UNIVERSIDAD AUTÓNOMA DE MADRID

FACULTY OF SCIENCES

Department of Molecular Biology

Protective role of mitochondrial uncoupling protein UCP3 and the transcription factor Nrf2 against cardiac ischemia-reperfusion injury and their involvement in ischemic preconditioning

Patricia Sánchez Pérez

Madrid, 2019

UNIVERSIDAD AUTÓNOMA DE MADRID

FACULTY OF SCIENCES

Department of Molecular Biology

Protective role of mitochondrial uncoupling protein UCP3 and the transcription factor Nrf2 against cardiac ischemia-reperfusion injury and their involvement in ischemic preconditioning

Thesis submitted by Patricia Sánchez Pérez, BSc in Biology, for the degree of Doctor of Philosophy (PhD) in Molecular Biosciences, with international PhD mention

The experimental work described in this thesis has been performed under the supervision of Dr. Susana Cadenas Álvarez at the Centro de Biología Molecular “Severo Ochoa” (CSIC-UAM)

Thesis research was supported by a predoctoral fellowship from the Universidad Autónoma de Madrid (FPI-UAM, 2014) and an associated mobility fellowship for a short stay at the University of Oslo (Norway).

Work in Dr. Cadenas´ laboratory was supported by grants from the Instituto de Salud Carlos III (ISCIII) FIS (PS09/00116, PI12/00933 and PI15/00448) cofounded by Fondos Europeos de Desarrollo Regional (FEDER) and by Comunidad de Madrid, Spain (S2011/BMD-2402).

A mi familia

“Nuestra mayor debilidad reside en rendirnos. La forma más segura de tener éxito es intentarlo siempre una vez más” Thomas A. Edison

“A diamond is just a piece of charchoal that handled stress exceptionally well” Anonymous

AGRADECIMIENTOS/ ACKNOWLEDGEMENTS

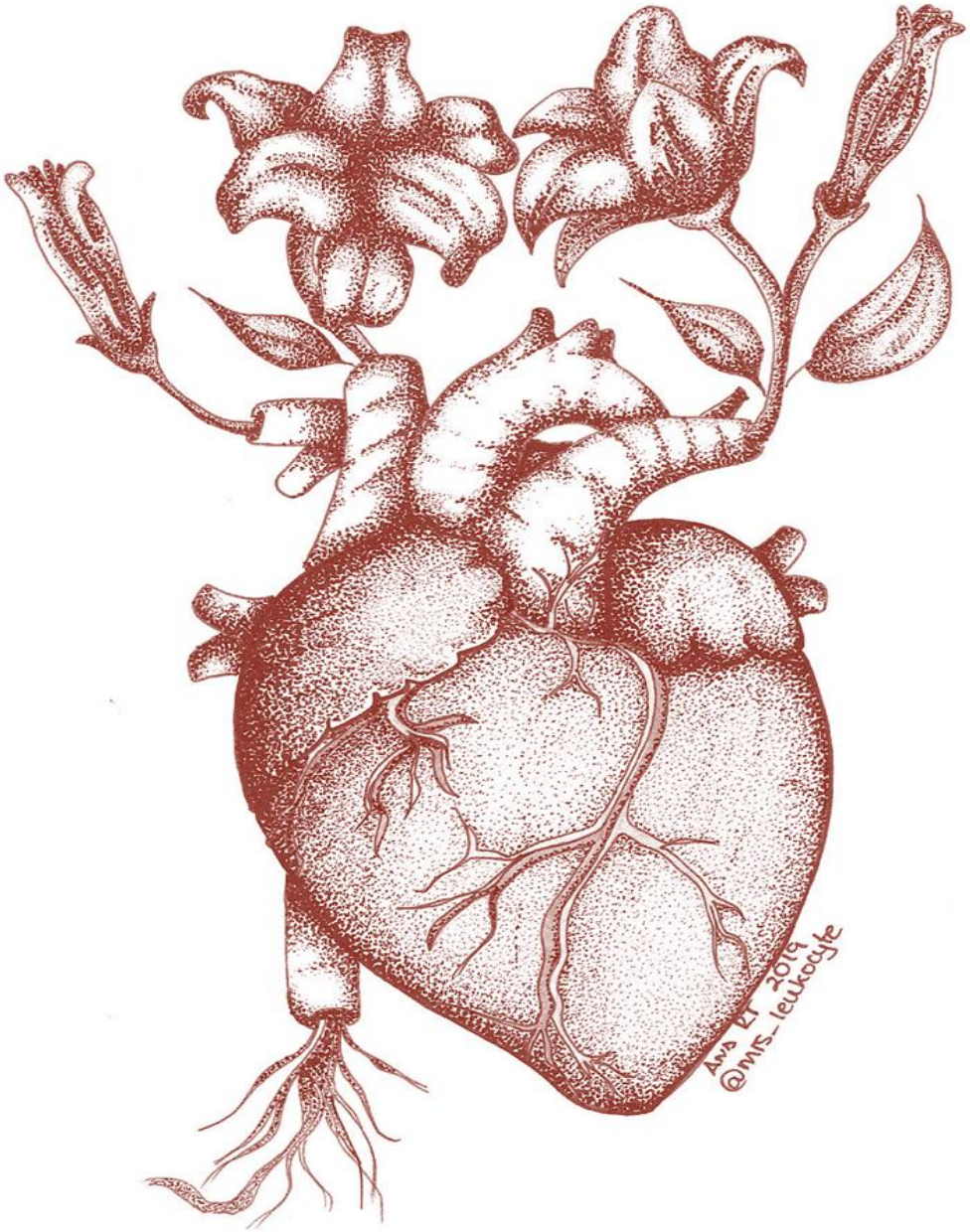

El corazón de uno florece gracias a la luz de las personas buenas que le rodean. Nunca dejes que se marchite por la oscuridad.

Nadie dijo que hacer la tesis fuera a ser fácil, pero quizá no sabía que iba a ser tan duro. Tras años de sudor, sangre y lágrimas ha llegado el momento de agradecer todo el apoyo recibido durante estos años. Siempre he pensado cómo sería escribir este apartado, ya que para mí es casi uno de los más importantes de la tesis. No sé qué hubiera hecho sin toda esta gente maravillosa que me ha apoyado, enseñado y acompañado durante todo este tiempo.

En primer lugar, quiero agradecer a la Dra. Susana Cadenas y su proyecto, sin el cual probablemente no hubiera podido conseguir la FPI-UAM 2014. Siempre recordaré el día que me entrevisté con ella para poder solicitar la FPI-UAM, me contó el proyecto y tras terminar me preguntó qué era lo que más me había gustado. Recuerdo que le dije, el equipo de los corazones (no sabía casi ni pronunciar bien su nombre), "el Langendorff," el cual luego se convirtió en mi gran aliado durante esta tesis. Al principio fue duro tener que aprender la técnica sin apenas referencias, hasta que Susana pudo traer un par de días a Igor y a Lin de Bristol para que me enseñasen y ayudasen a perfeccionar la técnica. Por ello debo darle las gracias por traerles y dejarme aprender esta técnica, poco común en España, pero que es increíble y ha dado la mayoría de los frutos de esta tesis. Poder mantener el corazón vivo fuera del cuerpo durante varias horas, verle latir, es algo fascinante como bióloga y que siempre me fascinará. También debo agradecerle el haber podido colaborar con el CNIC con el grupo del Dr. Borja Ibáñez, las unidades de imagen (Dr. Jesús J. Borreguero, Lorena Flores y María Villalba), animalario (Iria y Lorena), así como la unidad de histología (Antonio de Molina Iracheta) para uno de los estudios ecocardiográficos. Por último, he de agradecerle el resto de formación científica obtenida durante estos años, el que nunca falte de nada en el laboratorio, tanto medios instrumentales como económicos para la correcta consecución de esta tesis, y si me apuráis, hasta estudiantes.

A mis "pollitos", mis 6+1 estudiantes, porque bueno el 1, Rubén, era el estudiante de máster que estaba cuando entré. A ti te debo demasiadas cosas, tú me enseñaste todo del laboratorio cuando entré, me enseñaste hasta como poder orientar bien el corazón para canularlo en el Langendorff hasta que pudo venir Igor. Gracias también por cada momento, por esos memes, por recomendarme buena música, y por seguir siempre ahí aunque tuvieras que marcharte del lab. Durante ese primer año, se unió Alice para el TFG, que luego siguió para hacer el TFM junto con Rosa. Mis chicas "masterizadas", mis alegrías del lab, mis T-rex. Gracias por todos esos buenos momentos de risas, de alimentarme con chocolate, de dibujitos y frases de ánimo, de siempre ayudarme (sobre todo ese verano en el que os tenía a vosotras y a Laura y Jesús de prácticas, y no me daba la vida), etc. Por último, se unieron al lab Jesús e Irene, mis últimos pollitos a largo plazo. Entraron para hacer el TFG y en mis últimos años de tesis. Gracias por ser tan comprensivos conmigo, aplicados y aprender tan rápido, cuando a mí el tiempo también me apremiaba e iba estresada con todo. Para terminar, quiero dar las gracias a mis dos pequeñas polluelos Laura y Marta, que aunque sólo estuvieron 1 mes de prácticas, se esforzaron por aprender y aprovechar al máximo el tiempo. Unas chicas muy aplicadas, buenas personas, que me alegraron los días y que ya están llegando lejos. Como maestra Yoda, sólo deciros que estoy muy orgullosa de los 7, de ver vuestra evolución, de cómo habéis pasado de ser pollitos a ser grandes T-rex, ya estéis en una farma, haciendo la tesis con temas de la NASA o en el CNIC con FPU o TFG, siendo el nº2 del BIR, o estéis en Cambridge y Estocolmo estudiando. Para un maestro no hay mayor satisfacción que ver que sus polluelos progresan y bien por lo alto, aunque no olvidéis que yo sólo os he guiado, el trabajo

y mérito es y será siempre vuestro. Puede que yo os haya enseñado cosas del lab, pero vosotros me habéis enseñado muchas cosas de la vida y a ser buena profe y mentora (o eso creo). Gracias a todos y por seguir pendiente de mí aunque ya no estéis por el lab.

Special thanks (tusen takk) to everybody in Oslo, where I did my stay. Thank you Dr. William Louch (Bill) for giving me the opportunity to go to Oslo and let me know and collaborate with Magnus (the super-surgeon) and Dr. Kåre-Olav´s group. I am very grateful to have known you and worked with all of you. Thank you for listening all my ideas, rely on me and my work, and valuing all my work. Also, thank you for the good moments and lunches with all of you: the stories of Jarle, the long talks with Arsenii, the cakes from Tørun and MayKris...Thank you to Christina for the long hours at the animal facility depilating mice, doing echos and also surgeries with Magnus until 3 am while listening to music. Thanks to MayKris, the master Langendorffer to teach me about cardiomyocytes isolation, norwegian and share the same passions for HP and owls haha. Finally, thank you to Mariia for the long talks about whatever, the laughs and for organizing that fantastic Christmas dinner.

Esta tesis también es gracias a todos los servicios del CBMSO que de alguna otra manera me han echado una mano en numerosas ocasiones. Desde Paco y Fernando del servicio de instrumentación y la gente de mantenimiento para la instalación del Langendorff en la 1ª planta o cualquier arreglo hasta Mª José de limpieza, por su alegría por las tardes y sus ánimos con ¡venga que ya es viernes! También a todos los servicios científicos como los de microscopía (Carmen, Alfonsa, Maite, Ángeles y Alex, así como Maite y Milagros), de genómica (sobre todo Laura), cultivos, etc. Gracias sobre todo al servicio del animalario, donde tanto tiempo he pasado. Gracias a Elena y Fernando por siempre escuchar mis peticiones y ayudarme en todo momento con cualquier cosa que les pasara a nuestros ratoncillos. Gracias también a todo su equipo de técnicos, que siempre me han echado una mano en lo que he necesitado, desde que empecé hasta el final, ayudándome siempre y más cuando iba como un torbellino por los pasillos (con especial mención a José, que es el que más me ha sufrido y escuchado, el pobre).

He pasado casi 6 años en el CBMSO, si cuento que también hice mi PFC allí, aunque con el grupo del Dr. Santiago Lamas, con los que he seguido colaborando y manteniendo el contacto durante mi tesis. A ese Lab 427 (ahora 103) quiero agradecer mucho que Mª Ángeles fura mi "mami" pollito cuando empecé. Ella me enseñó todo lo que sé sobre cultivos, WB, citometría, ratones, organización del trabajo, paciencia, a no frustrarse, etc. Tú sembraste las bases para poder llegar hasta aquí. También quiero agradecer a Rosa, Óscar y José por siempre apoyarme y ayudarme. Quiero hacer una especial mención a Cris, la cual conocí como la chica "loca" del S.Lamas, mi tita molona; y que ahora se ha convertido en "mother of dragons", en mi mentora y próximamente en PI en EEUU. Estoy muy muy contenta y feliz por haberte conocido, por haber sido compi, pero sobre todo amiga. Gracias y un millón de gracias por cada uno de tus consejos, correcciones, paciencia, por hacer que siempre saque una sonrisa y apoyarme en la distancia pese al desfase horario. Gracias a ti también por presentarme a Vero, que aunque nos conocimos en el máster no entablamos amistad hasta que me la presentaste al volver al CBMSO. Vero y Tam, mis unicornias, compañeras y amigas de batallas, de risas hasta doler la tripa, de aventuras (Toledo, Oslo, y próximamente Bélgica), de bodas, quedadas, de hacer el tonto, de comidas, etc. Gracias por hacer mis días en el CBMSO geniales sobre todo durante la comida, que era la hora de desconexión, y gracias por

estar siempre ahí cuando he necesitado algo. A esta chupipandi se unieron, más adelante, Carlitos y Jessi. Gracias por esas comidas hablando de bioempresas locas, por aprender sobre uñas, esteticien y organización de bodas, por compartir conmigo esas tartas súper buenas de la madre de Jess, bombones o bollitos que traíais al lab, que aunque yo no formará parte físicamente, siempre me habéis hecho sentir como una más. Gracias por dejarme formar parte de vuestras vidas tanto dentro como fuera del lab.

En otra línea de palabras, quiero agradecer a Maca (sí, no me he olvidado de ti y tienes tu parrafito de gloria para cuando te sientes a leerlo) el haberme enseñado a valorar el trabajo de un técnico, el trabajar duro como nadie, el enseñarme junto con MA cultivos primarios durante mi PFC, luego a enseñarme a destetar, marcar e identificar ratones cuando empecé la tesis y tú ya trabajabas en el animalario. Gracias por seguir mi trayectoria tanto profesional como personal, por no perderte ni una aventura ni locura como la de la visita a Oslo, por regalarme momentos únicos de felicidad y de muchas risas. Tanto tú como Cris habéis seguido mi trayectoria desde que era un huevito hasta ahora y me habéis ayudado a crecer y evolucionar durante este arduo camino de la investigación.

Quiero agradecer también a mis compis de lab, tanto a los Wildfredos (César, Jorge, Ándres y Arancha), como a Tania (de microscopía e-), como a la pequeña extensión del 108 en el 127 (Marcos, Sandra, Jorge, Carlos, Elena, Mario...) por siempre darme conversación, por echarme una mano en lo que he necesitado, y hacer que no sólo sean compañeros de trabajo si no amigos con el tiempo. Gracias a mi amigo Nacho (del máster) que favoreció esta amistad, así como a Diana, que ha pasado de ser la compi de enfrente de la poyata y a hablar entre las baldas, a ser una buena amiga tanto dentro como fuera del lab, y que se ha unido a la chupipandi. También mencionar y dar las gracias a mis compis de otros labs como del CNIC y CNB, donde realicé el máster y las prácticas de la carrera, por su amistad y el haberme ayudado en mi formación como científica y persona (Sofi, Tania, Briane, Adrián, Luis, Samuel, Rui, Laura, Gliselle, Ginés, Susana, Lolo...). Así como a toda la gente maravillosa que he conocido durante esta etapa y del mundo de la divulgación científica (gente de Pint of Science, Apadrina, Cienciaterapia y La Biothèque).

Yéndome un poco atrás en el tiempo, quiero dar las gracias a mis amigos de la carrera por compartir la biología como pasión, por siempre hacer simbiosis, apoyarme y hacer por seguir manteniendo el contacto y como dice Emilio "ser amigos de los de toda la vida": Mery ("mi cousin", compi de clase, prácticas y de la vida), Gema (fuiste compi durante el PFC y sin buscarlo, te convertiste en una amiga esencial en mi vida), Belén (la psicóloga infiltrada en bio), Emilio (el amigo loco de la colina), Ana (artista del corazón de los agradecimientos y amiga desde el día 1 de la carrera), Adri, Pili, Claudia, Sonia... También, gracias a mis otros compis de la carrera, del máster del universo, de la tesis, de divulgación, de la vida, y no sé si de más se puede: Cris, José y Tania. Gracias a los 3 por aguantarme, por hacer que me pare cuando iba a mil/h por los pasillos, por sufrir y superar todos juntos esta etapa, por el apoyo incondicional, por las ¡"reunión"! en los pasillos para resolver dudas del doctorado y por hacer por vernos aunque fuera para comer y estuviéramos todos a tope.

Quiero dar las gracias también a todos mis amigos que en la distancia me mandan notas de apoyo, hacen por venir a Madrid o que quedemos en Murcia, Navarra, Toledo, etc cuando coincidimos, y espero que próximamente en Alemania: Juan Fran, María, MicroPatri. Gracias

también a mis chicas aventureras de Oslo, quién iba a decir que el mensaje de María en el facebook, nos iba a juntar a las 4 (María, Olga y Guille). Gracias por hacer de los 3 meses en Noruega una experiencia increíble, que la repetiría una y otra vez con vosotras. Gracias por todos los buenos momentos vividos allí. Por ello, y ya que no hemos cumplido la promesa de quedadas estacionales, queda pendiente el volver a Oslo y más ahora que Olgui está allí.

Voy a ir acortando que si no me enrollo, aunque quiero y espero que no se me olvide nadie. Quiero agradecer también a mis amigas de Rasca (Tania, Fransi y Lur), que siempre han hecho por escucharme y poner interés aunque no se enterasen mucho de lo que les contaba de la tesis. Gracias por esos findes desde pequeñas hasta ahora, por esos grandes momentos en bici y en la pisci, en el campo cogiendo moras y haciendo picnic, por hacer el gamba, por las reuniones en el "rollinski", por crecer juntas y seguir siempre unidas pase lo que pase.

Ya terminando, quiero agradecer a mi familia por estar siempre ahí, por confiar en que yo puedo con todo, por apoyarme incondicionalmente en todos los pasos que doy en la vida y ayudarme a levantarme si me caigo. Gracias a mis padres por darme su maravillosa genética y la mejor de las epigenéticas, y haber hecho que, tanto yo como Belén, podamos alcanzar nuestras metas y convertirnos en las personas que somos. Gracias por vuestro cariño y amor incondicional siempre, por inculcarnos los mejores valores y educación. Gracias por ayudarme siempre que lo necesito, por aguantarme, por valorar mi esfuerzo y trabajo, por vuestra comprensión y paciencia, sobre todo escuchándome horas y horas hablar de la tesis hasta que habéis acabado entiendo de lo que hablaba. Gracias también por luchar conmigo por mis sueños y compartir mi pasión por la biología. Gracias a Belén, no sólo por ser una gran hermana, si no también mi amiga, por la portada fabulosa que me has hecho, por siempre escucharme, por aliarnos, por los grandes momentos siempre y por todo. Os quiero mucho a los 3.

Por último, gracias a mi sol, a mi luz en la oscuridad, gracias a ti Rubén. Gracias por darme todo durante todos estos años, por aguantar y quererme como nadie, por ser un gran apoyo y estar ahí siempre que parece que voy a caer y tenderme tus manos. No sé qué hubiera hecho sin ti, sobre todo en estos últimos años dónde mis niveles de estrés ya estaban por las nubes. Gracias por enseñarme y caminar juntos, por ayudarme en todo, por siempre hacer que sonría y sea feliz. Gracias por hacerme vivir tan buenos momentos y que espero que sigan por mucho tiempo. Te quiero.

Espero no haberme dejado a nadie, pero por si acaso, muchísimas gracias a todas y cada una de las personas que habéis estado ahí en algún momento u otro de estos años o siempre. Todas habéis formado parte de esta tesis,

¡GRACIAS!

THANKYOU MERCI TAKK XIÈ XIÈ GRAZIE SPASIBA

TABLE OF CONTENTS

ABBREVIATIONS

A

ADP - Adenosine diphosphate

AMP - Adenosine monophosphate

ANOVA - Analysis of variance

ANT - Adenine nucleotide translocase

ARE - Antioxidant response element

ARNT - Aryl hydrocarbon receptor nuclear translocator

ATF-1 - cAMP-dependent transcription factor ATF-1, activating transcription factor 1

ATP - Adenosine triphosphate

B

BAT - Brown adipose tissue

BSA - Bovine serum albumin

bp - base pair

b-ZIP – Basic-region leucine zipper

C

cAMP - Cyclic AMP

CHX - Cycloheximide

CK - Creatine kinase

CoA - Coenzyme A

CBP - CREB-binding protein

CREB -cAMP response element-binding protein

D

DMEM - Dulbecco´s modified Eagle medium

DMSO - Dimethyl sulfoxide

DNA - Deoxyribonucleic acid

DTT - Dithiothreitol

E

E/A - Ratio of the peak velocity of early (E) to late (A) diastolic transmittal flow

ECG - Electrocardiogram

EDTA - Ethylenediaminetetraacetic acid

EF - Ejection fraction

ER - Endoplasmic reticulum

ETC - Electron transport chain

F

FAD - Flavin adenine dinucleotide (oxidized)

$FADH_2$ - Flavin adenine dinucleotide (reduced)

FCCP - Carbonyl cyanide p-trifluoromethoxyphenylhydrazone

FS - Fractional shortening

G

GPx - Glutathione peroxidase

Grx - Glutaredoxin

GR - Glutathione reductase

GSH - Glutathione (reduced)

GSSG - Glutathione (oxidized)

H

HIF-1 - Hypoxia inducible factor-1

HNE - 4-Hydroxy-2-nonenal

HO-1 - Heme oxygenase-1

HRE - Hypoxia responsive element

I

i.p. - Intraperitoneal

IMM - Inner mitochondrial membrane

IMS -Intermembrane space

IPC -Ischemic preconditioning

IR -Ischemia-reperfusion

IVS - Interventricular septum

K

Keap1 - Kelch-like ECH-associated protein 1

KO - Knockout

L

LAD - Left anterior descending

LDH - Lactate dehydrogenase

LV - Left ventricle

LVID - Left ventricle internal dimension

LVPW- Left ventricle anterior and posterior wall

M

Maf - Musculoaponeurotic fibrosarcoma

MAPK - Mitogen-activated protein kinase

MI - Myocardial infarction

Mn-SOD - Manganese superoxide dismutase

mPTP - Mitochondrial permeability transition pore

mRNA - Messenger ribonucleic acid

MTT - 3-(4,5-Dimethylthiazol-2-yl)-2,5-diphenyltetrazolium bromide

MV - Mitral valve

MyoD - Myogenic regulatory factor

N

NAC - N-Acetyl-L-cysteine

NAD^+ - Nicotinamide adenine dinucleotide (oxidized)

NADH - Nicotinamide adenine dinucleotide (reduced)

$NADP^+$ - Nicotinamide adenine dinucleotide phosphate (oxidized)

NADPH - Nicotinamide adenine dinucleotide phosphate (reduced)

NO - Nitric oxide

NOX - NADPH oxidase

Nrf2 - Nuclear factor erythroid 2-related factor 2

O

OGD - Oxygen-and glucose deprivation

OMM - Outer mitochondrial membrane

P

pATF-1 - Phosphorylated ATF-1

PAGE - Polyacrylamide gel electrophoresis

PBS - Phosphate-buffered saline

PCR - Polymerase chain reaction

PFA - Paraformaldehyde

PGC-1α - Peroxisome proliferator-activated receptor γ coactivator 1α

PPAR - Peroxisome proliferator-activated receptor

Prx - Peroxiredoxin

PSAX - Parasternal standard short axes

PSLAX - Parasternal standard long axes

PW - Pulse wave

p38 MAPK - p38 Mitogen-activated protein kinase

R

RET - Reverse electron transport chain

RIRR - ROS-induced ROS release

RNA - Ribonucleic acid

RNS - Reactive nitrogen species

ROS - Reactive oxygen species

RT - Room temperature

RV - Right ventricle

S

SDS - Sodium dodecyl sulphate

SEM - Standard error of the mean

SI - Simulated ischemia

SIR - Simulated ischemia-reperfusion

SOD - Superoxide dismutase

T

TBS - Tris-buffered saline

TCA - Tricarboxylic acid

TMRM - Tetramethylrhodamine methyl ester

Trx - Thioredoxin

TrxR - Thioredoxin reductase

TTC - 2,3,5-Triphenyltetrazolium chloride

U, W

UCP - Uncoupling protein

UQ - Ubiquinone (oxidized)

UQH_2 - Ubiquinol (reduced)

WT - Wild-type

Δ

Δ*p* - Protonmotive force

ΔpH - pH gradient

$\Delta\psi_m$ - Mitochondrial membrane potential

ABSTRACT/RESUMEN

Mitochondria are a main source of reactive oxygen species (ROS) in cells, particularly in pathological conditions such as ischemia-reperfusion (IR). Mitochondrial uncoupling proteins UCP2 and UCP3 play an important role in the control of ROS production by the electron transport chain. Besides, the transcription factor Nrf2 (nuclear factor-erythroid 2-related factor 2) is a master regulator of the cellular redox homeostasis. In this thesis, we aimed at analysing the regulation of UCP3 and Nrf2 in response to hypoxia and their protective effect against cardiac IR injury. We have found that hypoxia induces UCP3 expression and Nrf2 nuclear accumulation in C2C12 myotubes and HL-1 cardiomyocytes. These effects are mediated by the activation of p38 MAPK that in turn phosphorylates and activates ATF-1. Moreover, hypoxia/reoxygenation increases mitochondrial superoxide production and induces UCP3 expression and Nrf2 nuclear accumulation to a greater extent than hypoxia alone. Likewise, simulated ischemia and simulated ischemia-reperfusion (SIR) increase UCP3 expression and the activation of both Nrf2 and ATF-1 in HL-1 cells. Consistent with enhanced superoxide production after hypoxia/reoxygenation, SIR augments HNE-protein adducts, indicating increased oxidative stress. Nrf2 activation and ATF-1 phosphorylation also increase in isolated perfused hearts subjected to IR or ischemic preconditioning (IPC), from both UCP3-KO and wild-type mice, although this increase is higher in hearts lacking UCP3. Similarly, active caspase-3 expression is enhanced in these conditions, particularly in UCP3-KO hearts, which reflects increased damage. UCP3 plays a cardioprotective role against IR injury, since isolated perfused hearts from mice lacking this protein present larger infarct size than those from wild-type mice. Consistent with this result, creatine kinase activity in the coronary effluent is higher in UCP3-KO than in wild-type mice at reperfusion. The cardioprotective effect of UCP3 against IR injury is even more relevant in aged than in adult mice and is also evident after left anterior descending (LAD) coronary artery ligation followed by reperfusion, as the histological analysis showed that UCP3 knockout hearts present larger infarct size than wild-type hearts. Moreover, UCP3-KO mice have a tendency to exhibit increased signs of cardiac damage as evaluated by echocardiography. A metabolomics analysis showed that, in ischemic conditions, UCP3 affects on the accumulation of the Krebs cycle intermediates. These data suggest that lipid and energy metabolism are the pathways more likely to be modulated by UCP3. The transcription factor Nrf2 plays a cardioprotective role against IR injury, since isolated perfused hearts from mice lacking Nrf2 present larger infarct size than those from wild-type mice. Accordingly, creatine kinase activity in the coronary effluent is higher in Nrf2-KO than in wild-type mice at reperfusion. Our results indicate that Nrf2 is involved in IPC, since the absence of this factor abolishes IPC protective effects.

Las mitocondrias son una fuente principal de especies reactivas de oxígeno (ROS) en las células, particularmente en condiciones patológicas como la isquemia-reperfusión (IR). Las proteínas desacoplantes mitocondriales UCP2 y UCP3 juegan un papel importante en el control de la producción de ROS por la cadena de transporte de electrones. Además, el factor de transcripción Nrf2 (*nuclear factor-erythroid 2-related factor 2*) es un regulador maestro de la homeostasis redox celular. En esta tesis, nos planteamos analizar la regulación de UCP3 y Nrf2 en respuesta a la hipoxia y su efecto protector frente al daño cardiaco por IR. Hemos encontrado que la hipoxia induce la expresión de UCP3 y la acumulación nuclear de Nrf2 en los miotubos C2C12 y los cardiomiocitos HL-1. Estos efectos están mediados por la activación de p38 MAPK, que a su vez fosforila y activa a ATF-1. Además, la hipoxia/reoxigenación aumenta la producción de superóxido mitocondrial e induce la expresión de UCP3 y la acumulación nuclear de Nrf2 en mayor medida que la hipoxia sola. Asimismo, la isquemia simulada y la isquemia-reperfusión simulada (SIR) aumentan la expresión de UCP3 y la activación de Nrf2 y ATF-1 en las células HL-1. De acuerdo con la producción incrementada de superóxido tras la hipoxia/reoxigenación, la SIR también aumenta los aductos HNE-proteína, lo que indica un aumento del estrés oxidativo. La activación de Nrf2 y la fosforilación de ATF-1 también aumentan en los corazones aislados perfundidos y sometidos a IR o precondicionamiento isquémico (IPC), tanto de ratones UCP3-KO como de ratones de tipo silvestre, aunque este aumento es mayor en los corazones que carecen de UCP3. De forma similar, la expresión de la caspasa-3 activa aumenta en estas condiciones, particularmente en los corazones UCP3-KO, lo que refleja el daño aumentado en los mismos. UCP3 juega un papel cardioprotector frente al daño por IR, ya que los corazones aislados perfundidos de ratones que carecen de UCP3 presentan un tamaño de infarto mayor que los ratones de tipo silvestre. De acuerdo con este resultado, la actividad creatina quinasa en el efluente coronario es mayor en los ratones UCP3-KO que en los de tipo silvestre. El efecto cardioprotector de UCP3 frente al daño por IR es aún más relevante en ratones viejos que en adultos y también es evidente después de la ligadura de la arteria coronaria descendente anterior izquierda (LAD) seguida de reperfusión, ya que el análisis histológico mostró que los corazones que carecen de UCP3 presentan un tamaño de infarto mayor que los corazones de tipo silvestre. Además, los ratones UCP3-KO tienden a mostrar signos aumentados de daño cardiaco, según lo evaluado por la ecocardiografía. El análisis metabolómico mostró que, en condiciones de isquemia, UCP3 afecta a la acumulación de intermediarios del ciclo de Krebs. Los datos sugieren que el metabolismo de lípidos y el energético son las vías con mayor probabilidad de ser moduladas por UCP3. El factor de transcripción Nrf2 juega un papel cardioprotector frente al daño por IR, ya que los corazones aislados perfundidos de ratones que carecen de Nrf2 presentan un tamaño de infarto mayor que los de tipo silvestre. Asimismo, la actividad creatina quinasa en el efluente coronario es mayor en ratones Nrf2-KO que en ratones de tipo silvestre durante la reperfusión. Nuestros resultados indican que Nrf2 está implicado en el IPC, ya que la ausencia de este factor elimina los efectos protectores del IPC.

INTRODUCTION

1. Mitochondrial ROS production and oxidative stress

Mitochondria are the powerhouse of the cell. Their principal function is the generation of adenosine triphosphate (ATP) by oxidative phosphorylation, which is the main source of chemical energy in most cells (*Fig. 1*). Moreover, mitochondria generate reactive oxygen species (ROS), thereby modulating the cellular redox status (Zorov *et al.*, 2014). They also control the adaptation of cells to metabolic changes and the response to changes in substrate availability (Liesa and Shirihai, 2013). Besides, they regulate cell death (Galluzzi *et al.*, 2012). Therefore, malfunction of mitochondria and excessive ROS production lead to pathological conditions such as neurodegenerative diseases, cancer, diabetes and cardiovascular diseases, and also to the aging process (Brand, 2000; Chan, 2006; Fischer *et al.*, 2012).

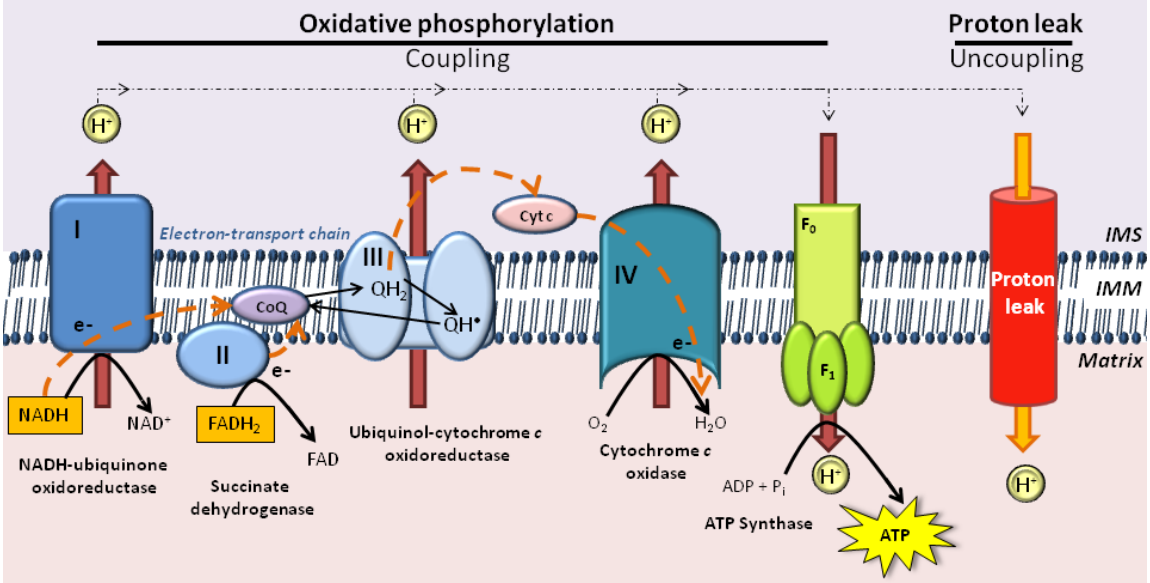

***Fig. 1.* The proton circuit across the inner mitochondrial membrane.** During the oxidation of substrates, complexes I, III and IV of the ETC translocate protons to the intermembrane space, generating an electrochemical proton gradient. The energy contained in this gradient drives ATP synthesis by the ATP synthase. The proton leak across the inner mitochondrial membrane mediated by UCPs uncouples oxidative phosphorylation, dissipating the energy of the proton gradient as heat. IMS, intermembrane space, IMM, inner mitochondrial membrane. Based on Cadenas (2018).

During the transfer of electrons in the ETC, protons are pumped across the inner mitochondrial membrane from the matrix into the intermembrane space by specific respiratory enzyme complexes (Lenaz and Genova, 2010) (*Fig. 1*). This proton pumping generates potential energy in the form of an electrochemical proton gradient, or protonmotive force (Δp), which consists of a pH gradient (ΔpH) and a membrane potential ($\Delta\psi_m$) across the inner mitochondrial membrane. The electrochemical proton gradient is used to drive ATP synthesis through the ATP synthase, a process termed oxidative phosphorylation (Mitchell, 1966). However, oxidative phosphorylation is not 100% efficient, since some protons return to the matrix independently of the ATP synthase, generating heat instead of ATP. This process is known as proton leak (Brand, 1990) (*Fig. 1*).

1.1. Mitochondrial ROS production

Mitochondria are the major source of ROS in the cell (Murphy, 2009). There are several mitochondrial sources of ROS generation, such as matrix dehydrogenases like α-ketoglutarate dehydrogenase or succinate dehydrogenase, aconitase, and mitochondrial monoamine oxidases (Lenaz, 2012). However, the respiratory chain in the inner mitochondrial membrane is a major source of ROS (Zorov *et al.*, 2014). ROS were initially considered as harmful by-products of cell respiration, but it is now well recognized that they play a dual role in aerobic cells, which depends on their concentration (Murphy, 2009; Nickel *et al.*, 2014). At low levels, ROS are important in cell signaling, acting as second messengers by activating the expression of several genes and signaling pathways. They are involved in processes such as senescence, cell proliferation and apoptosis, and have even been recognized as anti-tumorigenic species (Dröge, 2002; Forman *et al.*, 2008). By contrast, at high levels, ROS can produce macromolecular damage and oxidative stress. In cells, ROS are counterbalanced by antioxidants such as superoxide dismutase (SOD), catalase, glutathione peroxidase (GPx) or peroxiredoxin (Prx). In addition, the antioxidant tripeptide glutathione, which is reduced by glutathione reductase (GR), is the primary determinant of the cellular redox state (Handy and Loscalzo, 2012; Schafer and Buettner, 2001). An overproduction of ROS can trigger oxidative stress, as the capacity of the antioxidant system cannot compensate it (Sies, 1985). Oxidative stress, in turn, can lead to the development of pathological conditions (Balaban *et al.*, 2005).

Oxygen is the final acceptor of electrons in the respiratory chain. The transfer of four electrons at complex IV (cytochrome *c* oxidase) reduces oxygen to water. However, some of the redox centers of the respiratory complexes can transfer a single electron to oxygen, generating the superoxide radical ($O_2^{\bullet -}$) (Cadenas and Davies, 2000). Complex I (NADH-ubiquinone oxidoreductase) and complex III (ubiquinol-cytochrome *c* oxidoreductase) are the major centers able to transfer a single electron to O_2 (Murphy, 2009; Sena and Chandel, 2012) (***Fig. 2***). In particular, complex I produces high amounts of superoxide during reverse electron transport (RET), which occurs when the coenzyme Q pool becomes highly reduced and a large Δp forces electrons back from complex II driven by succinate oxidation (Chouchani *et al.*, 2014). This process occurs under conditions of ischemia-reperfusion (IR) (see Section 5.1). Importantly, complex I generates superoxide exclusively to the mitochondrial matrix, while complex III can produce superoxide to either the matrix or the intermembrane space (St-Pierre *et al.*, 2002). The topology of superoxide production is important for redox signaling and oxidative damage, as it determines the efficient removal of $O_2^{\bullet -}$ by the cellular antioxidant system. In addition to complexes I and III, other sites of superoxide production have been described (Brand, 2016), and the description of these sites allows the identification of therapeutic targets against oxidative damage, and some groups are working to design antioxidant compounds that target superoxide production at specific sites (Brand, 2016; Orr *et al.*, 2015).

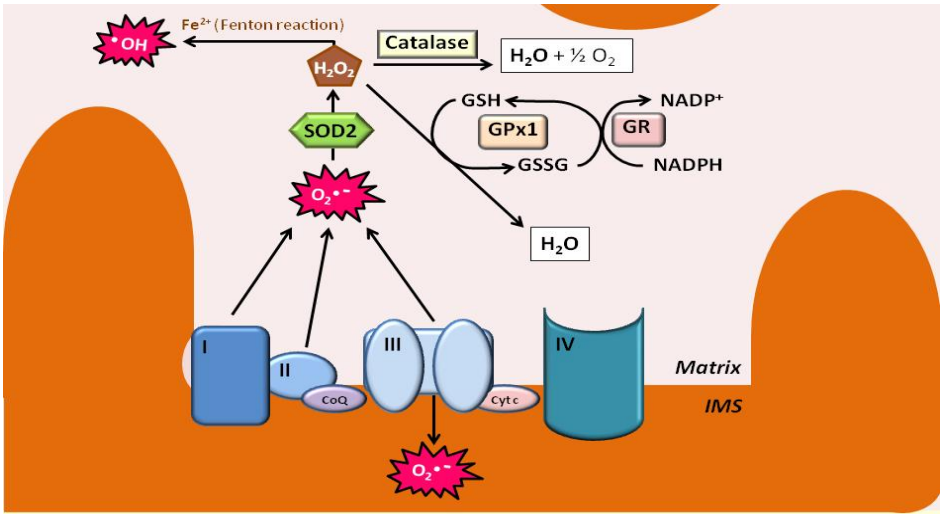

***Fig. 2*. Mitochondrial ROS generation and the antioxidant system.** Complexes I, II and III release superoxide ($O_2^{\bullet-}$) either into the matrix or into the intermembrane space. Mitochondria are equipped with defense mechanisms to prevent macromolecular damage. Mitochondrial SOD (Mn-SOD or SOD2) catalyzes the dismutation of $O_2^{\bullet-}$ into H_2O_2 and O_2. H_2O_2 is in turn removed by catalase and GPx, generating H_2O and O_2 (catalase) or H_2O and GSSG (GPx). GSSG is reduced to GSH by GR and NADPH. Some H_2O_2 molecules escape the antioxidant system and they are transformed into hydroxyl radicals ($OH^{\bullet}$) through the Fenton reaction. IMS, intermembrane space; GPx, glutathione peroxidase; GR, glutathione reductase; GSH, reduced glutathione; GSSG, oxidized glutathione; SOD, superoxide dismutase. Based on Fuhrmann and Brüne (2017).

1.2. Oxidative stress-mediated macromolecular damage

The term oxidative stress was coined by Helmut Sies in 1985 to refer to a shift in the prooxidant to antioxidant balance in favor of the former, leading to macromolecular damage (Sies, 2015, 1985). The term was then redefined from a mechanistic point of view as a disruption of redox signaling and control that causes cell dysfunction (Jones, 2006). Mitochondria have evolved mechanisms to process ROS into less toxic substances, thus helping to maintain metabolic homeostasis. Under normal conditions, mitochondrial $O_2^{\bullet-}$ is rapidly converted to hydrogen peroxide (H_2O_2) by the mitochondrial manganese superoxide dismutase (Mn-SOD). H_2O_2 is then reduced to H_2O by catalase, GPx or Prx (*Fig. 2*). Since H_2O_2 is more stable than $O_2^{\bullet-}$, it can escape from the mitochondrion and diffuse into the cytosol. Redox metal ions such as iron (Fe^{2+}) or copper (Cu^{+}) react with H_2O_2 to generate the hydroxyl radical ($OH^{\bullet}$) by the Fenton reaction. $OH^{\bullet}$ is an extremely reactive radical that is able to peroxidize membrane phospholipids and cause oxidative damage to proteins and DNA (Lenaz, 2012). Lipid peroxidation products, such as the reactive alkenal 4-hydroxy-2-nonenal (HNE) have generally been considered as toxic products of a deleterious process. These products can amplify ROS damage and are able to form adducts with proteins and DNA (Conklin *et al.*, 2007; Esterbauer *et al.*, 1991). Moreover, HNE is a very stable molecule so it can diffuse and disseminate the oxidative injury, amplifying the damage and playing an important pathogenic role in several diseases. However, at physiological concentrations, HNE acts as a potent mediator that regulates a variety of signaling pathways and cellular processes (Chapple *et al.*, 2013). The signaling effect of HNE originates from its ability to form adducts with

proteins involved in signal transduction and gene expression including receptors, kinases, phosphatases and transcription factors (Ullery and Marnett, 2012). HNE can also induce some cellular defense mechanisms against oxidative stress, thus being involved in its own detoxification. During the detoxification process, HNE consumes the bioavailable GSH in the cell to form non-reactive GSH-HNE catalyzed by GST (glutathione S-transferase). The decrease in GSH levels together with Nrf2 (nuclear factor-erythroid 2-related factor 2) activation leads to GSH synthesis by a positive feedback mechanism. In fact, HNE has been shown to modify Keap1 (the cytosolic repressor of Nrf2) and activate ARE (antioxidant response element) to induce the expression of ARE dependent genes (Levonen *et al.*, 2004). The ability of the cell to cope with oxidative stress and especially to detoxify HNE largely determines the balance between cell survival and cell death (Dalleau *et al.*, 2013).

2. Mitochondrial uncoupling proteins and oxidative stress

Mitochondrial uncoupling proteins (UCPs) are inner membrane proteins that belong to the superfamily of the mitochondrial anion carriers (Krauss *et al.*, 2005) (*Fig. 3*). UCPs have a molecular mass of around 32 kDa and a tripartite structure with three similar domains of 100 residues approximately. Each repeat contains two hydrophobic regions that form transmembrane α-helices. Within each repeat, a long hydrophilic loop, which is oriented towards the matrix side of the membrane, connects the two attached helices (Ledesma *et al.*, 2002). UCPs are able to dissipate the electrochemical proton gradient generated by the electron transport chain across the inner mitochondrial membrane, producing heat instead of ATP.

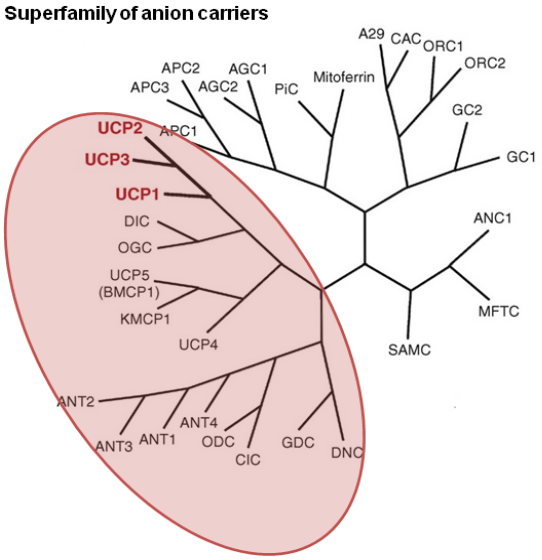

Protein	Aminoacid identity (%)
UCP1	**100**
UCP2	**59**
UCP3	**57**
DIC	35
UCP5 (BMCP1)	34
OGC	32
UCP4	30
ANT2	20
ANT3	20
ANT1	19

***Fig. 3.* Phylogenetic analysis of mitochondrial anions carriers and comparison of the sequence identity with UCP1.** Analysis of the mitochondrial anion carriers suggests that UCP1-3 belong to the same subfamily that does not include UCP4 or UCP5 (BMCP1). The figure shows the human SLC25 mitochondrial anion carrier members displayed using an unrooted topological algorithm. UCP2 and UCP3 share 59% and 57% amino acid sequence identity with UCP1, respectively, and UCP2 and UCP3 are 73% identical to each other. ANT, adenine nucleotide translocase; DIC, dicarboxylate carrier; OGC, oxoglutarate/malate carrier. Adapted from Azzu and Brand (2010a) and Krauss *et al.* (2005).

UCP1 was the first UCP identified, in brown adipose tissue (BAT) (Nicholls *et al.*, 1978). Its function is adaptive thermogenesis in brown adipocytes. UCP2 and UCP3 show around 60% sequence identity with UCP1 and around 70% identity with each other, which suggests similar biochemical properties and function. However, studies using UCP2 and UCP3 knockout mice showed that the physiological functions of UCP2 and UCP3 differ from that of UCP1, since they are not normally thermogenic or involved in the adaptive response to cold (Himms-Hagen and Harper, 2001). Moreover, these proteins have different expression patterns: UCP1 is specifically expressed in BAT (Bouillaud et al., 1985), UCP2 is ubiquitously expressed (Fleury *et al.*, 1997) and UCP3 is abundantly expressed in skeletal muscle and to a lesser extent in heart and BAT (Boss *et al.*, 1997). UCP2 and UCP3 do not transport protons in the absence of specific activators, as shown from the very low proton conductance in the absence of fatty acids of proteoliposomes containing UCP2 or UCP3 (Echtay *et al.*, 2001; Jabůrek and Garlid, 2003), and the lack of effect of UCP2 or UCP3 knockout on the basal proton conductance of isolated mouse mitochondria (Cadenas *et al.*, 2002; Krauss *et al.*, 2003). However, they catalyze a nucleotide-sensitive proton leak when activated by fatty acids, superoxide or alkenals derived from lipid peroxidation (Brand *et al.*, 2004).

2.1. Physiological roles of UCPs

As stated above, UCP1 mediates adaptive thermogenesis in BAT. By contrast, the physiological function of UCP2 and UCP3 is not clearly established yet. They have been involved in the control of mitochondrial ROS production and the protection against oxidative damage (Mailloux and Harper, 2011).

2.1.1. Physiological role of UCP1

UCP1 catalyzes the transfer of protons from the mitochondrial intermembrane space to the matrix, thus mediating non-shivering thermogenesis in BAT to produce heat in response to cold exposure (Cannon and Nedergaard, 2004; Nicholls and Locke 1984). This process allows hibernators, cold-adapted rodents and newborn mammals to generate heat without the necessity of shivering. UCP1 is activated by free fatty acids and inhibited by purine nucleotides (Locke *et al.*, 1982). Upon sympathetic stimulation of lipolysis in brown adipocytes, increased free fatty acid levels activate the proton leak catalyzed by UCP1 (Nicholls and Locke, 1984). However, the mechanism of UCP1 activation by fatty acids is still under debate. Two main models have been proposed: the *fatty acid cycling model*, in which fatty acids function as substrate (Breen *et al.*, 2006; González-Barroso *et al.*, 1998; Skulachev, 1991), and the *proton-buffering model*, in which fatty acids function as a prosthetic group (Klingenberg and Huang, 1999; Rial *et al.*, 2004; Winkler and Klingenberg, 1994). A more recent model *(functional competition model)* suggests that proton transport is independent of fatty acids, which act as allosteric ligands, regulating

conductance (Nicholls, 2006; Shabalina *et al.*, 2004). More recently, using direct patch-clamp measurements of UCP1 currents from the inner mitochondrial membrane of BAT mitochondria, Fedorenko *et al.* (2012) showed that UCP1 is a long-chain fatty acid anion/H^+ symporter *(shuttling model)*.

2.1.2. Physiological role of UCP2

UCP2 was identified in 1997 as a novel uncoupling protein that showed 59% amino acid identity with UCP1 (Fleury *et al.*, 1997) (*Fig. 3*). UCP2 mRNA is present in many tissues and cell types: adipose tissue, heart, lung, spleen, pancreas, kidney, thymus, lymphocytes and macrophages (Fleury *et al.*, 1997; Pecqueur *et al.*, 2001). UCP2 mediates proton leak in intact thymocytes (Krauss *et al.*, 2002). Importantly, UCP2 negatively regulates insulin secretion, being a critical link between obesity, β-cell dysfunction and type 2 diabetes (Zhang *et al.*, 2001). Endogenously produced mitochondrial superoxide activates UCP2-mediated proton leak, thus lowering ATP levels and impairing glucose-stimulated insulin secretion (GSIS) (Krauss *et al.*, 2003). UCP2 attenuates GSIS by lowering ROS production, which is an important signal in glucose sensing (Affourtit *et al.*, 2011). UCP2, therefore, has an important role in the pathogenesis of type 2 diabetes by inhibiting insulin secretion in pancreatic islet β-cells (Mattiasson and Sullivan, 2006). The inhibition of UCP2 with genipin reverses the deleterious effects of obesity and high glucose-induced pancreatic β-cell dysfunction, an effect achieved by the inhibition of UCP2-mediated proton leak (Zhang *et al.*, 2006). Moreover, Bouillaud (2009) proposed that UCP2 functions as a uniport for anionic pyruvate. More recently, Vozza *et al.* (2014) showed that UCP2 is able to export C4 metabolites out of mitochondria, thus regulating substrate oxidation by limiting mitochondrial oxidation of glucose and enhancing glutaminolysis.

2.1.3. Physiological role of UCP3

UCP3 was identified in 1997 as a protein that showed 57% amino acid identity to UCP1, and 73% identity to UCP2 (Boss *et al.*, 1997). This protein is expressed in skeletal muscle, BAT and heart. UCP3 was initially considered a candidate for mediating thermogenesis in muscle. However, UCP3 knockout mice are neither cold sensitive nor obese and have normal energy expenditure compared to wild-type mice (Himms-Hagen and Harper, 2001). Moreover, both fasting and starvation, conditions that require energy conservation, lead to UCP3 upregulation in skeletal muscle (Cadenas *et al.*, 1999). In addition, the presence of UCP3 in ectothermic fish and plants points to a function of this protein that is different from thermogenesis (Brand and Esteves, 2005).

UCP3 has also been suggested to play an important role in regulating fatty acid metabolism, acting as a transporter of fatty acid anions from the mitochondrial matrix (Himms-Hagen and Harper, 2001; Schrauwen *et al.*, 2001). Consistent with this idea, UCP3 overexpression increases

fatty acid transport and oxidation (Bezaire *et al.*, 2005). Seifert *et al.*, (2008) found that UCP3 is necessary for fasting-induced enhancement of fatty acid oxidation rate and capacity via mitigated oxidative stress. Nevertheless, these authors showed that UCP3 is not itself a fatty acid transporter, as it had been previously proposed (Himms-Hagen and Harper, 2001; Schrauwen *et al.*, 2006).

Proton leak mediated by UCP3 is activated by superoxide and reactive alkenals, and it was proposed that the mild uncoupling induced by proton transport attenuates mitochondrial ROS production and protects against oxidative damage (Azzu and Brand, 2010a; Mailloux and Harper, 2011). UCP3 neutralizes protein oxidation (Barreiro *et al.*, 2009) and reduces ROS production during exercise (Jiang *et al.*, 2009). Along the same line, skeletal muscle mitochondria from UCP3 knockout mice show higher levels of ROS production and enhanced markers of oxidative damage (Brand *et al.*, 2002; Vidal-Puig *et al.*, 2000), while mice overexpressing UCP3 exhibit reduced ROS production during aging (Nabben and Hoeks, 2008).

Similar to UCP2, UCP3 is also involved in insulin sensitivity. Several genetic association studies have related polymorphisms on the genes encoding UCPs to obesity and type 2 diabetes (Jia *et al.*, 2009; Musa *et al.*, 2012). Moreover, studies in type-2 diabetic patients showed decreased UCP3 expression in skeletal muscle, which was accompanied by a reduced insulin sensitivity and decreased metabolic flexibility (Schrauwen *et al.*, 2006). However, the treatment with rosiglitazone, a PPARγ (peroxisome proliferator-activated receptors) agonist, restored muscle UCP3 content and improved insulin sensitivity in these patients (Schrauwen *et al.*, 2006).

2.2. Regulation of UCP expression

Peroxisome proliferator-activated receptor (PPAR) subtypes mediate to a large extent the transcriptional regulation of the UCP genes, with a distinct relevance depending on the particular UCP gene and the tissue in which it is expressed (Villarroya *et al.*, 2007).

2.2.1. Regulation of UCP1

UCP1 mediates non-shivering thermogenesis in BAT, although its mechanism of action at the molecular level is still controversial. The induction of adaptive thermogenesis is highly regulated and leads to UCP1 activation, which dissipates mitochondrial protonmotive force as heat. Fatty acids provide not only the substrate for thermogenesis, but also induce UCP1 activity, overcoming inhibition by endogenous adenine nucleotides (Nicholls, 2001). In response to prolonged exposure to cold or chronic overfeeding, norepinephrine release from sympathetic nerves results in the induction of the thermogenic response. Importantly, norepinephrine stimulation of β-adrenergic receptors results in several steps: (1) activation of p38 mitogen-activated protein kinase (MAPK) pathways that upregulate UCP1 synthesis - these pathways involve the transactivation of the PPAR family by the transcriptional coactivator PGC1α (peroxisome proliferator-activated receptor γ coactivator 1α), as well as the activation of other transcription factors such as those of the CREB

(cAMP-responsive element-binding protein) family (Carmona *et al.*, 2005; Puigserver *et al.*, 1998); (2) activation of protein kinase A (PKA)-mediated pathways that initiate lipolysis and release fatty acids, activators of UCP1 (Locke *et al.*, 1982; Robidoux *et al.*, 2004); (3) inhibition of lysosomal pathways that degrade UCP1 via autophagy and affect UCP1 turnover. UCP1 half-life is around 1-4 days (Moazed and Desautels, 2002). Therefore, UCP1 is controlled at the synthesis, ligand-activation and proteolysis steps.

2.2.2. Regulation of UCP1 homologs: UCP2 and UCP3

Studies reconstituting UCP1, UCP2 and UCP3 into proteoliposomes suggest that all UCPs have comparable fatty acid-activation of proton conductance and similar inhibition by purine nucleotides (Jabůrek *et al.*, 1999; Žáčková *et al.*, 2003). Superoxide and reactive alkenals activate uncoupling in mitochondria via ANT and UCPs, which has been suggested as a feedback mechanism to control excessive mitochondrial ROS production and oxidative stress (Echtay *et al.*, 2003). Interestingly, the presence of fatty acids is required for superoxide stimulation of proton leak in mitochondria that express UCP2 and UCP3 (Echtay *et al.*, 2002). It is also known that glutathionylation maintains UCP2 and UCP3 in an inactive state, whereas an increase in ROS levels leads to their deglutathionylation and activation (Mailloux *et al.*, 2011).

Similar to UCP1, UCP2 is regulated at several levels: transcription, translation, modulation of protein activity and degradation. Several studies have shown that UCP2 is upregulated in diabetes, and that hyperglycemia and hyperlipidemia increase *Ucp2* mRNA expression via transcription factors, such as PPARs or FOXA-2 (forkhead box A-2) (Affourtit and Brand, 2008; Villarroya *et al.*, 2007). Sirt1 represses *Ucp2* gene expression by binding directly to its promoter in pancreatic β-cells, stimulating insulin secretion (Bordone *et al.*, 2006). In addition, Pecqueur *et al.* (2001) showed that an upstream ORF (open reading frame) located in exon two of the *Ucp2* gene strongly inhibits the expression of the protein, providing a mechanism for translational regulation of *Ucp2* mRNA by means of which its expression can be strongly and rapidly induced under stress conditions (Pecqueur *et al.*, 2001). At the translational level, physiological concentrations of glutamine stimulate UCP2 expression (Hurtaud *et al.*, 2007). Of note, UCP2 has a short half-life of approximately 1 h (Azzu *et al.*, 2008) and is degraded by the cytosolic ubiquitin-proteasome system, which allows for rapid variations in UCP2 levels in response to changes in nutrient supply (Azzu and Brand, 2010b).

UCP3 is upregulated in response to fasting and starvation (Cadenas *et al.*, 1999). Fatty acids control the transcription of the *Ucp3* gene via MyoD and PPAR-dependent pathways in human skeletal muscle (Solanes *et al.*, 2003). UCP3 expression is also induced by exercise, hypoxia and AMP-activated protein kinase in rat skeletal muscle (Zhou *et al.*, 2000). Likewise, thyroid hormones directly activate UCP3 transcription in skeletal muscle, which is mediated by binding to a TRE (thyroid hormone response element) in the proximal promoter region (Solanes *et al.*, 2005).

UCP3 has also a short half-life of 0.5-4 h, and it is turned over rapidly in a proteasome-dependent manner (Azzu *et al.*, 2010a, 2010b). Moreover, our group has recently shown that H_2O_2 and HNE upregulate UCP3, an effect mediated by the transcription factor Nrf2, which promotes cell survival under conditions of oxidative stress (Anedda *et al.*, 2013; López-Bernardo *et al.*, 2015)

2.3. Mild uncoupling of oxidative phosphorylation as a mechanism to control mitochondrial ROS production

Mitochondria are a main source of ROS. There is a strong positive correlation between the protonmotive force (Δp) and mitochondrial ROS production. Korshunov *et al.* (1997) reported that, above a threshold value of $\Delta\psi_m$, a very strong increase in H_2O_2 production takes place in isolated rat heart mitochondria respiring on complex II substrates (*Fig. 4A*). These findings were subsequently confirmed in rat brain mitochondria oxidizing NADH-dependent substrates (Starkov and Fiskum, 2003). Moreover, in *Drosophila* mitochondria, a 10 mV reduction in $\Delta\psi_m$ decreases ROS generation from complex I following reverse electron flow by 70%, without diminishing the efficiency of oxidative phosphorylation (Miwa and Brand, 2003). Mitochondrial uncoupling has been suggested to decrease ROS production, minimize oxidative damage to DNA and slow ageing (Brand, 2000). This mechanism has been identified as a cytoprotective strategy under conditions of oxidative stress, including diabetes, ischemia-reperfusion (IR) injury or aging (Cadenas, 2018b). Mild uncoupling of oxidative phosphorylation refers to a limited increase in proton conductance so that protonmotive force is slightly lowered and respiration rate is moderately increased but ATP can still be made (Brand and Esteves, 2005). Hence, the mild uncoupling of oxidative phosphorylation may represent a natural antioxidant mechanism for decreasing ROS production and protecting against oxidative stress (Mailloux and Harper, 2011; Skulachev, 1997).

Nègre-Salvayre *et al.* (1997) first suggested a role for the UCPs in reducing mitochondrial ROS production. They showed that the inhibition of UCP2 by GDP raised the membrane potential and increased mitochondrial H_2O_2 production. As previously mentioned, UCPs are activated by superoxide and by lipid peroxidation products such as HNE (Aguirre and Cadenas, 2010; Echtay *et al.*, 2002; Murphy *et al.*, 2003). The mild uncoupling induced by proton transport through the UCPs limits mitochondrial ROS production and represents a feedback response to the overproduction of superoxide by the ETC (Mailloux and Harper, 2011) (*Fig. 4B*). Even though UCP2 and UCP3 have been involved in mild uncoupling for ROS reduction (Mailloux and Harper, 2011), there is some controversy regarding the involvement of UCP1 in this mechanism. Some authors reported that UCP1 was not involved in the control of ROS production in BAT mitochondria (Nabben *et al.*, 2011; Shabalina and Nedergaard, 2012). They conclude that membrane depolarization may not necessarily decrease ROS production.

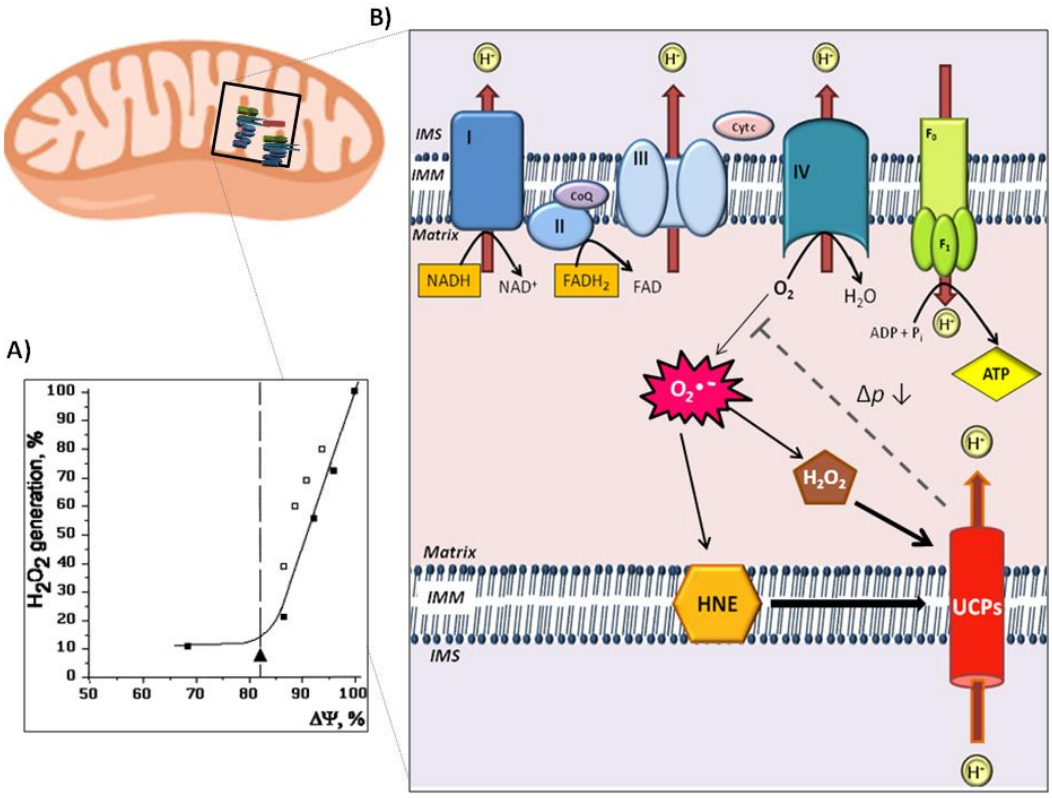

***Fig. 4*. Mild uncoupling of oxidative phosphorylation limits mitochondrial ROS production.** A) Relationship between membrane potential ($\Delta\psi_m$) and H_2O_2 production in rat heart mitochondria. The figure illustrates a very steep dependence of H_2O_2 formation upon $\Delta\psi_m$. Taken from Korshunov *et al*. (1997). B) During substrate oxidation, the pumping of protons by complexes of the ETC generates a protonmotive force (Δp) across the inner mitochondrial membrane. The final electron acceptor is O_2 that is reduced to H_2O at complex IV. However, some electrons escape from the reduced complexes, reacting with O_2 to form $O_2^{\bullet-}$, which can be transformed into H_2O_2 by Mn-SOD. $O_2^{\bullet-}$ can also peroxidize membrane phospholipids, generating HNE, which induces H^+ transport through UCPs. This lowers Δp and slightly stimulate electron transport (mild uncoupling), so that the complexes become more oxidized and the local O_2 concentration is reduced, both these effects reduce mitochondrial ROS production. The mild uncoupling induced by HNE limits mitochondrial ROS generation as a feedback response to an overproduction of superoxide by the ETC. Based on Echtay *et al*. (2003).

3. The antioxidant transcription factor Nrf2

An effective adaptive response to oxidative stress is essential for cell survival. The transcription factor nuclear factor erythroid 2-related factor 2 (Nrf2) is the master regulator of the cellular redox homeostasis. Nrf2 targets consist of genes encoding antioxidant enzymes, proteins involved in xenobiotic detoxification, repair and removal of damaged proteins, as well as other transcription factors (Hayes and Dinkova-Kostova, 2014).

3.1. Role of Nrf2 as a regulator of the cellular defense system

Nrf2 is encoded by the gene *Nfe2l2* and belongs to the family of basic leucine zipper (bZIP) transcription factors. It also contains an upstream cap'n'collar (CNC) domain that contributes to the DNA-binding specificity of this family (Moi *et al.*, 1994). In vertebrates, other members of the CNC-bZIP family of proteins include p45 NF-E2, Nrf1 (NF-E2-related factor 1) and Nrf3 (NF-E2-

related factor 3) (Motohashi *et al.*, 2002). All members of this family form heterodimers with small Maf (musculoaponeurotic fibrosarcoma) proteins, which are necessary for DNA binding (Kensler *et al.*, 2007). Essential to the expression of Nrf2 target genes is the presence of the antioxidant response element (ARE) in their regulatory DNA sequences (Itoh *et al.*, 1997; Rushmore *et al.*, 1991). The ARE, also known as electrophile response element (EpRE), is comprised of the 5´-TGACnnnGC-3´ core sequence (Venugopal and Jaiswal, 1996). This sequence mediates the transcription of genes encoding proteins involved in glutathione synthesis and conjugation, phase II xenobiotic metabolism, ROS elimination and drug transport, including phase I-II detoxifying enzymes, glutathione S-transferases, NAD(P)H quinone oxidoreductase 1 (NQO1), heme oxygenase-1 (HO-1) and multidrug resistance-associated proteins (MRP) (Bryan *et al.*, 2013; Nguyen *et al.*, 2003; Wasserman and Fahl, 1997). Importantly, Nrf2 also promotes NADPH production, which is required by many drug-metabolizing enzymes and antioxidant systems for their activity. NADPH serves as a major reducing resource in the body, and many oxidoreduction reactions in the cell, including reducing oxidized GSH and thioredoxin, are performed by oxidizing NADPH to $NADP^+$ (Wu *et al.*, 2011). In addition, some of the products of these Nrf2-regulated enzymes can activate Nrf2 signaling, thereby potentiating the Nrf2 adaptive response (Osburn and Kensler, 2008).

Studies using Nrf2 knockout mice showed the important role of this factor in the protection against oxidative stress, cell degradation and aging (Itoh *et al.*, 1997; Miller *et al.*, 2012). Although Nrf2 deficient mice are viable and fertile, the low expression of phase II enzymes and the increased sensitivity to oxidizing compounds and xenobiotics associate with oxidative pathology (Enomoto *et al.*, 2001; Motohashi and Yamamoto, 2004). Nrf2 is a critical factor for developing an appropriate innate immune response, which determines survival during septic shock. Thus, Nrf2 knockout mice have greater sensitivity to experimental sepsis compared to wild-type mice (Thimmulappa *et al.*, 2006). In this work, the authors demonstrated that the expression of genes encoding effectors of the innate immune response (cytokines, chemokines, adhesion molecules and receptors) was dysregulated in Nrf2 knockout mice in response to LPS (lipopolysaccharide). They also showed that Nrf2 suppresses inflammation by inhibiting NF-κB (nuclear factor kappa-light-chain-enhancer of activated B cells) activation through the maintenance of redox status. Other studies in Nrf2 deficient mice also showed that loss of expression of Nrf2 significantly enhances the susceptibility of mice to chemical carcinogens (Ramos-Gomez *et al.*, 2001). Of note, the chemical activation of Nrf2 by different agents including phytochemicals and derivatives such as sulforaphane and curcumin, therapeutics such as oltipraz and acetaminophen, environmental agents like paraquat, metals and endogenous inducers, is protective against pathologies related to excessive oxidative damage such as diabetes, cancer, and cardiovascular and neurodegenerative diseases (Espinosa-Diez *et al.*, 2015).

In addition to control cytoprotective mechanisms, Nrf2 has been reported to regulate intermediary metabolism and mitochondrial function (Hayes and Dinkova-Kostova, 2014; Itoh *et al.*, 2015). Thus, Nrf2 inhibits lipogenesis, supports β-oxidation of fatty acids, facilitates flux through the pentose phosphate pathway, and increases NADPH regeneration and purine biosynthesis. These observations suggest that Nrf2 directs metabolic reprogramming during stress, providing an interface between redox and intermediary metabolism (Dinkova-Kostova and Abramov, 2015; Hayes and Dinkova-Kostova, 2014). Likewise, Nrf2 has been involved in maintaining mitochondrial redox homeostasis by providing the reduced form of glutathione (GSH), the reducing cofactor NADPH and mitochondrial antioxidant enzymes such as GPx1, SOD2 and Prx3/5 (Ryoo and Kwak, 2018). Importantly, Nrf2 not only stimulates the transcription of antioxidant proteins, but also regulates both mitochondrial and cytosolic ROS production through NAD(P)H oxidase (NOX) (Kovac *et al.*, 2014). Furthermore, we showed that Nrf2 upregulates UCP3 in response to oxidative stress in mouse skeletal muscle and cardiac cells (Anedda *et al.*, 2013; López-Bernardo *et al.*, 2015). Holmström *et al.* (2013) reported that Nrf2 has an important impact on cellular bioenergetics by controlling substrate availability for mitochondrial respiration. Along the same line, the mitochondrial oxidation of fatty acids is depressed in the absence of Nrf2 and accelerated when Nrf2 is constitutively active (Ludtmann *et al.*, 2014). This metabolic role of Nrf2 in fatty acid oxidation has implications for chronic disease conditions, including cancer, metabolic syndrome and neurodegeneration.

3.2. Regulation of Nrf2 activity

Although Nrf2 is ubiquitously expressed, studies in mice showed that its expression is more abundant in lung, kidney and intestine, organs where detoxification reactions normally occur (Itoh *et al.*, 1997; McMahon *et al.*, 2001). Nrf2 gene expression is at least partly regulated by AHR (aryl hydrocarbon receptor) inducers that activate multiple XREs (xenobiotic response elements) in its promoter (Miao *et al.*, 2005). Likewise, LPS induces NQO1 and HO-1 expression in human monocytes via Nrf2 to modulate their inflammatory responsiveness (Rushworth *et al.*, 2008).

The basal activity of Nrf2 and its activation in response to stress are tightly controlled. Nrf2 has seven protein domains, called Nrf2-ECH homology (Neh) domains 1-7. The Neh1 domain contains the CNC-bZIP region that dimerizes with small Maf proteins and binds DNA. The Neh2 domain negatively controls Nrf2 activity as it recruits Keap1 (Kelch-like ECH-associated protein 1), a dimeric redox-sensitive substrate adaptor for the Cullin (Cul)3-RING box protein (Rbx)1 E3 ubiquitin ligase complex. The Neh4 and Neh5 regions represent transactivation domains that recruit cAMP response element-binding protein (CREB)-binding protein (CBP), and/or receptor-associated coactivator (RAC)3 (Hayes and Dinkova-Kostova, 2014).

Under normal conditions, Nrf2 is maintained at low levels because it is targeted constitutively by proteasomal degradation by ubiquitylation. The negative regulation of Nrf2 requires the

interaction of the Neh2 domain with the cytosolic protein Keap1 (Cullinan *et al.*, 2004; Itoh *et al.*, 1999). Keap1 negatively regulates Nrf2 function by controlling its subcellular localization (*Fig. 5*). Oxidants and electrophiles react with cysteine sensors within Keap1, causing a conformational change and disrupting the ability of Keap1 to target Nrf2 for degradation (Dinkova-Kostova *et al.*, 2002; Yamamoto *et al.*, 2008; Zhang and Hannink, 2003). This allows Nrf2 to translocate to the nucleus, where it heterodimerizes with a small Maf protein and subsequently binds to an ARE, activating the expression of its target genes (Itoh *et al.*, 1997; Rushmore *et al.*, 1991). Moreover, phosphorylation of Nrf2 by protein kinase RNA (PKR)-like endoplasmic reticulum (ER) kinase (PERK) or PKC (Ser-40) may also lead to ubiquitylation arrest (Cullinan *et al.*, 2003; Huang *et al.*, 2002; Niture *et al.*, 2009). Furthermore, CREB-binding protein (CBP)-induced acetylation of Nrf2 increases its binding to target gene promoters and Nrf2-dependent transcription (Kawai *et al.*, 2011; Sun *et al.*, 2009). The turnover of Nrf2 adapts in response to alterations on cellular redox state. Under homeostatic conditions, Nrf2 half-life is less than 10 min, whereas it increases to 40 min under oxidative stress in COS1 cells (McMahon *et al.*, 2004). This is accomplished through the Neh2 degron and the redox-sensitive recruitment of Nrf2 to Keap1 in the first case and the redox-insensitive Neh6 degron in the second.

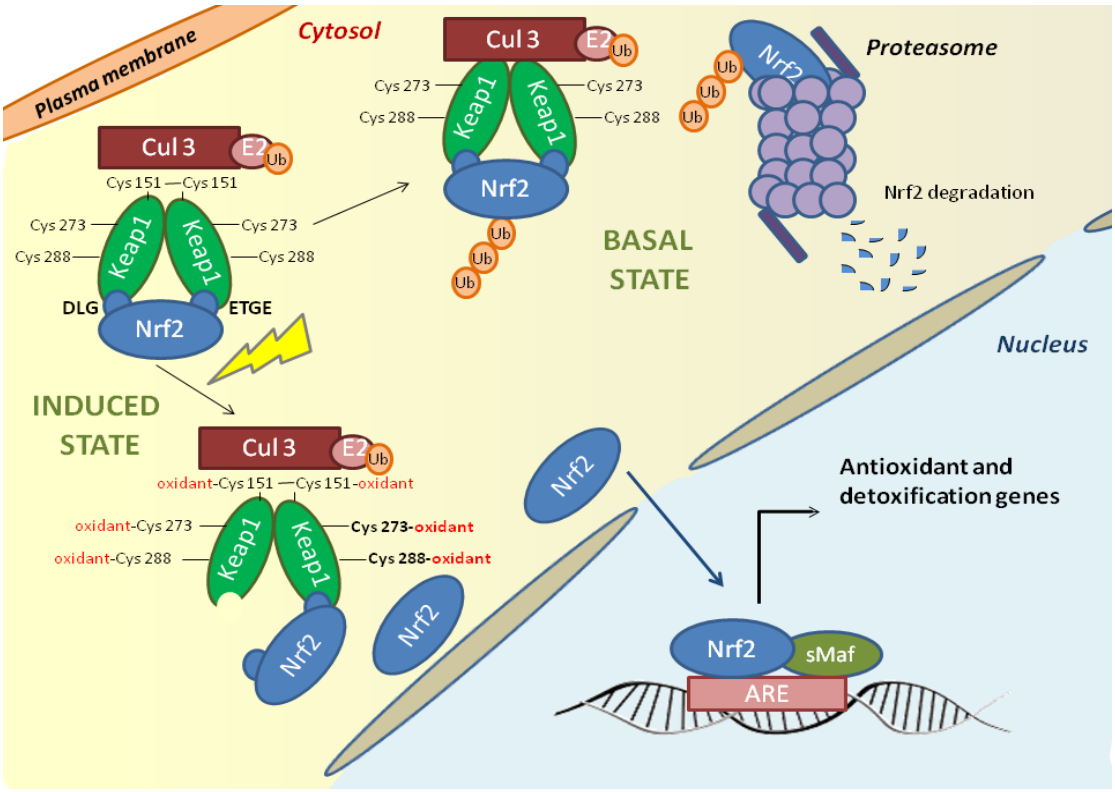

***Fig. 5.* Nrf2 is negatively regulated by Keap1.** Under basal unstressed conditions, a Keap1 homodimer interacts with one Nrf2 molecule at two binding sites, the ETGE and DLG motifs. Keap1 functions as substrate adaptor protein for the Cullin (Cul)3-containing E3-ligase complex and targets Nrf2 for ubiquitylation and proteasomal degradation. Inducers such as H_2O_2 or HNE react with specific cysteine residues in Keap1, inducing a conformational change that leads to the release of Nrf2 and its nuclear translocation. In the nucleus, Nrf2 heterodimerizes with a small Maf protein and binds to the ARE (antioxidant response element), activating the transcription of cytoprotective genes. Based on Espinosa-Diez *et al.* (2015).

In addition to the Cullin3-Rbx1 E3-ubiquitin ligase complex, two other ubiquitin ligase systems are involved in Nrf2 degradation. First, following phosphorylation by glycogen synthase kinase 3 (GSK-3) of a DSGIS motif in Neh6 domain, Nrf2 is degraded via β-transducin repeat-containing protein (β-TrCP)-Cull-based ubiquitin ligase (Chowdhry *et al.*, 2013). Thus, the activation of GSK-3 in Keap1-null mouse embryonic fibroblasts (MEFs) by inhibition of the phosphatidylinositol 3-kinase (PI3K)-protein kinase B (PKB)/Akt pathway markedly reduces endogenous Nrf2 protein and decreases the normal levels of mRNA for Nrf2-regulated enzymes (Chowdhry *et al.*, 2013). Second, synoviolin (Hrd1), located in the ER, has been identified as a novel E3 ubiquitin ligase for Nrf2 in the context of liver cirrhosis (Wu *et al.*, 2014). Interestingly, $p21^{Cip1/WAF1}$, a cyclin-dependent kinase inhibitor, competes with Keap1 for Nrf2 binding, compromising ubiquitylation of Nrf2 (Chen *et al.*, 2009). Similarly, the autophagy substrate p62 interacts with the Nrf2-binding site on Keap1, resulting in stabilization of Nrf2 and transcriptional activation of Nrf2 target genes (Komatsu *et al.*, 2010). Finally, redox sensitive microRNAs or 'redoximiRs' can regulate Nrf2 and Nrf2-mediated antioxidant gene expression (Cheng *et al.*, 2013; Espinosa-Diez *et al.*, 2015).

4. Cellular adaptations to hypoxia

The term hypoxia refers to reduced oxygen availability. For cells to adapt to hypoxic conditions, they must be able to sense changes in oxygen and respond accordingly. The initiation of these responses can be rapid and involve transcriptional and post-transcriptional mechanisms. The proposed oxygen sensors include the prolyl hydroxylase family of enzymes that require molecular oxygen for activity, the NAD(P)H oxidase family of enzymes that reduce oxygen to superoxide, oxygen sensitive ion channels and the electron transport chain (Giaccia *et al.*, 2004).

4.1. Hypoxia and ROS production

The effect of hypoxia on cellular ROS generation is controversial (Clanton, 2005). Early work by Chance and col. showed that the rate of endogenous H_2O_2 production in liver was directly related to the level of Po_2 (Boveris, 1977; Chance *et al.*, 1979). Similarly, using open-flow respirometry and fluorometry, it was reported that reduced oxygen availability decreased ROS production in isolated rat liver mitochondria (Hoffman *et al.*, 2007). By contrast, a proposed model of hypoxic cell signalling is that mitochondrial ROS generation increases in hypoxia (Dawson *et al.*, 1993; Hamanaka and Chandel, 2009). This increase could occur due to oxygen limitation at complex IV (cytochrome *c* oxidase), causing backup of electrons in the proximal chain and increased electron leak to form superoxide. Subsequently, a model was proposed in which hypoxia may induce a conformational change in complex III (ubiquinol cytochrome *c* oxidoreductase), which facilitates interaction between the ubisemiquinone radical and oxygen, to enhance superoxide generation (Brunelle *et al.*, 2005; Guzy *et al.*, 2005; Mansfield *et al.*, 2005). Another

possible mechanism consists of cytochrome *c* reduction due to oxygen limitation at complex IV, abolishing the ability of oxidized cytochrome *c* to scavenge superoxide (Butler *et al.*, 1975; Skulachev, 1998), thus enhancing mitochondrial ROS formation.

As explained above, changes in ambient P_{O_2} need to be sensed to allow adaptation of cellular functions via the regulation of gene activity, and the generation of ROS could be essential in the O_2 sensing pathway (Kietzmann *et al.*, 2000). Thus, cardiomyocytes increase mitochondrial ROS generation during hypoxia (Duranteau *et al.*, 1998), and these ROS participate in signal transduction pathways such as p38 MAPK phosphorylation, which is involved in adaptive responses, including ischemic preconditioning and gene transcription (Kulisz *et al.*, 2002). Therefore, ROS signaling leads to adaptation to hypoxia and cell survival, and is essential for the protection afforded by ischemic preconditioning (Das *et al.*, 1999).

4.2. Cellular response to hypoxia: the HIF pathway

The hypoxia-inducible factor-1 (HIF-1) was initially identified as a transcription factor that regulates erythropoietin gene expression in response to a decrease in oxygen availability in kidney tissue (Semenza and Wang, 1992), and is the master regulator of the cellular responses to hypoxia in mammals (Semenza, 2012). This transcription factor is a heterodimer composed of two subunits: HIF-1α and HIF-1β. HIF-1α is an oxygen sensitive subunit through its oxygen dependent degradation domain (ODDD), and its expression is induced under hypoxic conditions. By contrast, HIF-1β, also known as the aryl hydrocarbon nuclear translocator (ARNT), is constitutively expressed. These two subunits belong to the bHLH-PAS protein family, because their structures are related to two nuclear proteins found in *Drosophila* (Per and Sim, PAS) that have a basic helix-loop-helix (bHLH) motif (Wang *et al.*, 1995; Wang and Semenza, 1995).

Under normal oxygen tension, HIF-1α is bound by the Von Hippel-Lindau (VHL) tumor suppressor protein, which recruits an E3 ubiquitin ligase that targets HIF-1α for proteasomal degradation (Kaelin and Ratcliffe, 2008). VHL binding is dependent upon hydroxylation of a specific proline residue in HIF-1α by the iron-dependent enzyme prolyl hydroxylase PHD2, which uses O_2 as substrate such that its activity is inhibited under hypoxic conditions (Epstein *et al.*, 2001; Ivan and Kaelin, 2017; Srinivas *et al.*, 1999). Another oxygen-dependent major mechanism for negative regulation of HIF-1α under normoxia is the control of HIF-1α transactivation. Thus, oxygen-dependent hydroxylation of a HIF-1α asparagine residue by factor inhibiting HIF-1 (FIH-1), also known as asparaginyl hydroxylase, blocks HIF-1α mediated gene transcription by inhibiting the interaction with the transcriptional coactivator CBP/p300 (Ebert and Bunn, 1998; Lando *et al.*, 2002; Mahon *et al.*, 2001). By contrast, under hypoxia, HIF-1α is stabilized as PHD activity decreases, allowing the translocation of this subunit to the nucleus, where it dimerizes with HIF-1β (Dehne and Brüne, 2014). The resultant heterodimer binds to hypoxia response elements (HREs) in either the promoter or enhancer regions of target genes. Hypoxia also leads to the

recruitment of the CBP/p300 coactivator. The HRE contains the core sequence 5′-RCGTG-3′ (where R is A or G) and is present in several hundred genes involved in diverse biological processes that allow the adaptation to the hypoxic environment (Schodel *et al.*, 2011). Thus, HIF-1 contributes to the regulation of multiple adaptive responses to hypoxia, including cell proliferation, metabolism and angiogenesis (Semenza, 2013). Likewise, HIF-1 induces a metabolic reprogramming from oxidative to glycolytic metabolism and downregulates mitochondrial oxygen consumption (Cadenas *et al.*, 2010; Kim *et al.*, 2006; Papandreou *et al.*, 2006). Another adaptation to reduced oxygen levels is a subunit switch that occurs in complex IV, whereby the COX4-1 regulatory subunit is replaced by the COX4-2 isoform. This event is mediated by HIF-1, which activates the transcription of the genes encoding COX4-2 and LON, a mitochondrial protease required for the degradation of COX4-1 (Fukuda *et al.*, 2007). The aim of this subunit switch is to optimize the efficiency of electron transport and minimize superoxide production in hypoxic conditions. Similarly, the mitochondrial NDFUA4L2 protein, a HIF-1 target, reduces complex I activity under hypoxia (Tello *et al.*, 2011). Induction of NDUFA4L2 under hypoxia decreased respiration, prevented an increase in ROS production and preserved the membrane potential. In addition, the complex I transition from the catalytically active (A) to the de-active or dormant (D) state represents a mechanism that provides a fast response of the mitochondrial respiratory chain to oxygen deprivation, most likely to protect mitochondria form ROS generation at reperfusion (Babot *et al.*, 2014; Dröse *et al.*, 2016). Although the precise mechanism is not fully understood, the proteins NDUFA9, ND1 and ND3 of complex I are apparently involved (Ciano *et al.*, 2013). Interestingly, it was recently reported that HIF-1α expression might be involved in promoting the Nrf2-mediated antioxidant responses in skeletal muscle (Ji *et al.*, 2018).

As explained above, the molecular adaptation to hypoxia depends on the binding of HIF-1 to HRE in oxygen-regulated genes. In addition, adjacent sequences are required for hypoxia-inducible transcription. Thus, the binding of the multiprotein complex to the lactate dehydrogenase A (LDH-A) promoter involves HIF-1, CREB-1/ATF-1 and CBP/p300 (Ebert and Bunn, 1998), and the cooperation of these three proteins is essential for hypoxic induction (Firth *et al.*, 1995).

The CREB (cAMP-response element (CRE)-binding protein)/ATF-1 (activating transcription factor-1) family of transcription factors are basic leucine zipper (bZIP) proteins that are involved in cAMP and Ca^{2+}-induced transcriptional activation (West *et al.*, 2002). CREB regulates diverse cellular responses, including proliferation, survival and differentiation (Shaywitz and Greenberg, 1999). Both CREB and ATF-1 are essential for cell survival during early mouse development (Bleckmann *et al.*, 2002). They are induced by a variety of signals and subsequently mediate the transcription of genes containing CRE. The CREB family contains a kinase-inducible domain (KID) that includes a PKA phosphorylation site, as well as several phosphorylation sites for casein kinases I and II (Brindle *et al.*, 1993; Mayr and Montminy, 2001). PKA phosphorylates CREB at Ser-133, promoting transcription by the recruitment of the coactivator CREB-binding protein

(CBP) (Kwok *et al.*, 1994; Parker *et al.*, 1996). CBP and its paralogue p300 are thought to enhance CREB target gene expression by acetylating nucleosomal histones and recruiting RNA polymerase II complexes (Kee *et al.*, 1996; Ogryzko *et al.*, 1996). Fibroblast growth factor (FGF) and cellular stress regulate CREB and ATF-1 via a pathway involving p38 MAPK and MAP kinase-activated protein (MAPKAP) kinase-2 in SK-N-MC neuroblastoma cells (Tan *et al.*, 1996). Besides, hypoxia (5% O_2) induces CREB phosphorylation at Ser-133 in PC12, which is required for CREB-mediated transcriptional activation (Beitner-Johnson and Millhorn, 1998). Interestingly, UCP3 expression increases in hypoxia via ATF-1 phosphorylation by p38 MAPK in murine C2C12 myoblasts (Lu and Sack, 2008).

5. Cardiac ischemia-reperfusion injury

5.1. Mitochondrial ROS production in ischemia-reperfusion

The term ischemia refers to deficient blood supply to tissues due to obstruction of the arterial inflow. The extent of cell dysfunction, injury or death is influenced by both the magnitude and the duration of ischemia. The restoration of blood flow after prolonged ischemia, known as reperfusion, is essential for cardiomyocytes survival and to limit myocardial damage and cardiac dysfunction. Paradoxically, reperfusion itself exacerbates myocardial injury, a process termed reperfusion injury, and such damage attenuates the benefits of myocardial reperfusion (Braunwald and Kloner, 1985; Yellon and Hausenloy, 2007).

5.1.1. The ischemia-reperfusion process

During ischemia, the lack of oxygen and nutrient supply leads to several biochemical and metabolic changes within the myocardium (*Fig. 6*). Oxidative phosphorylation ceases to function in the absence of oxygen, leading to mitochondrial membrane depolarization, ATP depletion and inhibition of myocardial contractile activity. Moreover, cellular metabolism switches to anaerobic glycolysis, resulting in the accumulation of lactate that reduces the intracellular pH. The acidic conditions during ischemia prevent the opening of the mitochondrial transition pore (mPTP) and cardiomyocyte hypercontracture. The activity of ion pumps in ischemia leads to intracellular Ca^{2+} overload. In addition, as shown using isolated rat heart mitochondria, ischemic damage to the ETC increases both the capacity and the net production of H_2O_2 from complex I and complex III, creating the conditions for an increase in ROS production during reperfusion (Chen *et al.*, 2008).

As explained above, myocardial reperfusion exacerbates ischemic injury. Several factors mediate the detrimental effects of this reperfusion injury (*Fig. 6*). In the first few minutes of reperfusion, a burst of ROS is produced by a variety of sources (Braunersreuther and Jaquet, 2012; Henry *et al.*, 1990; Zweier *et al.*, 1987). This oxidative stress mediates myocardial injury and cardiomyocyte death through different mechanisms. Thus, ROS cause myocardial reperfusion injury by inducing the opening of the mPTP, acting as a neutrophil chemoattractant and mediating

dysfunction of the sarcoplasmic reticulum, which contributes to intracellular Ca^{2+} overload. Reperfusion eliminates lactic acid, resulting in the rapid restoration of physiological pH, which releases the inhibition on mPTP opening and cardiomyocyte contracture (Garcia-Dorado *et al.*, 2012; Griffiths and Halestrap, 1995; Halestrap and Richardson, 2015). The restoration of the mitochondrial membrane potential drives calcium into the mitochondria, which can also induce mPTP opening. Several hours after myocardial reperfusion, neutrophils accumulate in the infarcted myocardial tissue in response to the release of the chemoattractants ROS, cytokines and activated complement (Yellon and Hausenloy, 2007).

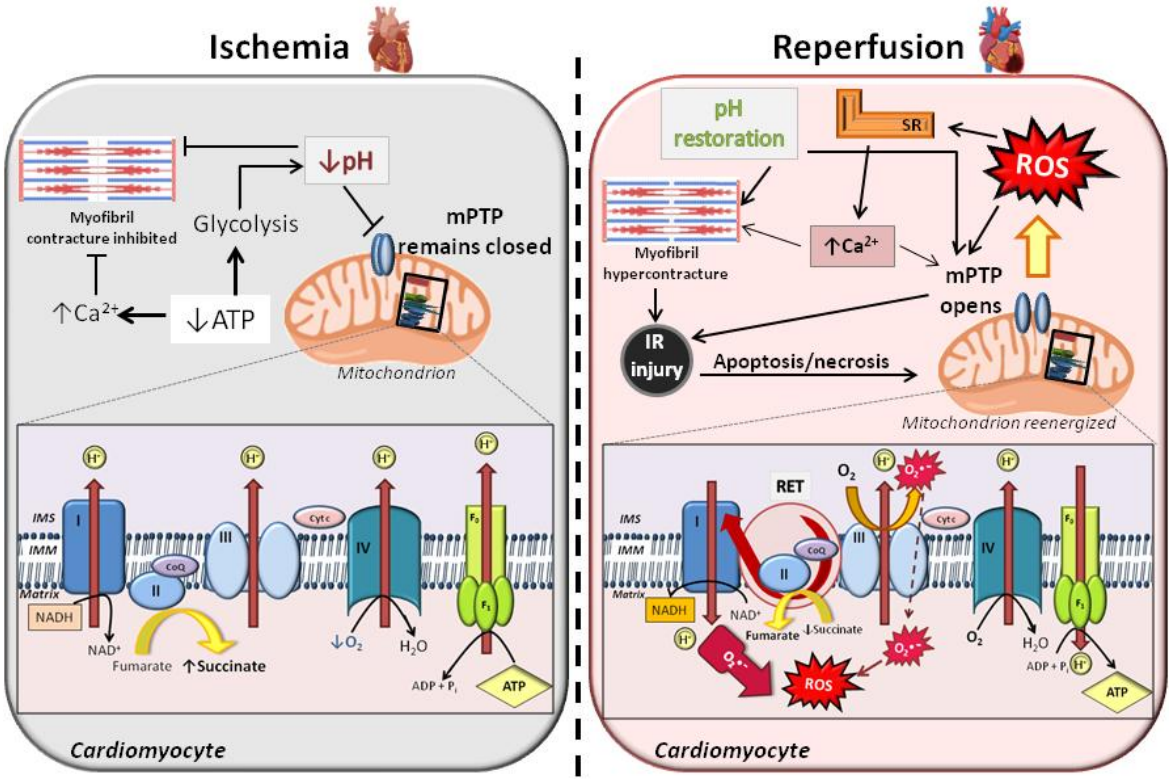

***Fig. 6.* Schematic illustrating the principal mediators of myocardial IR injury.** During ischemia, the absence of O_2 switches cellular metabolism to anaerobic glycolysis, resulting in the production of lactate and a decrease in the intracellular pH. The acidic conditions prevent mPTP opening and myocardial hypercontracture. During reperfusion, the ETC is reactivated, generating ROS from complex I by succinate-driven RET. Rapid restoration of physiological pH leads to mPTP opening and cardiomyocyte contracture. ROS and Ca^{2+} overload due to sarcoplasmic reticulum (SR) dysfunction contribute to mPTP opening. Besides, neutrophiles accumulate in the infarcted tissue in response to the release of the chemoattractans ROS, cytokines and activated complement. Based on Hausenloy and Yellon (2013).

5.1.2. Source of ROS production in ischemia-reperfusion

A variety of sources contributes to ROS generation at reperfusion. The ETC is reactivated during reperfusion, generating ROS. The mechanism underlying ROS production during IR involves succinate accumulation during ischemia and superoxide production at complex I by reverse electron transport (RET) driven by succinate oxidation (Chouchani *et al.*, 2016, 2014). In addition, other authors identified thiol modifications in complex I that enhanced ROS generation in isolated perfused rat hearts following IR (Tompkins *et al.*, 2006). By contrast, ROS from

complex III mediate cardioprotective effects by delaying the opening of mPTP in isolated mitochondria, improving the functional recovery and reducing infarct size in isolated hearts following IR (Madungwe *et al.*, 2016).

In addition to the mitochondrial respiratory chain, there are other sources of ROS that play an important role in IR injury, such as NAD(P)H oxidases from the NOX family (Cadenas, 2018b), xanthine oxidase and uncoupled NOS (Granger and Kvietys, 2015). The tendency of various ETC complexes to generate ROS in response to ROS exposure underlies the notion that mitochondrial ROS production is a self-amplifying process. This amplification of ROS production by the ETC has been termed "ROS-induced ROS release" (RIRR) (Zorov *et al.*, 2014). This process is also important for signalling events (Daiber, 2010; Schulz *et al.*, 2014). The fact that isolated perfused hearts from mice lacking Cu/Zn-SOD are more susceptible to IR injury than those from wild-type mice reflects the importance of ROS as mediators of IR injury (Yoshida *et al.*, 2000).

5.2. The cardioprotective phenomenon of ischemic preconditioning

Ischemic conditioning refers to an endogenous phenomenon in which one or more brief episodes of non-lethal ischemia and reperfusion confer protection against a subsequent lethal episode of IR. The conditioning stimulus can be applied before (ischemic preconditioning, IPC) or after (ischemic perconditioning) ischemia, or at the transition from ischemia to reperfusion (ischemic postconditioning) (Ferdinandy *et al.*, 2007; Hausenloy and Yellon, 2011; Murry *et al.*, 1986). Ischemic conditioning can be applied either directly to the heart or to a remote organ or tissue, such as a limb (remote ischemic preconditioning) (Hausenloy and Yellon, 2016; Venugopal *et al.*, 2009).

Since the original study demonstrating the protection of the myocardium by IPC (Murry *et al.*, 1986), several key mediators have been identified, such as adenosine, bradykinin, sub-lethal ROS and nitric oxide (NO) (Downey *et al.*, 2007; Heusch, 2015). ROS and NO share the same paradox with IR: little IR, ROS or NO protects whereas excessive IR, ROS or NO induces injury. All conditioning forms are dependent on complex signaling pathways, and the final effector is probably the mPTP, so that the signaling produces protection by preventing pore formation. Murry *et al.* (1990) proposed that preconditioning reduces myocardial energy demand during ischemia, which results in a reduced rate of ATP utilization and a reduced rate of anaerobic glycolysis. These authors concluded that either preservation of ATP or reduction of the cellular load of catabolites would be responsible for delayed ischemic cell death.

The protective effect of IPC occurs in two phases: an immediate effect that lasts for 2-3 h and a delayed effect that appears 24-48 h later (Hausenloy and Yellon, 2010). In the early phase, ROS activate cardioprotective signal transduction pathways through post-translational modifications of redox-sensitive proteins. The late phase is mediated by cardioprotective gene expression. Although

investigation on IPC has been extensive, the precise mechanism is not fully understood. Cardiac-delayed IPC leads to the upregulation of HIF-1α or some of its downstream genes, suggesting an essential role for this factor in IPC (Eckle *et al.*, 2008). Indeed, IPC-induced protection against myocardial ischemia is lost in partially deficient HIF-1α mice (Cai *et al.*, 2008). IPC upregulates key molecules in adenosine signaling through HIF-1α such as ecto-5'-nucleotidase CD73 that generates adenosine and the A2B adenosine receptor (A2BAR). Adenosine triggers Akt activation, which prevents opening of the mPTP conferring cardioprotection (Downey *et al.*, 2007; Hausenloy *et al.*, 2005; Solenkova *et al.*, 2006). Cardioprotection by preconditioning requires a complex signaling cascade that includes the opening of mitochondrial ATP-sensitive potassium channels (mitoK$_{ATP}$) (Paggio *et al.*, 2019; Penna *et al.*, 2009). In fact, diazoxide, a mitoK$_{ATP}$ opener, pharmacologically preconditions the heart through a redox-sensitive mechanism (Forbes *et al.*, 2001).

Survival signaling pathways provide cardioprotection against IR (Heusch, 2015). Two of the key pathways that have been identified are the Reperfusion Injury Salvage Kinase (RISK) and the Survivor Activating Factor Enhancement (SAFE) pathways (Hausenloy and Yellon, 2004; Lecour, 2009). The acute ischemic stress of non-lethal ischemia leads to the release of multiple stress-inducible factors that may activate through G-protein coupled receptors or receptor tyrosine kinases to induce the RISK cascade, or through inflammatory cytokines via the glycoprotein 130 or the TNF receptor to activate the SAFE pathway. This increase in survival signaling correlates with a reduction in infarct size (Hausenloy *et al.*, 2005). The RISK pathway is a combination of two parallel cascades, PI3K/Akt and MEK1-ERK1/2, whereas the SAFE pathway involves the activation of the transcription factor signal transducer and activator of transcription 3 (STAT-3). Both pathways target the inhibition of the mPTP opening to promote cardiomyocyte survival (Hausenloy *et al.*, 2011). A third signaling cascade based on the protein kinase G (PKG) and involving NO has been also proposed to mediate cardioprotection (Cohen and Downey, 2007).

5.3. Role of UCPs in cardioprotection

Mild uncoupling of oxidative phosphorylation mediated by UCPs lowers $\Delta\psi_m$ and might decrease mitochondrial superoxide production (see section 2). In fact, UCPs attenuate oxidative damage and cell death in cardiomyocytes, limiting infarct size after IR (Safari *et al.*, 2014). Supporting this idea, studies in isolated rat hearts using low doses of chemical uncouplers such as FCCP (carbonyl cyanide p-trifluoromethoxyphenylhydrazone) showed similar cardioprotective effects, reducing ROS and infarct size in IR hearts (Brennan *et al.*, 2006). Even though UCP2 and UCP3 have been involved in mild uncoupling for ROS reduction (Mailloux and Harper, 2011), there is some controversy regarding UCP1. Some authors reported that UCP1 is not involved in the control of ROS production in BAT mitochondria. They posit that membrane depolarization

may not necessarily decrease ROS production (Nabben *et al.*, 2011; Shabalina and Nedergaard, 2012).

We showed that UCP3 is upregulated in response to oxidative stress in mouse cardiomyocytes, an effect mediated by the transcription factor Nrf2 (Anedda *et al.*, 2013; López-Bernardo *et al.*, 2015). UCP3 is also upregulated in mouse skeletal muscle in response to hypoxia via ATF-1 and p38 MAPK (Lu and Sack, 2008). Moreover, UCP3 levels increase in response to IR in the rat (Safari *et al.*, 2014) and mouse heart (Anedda *et al.*, 2013). Furthermore, Ozcan *et al.* (2013) reported that UCP3 protects against cardiac IR injury. In this work, the authors showed that isolated perfused hearts from mice lacking UCP3 have larger infarct size after IR than hearts from wild-type mice, and UCP3 knockout mice have increased infarct size after *in vivo* IR (left coronary artery ligation). Of note, UCP3 knockout hearts generate more ROS than wild-type hearts, and the pretreatment with FCCP improves functional recovery after ischemia (Ozcan *et al.*, 2013). In addition, cardiomyocytes from UCP3 knockout mice showed mitochondrial dysfunction, increased ROS production and apoptotic cell death when compared to wild-type cells during *in vitro* hypoxia (Perrino *et al.*, 2013). Therefore, UCP3 regulates ROS levels and cell survival during hypoxia, decreasing infarct size in the ischemic heart. By contrast, UCP2 knockout mice have reduced infarct sizes after cerebral IR (De Bilbao *et al.*, 2004).

Several studies have shown a positive correlation between cardiac UCP3 levels and circulatory free fatty acids in failing hearts from humans (Murray *et al.*, 2004) and rats (Murray *et al.*, 2008). Increased levels of cardiac UCPs are associated with a reduction in cardiac efficiency (Boehm *et al.*, 2001). As mentioned earlier, a proposed function of UCP3 is the export of long chain fatty acids from the mitochondrial matrix to avoid excessive accumulation of potentially damaging long chain fatty acid anions in the matrix or to facilitate fatty acid oxidation (Himms-Hagen and Harper, 2001; Schrauwen *et al.*, 2001). It was recently reported that normal cardiac UCP3 levels are essential for recovery of long chain fatty acid oxidation, mitochondrial respiratory capacity and contractile function following IR (Edwards *et al.*, 2018; Ozcan *et al.*, 2013).

McLeod *et al.* (2005) showed that cardiac UCP2 and UCP3 expression (mRNA and protein) increase during IPC, and both proteins confer ischemia tolerance by decreasing infarct size and mitochondrial ROS production in preconditioned hearts. Besides, UCP3 mediates H_2O_2-induced cardioprotection by inhibiting mPTP opening (Chen *et al.*, 2014). Studies in UCP3 knockout mice showed that this protein is an important regulator of IPC, since preconditioning was abolished in these mice (Ozcan *et al.*, 2013). In this work, the authors showed that UCP3 prevents myocardial necrosis, contractile dysfunction and arrhythmias during IR injury, while maintaining myocardial ATP content and suppressing detrimental ROS production.

5.4. Role of Nrf2 in cardioprotection

Nrf2 is the master regulator of the adaptive response to oxidative stress (see section 3). Therefore, Nrf2 is an excellent candidate for protecting against cellular hypoxia-reoxygenation and cardiac IR (Shen *et al.*, 2019). Thus, Nrf2 knockdown with siRNA reduced cell survival by 50% during hypoxia/reoxygenation in H9c2 cardiomyoblasts (Kolamunne *et al.*, 2013). Studies in Nrf2 knockout mice demonstrated the importance of this protein in the protection of the heart against IR injury. In particular, Nrf2 knockout mice have an increased infarct size after *in vivo* regional IR and a reduced degree of cardiac protection by means of IPC (Xu *et al.*, 2014). Interestingly, cycles of brief ischemia and reperfusion (5 min ischemia/5 min reperfusion) that induce protection in wild-type hearts, causes *de novo* Nrf2 protein translation, thereby inducing the expression of ARE-containing genes such as HO-1 and GCLC (glutamate-cysteine ligase catalytic subunit) (Xu *et al.*, 2014). Likewise, H_2O_2 preconditioning counteracts oxidative stress-induced apoptosis by decreasing caspase-3 activity, increasing Bcl2 expression and increasing the expression and activity of antioxidants and phase II enzymes through Nrf1 and Nrf2 translocation to the nucleus in rat neonatal cardiomyocytes (Angeloni *et al.*, 2011). This mechanism involves PI3K/Akt and p38 MAPK activation. The induction of Nrf2 and its target genes also occurs in renal tissue after IR and renal epithelial cells exposed to hypoxia-reoxygenation (Leonard *et al.*, 2006).

Several studies have demonstrated the cardioprotective role of Nrf2 through its activation by a large variety of compounds. For example, low doses of HNE activate Nrf2, increasing the intracellular GSH, which results in cardioprotective effects in cardiomyocytes subjected to glucose-free anoxia followed by reoxygenation and improves the functional recovery of the left ventricle after IR in isolated perfused hearts (Zhang *et al.*, 2010). HNE also enhances UCP3 expression via Nrf2, increasing cardiomyocyte survival under oxidative stress (López-Bernardo *et al.*, 2015). Moreover, the natural compound sulforaphane, a well-established Nrf2 activator found in cruciferous vegetables, markedly decreases the infarct size and attenuates the increased LDH level in the effluent during reperfusion in Langendorff-perfused rat hearts (Piao *et al.*, 2010). This compound also protects the heart from IR injury after experimental transplantation (Li *et al.*, 2013).

OBJECTIVES

The overall objective of this doctoral thesis is to contribute to the understanding of the mechanisms of tolerance to ischemia-reperfusion injury and those involved in the cardioprotective phenomenon of ischemic preconditioning.

The specific objectives are:

1. To analyze the regulation of UCP3 expression and the activation of the transcription factor Nrf2 in response to hypoxia, hypoxia/reoxygenation and simulated ischemia-reperfusion, and the signaling pathways involved.

2. To evaluate the cardioprotective role of UCP3 against IR injury and its impact on cardiac physiology and metabolite levels.

3. To investigate cardioprotective role of Nrf2 against IR injury and its involvement in IPC.

MATERIALS AND METHODS

1. Cell culture and treatments

1.1. HL-1 cell line

HL-1 is a cardiac muscle cell line derived from the AT-1 mouse atrial cardiomyocyte tumor lineage (Claycomb *et al.*, 1998). These cells are able to contract and retain phenotypic characteristics of the adult cardiomyocytes.

HL-1 cells were grown and maintained using 0.02% gelatin/fibronectin-coated plates and Claycomb medium (Sigma-Aldrich, 51800C) supplemented with 10% (v/v) HyClone fetal bovine serum (GE Healthcare, SV30160.03), 100 µM norepinephrine (Sigma-Aldrich, A0937), 1% (v/v) GlutaMAX™ (Gibco, Life Technologies, 35050-061) and an antibiotic mix (100 U/ml penicillin and 100 µg/ml streptomycin; GE Healthcare, Life Technologies, PAA P11-010). These supplements allow the maintenance of their differentiated phenotype and contractile activity. Cells (*Fig. 7A*) were cultured at high confluence and were split 1 to 2 every three days.

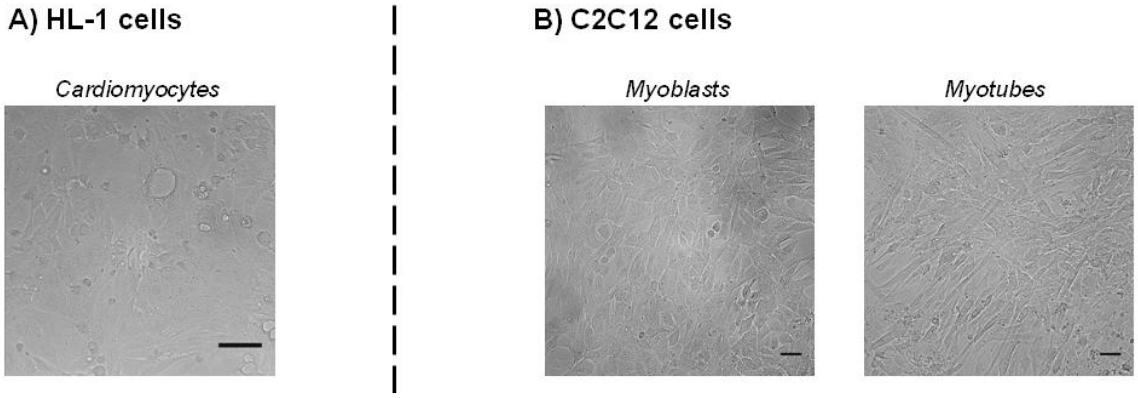

***Fig. 7.* Representative images of the cell lines used in this study.** A) HL-1 cells: pictures taken with a Leica AF 6000 LX microscope (60x objective). B) C2C12 cells: undifferentiated myoblasts and myotubes after 5 days of differentiation; pictures taken with a Zeiss Axiovert200 microscope coupled to a sCMOS monochrome-colour Camera from Hamamatsu (40x objective).

1.2. C2C12 cell line

C2C12 is an immortalized mouse myoblast cell line, obtained from dystrophic mouse muscle (Yaffe and Saxel, 1977). C2C12 cells were acquired from The American Type Culture Collection. They were cultured in Dulbecco's modified Eagle's medium (DMEM) (Gibco, Life Technologies, 52100) supplemented with 10% (v/v) fetal bovine serum (Sigma-Aldrich, F7524), 1 mM sodium pyruvate (Sigma-Aldrich, S8636), 2 mM L-glutamine (Merck, 1.00289) and an antibiotic mix (100 U/ml penicillin and 100 µg/ml streptomycin; GE Healthcare, Life Technologies, PAA P11-010).

Once the cells reached 70% confluence (*Fig. 7B*), they were differentiated for 4 days in DMEM supplemented with 2% (v/v) horse serum (Gibco, Life Technologies, 26050-088), 1 mM sodium pyruvate (Sigma-Aldrich, S8636), 2mM L-glutamine (Merck, 1.00289) and an antibiotic

mix (100 U/ml penicillin and 100 µg/ml streptomycin; GE Healthcare, Life Technologies, PAA P11-010).

1.3. Cell treatments

Cells were either treated with different compounds or subjected to several conditions as explained below:

1.3.1. UCP3 expression and Nrf2 activation in response to oxidative stress conditions

To study the effect of oxidative stress on UCP3 expression and Nrf2 activation, HL-1 cells were treated with 300 µM H_2O_2 (Sigma-Aldrich, H-1009) or with 20 µM HNE (Cayman chemical, 32100) for 5 h. Some cells were pretreated with 5 mM NAC (N-acetylcysteine) (Sigma-Aldrich, A9165) for 1 h to test the protective role of this compound and its effects on UCP3 protein levels and Nrf2 nuclear translocation.

1.3.2. UCP3 expression and Nrf2 and ATF-1 activation in response to hypoxia

To study the expression of UCP3 as well as the activation of Nrf2 and ATF-1 in response to hypoxia, both HL-1 and C2C12 cells were incubated in a hypoxic chamber (Whitley H35 Hypoxystation, Don Whitley Scientific Ltd.) at 1% O_2 and 37ºC at different times. Some cells were treated with 10 µg/mL CHX (cycloheximide) (Sigma-Aldrich, C7698), an inhibitor of protein synthesis, under hypoxic conditions. Control cells were treated with ethanol, since CHX was dissolved in this alcohol.

1.3.3. Regulation of UCP3 expression and Nrf2 activation by ATF-1 via p38 MAPK under hypoxic conditions

To test the involvement of ATF-1 in the induction of UCP3 and Nrf2 under hypoxic conditions, HL-1 and C2C12 cells were treated with 30 µM SB203580 (Sigma-Aldrich, S8307), a p38 MAPK inhibitor, for 24 h at 1% O_2 in a hypoxic chamber (Whitley H35 Hypoxystation, Don Whitley Scientific Ltd.). DMSO (SB203580 vehicle) was used in the control cells.

1.3.4. Effect of hypoxia/reoxygenation and simulated ischemia-reperfusion on UCP3 expression and Nrf2 and ATF-1 activation

HL-1 cells were subjected to hypoxia/reoxygenation and oxygen and glucose deprivation (OGD). For these experiments, HL-1 cells were incubated at 1% O_2 in a hypoxic chamber (Whitley H35 Hypoxystation, Don Whitley Scientific Ltd.) for 24 h. Then, the cells were reoxygenated with fresh medium at 21% O_2 in a 37ºC cell incubator for 4 h. Control cells were maintained in normoxic conditions (21% O_2, 5% CO_2 at 37ºC) for 24 h.

For OGD experiments, which simulate *in vitro* a process of ischemia-reperfusion, HL-1 cells were first washed with a saline buffer containing 3.6 mM KCl, 140 mM NaCl, 1.2 mM $MgSO_4$, 1.3 mM $CaCl_2$ and 20 mM Hepes with or without 5 mM glucose, pH 7.4 (Sarri *et al.*, 2006). Then,

the cells underwent 1% O_2 and glucose deprivation for 2 h in a hypoxia chamber (Whitley H35 Hypoxystation, Don Whitley Scientific Ltd.), simulating *in vitro* an ischemic process. After OGD, the cells were reoxygenated and exposed to 5 mM glucose for 4 h. Control cells were maintained in normoxia (21% O_2) with 5 mM glucose for 6 h.

1.4. Determination of cell viability by the MTT assay

The MTT assay is a colorimetric assay to determine cell viability using the MTT dye 3-(4,5-dimethylthiazol-2-yl)-2,5-diphenyltetrazolium bromide (Sigma-Aldrich, M2128). This dye is reduced to purple formazan, an insoluble compound produced in living cells due to their metabolic activity, which is dependent on the NAD(P)H flux produced by the NAD(P)H-dependent oxidoreductase enzymes in the cytosolic compartment of these cells (*Fig. 8*).

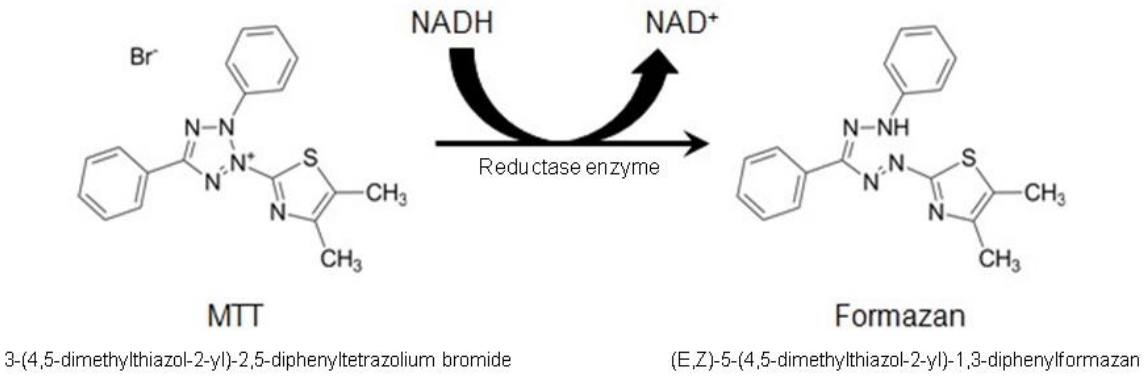

***Fig. 8.* Chemical reaction produced inside living cells in the presence of MTT.** MTT dye is reduced by NAD(P)H-dependent oxidoreductases into a purple formazan, which is detected with a spectrophotometer at 570 nm. Modified from Riss *et al.*, (2013).

HL-1 cells were seeded in gelatin/fibronectin-coated 96-well plates at 32,000 cells/well, and incubated for 24 h at 37°C in 5% CO_2. The cells were then cultured in a hypoxic chamber (Whitley H35 Hypoxystation, Don Whitley Scientific Ltd.) at 1% O_2 for 24 h at 37ºC. After hypoxia, the cells were reoxygenated at 21% O_2 for 4 h at 37ºC. Some cells were treated with 1 mM H_2O_2 for 5 h as a positive control for low cell viability. At the end of the treatments, MTT (5 mg/mL in PBS) was diluted 1/10 in cell culture medium and added to the cells for 4 h at 37ºC in the dark. Then, the culture medium (100 µL) was removed and the same volume of HCl-SDS (41.3 µL of 37% HCl in 50 mL of 10% SDS) was added to each well (100 µL). Plates were incubated overnight at 37ºC. After incubation, the formazan crystals were carefully resuspended with the pipette. Finally, cell viability was assessed by measuring the absorbance at 570 nm in a FLUOstar OPTIMA Microplate Reader (BMG Labtech).

1.5. Determination of protein expression by immunoblotting

1.5.1. Cell fractionation and protein quantification

Cells were grown in 60 mm culture plates until they reached confluence. Upon completion of cell treatments, the cells were harvested by centrifugation at 300 x *g* for 5 min at room temperature (RT). The pellets were resuspended in a volume of buffer A (Cell Fractionation Kit-Standard; Abcam, ab109719) at a density of 6.6 x 10^6 cells/mL.

Cellular fractions (cytosol, mitochondria and nucleus) were separated using the Cell Fractionation Kit-Standard (Abcam, ab109719), following the manufacturer's instructions. The kit is based on sequential detergent-extraction of cytosolic and mitochondrial proteins, without the need for mechanical disruption of the cells. The nuclear fractions were vortexed vigorously for 2 min and then sonicated by 6 cycles of 3 s separated by 10 s interval at 30% magnitude and at 4ºC. This allowed DNA shearing to obtain less viscous samples.

Protein concentration of the samples was determined with the Pierce™ BCA Protein Assay Kit (Thermo Scientific, #23225), according to the manufacturer's instructions.

1.5.2. Immunoblot analysis

For protein analysis, the desired amount of protein extracts (30-80 µg) of each fraction was mixed 1/5 (v/v) with SDS Sample Buffer 5X (Cell Fractionation Kit-Standard, Abcam, ab109719) and heated at 60ºC in a water bath for 10 min. The samples were then centrifuged at 11,000 x *g* for 5 min at RT. The proteins were separated by electrophoresis using 10% (nuclear fraction) or 12%-15% (mitochondrial and cytosolic fractions) acrylamide/bis-acrylamide gels under denaturalizing conditions (10% SDS-PAGE). The gels were resolved using 120 V for 2 h in TGS buffer [25 mM Tris, 192 mM glycine, 0.1% (w/v) SDS, pH 8.3] (Bio-Rad Laboratories, 161-0772). After electrophoresis, the proteins were transferred to nitrocellulose membranes (0.45 µm, GE Healthcare, 10600007) at 400 mA for 1 h in TG buffer [25 mM Tris, 192 mM glycine, pH 8.3] (Bio-Rad, 161-0771) plus 20% methanol (v/v) (Fluka, 32213-2), using a Mini-PROTEAN Tetra Blotting Module (Bio-Rad). Once the transfer was finished, the nitrocellulose membranes were stained with a Ponceau S solution containing 0.1% (w/v) powered red Ponceau S (Sigma-Aldrich, P3504) in 5% (v/v) acetic acid (Merck, 1.00063) to check protein loading and transfer efficiency.

For protein immunodetection, the membranes were washed briefly with TBS-T buffer [20 mM Tris-HCl pH 7.5, 150 mM NaCl, 0.1% Tween-20] to eliminate Ponceau S remnants, and incubated in blocking solution [5% (w/v) non-fat dry milk in TBS-T] for 1 h at RT. Finally, for protein immunodetection, the membranes were incubated with the pertinent primary antibody dilution (in 5% milk, TBS-T solution) overnight at 4ºC (*Table 1*).

Antibody	Predicted MW (kDa)	Company and reference	Dilution	Source
Mitochondria				
anti-UCP3	34	Thermo Scientific Ref. PA1-0155	1:500	Rabbit
anti-Porin	30	Abcam Ref. ab14734 [20B12AF2]	1:2000	Mouse
Nucleus				
anti-Nrf2	95	Santa Cruz Biotech. Ref. sc.13032	1:250	Rabbit
anti-ATF-1	35	Santa Cruz Biotech. Ref. sc-243	1:200	Mouse
anti-pATF-1 (S63) [EP1591(2)Y]	35	Abcam Ref. ab76085	1:1000	Rabbit
anti-Lamin A/C	60-70	Cell signalling Ref. #2032	1:500	Rabbit
anti-Hsp90	90	Santa Cruz Biotech. Ref. sc-13119	1:1000	Mouse
Cytosol				
anti-HO-1	32	Santa Cruz Biotech. Ref. sc-136960	1:200	Mouse
anti-HNE-protein adducts	Adducts (50-120)	Abcam Ref. ab48506	1:500	Mouse
anti-Caspase-3 (ASP175)	17	Cell signalling Ref. #9661	1:500	Rabbit
anti-Tubulin	55	Sigma-Aldrich Ref. T6199	1:2000	Mouse

Table 1. **Primary antibodies used for immunoblot analysis.** Dilutions were made in blocking solution (5% non-fat dry milk in TBS-T).

Next day, the membranes were washed 3 times for 10 min with TBS-T before the incubation for 1 h at room temperature with the required horseradish peroxidase-conjugated secondary antibody dilution (in 5 % milk, TBS-T solution) (*Table 2*). The membranes were then washed again 3 times for 10 min with TBS-T and the immunoreactive bands were detected by using enhanced chemiluminescence (SuperSignal® West Femto Chemiluminescent Substrate, Thermo-Scientific, 34095), following the manufacturer's instructions. The specific band intensity was detected using a CCD camera of the Amersham Imager 680 (GE Healthcare, Life Sciences). The analysis of the images and quantification of the bands were carried out using the ImageJ software v1.8e (National Institutes of Health, USA).

Antibody	Company and reference	Dilution	Source
anti-HRP-Protein A (anti-Rabbit)	Invitrogen Ref. 10.1023	1:5000	Goat
anti-Mouse	Santa Cruz Biotech. Ref. sc-2005	1:5000	Goat

Table 2. **Secondary antibodies used for immunoblot analysis.** Dilutions were made in 5% non-fat dry milk in TBS-T solution.

1.6. Analysis of mitochondrial superoxide production and mitochondrial membrane potential by fluorescence microscopy

HL-1 cells were seeded over 13 mm diameter and 0.16 mm thickness gelatin/fibronectin-coated cover glasses (VWR International, 631-0150) inside 24-well plates at 65,000 cells/well. C2C12 cells were cultured directly over cover glasses at 47,000 cells/well and, at 70% confluence, they were differentiated for 4 days.

The cells were subjected to hypoxia (1% O_2) for 24 h and reoxygenation (21% O_2) for 4 h as described above. To detect mitochondrial superoxide ($O_2^{\bullet-}$), the cells were incubated with 4 μM MitoSOX™ Red (Molecular Probes, Life Technologies, M36008). MitoSOX™ Red was prepared at 5 mM in DMSO and then diluted for the experiment to 4 μM in HBSS (Hank's Balanced Salt Solution) (Lonza, BE10-527F). Some cells were treated with 20 μM rotenone for 40 min at 37ºC as a positive control of $O_2^{\bullet-}$ production. Then, all cells were incubated with MitoSOX™ Red for 10 min at 37ºC in the dark. As a negative control, some cells were incubated with MitoSOX™ Red for 10 min at 4ºC.

In order to determine the mitochondrial membrane potential, TMRM (tetramethylrhodamine methyl ester) (Molecular probes, Life Technologies, T668) was prepared at 10 mM in DMSO and then diluted to 50 nM in differentiation medium for C2C12 cells or to 150 nM in culture medium for HL-1 cells. The cells were incubated with TMRM for 30 min at 37ºC in the dark. As a control of increased membrane potential, some cells were treated with 1.6 μg/ml oligomycin for 3 h (C2C12 cells) or 2 μg/ml oligomycin for 90 min (HL-1 cells). As a control of decreased membrane potential, some cells were treated with 20 μM FCCP (carbonyl cyanide 4-(trifluoromethoxy) phenylhydrazone) for 5 min at 37ºC.

After the incubation with MitoSOX™ Red or TMRM, the cells were washed 3 times with HBSS or 6 times with PBS, respectively, and then fixed with 4% paraformaldehyde (PFA) in PBS for 15 min at room temperature. After fixation, the cells were washed 3 times with PBS and the cover glasses were mounted on the slides using ProLong (Life Technologies, P36930) as the mounting media. The slides were incubated overnight at room temperature in the dark until the analysis under the microscope.

Images were taken the following day using an Axiovert200 inverted epifluorescence microscope (Zeiss) coupled to a sCMOS monochrome Camera (Hamamatsu), using the Metamorph 7.10.1.16 (Molecular Devices) image acquisition software in Windows7. For each condition, 5 images were taken in different positions with a 40x/1.3 oil objective. MitoSOX™ Red is excited at 510 nm with an emission detection of 580 nm (texas-red channel). TMRM excitation wave length is 448 nm with the emission detection at 574 nm (rhodamine channel). Quantification of the images and data analysis were made with the ImageJ software v1.8e (National Institutes of Health, USA), subtracting the background and establishing the same threshold for all images using Huang's algorithm (Huang and Wang, 1995).

2. Animals

2.1. Mouse lines and genotyping

Mouse was used as an animal model. All the experiments were performed under the "Guide for the Care and Use of Laboratory Animals" within the European Parliament Directive 2010/63/EU, and approved by the local representation of the National Animal Research Authority in Spain.

For the experiments presented in this thesis, we used mice lacking the mitochondrial uncoupling protein UCP3 (Gong *et al.*, 2000) and mice deficient in the transcription factor Nrf2 (Itoh *et al.*, 1997). Both lines were maintained on standard rodent diet and had *ad libitum* access to food and water. All mice were bred and housed at the animal facility of the Centro de Biología Molecular "Severo Ochoa" (UAM-CSIC).

Mice were weaned 21 days after birth and they were separated by sex and labeled in the ears for identification. A tail biopsy was taken for genotyping. Genomic DNA was extracted from the tail biopsies using the Extract-N-Amp™ Tissue PCR Kit (Sigma-Aldrich, XNAT2) following the manufacturer's instructions. The obtained DNA was amplified by a double PCR using the following oligonucleotides for each mouse line (*Tables 3 and 4*):

Oligonucleotides	Sequence	Allele	PCR product size (bp)
Ucp3-Fw general (P3)	5'-CTTTATGGTTTACACAGC-3'	Common strand	-
Ucp3-Rv WT (P2)	5'-CATAGGCAGCAAAGGAAC-3'	Wild-type strand	400
Ucp3-Rv KO (P1)	5'-GCAAAACCAAATTAAGGG-3'	Knockout strand	490

***Table 3*. Oligonucleotides used for genotyping UCP3 knockout mice.**

Oligonucleotides	Sequence	Allele	PCR product size (bp)
Nrf2-Fw general	5´-ACAAGCAGCTGGCTGATACTACC-3´	Common strand	-
Nrf2-Rv WT	5´-CACTATCTAGCTCCTCCATTTCCGAG-3´	Wild-type strand	537
Nrf2-Rv KO β-gal	5´-TGGGATAGGTTACGTTGGTGTAGATGG-3´	Knockout strand	684

***Table 4*. Oligonucleotides used for genotyping Nrf2 knockout mice.**

In Nrf2-KO mice, a fragment of DNA coding for bacterial β-galactosidase (*LacZ* gene) followed by the positive selection neomycin cassette replaces part of Exon 4 and all Exon 5 of the *Nrf2* gen, abolishing gene function by deleting the cap 'n'collar leucine zipper regions (CNC, bZIP) (Chan *et al.*, 1996). The deletion of these CNC bZIP regions produces a distinguishable phenotype for Nrf2-KO mice. Nrf2 deficiency causes teeth decolorization (*Fig. 9*) due to a reduced iron transport capacity in the enamel organ as described by Yanagawa *et al.*, (2004). This phenotype makes them distinguishable from their heterozygous and wild-type littermates.

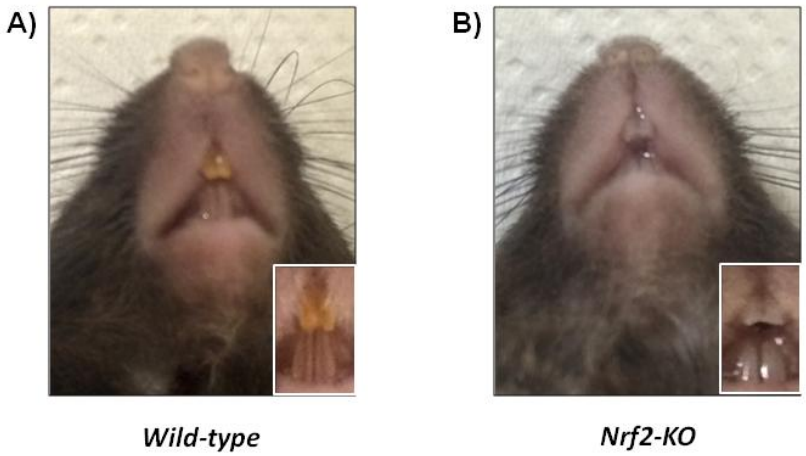

Fig. 9. Characteristic teeth decolorization in the Nrf2-KO mice. The pictures show the brownish-yellow color in the wild-type (A) and the grayish-white color in the Nrf2-deficient mice.

For each PCR reaction, we used 0.4 µM of each primer (Metabion), 0.2 mM dNTPs (Biotools, 20031), green loading buffer, 3 mM $MgCl_2$, 0.625 U GoTaq Polymerase (Promega, M7801) and genomic DNA. The reaction volume was completed until 25 µL with ultrapure Milli-Q water. The PCR protocol varied slightly depending on the mouse line analyzed (Table 5).

A)

UCP3 PCR Program

1. 95 ºC 5 min
2. 95 ºC 30 s
3. 55ºC 30 s
4. 72 ºC 1 min
5. Go to 2nd step
6. 72 ºC 5 min
7. 4 ºC ∞

x 35 cycles

B)

Nrf2 PCR Program

	WT		*KO*	
1.	95 ºC 5 min		95 ºC 5 min	
2.	95 ºC 1 min	x 39	95 ºC 1 min	x 35
3.	58ºC 30 s		55 ºC 1 min	
4.	72 ºC 1 min		72 ºC 1 min	
5.	Go to 2nd step		Go to 2nd step	
6.	72 ºC 5 min		72 ºC 5 min	
7.	4 ºC ∞		4 ºC ∞	

***Table 5.* Cycling parameters for the amplification of genomic DNA from UCP3-KO and Nrf2-KO mice.** A) UCP3 PCR program: 4 µL of genomic DNA was needed for amplification. The WT and KO alleles could be amplified within the same PCR reaction. B) Nrf2 PCR program: the WT and KO alleles had to be amplified in two different PCR reactions due to oligonucleotide competition. Different genomic DNA quantities were needed for detecting each allele: 1 µL for the WT reaction and 3 µL for the KO reaction.

The DNA amplification products (*Tables 3-5* and *Figs. 10-11*) were resolved in 1.8% agarose gel in TAE containing ethidium bromide (0.5 µg/mL) as the fluorescent dye for later ultraviolet DNA detection in the Slite 200W 15 GelDoc System (Avegene, Taipei, Taiwan).

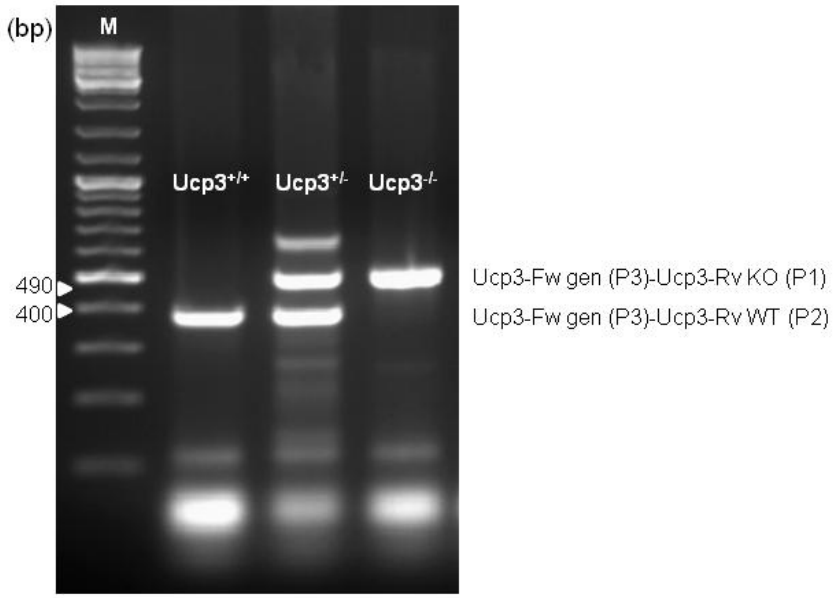

***Fig. 10*. DNA bands from UCP3 genomic DNA visualized by ultraviolet light.** The PCR products were detected by agarose gel electrophoresis (1.8%) containing ethidium bromide. +/+ = wild-type genotype (400 bp), +/- = heterozygous (400 pb and 490 bp) and -/- = knockout (490 bp). M, DNA ladder mix (10,000 bp).

For the experiments, 20-22 (adult group) or 78-80 (aged group) week old wild-type or knockout male mice were used. The animals were killed by cervical dislocation, and their hearts were quickly excised and used for *ex vivo* experiments or frozen in liquid nitrogen for subsequent studies.

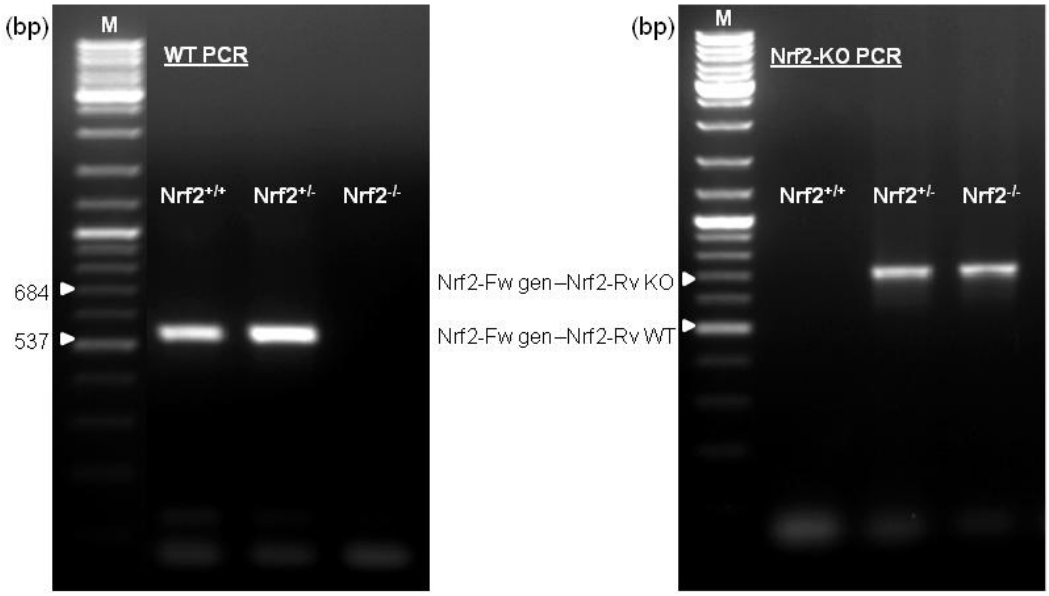

***Fig. 11*. DNA bands from Nrf2 genomic DNA visualized by ultraviolet light**. The PCR products were detected by agarose gel electrophoresis (1.8%) containing ethidium bromide. +/+ = wild-type genotype (537 bp), +/- = heterozygous (537 and 684 bp) and -/- = knockout (684 bp). M, DNA ladder mix (10,000 bp).

2.2. *Ex vivo* ischemia-reperfusion experiments in isolated perfused mouse hearts

2.2.1. The Langendorff perfusion system

For heart perfusion experiments, mice were killed by cervical dislocation. The hearts were immediately excised after clamshell thoracotomy, rinsed with ice-cold Krebs-Henseleit buffer solution, and cannulated via the aorta (Ø = 0.8 mm cannula) on a Langendorff perfusion system (Langendorff, 1895). The hearts were then perfused retrogradely with warm (37ºC) Krebs-Henseleit buffer using a setup consisting of a peristaltic pump (REGLO *Digital* MS-4/8, ISMATEC International, Wertheim, Germany), a pressure transducer and the corresponding amplifier (CIBERTEC S.A., Madrid, Spain), and a circulating water bath (TC120, Grant Instruments, Cambridgeshire, UK). Data recording was performed using a PowerLab 2/20 (ADInstruments, Oxfordshire, UK) and the PowerLab Chart software (ADInstruments) (*Fig. 12*).

The Krebs-Henseleit buffer solution is composed of 120 mM NaCl, 25 mM $NaHCO_3$, 11 mM glucose, 1.2 mM KH_2PO_4, 1.2 mM $MgSO_4$, 4.8 mM KCl and 2 mM $CaCl_2$. The Krebs buffer was bubbled with 95% O_2/5% CO_2 throughout the protocol to maintain pH 7.4 at 37ºC via water-jacketed glassware reservoirs.

2.2.2. Experimental heart perfusion protocols

The flow was maintained at 0.8 mL/min during heart cannulation. Once the heart was securely attached to the cannula, the flow was manually increased to 1.5-2.5 mL/min in order to achieve an aortic pressure of approximately 70-80 mmHg. The aortic pressure was monitored continuously by a pressure transducer located above the cannula. The set flow was maintained constant throughout the experiment (*Fig. 12*). For exclusion criteria, all experiments in which the flow was outside this range (1.5-2.5 mL/min) were discarded.

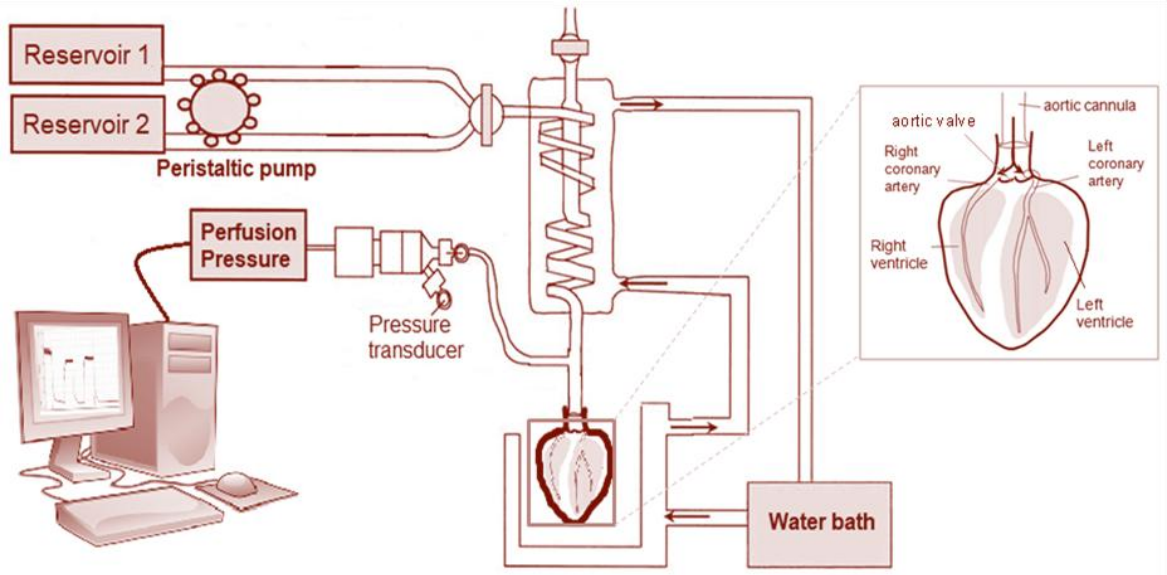

***Fig. 12*. The Langendorff perfusion setup used for *ex vivo* cardiac IR experiments.** This is a constant flow Langendorff system, in which the peristaltic pump controls the perfusion flow that is stabilized and kept constant once the heart is cannulated and secured to the cannula with silk suture. The perfusion solution flows retrogradely from the aorta through the coronary arteries, as the aortic valve closes under the pressure exerted by the perfusion buffer. The pressure transducer transmits the aortic pressure signal to the Power Lab system. During the whole IR protocol, the heart is partially immersed in warmed Krebs buffer. Modified from Dhein (2005).

Once the hearts were attached to the cannula and successfully beating, and the aortic pressure reached approximately 70 mmHg, they were subjected to the following protocols (*Fig. 13*):

- *Control (C)*: hearts were perfused with oxygenated Krebs buffer at 37ºC for 120 min.

- *Ischemia (I)*: hearts were allowed to stabilize for 20 min before the flow was stopped to produce global normothermic ischemia for 40 min.

- *Ischemia-reperfusion (IR):* hearts were allowed to stabilize for 20 min before the flow was stopped to generate ischemia for 40 min. Then, the flow was restored and the hearts were reperfused for 60 min.

- *Ischemic preconditioning + ischemia-reperfusion (IPC+IR)*: following the 20 min of stabilization, the hearts were subjected to two cycles of 5 min ischemia plus 5 min reperfusion. Then, they were subjected to 40 min of ischemia plus 60 min of reperfusion.

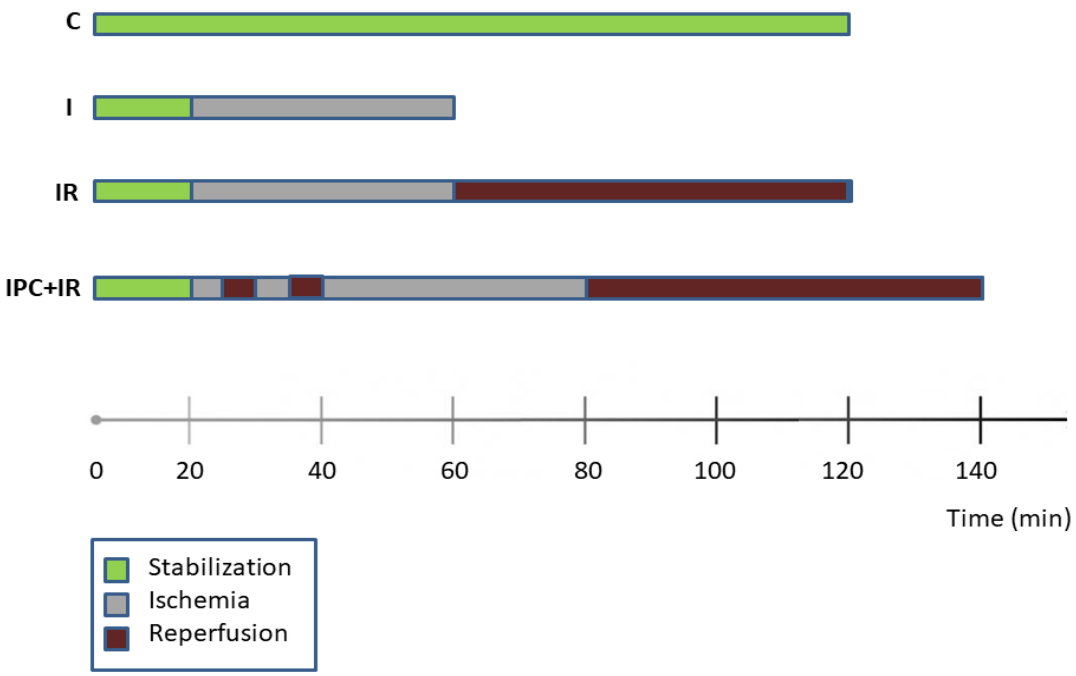

***Fig. 13*. Illustration of the different perfusion protocols applied to the isolated hearts for the Langendorff experiments.** C, control; I, ischemia; IR, ischemia-reperfusion; IPC+IR, ischemic preconditioning + ischemia-reperfusion. Color code: stabilization, green; ischemia, grey; reperfusion, brown.

Once the perfusion protocols were completed, some hearts were subjected to 2,3,5-triphenyltetrazolium chloride (TTC) staining for infarct size analysis (Section 2.2.3.1). Other hearts were directly removed from the cannula and, in this case, the atria were discarded, while the ventricles were immediately frozen in liquid nitrogen and then stored at -80ºC until they were processed for protein expression analysis (Section 2.2.3.3).

2.2.3. Analysis of the isolated perfused hearts

1. TTC staining for infarct size measurements

Infarct size measurements were performed by staining the hearts with 2,3,5-triphenyltetrazolium chloride (TTC; Sigma-Aldrich, T8867). TTC is a white water-soluble powder that acts as a redox indicator, as it is enzymatically reduced to red 1,3,5-triphenylformazan (TPF) in living tissues due to the activity of different dehydrogenases. Thus, living tissues will become red due to the TTC conversion to TPF, while necrotic tissue will remain white.

For heart staining, 1% (w/v) TTC was prepared in PBS, warmed at 37ºC and protected from light. After completion of the perfusion protocol, the heart was perfused with the TTC solution

through the cannula at 1.2 mL/min for 10 min. The heart was then removed from the cannula, immersed in pre-warmed PBS (37ºC) for 5 min and cut into 5-6 slices using a 2.0 mm acrylic coronal heart slicer matrix (Harvard Apparatus, Holliston, MA, USA). The slices were embedded overnight in 4% PFA for tissue fixation. Next day, the slices were washed with ultrapure water and scanned by both sides for image quantification. To assess the contribution of each slice to the total infarct, they were allowed to dry over desiccant paper for 24 h and weighted.

The infarct size was quantified by analyzing the scanned images using the AlphaEaseFC software (Alpha Innotech, San Leandro, CA, USA). The percentage of infarcted volume of the whole heart was represented as the ratio between the white death zone and the total risk zone (the area inside the slice perimeter). The final percentage was calculated considering the images from both sides of each slice, and the contribution of each particular slice to the total dried weight of the heart.

2. Creatine kinase activity assay

Creatine kinase (CK) activity was determined in the coronary effluent to estimate reperfusion injury. CK is found primarily in cardiac muscle, skeletal muscle and brain. This enzyme is a dimer that exists as three isoenzymes: MM, MB and BB. CK-MM is found in skeletal muscle, CK-MB is more concentrated in the cardiac muscle and CK-BB is found in the brain. CK is released from the cytosol into the systemic circulation when cell membranes are disrupted due to tissue damage. Therefore, the determination of CK activity provides a sensitive marker for the diagnosis of skeletal muscle diseases, as well as for the detection of myocardial infarction and cerebrovascular accidents.

CK activity was determined using the CK NAC-Activated assay (Randox Laboratories, CK522). Aliquots of coronary effluent (4 drops) were collected at the end of the stabilization period (basal levels) and at different time points during reperfusion (1, 3, 5, 7, 9, 15, 23, 30, 45 and 60 min). The samples were maintained at 4ºC and CK activity was determined the same day of the experiment. The determination of CK activity is based on the conversion of creatine phosphate and ADP into creatine and ATP (*Fig. 14*). The samples were incubated for 3 min and then the absorbance was measured at 340 nm every 1 min for 3 min at RT, using an Ultrospec 2100 *pro* UV/Visible spectrophotometer (GE Healthcare, Buckinghamshire, UK). The absorbance increment (ΔAbs) per min was recorded. For calculation, the equation shown in *Fig. 14B* was used. To estimate total CK release, the area under the curve (AUC) was calculated using the trapezoidal rule (Abdul-Ghani *et al.*, 2014).

A)

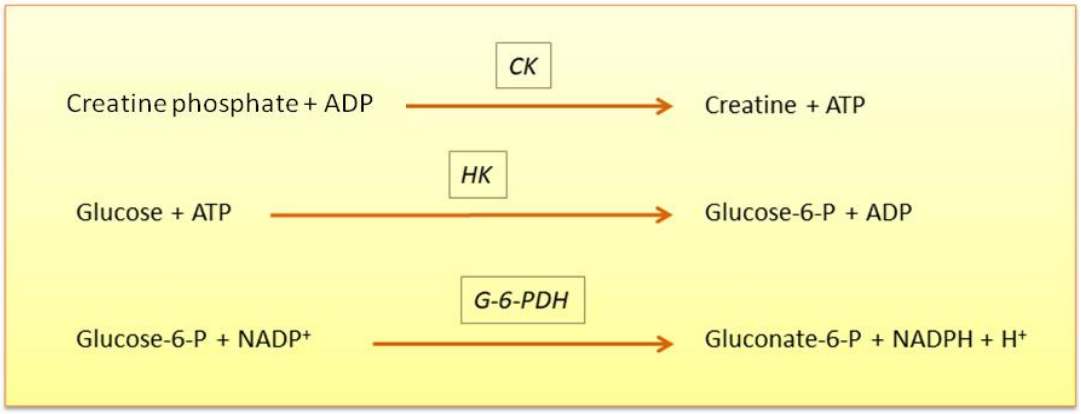

B)

$$CK\ activity\ (Units/L) = 4127 \times \Delta Abs\ (at\ 25°C/30°C)$$

Fig. 14. **CK activity assay**. A) The CK-NAC assay (Randox, UK) is based on the use of creatine phosphate and ADP as substrates, rather than creatine and ATP, for the determination of CK activity. This allows a faster reaction rate resulting in greater sensitivity. The assay includes N-acetyl-L-cysteine (NAC) to prevent the oxidation of sulphydryl groups in the active site of CK. B) Equation used to calculate the CK activity as recommended by the manufacturer at 25 ºC/30ºC.

3. Tissue protein extraction

Frozen hearts were finely minced with sharp scissors in 6 mL/g heart tissue of supplemented RIPA buffer (Sigma-Aldrich, R0278) [1 mM DTT (Sigma-Aldrich, D0632), 1 mM Pefablock (Roche, 11585916001), phosphatase inhibitor cocktail (Roche, 04906845001), protease inhibitor cocktail (Roche, 05892970001)] and then lysed on ice for 25 min, mixing the samples every 5 min. The homogenized lysates were separated into two equal parts to obtain two cellular fractions (total and nuclear fractions):

- For *total extracts*, the lysates were centrifuged at 12,000 x *g* for 10 min at 4ºC. The supernatants were collected as the total fraction and stored at -80ºC.
- For *nuclear extracts*, the lysates were centrifuged at 500 x *g* for 10 min at 4ºC. The supernatants were discarded and the pellets were resuspended in 150 µL of supplemented RIPA buffer and allowed to lyse for another 10 min on ice. Then, the samples were centrifuged at 12,000 x *g* for another 10 min at 4ºC, and the supernatants were collected as the nuclear fraction and stored at -80ºC.

Protein concentration was determined by the Pierce™ BCA Protein Assay Kit (Thermo Scientific, #23225). Nrf2, ATF-1 and pATF-1 (nuclear fraction), and UCP3, HO-1 and caspase-3 (total fraction) expression levels were analyzed by immunoblot as previously described (section 1.5).

4. Metabolomics analysis

Isolated hearts from wild-type and UCP3-KO mice were perfused using the Langendorff system according to the protocols described in section 2.2.2. Once the perfusion was completed, the hearts were removed from the cannula and cut along the longitudinal and transversal axis into 4 pieces. The upper left and lower right pieces were weighted together, frozen in liquid nitrogen for 5 min and stored at -80ºC. The same procedure was carried out for the other two pieces.

For the hydrophilic extraction of intracellular metabolites, the frozen hearts were homogenized using glass homogenizers at 4ºC, in 250 µL of cold extraction solution (50% methanol, 30% acetonitrile and 20% water, plus 100 ng/mL HEPES) per 10 mg of homogenized tissue. Next, the samples were vortex-mixed for 2 min and centrifuged at 16,000 x *g* at 4ºC for 10 min. The supernatants were collected and stored at -80ºC.

The samples were coded and shipped on dry ice to Dr. C. Frezza laboratory at the MRC Cancer Unit (University of Cambridge, Cambridge, UK) for metabolite analysis by liquid chromatography coupled to mass spectrometry (LC-MS). The metabolites analyzed included metabolites involved in fatty acid metabolism, Krebs cycle, aminoacid and nucleotide metabolism, as well as vitamins and cofactors.

3. *In vivo* ischemia-reperfusion study in wild-type and UCP3-KO mice

3.1. Left anterior descending (LAD) coronary artery ligation

For the left anterior descending (LAD) coronary artery ligation model, we performed two complementary *in vivo* studies in wild-type (C57BL/6J) and UCP3-KO mice. In one study, carried out in collaboration with Dr. L.J. Jiménez Borreguero at CNIC (Centro Nacional de Investigaciones Cardiovasculares, Madrid), we used 28-week old male mice. In the other study, in collaboration with Dr. W.E. Louch and Dr. K.O. Stensløkken from the University of Oslo (Oslo, Norway), we used 21-week old male mice.

The 28-week old mice were anesthetized with pentobarbital (50 mg/kg i.p.), while the 21-week old mice were anesthetized with inhaled isoflurane (1.5%-2.0%). The adequacy of anesthesia was evaluated by continuously monitoring of the heart rate, the respiratory rate and the electrocardiogram (ECG) through four leads, as well as the loss of the pedal reflex. Optimal anesthesia was maintained during the procedure, adjusting the isoflurane dose or given additional doses of pentobarbital when required.

Once the mice were anesthetized, they were intubated and ventilated with a small rodent ventilator (Harvard Apparatus, Holliston, MA, USA). The core temperature was maintained at 37°C with a heating pad. A small thoracotomy was performed in the intercostal space of the left side. Then, the LAD coronary artery was ligated with an 8–0 nylon suture, and the heart was

subjected to 45 min (28-week old mice) or 30 min (21-week old mice) of ischemia. After ischemia, the LAD ligation suture was removed and the chest was closed using a 6-0 nylon suture. Some analgesics were supplied after surgery in the drinking water or by i.p. injection. All procedures were terminal at day 21 post-surgery, when the animals were killed by cervical dislocation.

3.2. Echocardiography

Transthoracic echocardiography was performed to evaluate heart damage after *in vivo* IR in wild-type and UCP3-KO mice. Echocardiographies were carried out 3-4 days before surgery (basal condition) and 3, 7 and 21 days after IR, using a high-frequency ultrasound system: a 45-MHz probe, VisualSonics Vevo 770 (Toronto, Canada) for the 28-week old mice, or a 30-MHz probe, VisualSonics Vevo 3100 for the 21-week old mice. All animals were under light inhaled anesthesia (1.5 % isoflurane at 0.8-1.0 L/min of O_2) administered by a nose cone and ensuring a heart rate (HR) of 450±50 bpm. The mice were placed in supine position on a heating platform at 37ºC. A warmed ultrasound gel was used to maintain normothermia while the images were taken with a linear array transducer. The body temperature was monitored using an anal temperature probe, and the base-apex ECG was continuously monitored. Both data acquisition and analysis were blinded.

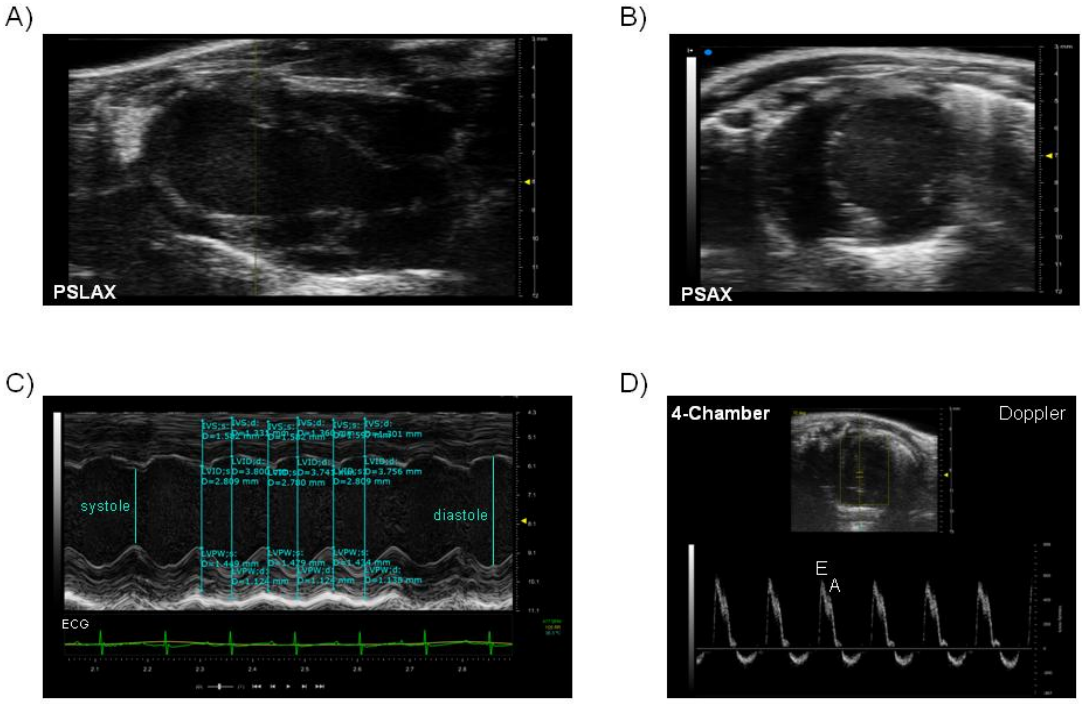

Fig. 15. **Images of echocardiographic measurements from a UCP3-KO mice.** A) PSLAX axes image at the level of papillary muscles. B) PSAX axes image at the level of papillary muscles. C) Left ventricular cavity dimensions, wall and septum thickness in systole and diastole at the level of papillary muscles. The ECG is also represented. D) Four-chamber image acquisition at the mitral valve level. The E and A waves of the blood flow through the mitral valve are represented. PSAX and PSLAX, parasternal standard short and long axes, respectively.

Two-dimensionally (2D) guided M-mode images of the left ventricle (LV) were acquired in the parasternal standard long (PSLAX) and short axes (PSAX) with a frame rate > 200 frames per second. The M-mode sample gate was placed at the level of the papillary muscles. These images were acquired to assess the left ventricle internal dimension (LVID) or volume (LVVol) in systole and diastole, the anterior and posterior wall (LVPW), the interventricular septum (IVS) thickness in systole and diastole and the aorta diameter. The fractional shortening (FS) was automatically calculated using the equation:

$$[(LVIDd-LVIDs)/LVIDd] \times 100\%$$

Likewise, the ejection fraction (EF) was calculated using the LVID or LVVol parameters and the equations:

$$[((LVIDd)^3-(LVIDs)^3)/(LVIDd)^3] \times 100\% \text{ or } [((LVVold)-(LVVols))/(LVVold)] \times 100\%$$

In addition, pulse wave (PW) Doppler images were taken to study diastolic dysfunction. For this, the mitral valve (MV) flow was analyzed by measuring the early (E) and late (A) diastolic velocity peak wave, their ratio (E/A) and the blood flow direction, using a four-chamber apical view and a pulse repetition frequency of 40 kHz. Once the images were acquired (*Fig. 15*), they were transferred to a computer for subsequent off-line analysis using the Vevo LAB Workstation software (Visual Sonics, Toronto, Canada).

In the 28-old mice, we also analyzed the infarct size by evaluating the regional left ventricular function in the PSLAX axes. The LV wall was divided into six segments: basal, mid and apical, in the anterior and posterior walls. Each segment was given score as described by the American Society of Echocardiography, according to its motion and systolic thickening: 1, normal or hyperkinetic; 2, hypokinetic; 3, akinetic, negligible thickening; 4, dyskinetic, paradoxical systolic motion; 5, aneurysmal, diastolic deformation. The number of dysfunctional segments and the sum of the individual scores of the six segments from the same heart were calculated to estimate the infarct size.

3.3. Histological analysis

Once the 21-day post-surgery echocardiography was performed, the mice were killed by cervical dislocation and the hearts were excised and processed for histological analysis. The hearts were washed with PBS and fixed in 4% PFA (diluted in PBS) at 4ºC overnight. Then, the samples were dehydrated with increasing concentrations of ethanol (30, 50 and 70%) and embedded in paraffin at the CNIC Histology Unit. Cross-sectional 4 μm slices of paraffin-embedded heart tissue were stained with hematoxylin-eosin or Masson's trichrome. For image analysis, the samples were digitalized with a scanner (Nanozoomer-RS C110730®, Hamamatsu) and analyzed using image analysis software (Tissuemorph®, Visiopharm).

4. Statistical analysis

The data are presented as the mean ± SEM. The statistical significance of the differences between means was calculated using a two-tailed Student *t* test for pairwise comparisons, and one-way ANOVA followed by a Tukey *post hoc* test for multiple comparisons. All data were tested for normal distribution using the Kolmogorov-Smirnov test. A *P* value of < 0.05 was considered statistically significant.

RESULTS

PART I. *Effects of hypoxia and hypoxia/reoxygenation on mitochondrial superoxide production and the regulation of UCP3 expression: implication of the transcription factors ATF-1 and Nrf2 on UCP3 upregulation*

1. Oxidative stress regulates UCP3 expression and Nrf2 activation

Mitochondrial uncoupling proteins (UCPs) are involved in the control of mitochondrial ROS production. UCP3 in particular might have a protective role against oxidative damage in the heart (Cadenas, 2018a). Previous work from our laboratory showed that sub-lethal concentrations of both hydrogen peroxide (H_2O_2) and the lipid peroxidation product 4-hydroxy-2-nonenal (HNE) are able to induce the activation of the transcription factor Nrf2, which in turn regulates redox homeostasis and induces UCP3 expression (Anedda *et al.*, 2013; López-Bernardo *et al.*, 2015). To confirm that low concentrations of H_2O_2 and HNE induce the accumulation of Nrf2 in the nucleus and increase the expression of UCP3, HL-1 cardiomyocytes were treated with 300 μM H_2O_2 and 20 μM HNE for 5 h. As expected, both treatments increased Nrf2 levels in the nuclear fraction and enhanced the expression of UCP3 in the mitochondrial fraction (*Fig. 16*).

To test whether the increase in Nrf2 nuclear accumulation and in UCP3 expression was due to the cellular stress induced by the treatment with H_2O_2 or HNE, some HL-1 cells were pretreated with the antioxidant N-acetylcysteine (NAC, 5 mM) for 1 h before the addition of H_2O_2 or HNE. As shown in *Fig. 16*, NAC was able to partially prevent UCP3 upregulation as well as the nuclear accumulation of Nrf2 in response to H_2O_2 or HNE.

NAC prevents the oxidation of reactive cysteine residues in Keap1, which impedes the conformational change of this protein that releases and activates Nrf2. Consequently, in the presence of NAC, Nrf2 is ubiquitinated and degraded by the ubiquitin proteasome system. NAC also modulates the intracellular thiol levels, increasing the intracellular levels of glutathione (GSH), which responds to oxidative stress and it is known to regulate UCP3 function (Mailloux *et al.*, 2011). Therefore, our results indicate that both the nuclear accumulation of Nrf2 and the increase in UCP3 expression are mediated by enhanced oxidative stress induced by H_2O_2 or HNE.

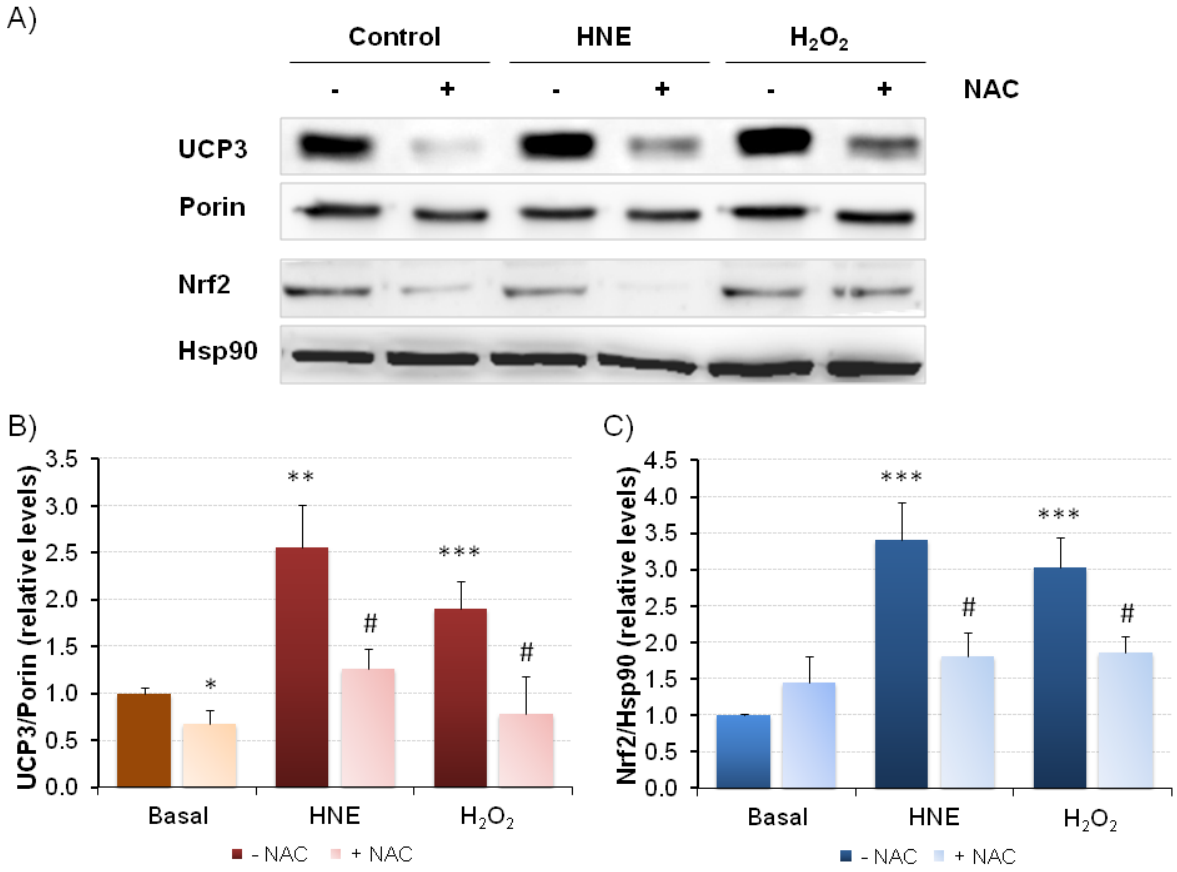

***Fig. 16.* Effects of HNE, H_2O_2 and the antioxidant N-acetylcysteine on UCP3 expression and Nrf2 nuclear accumulation.** A) Representative immunoblots of UCP3 protein levels in mitochondrial extracts and Nrf2 protein levels in nuclear extracts from HL-1 cells exposed to 20 µM HNE or 300 µM H_2O_2 for 5 h with (+) or without (-) a pretreatment with 5 mM N-acetylcysteine (NAC) for 1 h. Porin (VDAC) and Hsp90 were used as mitochondrial and nuclear loading controls, respectively. B, C) Histograms showing UCP3 expression (B) and Nrf2 nuclear accumulation (C) in HL-1cells. The histograms show the means ± SEM from 8 independent experiments. Basal, control untreated cells. **P* < 0.05, ***P* < 0.01, ****P* < 0.001 with respect to basal. $^{\#}P$ < 0.05 with respect to the oxidative stress condition (HNE or H_2O_2). HNE, 4-hydroxy-2-nonenal; H_2O_2, hydrogen peroxide; NAC, N-acetylcysteine.

2. Regulation of UCP3 expression and Nrf2 activation in hypoxia

A reduced level of oxygen (hypoxia) occurs in some pathological conditions, affecting the skeletal muscle and the heart, tissues that express UCP3. Given that hypoxia has been reported to increase intracellular ROS production (Bejma and Ji, 1999; Mohanraj *et al.*, 1998), and considering our finding that oxidative stress induces UCP3 expression and Nrf2 activation (*Fig. 16*), we wondered whether low oxygen levels could also upregulate UCP3 and activate Nrf2.

To analyze this question, we tested the effect of hypoxia (1% O_2) on UCP3 expression and Nrf2 nuclear accumulation at different time points in both C2C12 cells (mouse skeletal muscle cells) and HL-1 cells (mouse cardiomyocytes).

2.1. Hypoxia increases UCP3 expression, an effect due to new protein synthesis

In order to study the effect of hypoxia on UCP3 expression, cells were incubated in a hypoxic chamber (Whitley H35 Hypoxystation) at 1% O_2 for increasing periods of time (1, 2, 4, 8, 16 and 24 h). To determine whether increased protein expression was due to new protein synthesis, some cells were treated with 10 µg/mL cycloheximide (CHX), an inhibitor of protein synthesis.

UCP3 protein levels increased significantly at 16 and 24 h in response to hypoxia (*Fig. 17*) in both cell lines (C2C12 data not shown). Moreover, the treatment with CHX prevented the increase in UCP3 expression, indicating that UCP3 was newly synthesized under these conditions.

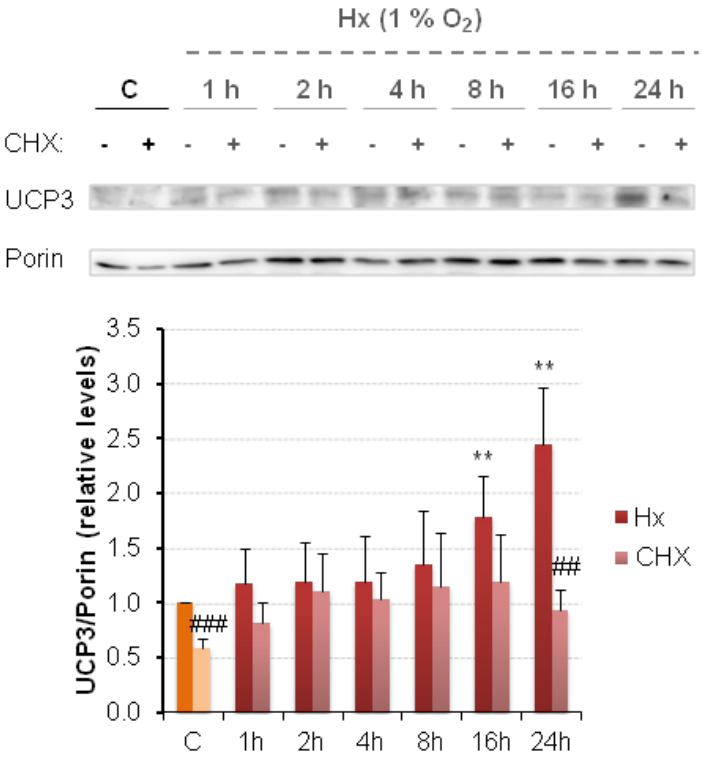

***Fig. 17*. Time course of UCP3 expression levels in response to hypoxia.** HL-1 cardiomyocytes were subjected to hypoxia (1% O_2) for increasing periods of time (1, 2, 4, 8, 16 and 24 h) in the presence (+) or the absence (-) of 10 µg/mL CHX. Cells exposed to normoxia (21% O_2) in the presence (+) or the absence (-) of CHX were used as controls. Representative immunoblots and histogram of UCP3 protein levels in mitochondrial extracts from HL-1 cells. Porin was used as protein loading control. The histograms show the means ± SEM from 6 independent experiments. $^{*}P < 0.05$, $^{**}P < 0.01$, $^{***}P < 0.001$ with respect to C. $^{\#}P < 0.05$, $^{\#\#}P < 0.01$ with respect to Hx. C, normoxic control; Hx, hypoxia; CHX, cycloheximide.

2.2. Hypoxia induces the nuclear accumulation of the transcription factor Nrf2

As shown in *Fig. 16*, we found that oxidative stress increases UCP3 expression and Nrf2 nuclear accumulation. Given that hypoxia induces the synthesis of UCP3 (*Fig. 17*), we wondered whether this condition could also activate Nrf2 and induce its translocation to the nucleus. To test this hypothesis, cells were subjected to hypoxia in the presence or absence of CHX as described in the previous section. Then, the accumulation of Nrf2 was analyzed in the nuclear fraction.

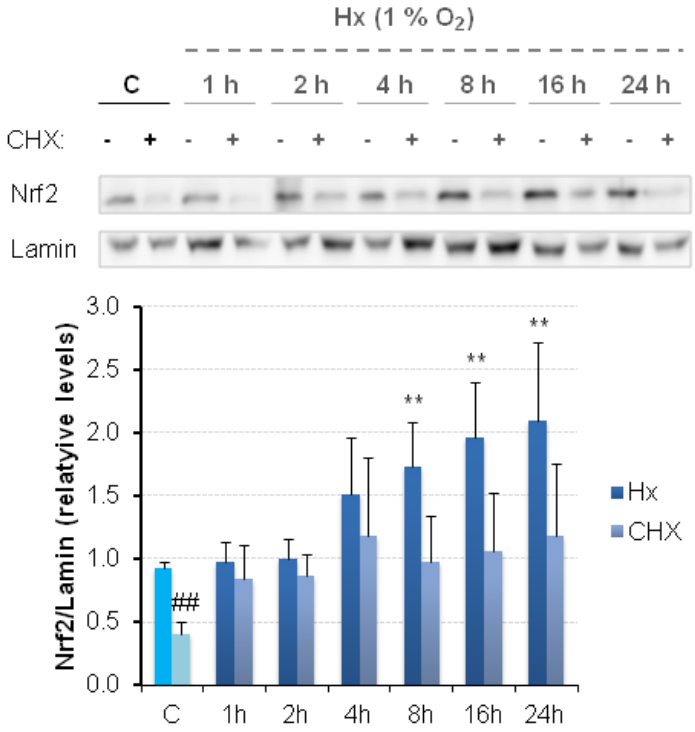

***Fig. 18*. Time course of Nrf2 nuclear accumulation in response to hypoxia.** HL-1 cardiomyocytes were subjected to hypoxia (1% O_2) for increasing periods of time (1, 2, 4, 8, 16 and 24 h) in the presence (+) or the absence (-) of 10 µg/mL of CHX. Cells exposed to normoxia (21% O_2) in the presence (+) or the absence (-) of CHX were used as controls. Representative immunoblots and histogram of the nuclear accumulation of Nrf2 in HL-1 cells. Lamin A/C was used as protein loading control. The histograms show the means ± SEM from 6 independent experiments. $^{*}P < 0.05$, $^{**}P < 0.01$, $^{***}P < 0.001$ with respect to C. $^{\#\#}P < 0.01$ with respect to Hx. C, normoxic control; Hx, hypoxia; CHX, cycloheximide.

Fig. 18 shows that the exposure to 1% O_2 increases the nuclear accumulation of Nrf2 in HL-1 cells. The increase started at 4 h in HL-1 cells and it reached statistical significance at 8 h in both cell lines (C2C12 data not shown). The maximum values for Nrf2 accumulation were obtained at 24 h in both HL-1 (*Fig. 18*) and C2C12 cells (data not shown). The treatment with CHX partially prevented the nuclear accumulation of Nrf2, suggesting that only a fraction of Nrf2 is newly synthesized. The increase in Nrf2 nuclear accumulation correlated with the increment in UCP3 protein expression (*Fig. 17*), suggesting that Nrf2 could mediate UCP3 induction under hypoxic conditions.

3. Effects of hypoxia and hypoxia/reoxygenation on UCP3 expression, Nrf2 activation, mitochondrial superoxide production and cell death

3.1. Hypoxia/reoxygenation increases UCP3 expression and the nuclear accumulation of Nrf2 to a greater extent than hypoxia alone

Cells subjected to hypoxia reached the highest peak in UCP3 expression and Nrf2 nuclear accumulation after 24 h of exposure to 1% O_2. We next wondered whether UCP3 and Nrf2 protein levels would also increase in cells subjected to a hypoxia/reoxygenation process.

To study the effect of hypoxia/reoxygenation on UCP3 expression and Nrf2 nuclear accumulation, HL-1 cells were exposed to hypoxia (1% O_2) for 24 h followed by reoxygenation (21% O_2) for 4 h. Then, UCP3 protein levels were determined by immunoblot in the mitochondrial fraction and, Nrf2 accumulation was determined in the nucleus (*Fig. 19*). The expression of the HO-1 Nrf2 target was also analyzed.

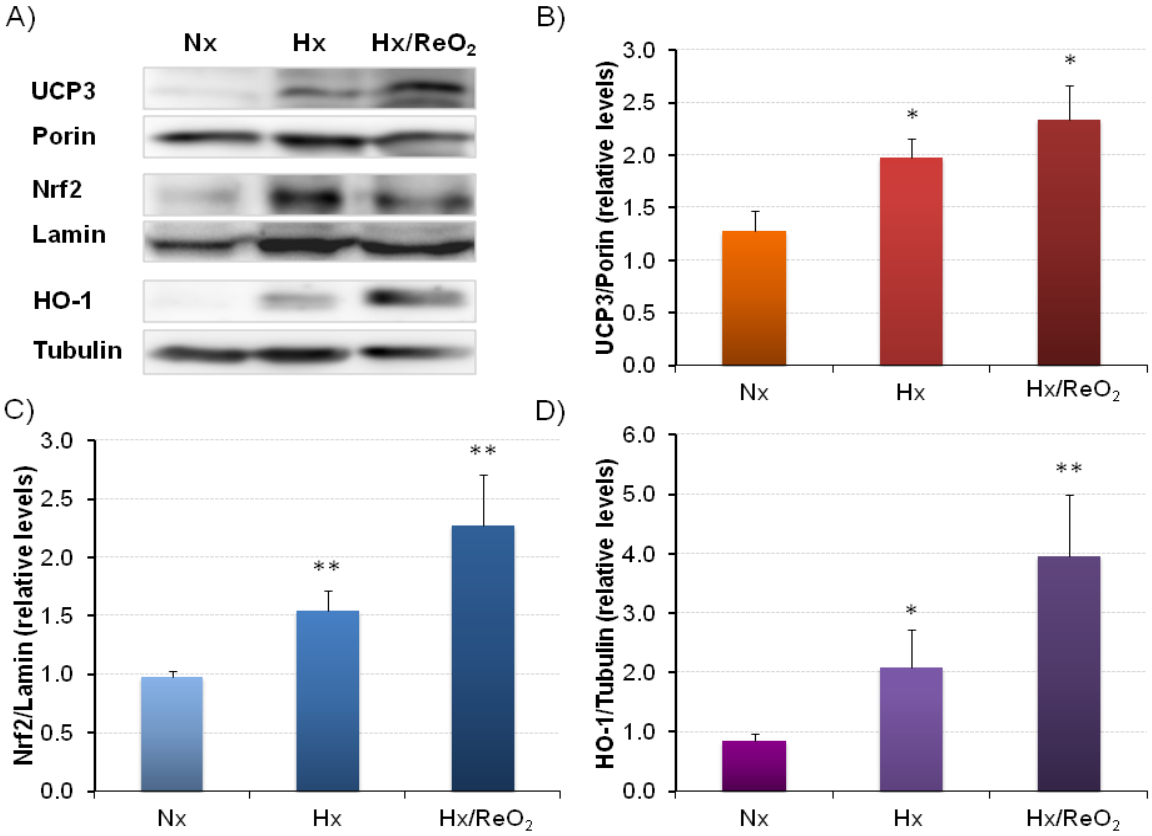

***Fig. 19.* Effects of hypoxia/reoxygenation on UCP3 expression, Nrf2 nuclear accumulation and HO-1 expression in HL-1 cells.** A) Representative immunoblots of UCP3, Nrf2 and HO-1 protein levels in the mitochondria, nucleus and cytosol, respectively, after 24 h Hx (1% O_2) or 24 h Hx followed by 4 h ReO_2 at 21% O_2 (Hx/ReO_2). Porin, lamin A/C and tubulin were used as protein loading controls in mitochondria, nucleus and cytosol, respectively. B) Histogram of UCP3 expression after Hx or Hx/ReO_2 in the mitochondrial fraction obtained from HL-1 cells. C) Histogram of the Nrf2 nuclear accumulation after Hx or Hx/ReO_2. D) Histogram of HO-1 expression after Hx or Hx/ReO_2. The histograms show the means ± SEM of 9 independent experiments. **P* < 0.05, ***P* < 0.01, with respect to Nx. Nx, normoxic control; Hx, hypoxia; Hx/ReO_2, hypoxia/reoxygenation.

As shown in *Fig. 19*, there was a significant increase in UCP3 expression and Nrf2 nuclear accumulation after the exposure to hypoxia for 24 h, consistent with data in *Figs. 17 and 18*. The increase in UCP3 protein levels and Nrf2 nuclear accumulation were even more evident when hypoxia was followed by reoxygenation (*Fig. 19*). We also determined the expression levels of the phase II detoxifying and antioxidant enzyme heme oxygenase-1 (HO-1), a direct target of Nrf2. As expected, the expression of HO-1 increased after hypoxia and hypoxia/reoxygenation in parallel with Nrf2 nuclear accumulation (*Fig. 19*).

3.2. Mitochondrial superoxide production decreases in hypoxia but increases after reoxygenation

UCP3 expression and Nrf2 nuclear accumulation increased after hypoxia and this increase is even higher after hypoxia/reoxygenation (*Fig. 19*). We have also shown that cells respond to H_2O_2 and HNE by increasing UCP3 and Nrf2 protein levels (*Fig. 16*). Next, we wondered if the increase in UCP3 expression and Nrf2 nuclear accumulation observed after hypoxia and hypoxia/reoxygenation could correlate with enhanced ROS levels in these conditions. To answer this question, we analyzed mitochondrial superoxide ($O_2^{\bullet-}$) levels after exposing the cells to hypoxia and hypoxia/reoxygenation. For these experiments, C2C12 myotubes and HL-1 cardiomyocytes were subjected to hypoxia (1% O_2) for 24 h followed or not by reoxygenation (21% O_2) for 4 h. Then, the cells were incubated with the probe MitoSOX Red, which was detected by fluorescence microscopy (*Fig. 20*). Cells treated with the complex I inhibitor rotenone were used as a positive control for mitochondrial superoxide production (Li *et al.*, 2003), whereas cells incubated with MitoSOX Red at 4ºC were used as a negative control.

Surprisingly, superoxide levels decreased in hypoxia compared to normoxia (*Fig. 20*) despite the fact that UCP3 expression and Nrf2 nuclear accumulation significantly increase at 24 h of exposure to hypoxia in both cell lines (*Figs. 17 and 18*). As expected, there was a significant increase in superoxide production after 4 h of reoxygenation (*Fig. 20*). This large amount of superoxide production after reoxygenation correlated with the high expression of UCP3 in mitochondria and of Nrf2 in the nucleus of HL-1 cells subjected to hypoxia/reoxygenation (*Fig. 19*).

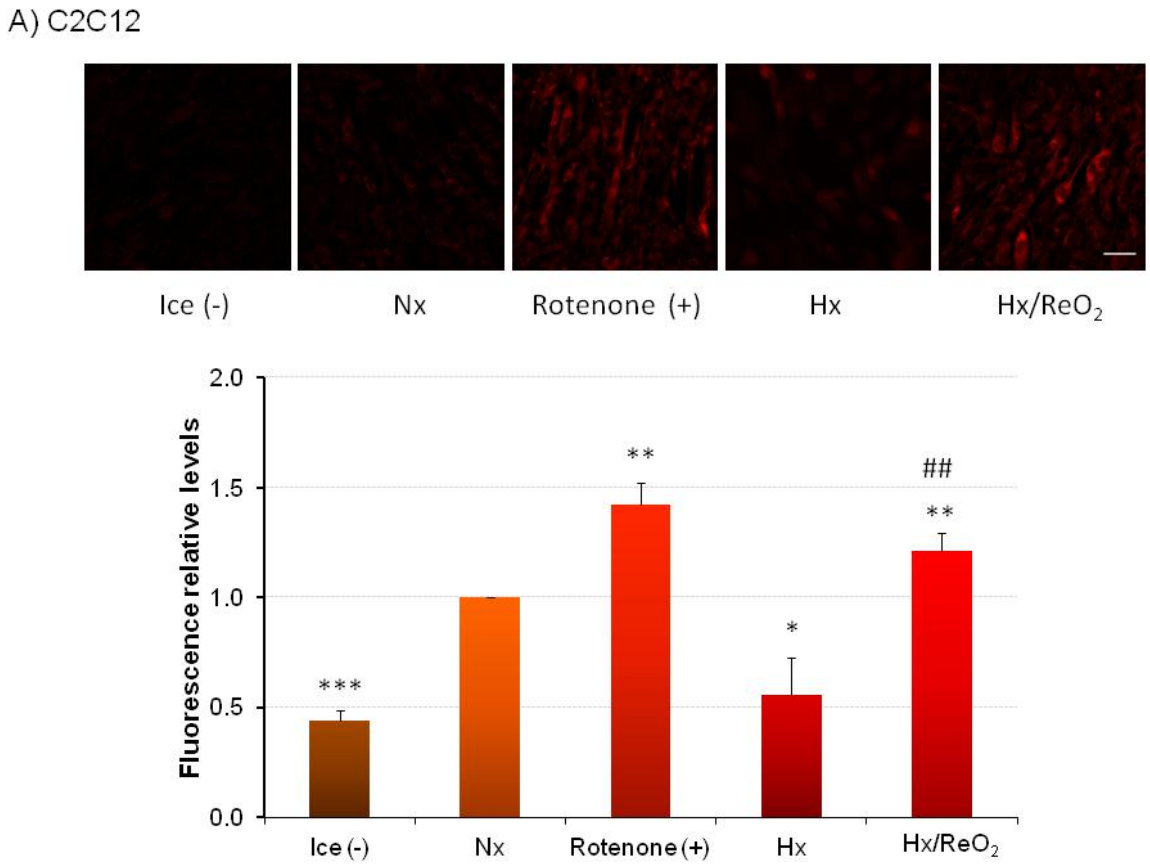

***Fig. 20*. Mitochondrial superoxide production after hypoxia and hypoxia/reoxygenation.** C2C12 myotubes (A) and HL-1 cardiomyocytes (B) were cultured under different conditions: Nx, normoxia (21% O_2); Hx, 1% O_2 for 24 h; Hx/ReO_2, 1% O_2 for 24 h followed by 21% O_2 for 4 h; 20 μM rotenone

(positive control) for 40 min. MitoSOX Red was incubated at 4 μM for 10 min at 37ºC, except for the negative control, which was incubated at 4ºC. Images were taken with a fluorescence microscope coupled to a sCMOS monochrome camera. Representative images of the different conditions in C2C12 (A) and HL-1 (B) cells are shown. The histograms represent the means ± SEM of 7-8 independent experiments. $*P < 0.05$, $**P < 0.01$, $***P < 0.001$ with respect to Nx. $^{\#\#}P < 0.01$ with respect to Hx. Nx, normoxia; Hx, hypoxia; Hx/ReO_2, hypoxia/reoxygenation.

Since MitoSOX Red is a cationic probe, its entry into the mitochondrion depends on the mitochondrial membrane potential ($\Delta\psi_m$). We therefore measured $\Delta\psi_m$ after hypoxia and hypoxia/reoxygenation.

To determine $\Delta\psi_m$, C2C12 and HL-1 cells were subjected to hypoxia (1% O_2) for 24 h and to hypoxia for 24 h followed by reoxygenation (21% O_2) for 4 h. Subsequently, the cells were incubated with the TMRM probe, which was detected by fluorescence microscopy. The values of $\Delta\psi_m$ in hypoxia and hypoxia/reoxygenation were compared to the normoxic basal levels (21% O_2). The inhibitor of the ATP synthase oligomycin, and the uncoupler FCCP were used as positive and negative controls for $\Delta\psi_m$, respectively.

After hypoxia/reoxygenation, $\Delta\psi_m$ did not change with respect to normoxia (*Fig. 21*). Therefore, our measurements of superoxide levels with MitoSOX Red after hypoxia/reoxygenation were comparable (*Fig. 20*). We then confirmed that reoxygenation after hypoxia stimulates superoxide production. By contrast, $\Delta\psi_m$ increased significantly after hypoxia compared to both normoxia and reoxygenation. Hence, the increase in superoxide levels detected with MitoSOX Red (*Fig. 20*) could have been overestimated. Taken together, these results indicate that superoxide production decreases after hypoxia but increases after hypoxia/reoxygenation.

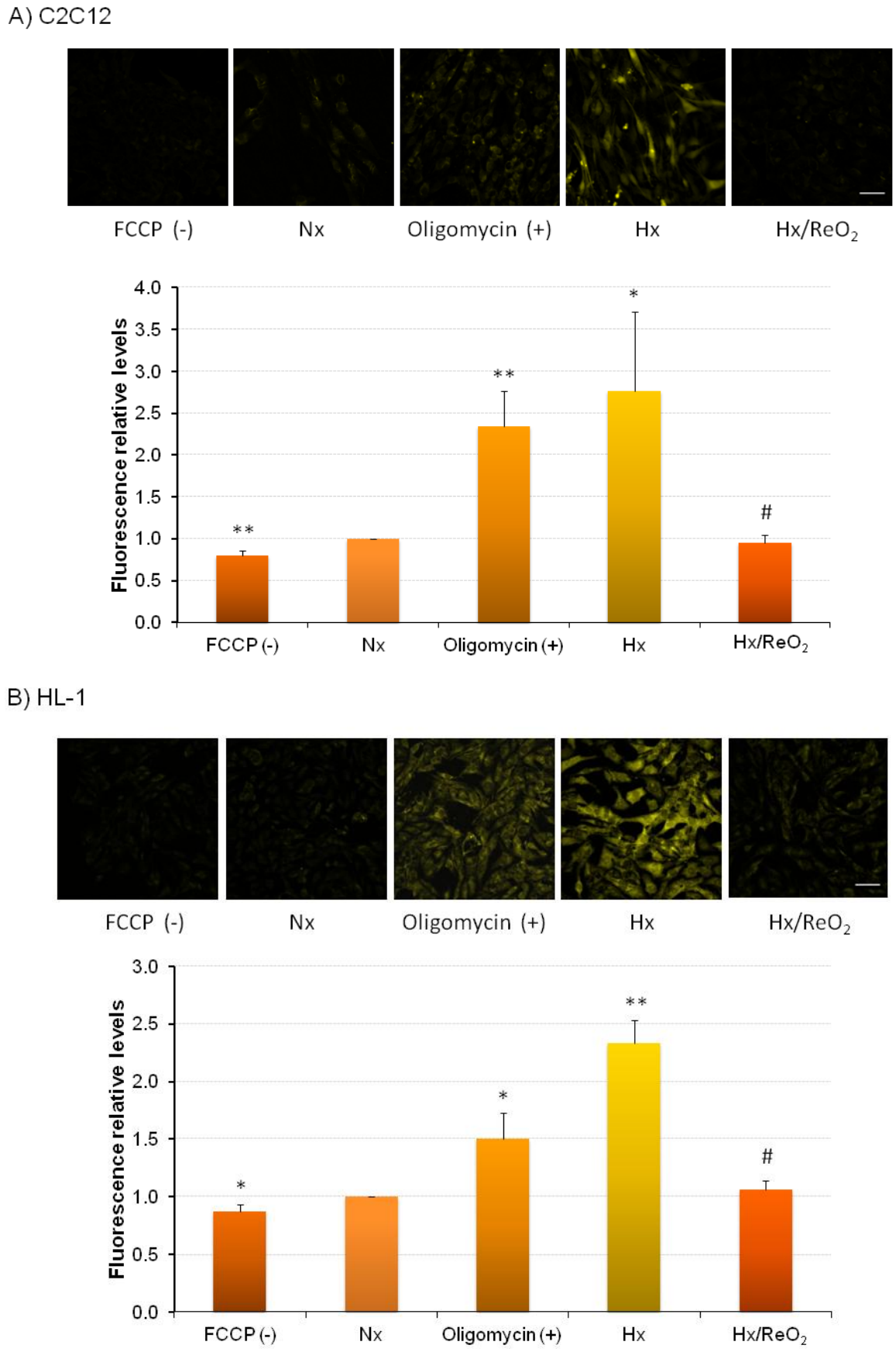

***Fig. 21*. Mitochondrial membrane potential after hypoxia and hypoxia/reoxygenation.** C2C12 myotubes (A) and HL-1 cardiomyocytes (B) were cultured under different conditions: Nx, (21% O_2); 20 µM FCCP (negative control) for 5 min; 1.6 µg/mL oligomycin (positive control) for 3 h in C2C12 cells and 2 µg/mL oligomycin for 90 min in HL-1 cells; Hx, 1% O_2 for 24 h; Hx/ReO_2, 1% O_2 for 24 h followed by

21% O_2 for 4 h. TMRM was incubated at 50 nM in C2C12 cells and at 150 nM in HL-1 cells for 30 min at 37ºC. Images were taken with a fluorescence microscope coupled to a sCMOS monochrome camera. Representative images of the different conditions in C2C12 (A) and HL-1 (B) cells are shown. The histograms represent the means ± SEM of 7-8 independent experiments. **P* < 0.05, ***P* < 0.01 with respect to Nx. $^{\#}P$ < 0.05 with respect to Hx. Nx, normoxia; Hx, hypoxia; Hx/ReO_2, hypoxia/reoxygenation.

3.3. Caspase-3 is activated after hypoxia and hypoxia/reoxygenation, although cell viability is not compromised after hypoxia

In contrast to hypoxia, hypoxia/reoxygenation induced a large increase in superoxide production (*Fig. 20*). As mentioned before, excessive superoxide production can induce oxidative stress and compromise cell viability. Hence, we assessed cell viability under these conditions. For this, we determined active caspase-3 by immunoblot as a marker of apoptosis and cell viability by the MTT assay in HL-1 cells.

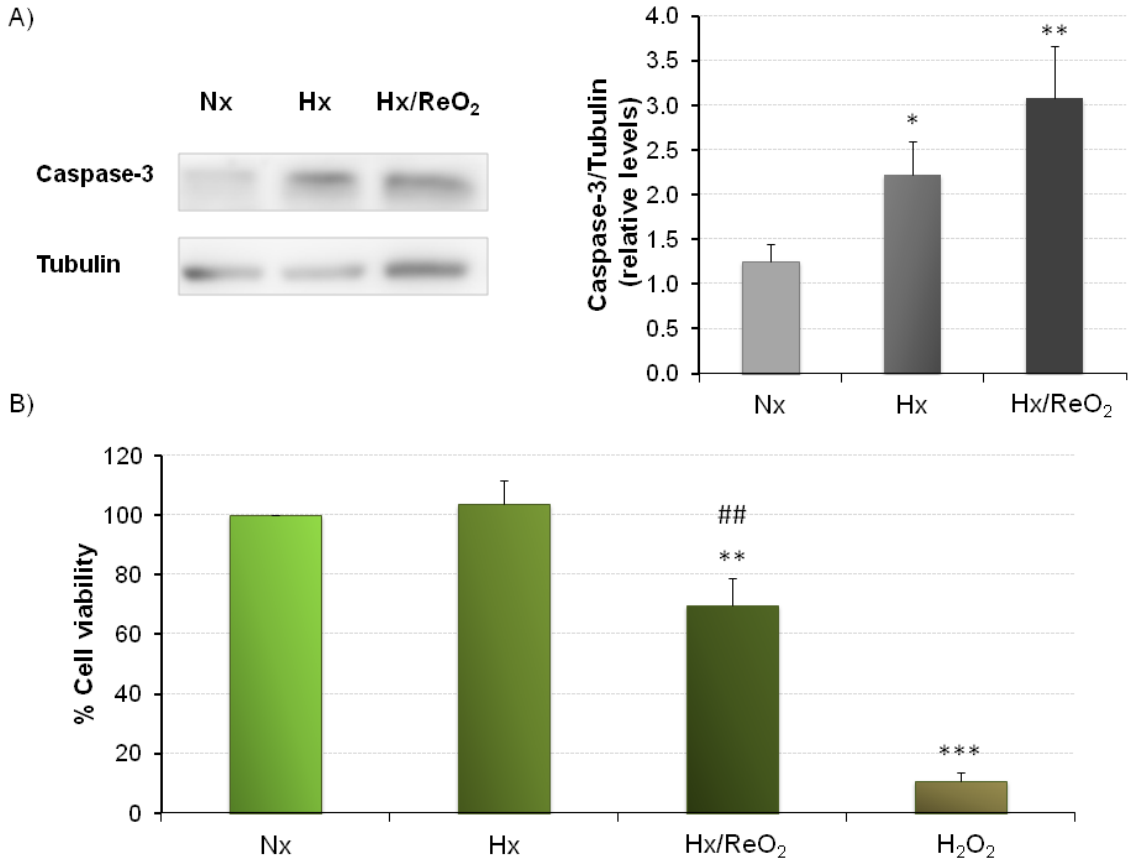

***Fig. 22*. Effects of hypoxia and hypoxia/reoxygenation on caspase-3 activation and cell viability in HL-1 cells.** A) Representative immunoblot of active caspase-3 after hypoxia (1% O_2, 24 h) and hypoxia/reoxygenation (1% O_2, 24 h followed by 21% O_2, 4 h). The histogram represents the means ± SEM of 9 independent experiments. B) Cell viability (%) obtained with the colorimetric MTT assay after hypoxia (1% O_2, 24 h) and hypoxia/reoxygenation (1% O_2, 24 h followed by 21% O_2, 4 h). As a positive control for cell death, HL-1 cells were treated with 1 mM H_2O_2 for 5 h. Six replicates per condition were performed. The histogram represents the means ± SEM of 9 independent experiments. **P* < 0.05, ***P* < 0.01, ****P* < 0.001, with respect to Nx. $^{\#\#}P$ < 0.01 with respect to Hx. Nx, normoxia; Hx, hypoxia; Hx/ReO_2, hipoxia/reoxygenation, H_2O_2, hydrogen peroxide.

The results shown in *Fig. 22* indicate that, although hypoxia significantly increased active caspase-3, it did not affect cell viability. By contrast, hypoxia/ reoxygenation caused high levels of active caspase-3 with a significant decrease in cell survival with respect to basal conditions (normoxia). The burst of ROS observed after hypoxia/reoxygenation (*Fig. 20*) resulted detrimental for cells, thus activating the apoptotic pathway through active caspase-3 and compromising cell viability (*Fig. 22*). As expected, a high concentration of H_2O_2 (1 mM) significantly decreased cell viability.

4. Regulation of UCP3 expression and Nrf2 activation by pATF-1 via p38 MAPK in hypoxia

In the previous sections, we found that hypoxia/reoxygenation increased superoxide production and decreased cell viability. Moreover, these conditions upregulated UCP3 expression and induced Nrf2 nuclear accumulation. By contrast, exposure of the cells to hypoxia for 24 h significantly decreased superoxide production with no effect on cell viability. However, the levels of UCP3 in mitochondria and those of Nrf2 in the nucleus increased with respect to normoxia. These results indicate that UCP3 upregulation and Nrf2 nuclear accumulation in hypoxia are not induced by increased ROS.

We next studied whether UCP3 upregulation in hypoxia could be mediated by the transcription factor ATF-1, as previously reported (Lu and Sack, 2008). This factor has been involved in the regulation of transcription by hypoxia (Ebert and Bunn, 1998; see introduction, section 4.2). In addition, AMPK and CREB-1 phosphorylation lead to Nrf2 nuclear translocation and upregulation of its target, HO-1 (Al-Rashed *et al.*, 2018). Hence, we decided to study the involvement of ATF-1 in UCP3 upregulation and Nrf2 nuclear accumulation in response to hypoxia.

4.1. ATF-1 phosphorylation increases in response to hypoxia

We first studied the phosphorylation of ATF-1 in response to hypoxia. For this purpose, C2C12 myotubes and HL-1 cardiomyocytes were incubated in a hypoxic chamber (Whitley H35 Hypoxystation) at 1% O_2 during increasing periods of time up to 24 h. As shown in *Fig. 23*, the phosphorylation of ATF-1 at Ser-133 increased gradually during hypoxia, reaching a peak at 16 and 24 h in both cell types (C2C12 data not shown). This increase occurred in parallel with the upregulation of UCP3 and the nuclear accumulation of Nrf2 (*Figs. 17 and 18*).

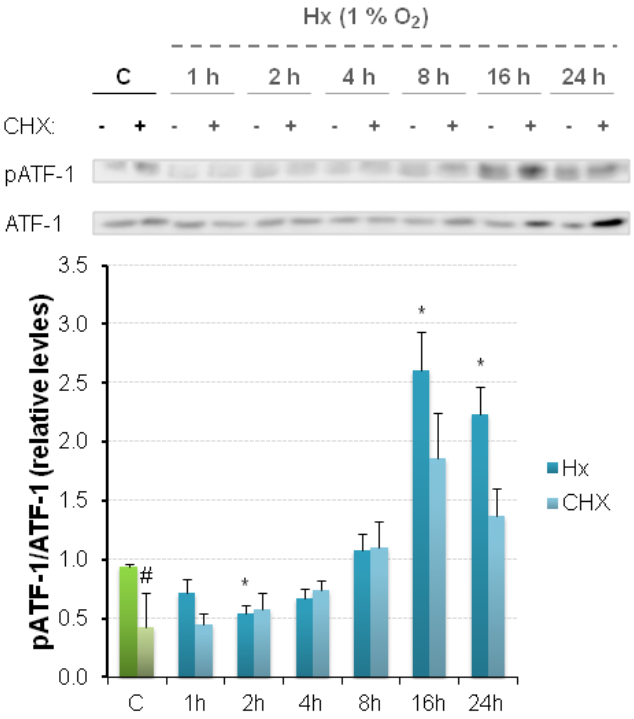

***Fig. 23*. Time course of ATF-1 phosphorylation in response to hypoxia.** HL-1 cardiomyocytes were subjected to hypoxia (1% O_2) with (+) or without (-) 10 µg/mL cycloheximide (CHX) for increasing periods of time up to 24 h. Cells incubated in normoxia (21% O_2) with or without CHX were used as controls. Representative immunoblots and histogram of pATF-1/ATF-1 in nuclear extracts from HL-1 cells. The histograms show the means ± SEM from 5-6 independent experiments. $^{*}P < 0.05$, $^{**}P < 0.01$ with respect to C. $^{\#\#}P < 0.01$ with respect to Hx. C, normoxic control; Hx, hypoxia; CHX, cycloheximide.

We also determined the phosphorylation of ATF-1 in response to hypoxia in the presence of the inhibitor of protein synthesis CHX. As expected, phosphorylated ATF-1 was accumulated at 16 and 24 h in the presence of this compound (*Fig. 23*), indicating that ATF-1 nuclear accumulation and phosphorylation in response to hypoxia are independent of new protein synthesis.

4.2. ATF-1 is phosphorylated via p38 MAPK in response to hypoxia

In the study mentioned above (Lu and Sack, 2008), the authors showed that ATF-1 phosphorylation at 5% O_2 was mediated by p38 MAPK (p38 mitogen-activated protein kinase). Therefore, we set out to study the involvement of this kinase in the phosphorylation of ATF-1 during hypoxia (1% O_2) using the p38 MAPK inhibitor SB203580 in C2C12 and HL-1 cells.

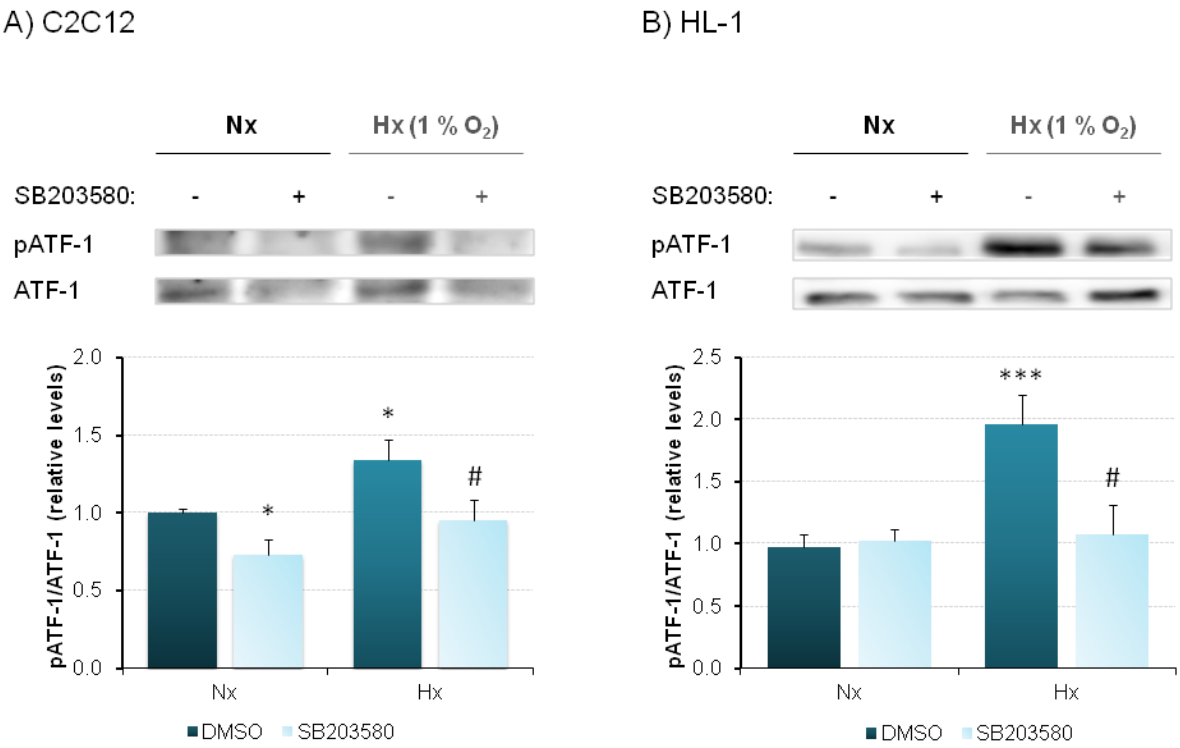

***Fig. 24*. Effect of p38 MAPK inhibition on ATF-1 phosphorylation in response to hypoxia in C2C12 and HL-1 cells.** C2C12 myotubes and HL-1 cardiomyocytes were subjected to normoxia (21% O_2) or hypoxia (1% O_2) for 24 h with (+) or without (-) 30 μM SB203580, a p38 MAPK inhibitor. A, B) Representative immunoblots and histograms of pATF-1/ATF-1 in nuclear extracts from C2C12 (A) and HL-1 (B) cells. The histograms show the means ± SEM from 6-8 independent experiments. **P* < 0.05, ****P* < 0.001 with respect to Nx. $^{\#}P$ < 0.05 with respect to Hx. Nx, normoxia; Hx, hypoxia. DMSO was used as the control vehicle.

Our results (*Fig. 24*) indicate that, under hypoxic conditions (1% O_2), the phosphorylation of ATF-1 at Ser-133 is mediated by p38 MAPK in both cell lines. Our data are in agreement with those obtained by Lu and Sack (2008) in C2C12 cells at 5% O_2, suggesting that this pathway is also activated at a lower O_2 concentration in HL-1 cells.

We next wondered whether the phosphorylation of ATF-1 by p38 MAPK under hypoxia was required for the induction of the expression of UCP3 and the activation of Nrf2 in these conditions.

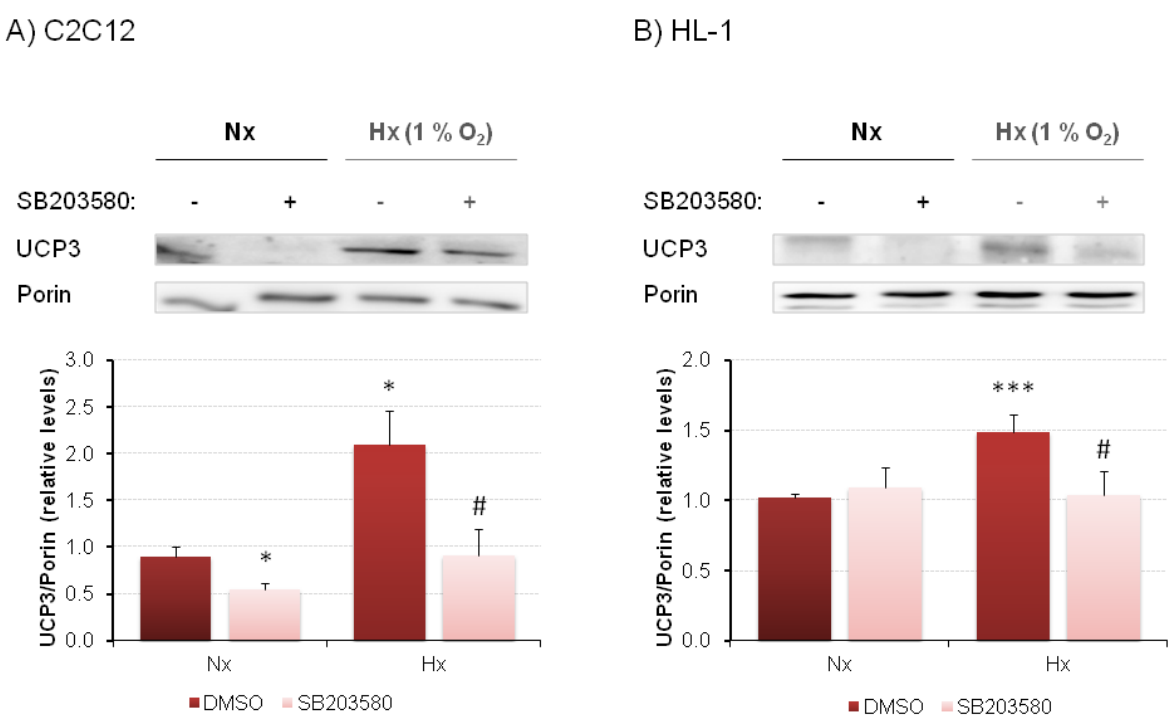

***Fig. 25*. Effect of p38 MAPK inhibition on UCP3 expression in response to hypoxia in C2C12 and HL-1 cells.** C2C12 myotubes and HL-1 cardiomyocytes were incubated under normoxia (21% O_2) or hypoxia (1% O_2) for 24 h with (+) or without (-) 30 µM SB203580, a p38 MAPK inhibitor. A, B) Representative immunoblots and histograms of UCP3 protein levels normalized with porin in the mitochondrial extracts from C2C12 (A) and HL-1 (B) cells. The histograms show the means ± SEM from 6-8 independent experiments. **P* < 0.05, ****P* < 0.001 with respect to Nx. $^{\#}P$ < 0.05 with respect to Hx. Nx, normoxia; Hx, hypoxia. DMSO was used as the control vehicle.

As shown in *Fig. 25*, UCP3 expression increased in hypoxia. However, the treatment with SB203580 prevented the induction of UCP3, suggesting that p38 MAPK in involved in UCP3 upregulation.

To test whether p38 MAPK inhibition could also affect Nrf2 activation in hypoxia, the cells were treated with SB203580 and subjected to hypoxia (1% O2) for 24 h. Then, we studied Nrf2 nuclear accumulation and the expression of its target HO-1. In agreement with our previous result (*Fig. 18*), the accumulation of Nrf2 in the nucleus increased after the incubation of the cells in hypoxia for 24 h (*Fig. 26*). As expected, HO-1 expression also increased in these conditions (*Fig. 26*). However, the increase in the expression of both proteins (Nrf2 and HO-1) in hypoxia was prevented when the cells were treated with SB203580 (*Fig. 26*). Hence, like UCP3, Nrf2 activation is regulated by p38 MAPK possibly via pATF-1 in response to hypoxia.

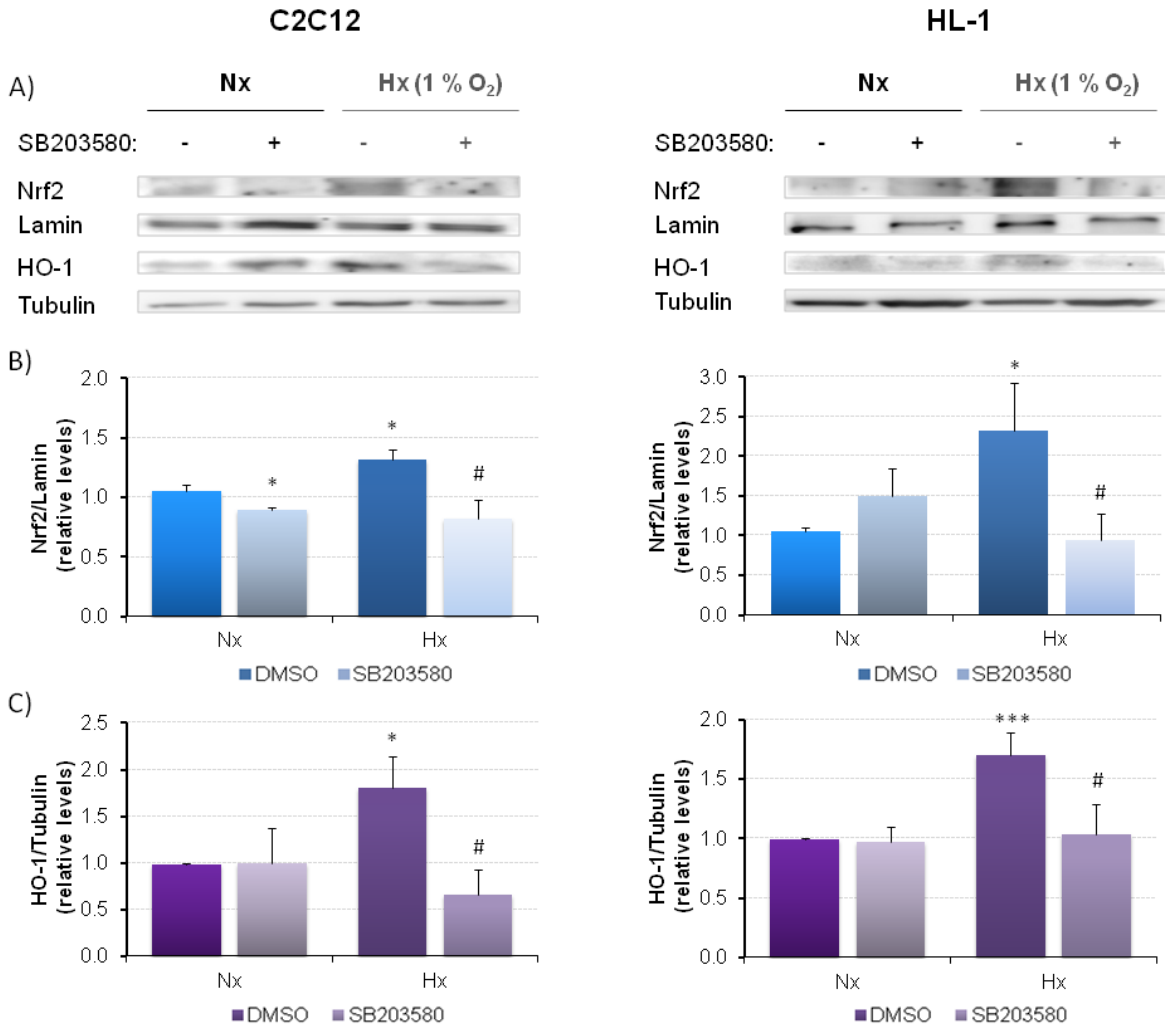

Fig. 26. **Effect of p38 MAPK inhibition on Nrf2 nuclear accumulation and HO-1 expression in response to hypoxia in C2C12 and HL-1 cells.** C2C12 myotubes and HL-1 cardiomyocytes were subjected to normoxia (21% O_2) or hypoxia (1% O_2) for 24 h with (+) or without (-) 30 μM SB203580, a p38 MAPK inhibitor. A, B) Representative immunoblots and histograms of the Nrf2 nuclear accumulation in nuclear extracts from C2C12 and HL-1 cells. Lamin A/C was used as loading control. A, C) Representative immunoblots and histograms of the Nrf2-direct target HO-1 in the cytosol of C2C12 and HL-1 cells. The HO-1 levels were normalized with tubulin. The histograms show the means ± SEM from 6-8 independent experiments. $*P < 0.05$, $***P < 0.001$ with respect to Nx. $^{\#}P < 0.05$ with respect to Hx. Nx, normoxia; Hx, hypoxia. DMSO was used as the control vehicle.

We have shown that the exposure of the cells to hypoxia (1% O_2) for 24 h decreases superoxide production compared to control cells (*Fig. 20*). Besides, HL-1 cells presented increased levels of caspase-3 in hypoxia, although cell viability was not affected (*Fig. 22*). To study whether p38 MAPK signaling was important for survival in hypoxia, we analyzed active caspase-3 levels in C2C12 and HL-1 cells subjected to hypoxia (1% O_2) for 24 h and treated with the p38 MAPK inhibitor SB203580. *Fig. 27* shows that caspase-3 levels increased in hypoxia in HL-1 cells, as shown before (*Fig. 22*), but this protein did not increase in hypoxia in C2C12 cells, indicating that these cells are relatively tolerant to hypoxia compared to cardiac cells. Caspase-3 levels increased

in both cell types when the cells were treated with SB203580 both in normoxia and hypoxia, suggesting that the p38 MAPK signaling pathway is important for cell survival.

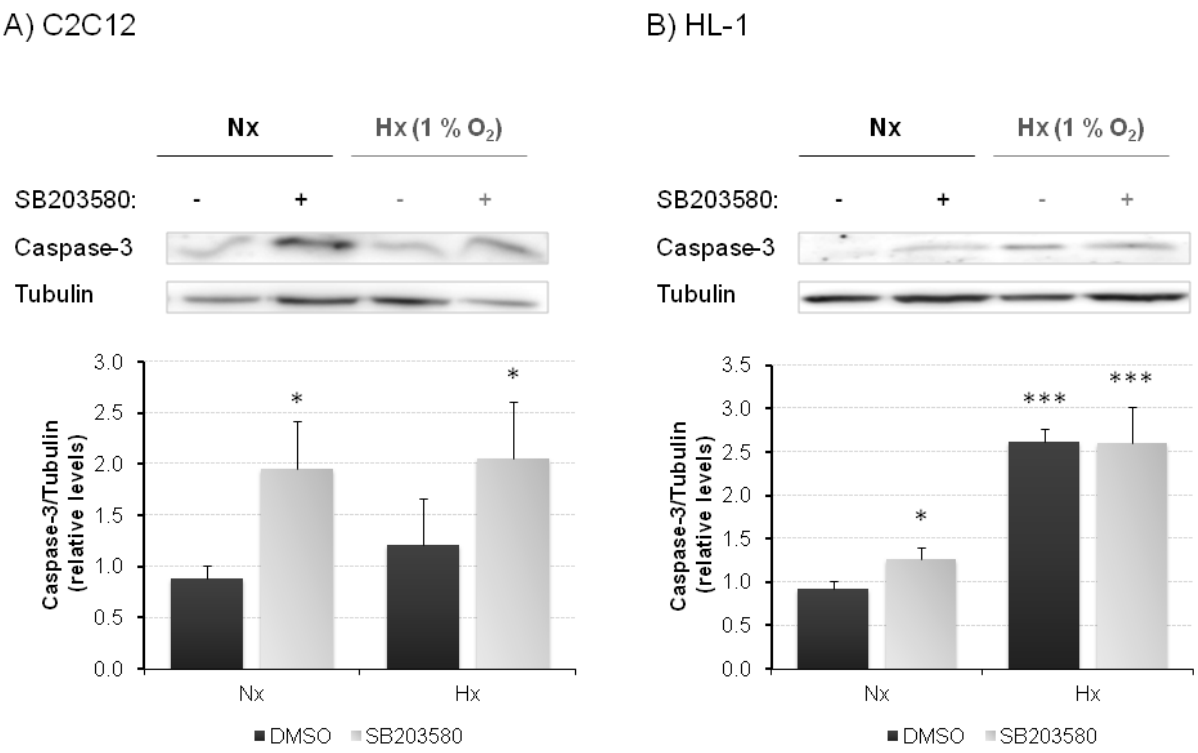

***Fig. 27.* Effect of p38 MAPK inhibition on caspase-3 activation in response to hypoxia in C2C12 and HL-1 cells.** C2C12 myotubes and HL-1 cardiomyocytes were incubated under normoxia (21% O_2) or hypoxia (1% O_2) for 24 h with (+) or without (-) 30 μM SB203580, a p38 MAPK inhibitor. A, B) Representative immunoblots and histograms of activated caspase-3 in cytosolic extracts from C2C12 (A) and HL-1 (B) cells. Tubulin was used as loading control. The histograms show the means ± SEM from 6-8 independent experiments. **P* < 0.05, ****P* < 0.001 with respect to Nx. Nx, normoxia; Hx, hypoxia. DMSO was used as the control vehicle.

ATF-1 phosphorylation in hypoxia increased in parallel to UCP3 expression and Nrf2 nuclear accumulation (*Figs. 17, 18 and 23*). Moreover, the inhibition of ATF-1 phosphorylation by p38 MAPK in hypoxia prevented UCP3 upregulation and Nrf2 activation (*Figs. 24-26*). Taken together, these results indicate that UCP3 expression and Nrf2 nuclear accumulation could be regulated by the p38 MAPK/pATF-1 pathway in response to hypoxia. The activation of this pathway in hypoxia might protect against cell death.

4.3. Reoxygenation after hypoxia reduces ATF1 phosphorylation compared to hypoxia alone

Since ATF-1 is phosphorylated in hypoxia (*Figs. 23 and 24*), we wondered whether it would also be phosphorylated upon reoxygenation. To test this, HL-1 cells were subjected to hypoxia (1% O_2) for 24 h followed by reoxygenation (21% O_2) for 4 h.

Interestingly, the pATF-1/ATF-1 after hypoxia/reoxygenation was still significantly higher than in normoxia (*Fig. 28*), but lower than in hypoxia. These results indicate that ATF-1 is activated in hypoxia, but the phosphorylation levels are reduced upon reoxygenation.

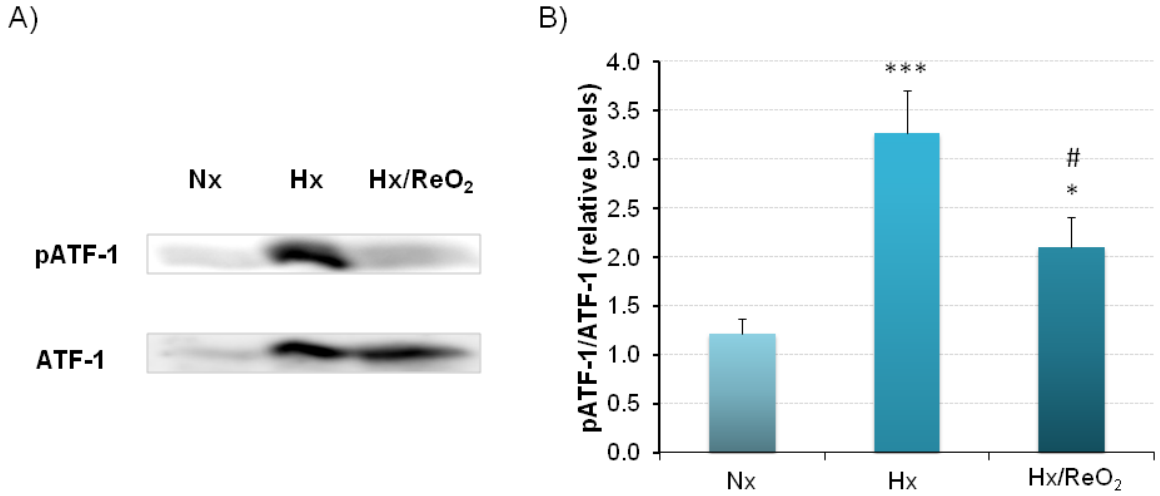

***Fig. 28*. Effects of hypoxia and hypoxia/reoxygenation on ATF-1 phosphorylation.** HL-1 cells were cultured in hypoxia (1% O_2) for 24 h or hypoxia (1% O_2) for 24 h followed by reoxygenation (21% O_2) for 4 h. A) Representative immunoblot of pATF-1 (Ser-133) and total ATF-1 after hypoxia and hypoxia/reoxygenation. B) The histogram shows the means ± SEM of 9 independent experiments. $*P < 0.05$, $***P < 0.001$ with respect to Nx. $^{\#}P < 0.05$ with respect to Hx. Nx, normoxia; Hx, hypoxia; Hx/ReO_2, hypoxia/reoxygenation.

5. Simulated ischemia or ischemia-reperfusion upregulates UCP3 expression and activates Nrf2 and ATF-1

Our previous data showed that hypoxia/reoxygenation induced the expression of UCP3, the activation of Nrf2, as well as the phosphorylation of ATF-1 in HL-1 cells. To test whether these changes also occurred during simulated ischemia (SI) or simulated ischemia-reperfusion (SIR), HL-1 cells were subjected to oxygen and glucose deprivation (OGD) or OGD followed by reoxygenation, respectively.

Similar to hypoxia and hypoxia/reoxygenation, SI and SIR significantly increased UCP3 expression and the activation of Nrf2 and ATF-1 (*Figs. 29 and 30*).

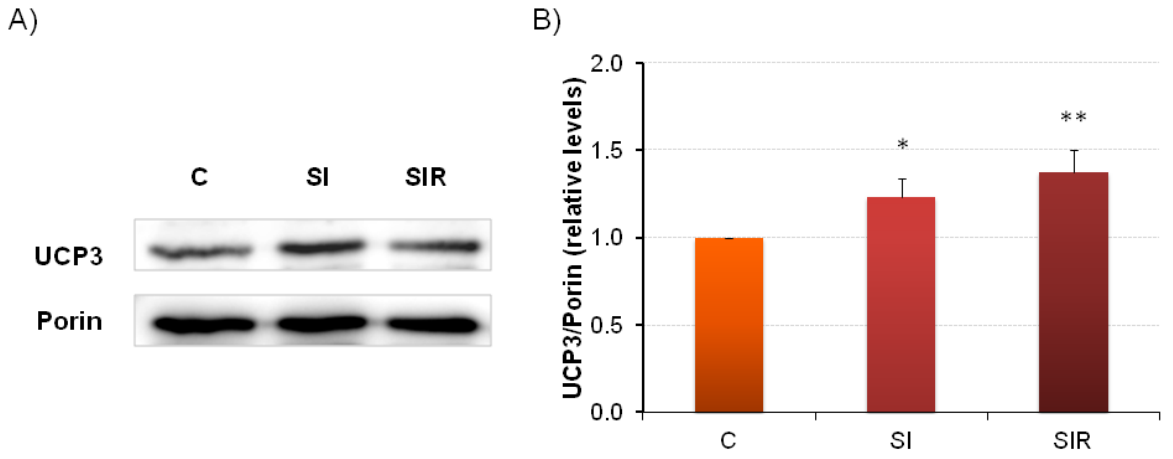

***Fig. 29*. Effects of simulated ischemia (SI) and simulated ischemia-reperfusion (SIR) on UCP3 expression in HL-1 cells.** HL-1 cells were subjected to simulated ischemia (SI) for 2 h or SI for 2 h followed by reperfusion (SIR) for 4 h. A) Representative immunoblot of UCP3 expression in the mitochondrial fraction of HL-1 cells. B) The histogram shows the means ± SEM of 9 independent experiments. Porin was used as loading control. **P* < 0.05, ***P* < 0.01 with respect to C. C, control; SI, simulated ischemia; SIR, simulated ischemia-reperfusion.

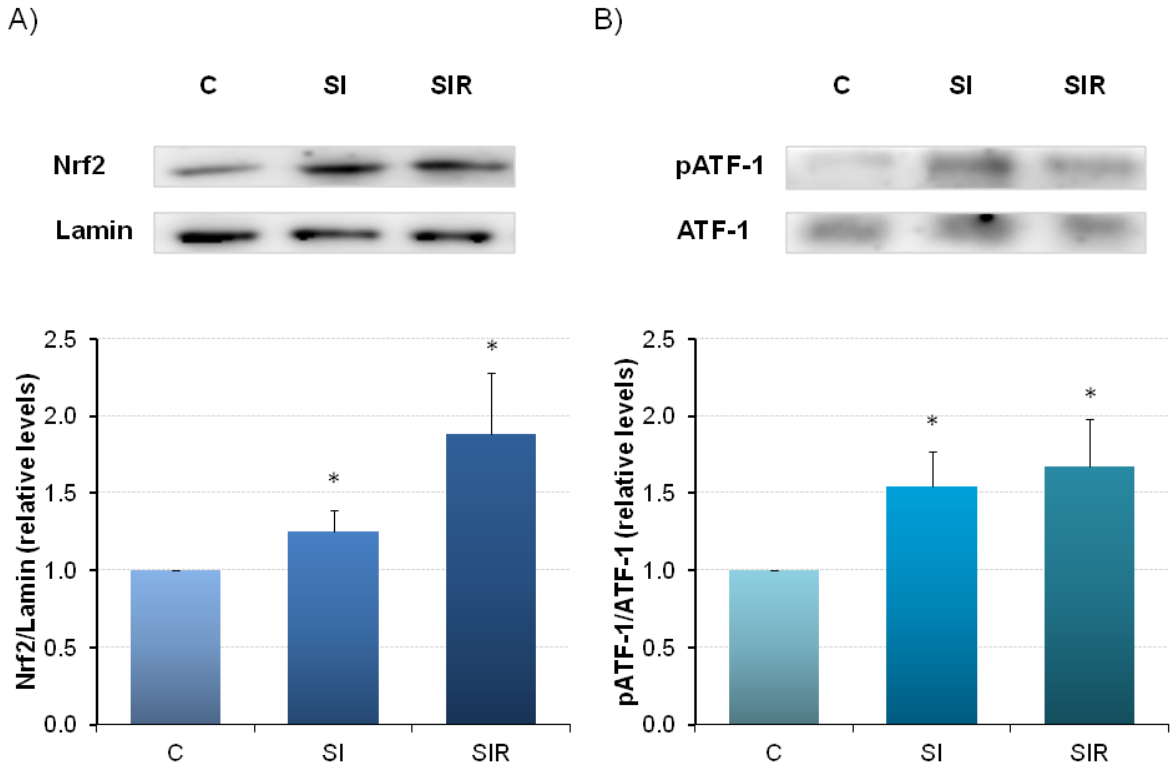

***Fig. 30*. Effects of simulated ischemia (SI) and simulated ischemia-reperfusion (SIR) on the activation of Nrf2 and ATF-1 in HL-1 cells.** HL-1 cells were subjected to simulated ischemia (SI) for 2 h or SI for 2 h followed by reperfusion (SIR) for 4 h. A) Representative immunoblot and histogram of the Nrf2 nuclear accumulation in HL-1 cells. Lamin A/C was used as loading control. B) Representative immunoblot and histogram of pATF-1/ATF-1. The histograms show the means ± SEM of 8-9 independent experiments. **P* < 0.05 with respect to C. C, control; SI, simulated ischemia; SIR, simulated ischemia-reperfusion.

We finally analyzed whether SI or SIR increases oxidative damage. For this, we determined the levels of 4-hydroxynonenal (HNE)-protein adducts by immunoblot, as a marker of oxidative stress. During oxidative stress, HNE is able to react with cysteine or lysine residues of proteins or with low-molecular-weight compounds and macromolecules, affecting their function and fate. The HNE-modified proteins can play pathogenic roles in several diseases.

Fig. 31 illustrates the levels of HNE-protein adducts after SI or SIR. SI did not affect the HNE-protein adducts, whereas SIR increased (p-value = 0.071) the accumulation of these compounds in the cytosol. These data are consistent with our previous results showing that superoxide levels increased in hypoxia/reoxygenation with respect to normoxia and hypoxia (*Fig. 20*). Therefore, our results show that the supply of oxygen and nutrients after ischemia generates oxidative stress in HL-1 cells.

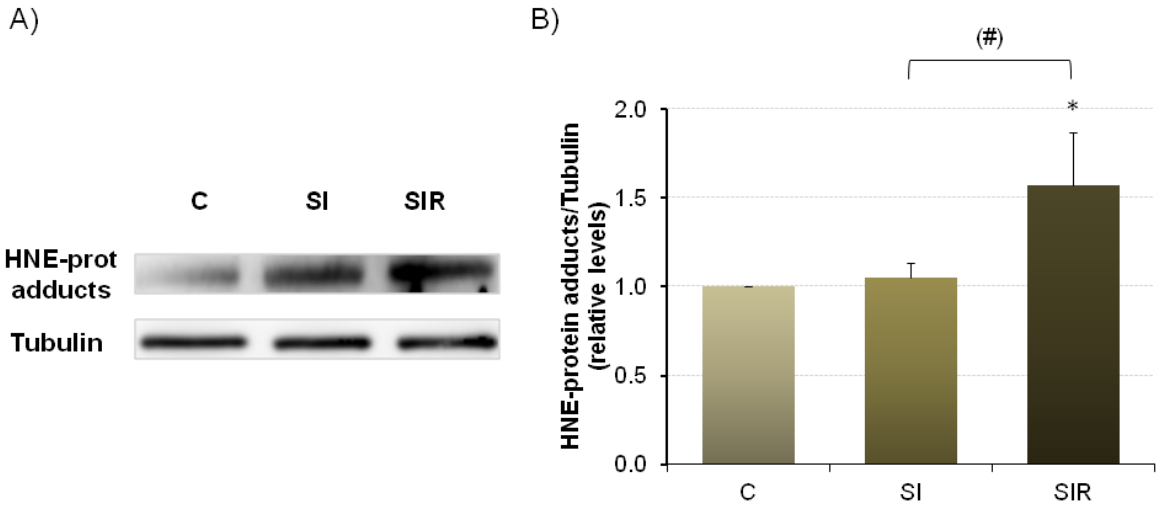

***Fig. 31*. Effects of simulated ischemia (SI) and simulated ischemia-reperfusion (SIR) on HNE-protein adducts in HL-1 cells.** HL-1 cells were subjected to simulated ischemia (SI) for 2 h or SI for 2 h followed by reperfusion (SIR) for 4 h. A) Representative immunoblot of HNE-protein adducts generated in the cytosolic fraction of HL-1 cells. Tubulin was used as loading control. B) The histogram shows the means ± SEM of 7 independent experiments. $*P < 0.05$ with respect to C. $^{(\#)}P = 0.071$ with respect to SI. C, control; SI, simulated ischemia; SIR, simulated ischemia-reperfusion.

The results obtained in this section show that UCP3 is upregulated in response to SI and SIR and that the transcription factors Nrf2 and ATF-1 are activated in these processes (*Figs. 29 and 30*). It remains to be elucidated whether they are involved in UCP3 upregulation and whether UCP3 plays a protective role against the oxidative stress generated in these conditions.

PART II. *Cardioprotective role of UCP3 against ischemia-reperfusion injury and its involvement in ischemic preconditioning*

In the first part of this thesis, we have shown that hypoxia/reoxygenation and SIR enhance UCP3 expression and induce both Nrf2 nuclear accumulation and ATF-1 phosphorylation in HL-1 cardiomyocytes. Moreover, our data indicate that oxidative stress and cell death are greatly enhanced upon reperfusion.

To test the relevance of these findings in a pathophysiological setting, we studied isolated perfused hearts from UCP3 knockout (UCP3-KO) and wild-type mice subjected to IR, using the Langendorff perfusion system (Materials and Methods, section 2.2.1). We also performed in these mice an *in vivo* model of myocardial infarction, the left anterior descending (LAD) coronary artery ligation (Materials and Methods, section 3.1).

1. Cardioprotective role of UCP3 against ischemia-reperfusion (IR) injury and its involment in ischemic preconditioning (IPC)

Previous work from our group showed that UCP3 expression is increased in isolated perfused hearts from wild-type mice subjected to IR and ischemic preconditioning (IPC) (Anedda *et al.*, 2013). Since the results obtained in this thesis indicate that Nrf2 and ATF-1 are activated in HL-1 cells subjected to hypoxia/reoxygenation or SIR, in parallel with an upregulation of UCP3, we set out to study the activation of both transcription factors in isolated perfused hearts after IR. We therefore analyzed the nuclear accumulation of Nrf2 and the phosphorylation of ATF-1 in isolated hearts from UCP3-KO and wild-type mice subjected to IR and IPC.

1.1. Nrf2 nuclear accumulation and ATF-1 phosphorylation are higher in UCP3-KO than in wild-type hearts after IR and IPC

To analyze protein levels, isolated perfused UCP3-KO and wild-type hearts were subjected to IR or IPC followed by IR using the Langendorff perfusion system as described in the Materials and Methods, section 2. Briefly, the hearts were perfused for 20 min (stabilization) and then they were subjected to 40 min ischemia followed or not by 1 h reperfusion. For IPC, the hearts were subjected to two cycles of 5 min ischemia plus 5 min reperfusion after stabilization, followed by IR as described above. Finally, the hearts were removed from the cannula and processed for protein extraction (Materials and Methods, section 2.2.3).

We first analyzed Nrf2 levels in the nucleus, as well as the expression of its target HO-1, in hearts from UCP3-KO and wild-type mice. We found a significant increase in Nrf2 nuclear accumulation and HO-1 expression when the hearts were subjected to IR or IPC, regardless of the genotype (*Fig. 32*). However, the increase in Nrf2 and HO-1 levels after IR was significantly higher in UCP3-KO than in wild-type mice.

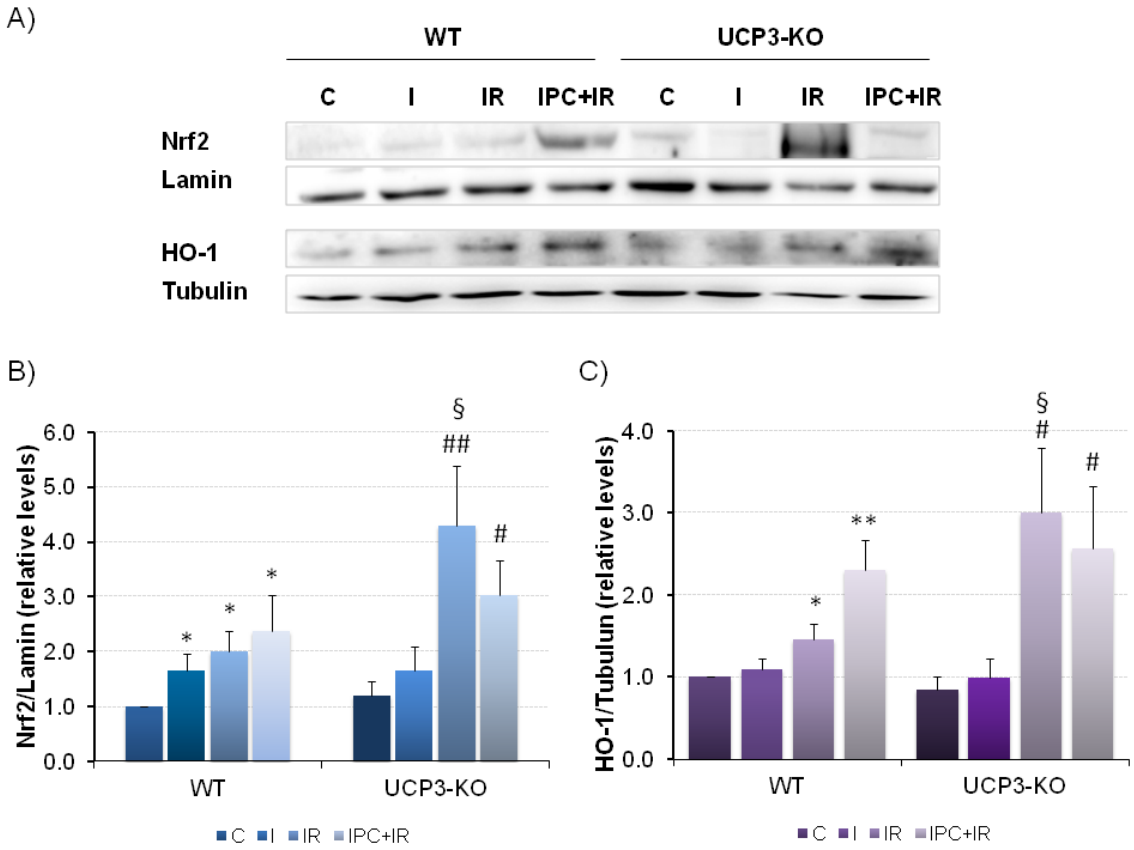

***Fig. 32*. Expression levels of Nrf2 and its target HO-1 after I, IR and IPC in UCP3-KO and wild-type hearts**. A) Representative immunoblots of the nuclear accumulation of Nrf2 and HO-1 expression in cytosol of UCP3-KO and wild-type (WT) hearts. Lamin A/C and tubulin were used as nuclear and cytosolic loading controls, respectively. B, C) Histograms of Nrf2 levels in the nucleus (B) and HO-1 in the cytosol (C). The histograms show the means ± SEM from 4-5 hearts per group. $*P < 0.05$, $**P < 0.01$, with respect to WT control. $^{\#}P < 0.05$, $^{\#\#}P < 0.01$ with respect to UCP3-KO control. $^{\S}P < 0.05$, UCP3-KO with respect to WT of the same condition. C, control; I, ischemia; IR, ischemia-reperfusion; IPC, ischemic preconditioning.

We also analyzed the phosphorylation of ATF-1 in hearts from UCP3-KO and wild-type mice after ischemia, IR and IPC. ATF-1 phosphorylation was significantly increased after IR and IPC in both genotypes (*Fig. 33*). However, the increase in ATF-1 phosphorylation was higher in both IR and IPC from UCP3-KO hearts than in wild-type hearts, although this difference between genotypes only reached statistical significance for the IR protocol. Moreover, ATF-1 phosphorylation increased in ischemia in both genotypes (*Fig. 33*).

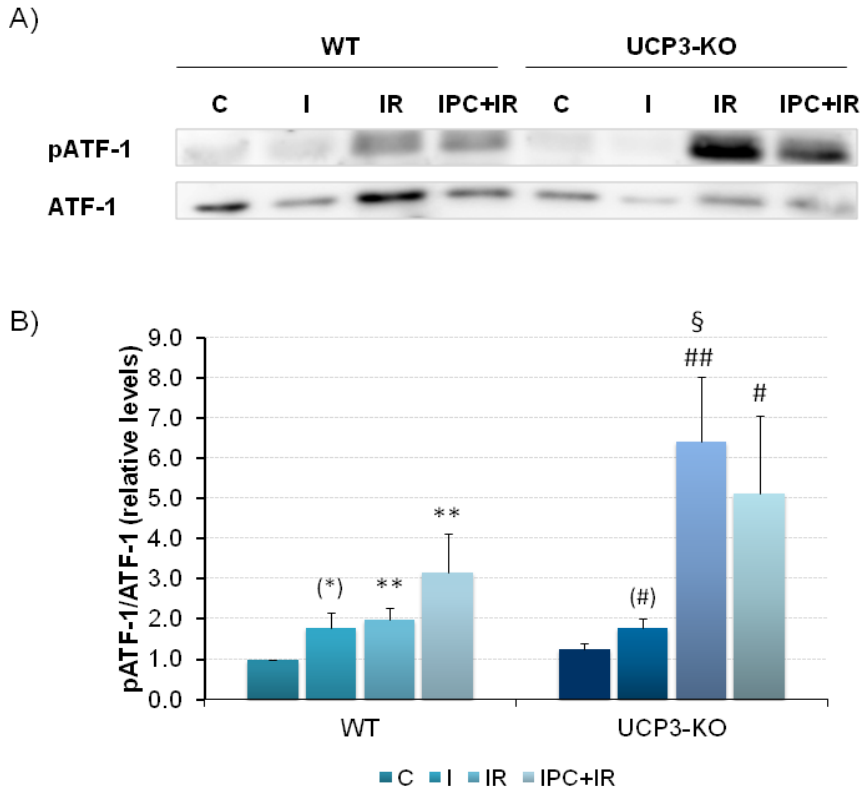

***Fig. 33*. ATF-1 phosphorylation after I, IR and IPC in UCP3-KO and wild-type hearts.** A) Representative immunoblots of the phosphorylated and total ATF-1 in UCP3-KO and wild-type (WT) hearts. B) Histogram of phosphorylated ATF-1 respect to total ATF-1 in the nucleus. The histogram shows the means ± SEM from 4-5 hearts per group. $^{**}P < 0.01$, $^{(*)}P = 0.055$ with respect to WT control. $^{\#}P < 0.05$, $^{\#\#}P < 0.01$, $^{(\#)}P = 0.078$, with respect to UCP3-KO control. $^{\S}P < 0.05$, UCP3-KO with respect to WT of the same condition. C, control; I, ischemia; IR, ischemia-reperfusion; IPC, ischemic preconditioning.

In summary, the results show that, regardless of the mouse genotype, IR and IPC increase the activation of the transcription factors Nrf2 and ATF-1 in the nucleus, as well as the expression levels of HO-1 in the cytosol, with respect to control hearts (*Figs. 32 and 33*). Of note, UCP3-KO hearts presented higher levels of these proteins after the IR and IPC than wild-type hearts. However, the differences between both genotypes were only statistically different after IR. These results are consistent with the activation of Nrf2 and ATF-1 *in vitro* after hypoxia/reoxygenation (*Figs. 19 and 28*) and SIR experiments (*Fig. 30*).

1.2. Active caspase-3 levels are higher in UCP3-KO than in wild-type hearts after IR and IPC

We have shown that hypoxia/reoxygenation induces cell death as determined by an increase in pro-apoptotic caspase-3 in HL-1 cells (*Fig. 22*). We then wondered whether IR also induced the expression and activation of caspase-3 in the hearts of UCP3-KO and wild-type mice and if this effect was affected by IPC.

Caspase-3 was activated after reperfusion (1 h) following ischemia (40 min) in both UCP3-KO and wild-type hearts, and it was also activated in hearts from both genotypes subjected to IPC

followed by IR (*Fig. 34*). Thus, this indicates that the reperfusion process may trigger the apoptotic cell death pathway. However, activated-caspase-3 levels were higher in UCP3-KO than in wild-type hearts in both protocols, although the difference between genotypes was statistically significant only in UCP3-KO after IR.

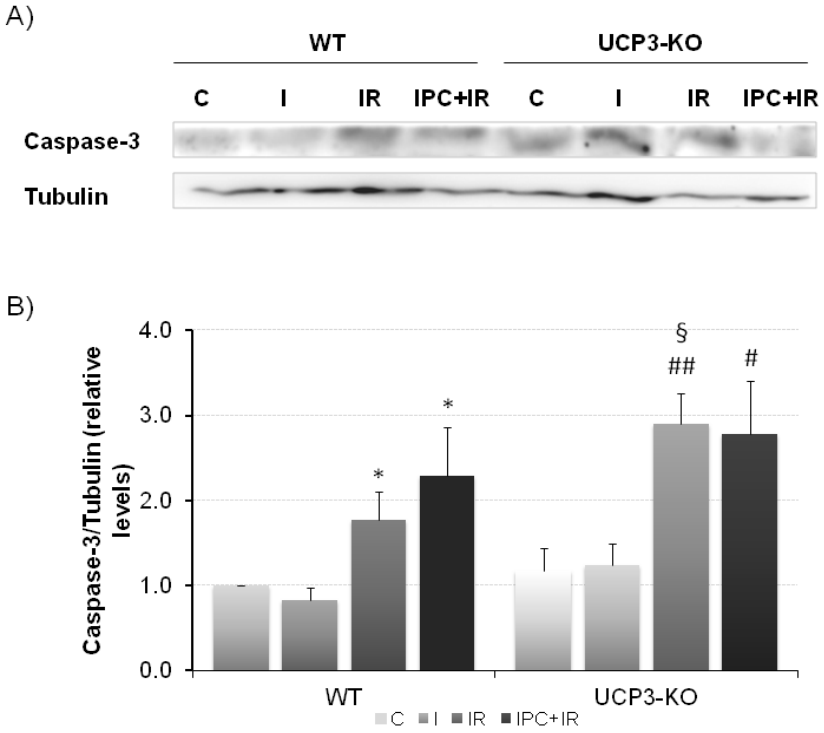

***Fig. 34*. Active caspase-3 protein levels after I, IR and IPC in UCP3-KO and wild-type hearts.** A) Representative immunoblots of cytosolic active caspase-3 in UCP3-KO and wild-type (WT) hearts. Tubulin was used as cytosolic loading control. B) Histogram of caspase-3 activation in the cytosol. The histogram shows the means ± SEM from 4-5 hearts per group. $^{*}P < 0.05$, with respect to WT control. $^{\#}P < 0.05$, $^{\#\#}P < 0.01$, with respect to UCP3-KO control. $^{\S}P < 0.05$, UCP3-KO with respect to WT of the same condition. C, control; I, ischemia; IR, ischemia-reperfusion; IPC, ischemic preconditioning.

The activation of capase-3 after IR and IPC in UCP3-KO and wild-type hearts (*Fig. 34*) increased in parallel with the expression levels of ATF-1, Nrf2 and HO-1 (*Figs. 32 and 33*).

2. Adult and aged UCP3-KO mice have larger infarct sizes and creatine kinase activity than age-matched wild-type mice

Given that UCP3 has been reported to decrease mitochondrial superoxide production and oxidative damage (Mailloux and Harper, 2011), we hypothesized that UCP3 could play a protective role against IR injury in the heart.

To test the role of UCP3 in cardioprotection against IR injury, UCP3-KO and wild-type hearts from adult mice (20-22 weeks) were subjected to IR using the Langendorff system (*Fig. 35*). At the end of the perfusion protocol, the hearts were stained with tetrazolium chloride (TTC) to determine the infarct size. *Fig. 35* shows that the infarct size, which was calculated as the

percentage of the infarct area (white) divided by the area at risk (total), was significantly larger in hearts lacking UCP3 (75.2%) than in wild-type mice (58.3%). A similar study was performed in aged mice (78-80 weeks). In this case, the difference in infarct size between both genotypes was larger in these mice than in adult mice: 82.0% for UCP3-KO compared to 60.4 % for wild-type mice. Thus, the infarct size in aged UCP3-KO mice was larger than in adult UCP3-KO mice after IR. These results indicate that UCP3 plays a cardioprotective role against IR injury that it is even more relevant in aged than in adult mice.

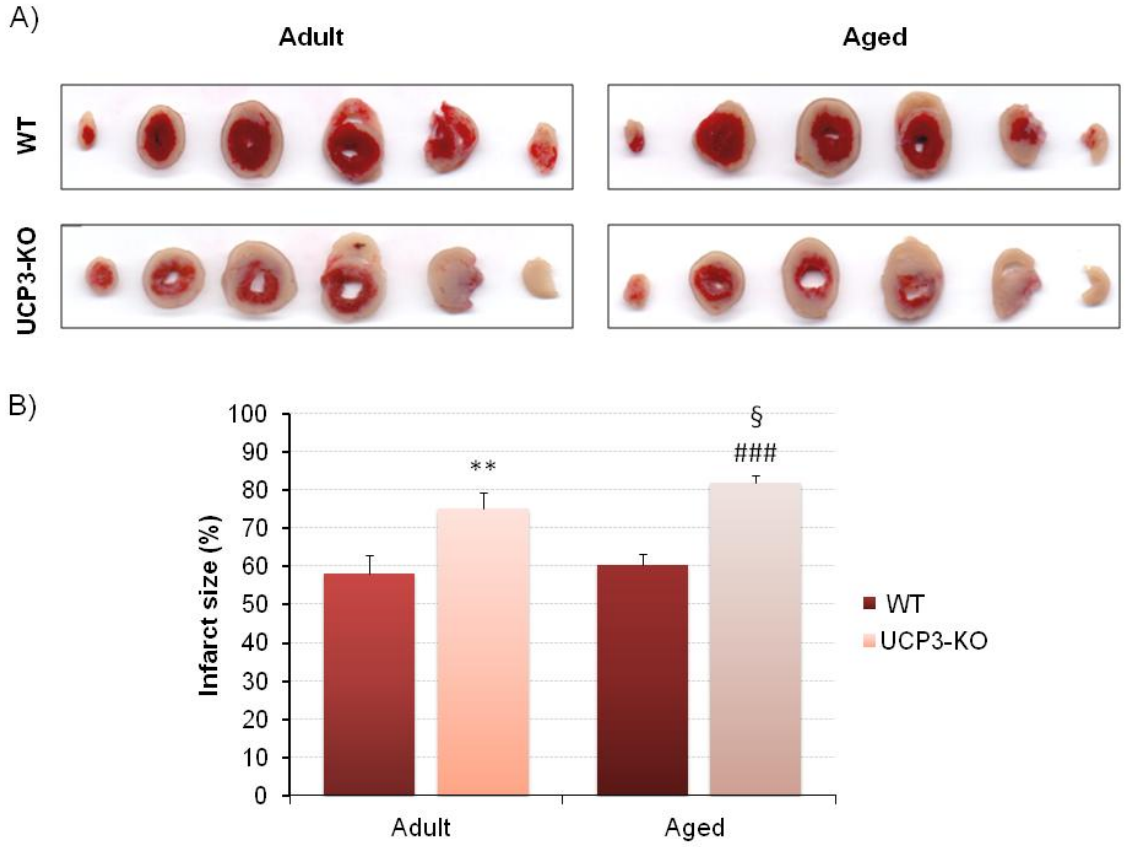

***Fig. 35*. Infarct size in adult and aged hearts from UCP3-KO and wild-type mice after IR.** A) Representative images of heart slices stained with tetrazolium chloride (TTC) from adult (20-22 weeks) and aged (78-80 weeks) mice from UCP3-KO and wild-type (WT) mice after IR. The viable zone was stained in red, while the infarcted area remained white. B) The histogram shows the means ± SEM of the percentage of infarct size (infarct area divided by area at risk) from 10-12 hearts per group. $^{**}P < 0.01$ with respect to adult WT mice, $^{\#\#\#}P < 0.001$ with respect to aged WT mice. $^{\S}P < 0.05$ with respect to adult UCP3-KO mice.

We also measured creatine kinase (CK) activity in the coronary effluent of the heart during reperfusion. This enzyme is present in skeletal muscle, myocardium and brain, and is released from the cytosol of damaged cells to the systemic circulation. Thus, elevated levels of CK have been used as a sensitive marker of myocardial infarction (Cabaniss, 1990).

To determine CK activity, hearts from adult (20-22 weeks) and aged (78-80 weeks) UCP3-KO and wild-type mice were subjected to IR using the Langendorff system. CK activity was determined in the coronary effluent of the perfused hearts: basal levels were determined after

stabilization and just before ischemia (time 0), whereas reperfusion levels were determined at increasing times up to 60 min during reperfusion.

During reperfusion, the highest values of CK activity were detected at 1-5 min, and CK activity was higher in the effluent of UCP3-KO hearts than in that of wild-type mice. Moreover, the activity was higher in aged than in adult hearts.

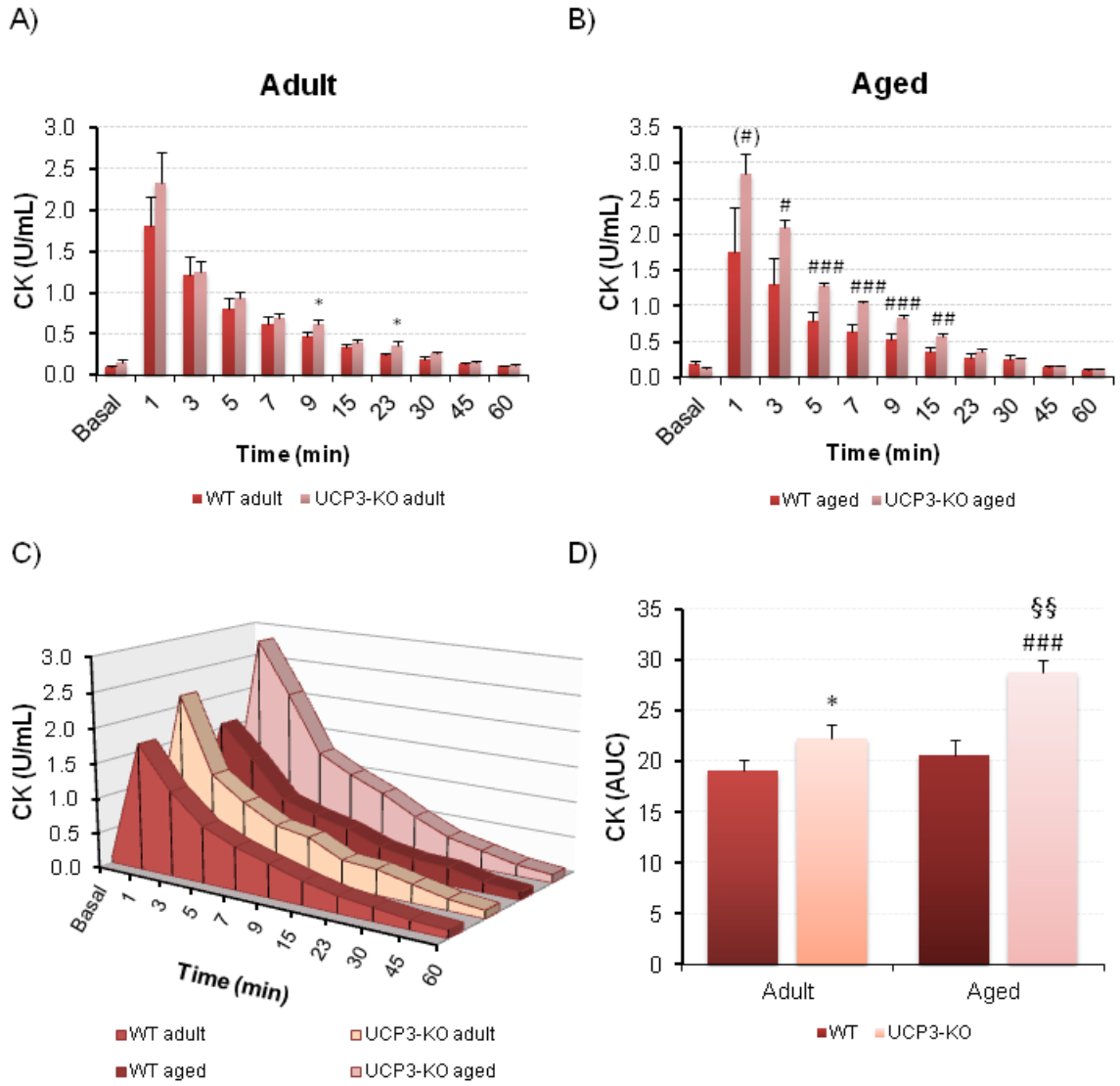

***Fig. 36*. Reperfusion levels of creatine kinase (CK) activity in the coronary effluent of isolated perfused hearts from adult and aged UCP3-KO and wild-type mice.** Creatine kinase (CK) activity (U/mL) measured in the coronary effluent at different times during reperfusion in isolated perfused hearts from adult (20-22 weeks) (A) and aged (78-80 weeks) (B) UCP3-KO and wild-type (WT) mice. C) Total CK activity (U/mL) measured during reperfusion. D) Area under the curve (AUC) of the total CK activity measured at reperfusion in panel C. The histograms show the means ± SEM of CK activity (U/mL) or AUC from 10-12 hearts per group. **P* < 0.05 with respect to adult WT mice. $^{(\#)}P = 0.07$; $^{\#}P < 0.05$, $^{\#\#}P < 0.01$, $^{\#\#\#}P < 0.001$ with respect to aged WT mice. $^{\S\S}P < 0.01$ with respect to adult UCP3-KO mice.

These results are consistent with the data obtained for infarct size (*Fig. 35*) and confirm that isolated perfused hearts from mice lacking UCP3 have more damage than those from wild-type

mice after IR. Likewise, they indicate that the infarct damage is exacerbated with age in UCP3-KO mice (*Figs.35 and 36*). UCP3, therefore, has a protective role against cardiac IR injury.

3. Myocardial infarct size is larger in UCP3-KO compared to wild-type mice after *in vivo* IR

In the previous section, we showed that UCP3 protects against IR injury in isolated perfused hearts. To test whether this protein also plays a cardioprotective role *in vivo*, we performed left anterior descending (LAD) coronary artery ligation followed by reperfusion in adult UCP3-KO and wild-type mice. Tissue damage was determined by echocardiography and histology. The echocardiography images were taken 3-4 days before surgery and 3, 7 and 21 days after surgery. After the last echocardiography (21 days), the mice were sacrificed by cervical dislocation and their hearts were used for histological analysis.

We performed two independent studies for the LAD coronary artery ligation model to generate local ischemia (Materials and Methods, section 3.1). In one study, LAD ligation was performed for 45 min, while in the other study, LAD ligation was performed for 30 min. We determined left ventricle (LV) size and function by echocardiography. For this, we measured the left ventricle (LV) internal dimension at end-systole (LVID;s) and end-diastole (LVID;d) as well as the LV volume at end-systole (LVVol;s) and end-diastole (LVVol;d), which were used to calculate the ejection fraction (EF) following the equations shown previously (Materials and Methods, section 3.2). In addition, after 45 min LAD ligation, we also measured the mitral flow (E:A ratio) and the electrocardiogram (ECG) (*Table 6*), while after 30 min LAD ligation we also measured the LV posterior wall (LVPW), the interventricular septum (IVS) thickness, the aorta diameter, the left atrial diameter (LAd) and the fractional shortening (FS) (*Table 7*).

45 min LAD ligation	3 days pre-MI		3 days post-MI		21 days post-MI	
	WT	UCP3-KO	WT	UCP3-KO	WT	UCP3-KO
EF (%)	50.8 ± 2.2	49.0 ± 3.7	29.4 ± 2.6	29.7 ± 4.2	27.3 ± 3.0	31.5 ± 4.6
LVVol (µL)	47.0 ± 6.8	50.3 ± 7.0	39.6 ± 3.0	50.6 ± 6.3	50.6 ± 5.0	66.4 ± 8.4
LVVol;d (µL)	61.7 ± 7.2	68.6 ± 7.5	54.3 ± 3.3	58.8 ± 2.2	67.6 ± 5.3	81.8 ± 7.4
LVVol;s (µL)	34.5 ± 3.1	36.4 ± 6.8	38.0 ± 2.5	37.7 ± 4.2	49.4 ± 5.0	57.2 ± 8.1
E:A	1.26 ± 0.1	1.21 ± 0.1	2.12 ± 0.3	2.03 ± 0.4	1.61 ± 0.1	1.58 ± 0.1
HR (bpm)	497 ± 16	472 ± 13	479 ± 12	498 ± 13	447 ± 27	448 ± 30
PR (ms)	42.1 ± 1.5	40.6 ± 1.0	39.8 ± 1.5	38.5 ± 2.5	46.7 ± 2.5	44.7 ± 3.4
QRS (ms)	25.1 ± 1.7	23.1 ± 1.8	20.4 ± 1.5	24.0 ± 3.0	17.9 ± 0.8	23.0 ± 2.5*

***Table 6*. Cardiac function of UCP3-KO and wild-type mice 3 days before and 3 and 21 days after the induction of myocardial infarction by 45 min LAD ligation.** The table shows the means ± SEM of the parameters analyzed from 9-10 mice per group. Echocardiography was performed in the M-Mode in the parasternal long (PSLAX) and short axis (PSAX) at the level of the papillary muscles, 3 days before surgery (basal data) and 3 and 21 days after surgery to evaluate the evolution of tissue damage. MI, myocardial infarction; EF, ejection fraction; LVVol, left ventricle volume; d, diastole; s, systole; E:A, ratio

of early (E) and late (A) wave from mitral flow; HR, heart rate; bpm, beats per minute; PR, distance between the onset of the P-wave to the onset of the QRS complex in the electrocardiogram (ECG), it indicates atrial depolarization (activation); QRS, time interval from the onset to the end of this QRS complex in the ECG, it indicates ventricle depolarization. *$P < 0.05$ with respect to wild-type (WT).

30 min LAD ligation	4 days pre-MI		3 days post-MI		7 days post-MI		21 days post-MI	
	WT	UCP3-KO	WT	UCP3-KO	WT	UCP3-KO	WT	UCP3-KO
EF (%)	55.0 ± 4.7	59.9 ± 4.1	62.7 ± 2.7	60.1 ± 6.9	64.7 ± 1.2	66.5 ± 8.7	57.3 ± 5.3	57.3 ± 8.0
FS (%)	23.7 ± 2.6	26.7 ± 2.4	28.2 ± 1.8	27.6 ± 4.0	29.4 ± 0.8	32.6 ± 5.1	25.4 ± 3.5	26.4 ± 5.0
LVID;d (mm)	4.07 ± 0.1	4.05 ± 0.1	3.02 ± 0.4	3.61 ± 0.4	3.49 ± 0.2	3.79 ± 0.4	3.52 ± 0.2	4.06 ± 0.4
LVID;s (mm)	3.11 ± 0.2	2.98 ± 0.1	2.19 ± 0.3	2.68 ± 0.5	2.46 ± 0.1	2.65 ± 0.5	2.65 ± 0.2	3.08 ± 0.5
IVS;d (mm)	0.86 ± 0.0	0.83 ± 0.0	1.27 ± 0.1	1.39 ± 0.1	1.33 ± 0.1	1.17 ± 0.1	0.99 ± 0.1	1.05 ± 0.1
IVS;s (mm)	1.16 ± 0.1	1.05 ± 0.1	1.50 ± 0.1	1.72 ± 0.1	1.54 ± 0.1	1.48 ± 0.1	1.21 ± 0.1	1.32 ± 0.2
LVPW;d (mm)	0.81 ± 0.0	0.78 ± 0.1	1.24 ± 0.2	0.97 ± 0.1	1.11 ± 0.1	0.96 ± 0.1	1.30 ± 0.1	1.16 ± 0.1
LVPW;s (mm)	1.03 ± 0.1	1.06 ± 0.1	1.41 ± 0.1	1.30 ± 0.1	1.53 ± 0.1	1.37 ± 0.1	1.55 ± 0.1	1.46 ± 0.1
Aorta (mm)	1.41 ± 0.0	1.45 ± 0.1	1.45 ± 0.1	1.46 ± 0.1	1.44 ± 0.0	1.41 ± 0.0	1.47 ± 0.1	1.47 ± 0.1
LAd (mm)	1.67 ± 0.1	1.69 ± 0.1	1.72 ± 0.1	1.58 ± 0.2	1.82 ± 0.1	1.73 ± 0.2	2.29 ± 0.1	2.21 ± 0.1

***Table 7*. Cardiac function of UCP3-KO and wild-type mice 4 days before and 3, 7 and 21 days after the induction of myocardial infarction by 30 min LAD ligation.** The table shows the means ± SEM of the parameters analyzed from 6-7 mice per group. Echocardiography was performed in the M-Mode in the parasternal long axis (PSLAX) at the level of the papillary muscles, 4 days before surgery (basal data) and 3, 7 and 21 days after surgery to evaluate the evolution of tissue damage. MI, myocardial infarction; EF, ejection fraction; FS, fractional shortening; LVID, left ventricular internal dimensions, d; diastole; s, systole; IVS, interventricular septum; LVPW, left ventricular posterior wall thickness; LAd, left atrial diameter.

The results of these studies show that mice lacking UCP3 tend to exhibit increased signs of cardiac damage in the functional parameters evaluated, particularly after 45 min LAD ligation. We found that 3 and 21 days after 45 min LAD ligation, both UCP3-KO and wild-type mice presented a significant reduction in the EF ($P < 0.005$) with respect to their basal echocardiography, which evidences left ventricle dysfunction (*Table 6*). The total LVVol and LVVol;d were higher in UCP3-KO mice than in wild-type mice at 21 days, although the increase was not statistically significant between genotypes for each LVVol measure ($P = 0.098$ and $P = 0.092$, respectively). This result also reflects some degree of left ventricle dysfunction. By contrast, the effect of cardiac IR on the EF was not evident after 30 min LAD ligation, and there was no effect of this protocol on the FS either (*Table 7*). After this protocol, however, both types of mice presented significantly

increased values for LVPW thickness and the LAd ($P < 0.01$ and $P < 0.005$, respectively) from 3 days post-surgery to 21 days post-surgery compared to the basal values from 4 days pre-surgery (*Table 7*). However, the degree of LVPW and LAd increase was not significantly different between genotypes. The IVS thickness after 21 days of 30 min LAD ligation was slightly higher in UCP3-KO mice with respect to wild-type mice (*Table 7*). Despite this parameter was not statistically significant, it also indicates major cardiac dysfunction in UCP3-KO mice. Interestingly, the QRS complex was different between wild-type mice and UCP3-KO after 21 days after 45 min LAD ligation (*Table 6*). Although the interpretation of these alterations is not obvious, this could account for the reported arrhythmias shown in these mice after LAD ligation (Ozcan *et al.*, 2013).

We also analyzed by echocardiography the infarct damage in UCP3-KO and wild-type mice subjected to 45 min LAD ligation. For this, the LV was divided into six different segments to evaluate the damage according to their motion and systolic thickening, as described in the Guide of the American Society of Echocardiography. The analysis showed that the scores in UCP3-KO were higher than in wild-type mice, although the difference did not reach statistical significance (*Table 8*).

45 min LAD ligation	3 days post-MI		21 days post-MI	
	WT	UCP3-KO	WT	UCP3-KO
SCORE	3.7 ± 0.57	4.3 ± 0.87	4.0 ± 0.72	4.6 ± 0.88

***Table 8*. Cardiac motility and infarct expansion score in the PSLAX of the left ventricle from UCP3-KO and wild-type hearts**. The table shows the total score for the left ventricle (LV) wall motion and thickening from UCP3-KO and wild-type (WT) hearts after 3 and 21 days post-myocardial infarction. The wall motility was scored as: 1, normal or hyperkinetic; 2, hypokinetic; 3, akinetic (negligible thickening); 4, dyskinetic (paradoxical systolic motion); and 5, aneurysmal (diastolic deformation). Means ± SEM represented the total score of all the 6 LV segments with abnormal motility from 8-10 mice per group.

Taken together, these results show that 21 days allow the heart to recover from 30 min LAD ligation whereas the heart function does not recover completely from 45 min LAD ligation, especially in UCP3-KO mice, which show a tendency to present increased signs of cardiac damage.

The mice survival curves for both protocols and genotypes were very similar as shown in *Fig. 37*. The Kaplan-Meier estimate of the mice survival over-time showed that, during the first 3-4 days after LAD ligation, mice survival was notably reduced in both protocols and genotypes (*Fig. 37*). After 45 min LAD ligation, UCP3-KO survival was reduced to 60.0% of total mice, while wild-type mice survival was reduced to 55.6%. By contrast, survival 3 days after the less aggressive 30 min LAD ligation for wild-type mice resulted in 77.8% of total mice, while for

UCP3-KO mice presented a similar survival curve as for 45 min LAD ligation (58.3%). These data indicate that the first 3-4 days after surgery are critical for mice survival. In addition, LAD ligation affected viability differently depending on the protocol. Whereas 45 min LAD ligation affected similarly to both types of mice, 30 min LAD ligation had less effect on wild-type than on UCP3-KO mice, indicating that these mice are more susceptible to *in vivo* IR.

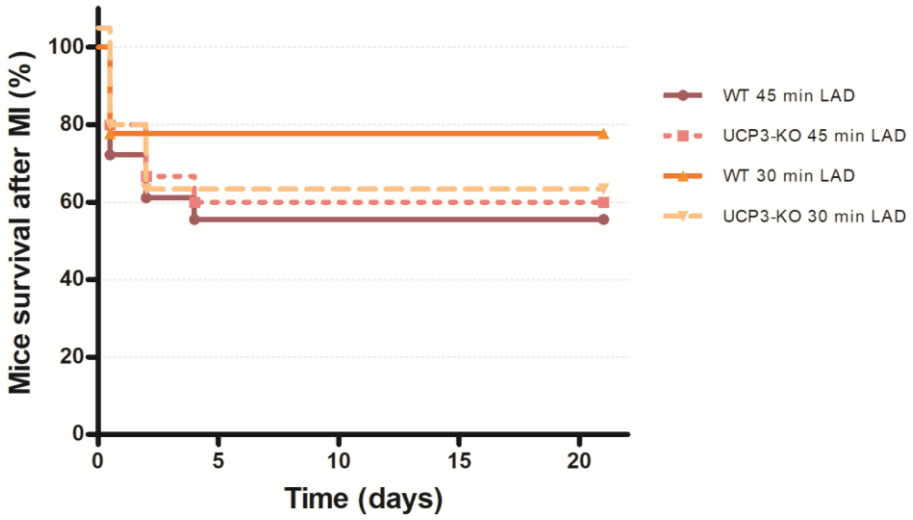

***Fig. 37*. Mice survival curves after 30 or 45 min LAD ligation.** The Kaplan-Meier curve estimates the mice survival at the beginning of the experiment (before surgery; 100% mice), on the same day of surgery (day 0; mice died during or immediately after surgery) and during the following days: 3 or 21days post-surgery. Each curve represents the percentage of UCP3-KO or wild-type (WT) mice alive after LAD ligation for 30 or 45 min. The initial number of mice (100%) for 30 min LAD ligation was 9 wild-type and 12 UCP3-KO mice, while for 45 min LAD ligation was 18 wild-type and 15 UCP3-KO mice.

In addition to the echocardiographic study, we analyzed the infarct size in mice subjected to LAD ligation for 45 min by histology. Once the 21 day post-surgery echocardiography was performed, the hearts were processed for histological analysis and hematoxylin-eosin (H-E) and Masson's trichrome staining (*Fig. 38*).

From the results of the histological analysis, we conclude that the hearts from UCP3-KO mice have larger infarct area than those from wild-type mice after an *in vivo* process of IR, thus confirming the cardioprotective role of UCP3 against this type of damage.

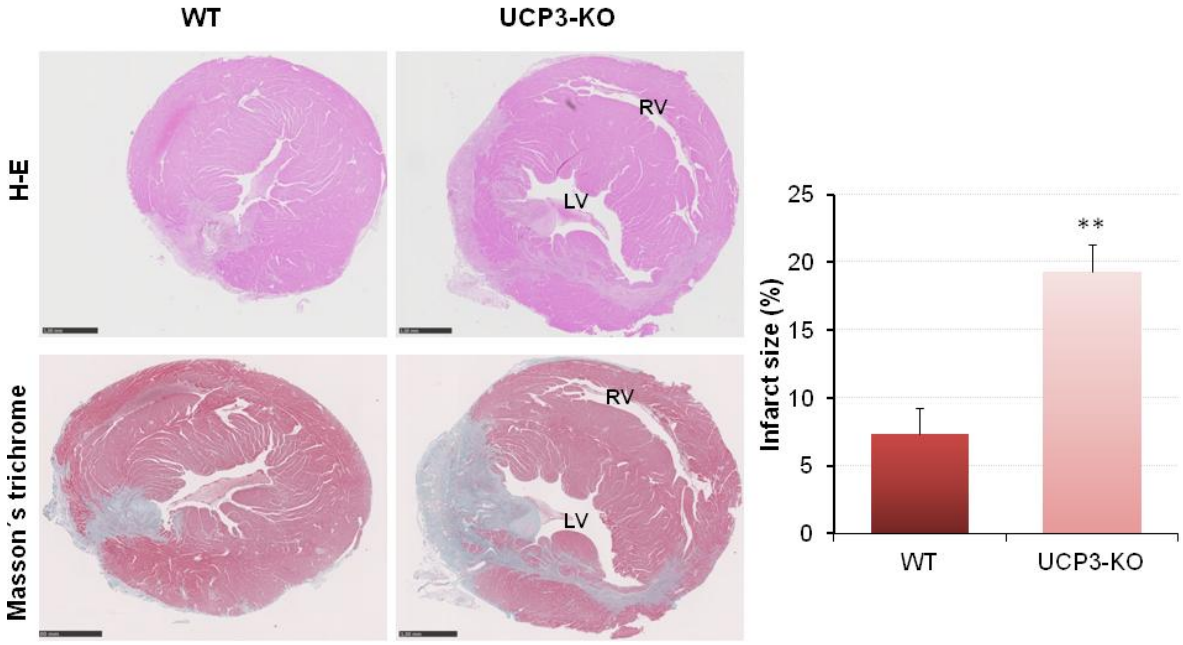

***Fig. 38*. Myocardial infarct area in UCP3-KO and wild-type hearts subjected to LAD ligation for 45 min.** Representative sections from infarcted UCP3-KO and wild-type (WT) hearts, stained with H-E (infarct area, stained in light magenta) or with Masson's trichome (collagen fibers, stained in blue). Scale bar 1.0 mm. The histogram shows the means ± SEM of the infarct size from the H-E staining sections from 8-9 mice per group. RV, right ventricle; LV, left ventricle. $^{**}P < 0.01$.

4. Metabolic changes in cardiac metabolites in UCP3-KO and wild-type mice after IR and IPC

The heart requires a constant supply of energy for contraction. Cardiomyocytes are able to use different substrates for producing ATP, mainly fatty acids, carbohydrates and, to a lesser extent, amino acids (Opie, 2014). Although fatty acids are the predominant substrate utilized in the adult myocardium, the cardiac metabolic network is highly flexible in utilizing other substrates when they become abundantly available (Kolwicz *et al.*, 2013).

To study the possible metabolic alterations that could explain the enhanced IR injury in UCP3-KO compared to wild-type hearts, and the lack of protection provided by IPC, we performed a metabolic analysis. For this, isolated perfused hearts from UCP3-KO and wild-type mice were subjected to ischemia, IR or IPC, and the intracellular metabolites were extracted and analyzed by targeted LC-MS metabolomics (Materials and Methods, section 2.2.3-4).

The metabolites analyzed were involved in carbohydrate, lipid, amino acid and nucleotide metabolism, or they were cofactors and vitamins. The metabolites were grouped in clusters of related pathways in the dendrogram associated to the heat map (*Fig. 39*).

The heat map shows the set enrichment of the metabolites for each protocol and each genotype with two colors that represent the abundance: the blue color indicates low abundance and

the red color indicates high abundance (*Fig. 39*). Metabolite abundance was calculated as log2 of the fold change (FC) of every group compared to the control protocol.

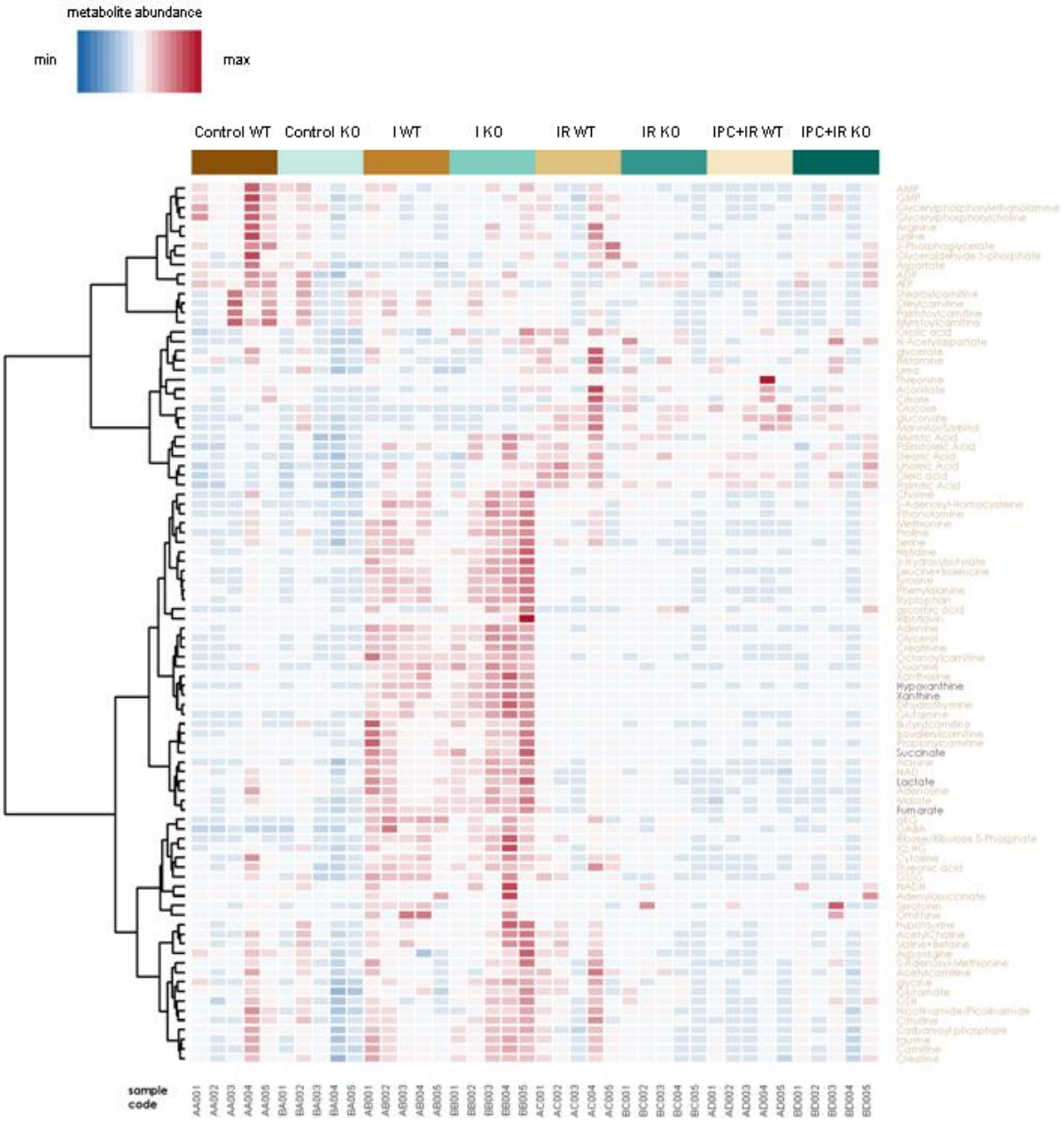

***Fig. 39*. Heat map analysis and hierarchical clustering dendrogram of LC-MS metabolomics obtained from hearts from UCP3-KO and wild-type mice subjected to I, IR and IPC.** The heat map shows the abundance of each metabolite in each individual heart (coded samples) from isolated perfused hearts from UCP3-KO and wild-type (WT) mice, subjected to I, IR and IPC. Each row represents a metabolite and each column represents a sample. The blue color indicates low abundance and red indicates high abundance. The associated hierarchical clustering dendrogram (on the left) represents groups of metabolites from related pathways. C, control; I, ischemia; IR, ischemia-reperfusion; IPC, ischemic preconditioning.

We found that, as expected, several metabolites increased in ischemia including the product of anaerobic glycolysis lactate (*Fig. 41*), and the products of the catabolism of purine nucleotides xanthine and hypoxanthine (*Fig. 40*). The intermediary of the metabolism of thymine, dihydrothymine, also increased in ischemia. These metabolites increased regardless of the mouse genotype and returned to basal values after reperfusion. Moreover, glucose decreased in ischemia in both genotypes (*Fig. 41*). Similarly, glycerate was less abundant in ischemia in both types of mice. Metabolites involved in the Krebs cycle such as succinate, fumarate, malate and α-ketoglutarate, were more abundant in ischemic hearts, as described before (Chouchani *et al.*, 2014), and returned to basal values after reperfusion (*Fig. 42*). Moreover, UCP3-KO hearts had a tendency to present higher levels of these metabolites that wild-type hearts. By contrast, the abundance of metabolites related to fatty acid metabolism showed differences between both groups of mice. Thus, carnitine significantly increased during ischemia and decreased after IR in UCP3-KO compared to wild-type mice, whereas acyl-carnitine followed a similar pattern although the differences were not statistically significant. The long-chain fatty acids oleic and linoleic significantly increased with all treatments compared to the control condition, but the increase was lower in UCP3-KO mice with respect to wild-type mice after IR or IPC (*Fig. 43*).

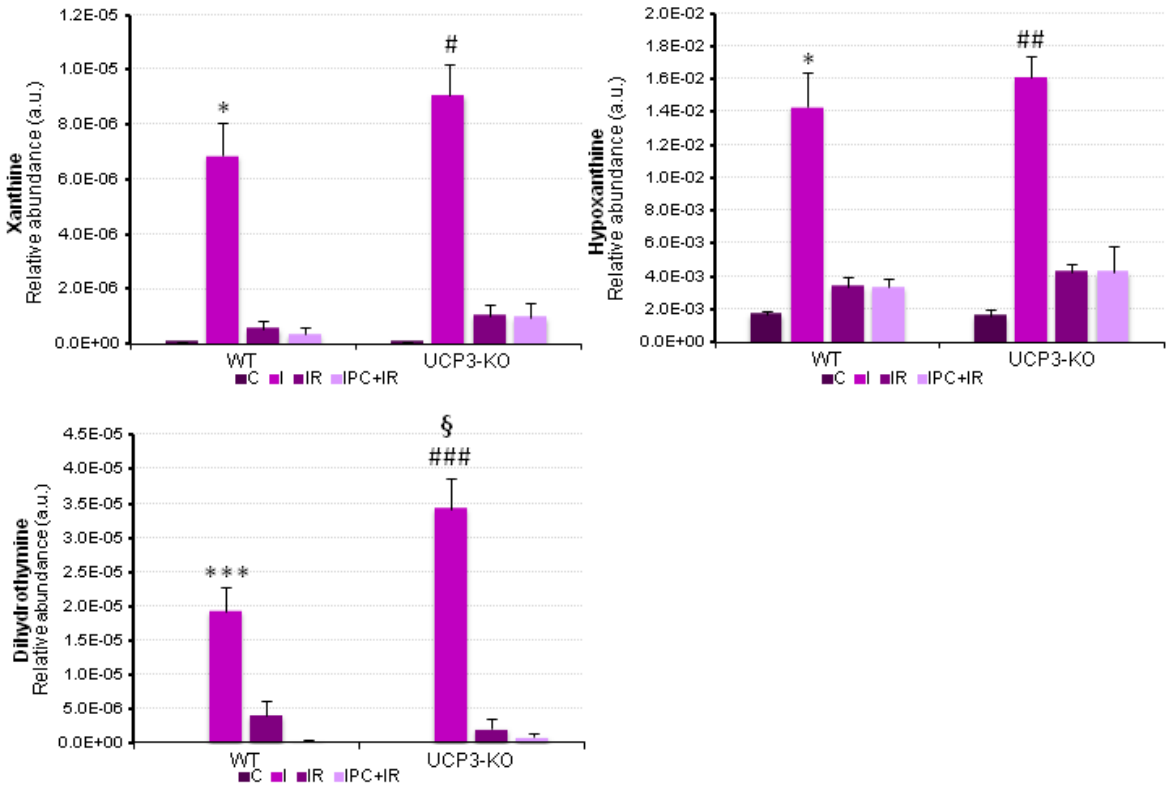

***Fig. 40*. Abundance of metabolites related to the catabolism of purine and pyrimidine nucleotides in hearts from UCP3-KO and wild-type mice subjected to I, IR and IPC**. The histograms show the means ± SEM of 5 hearts per group. **P* < 0.05, ****P* < 0.001 with respect to wild-type control group. $^{\#}P < 0.05$, $^{\#\#}P < 0.01$, $^{\#\#\#}P < 0.001$ with respect to UCP3-KO control group. $^{\S}P < 0.05$ UCP3-KO with respect to wild-type from the same condition. I, ischemia; IR, ischemia-reperfusion; IPC, ischemic preconditioning.

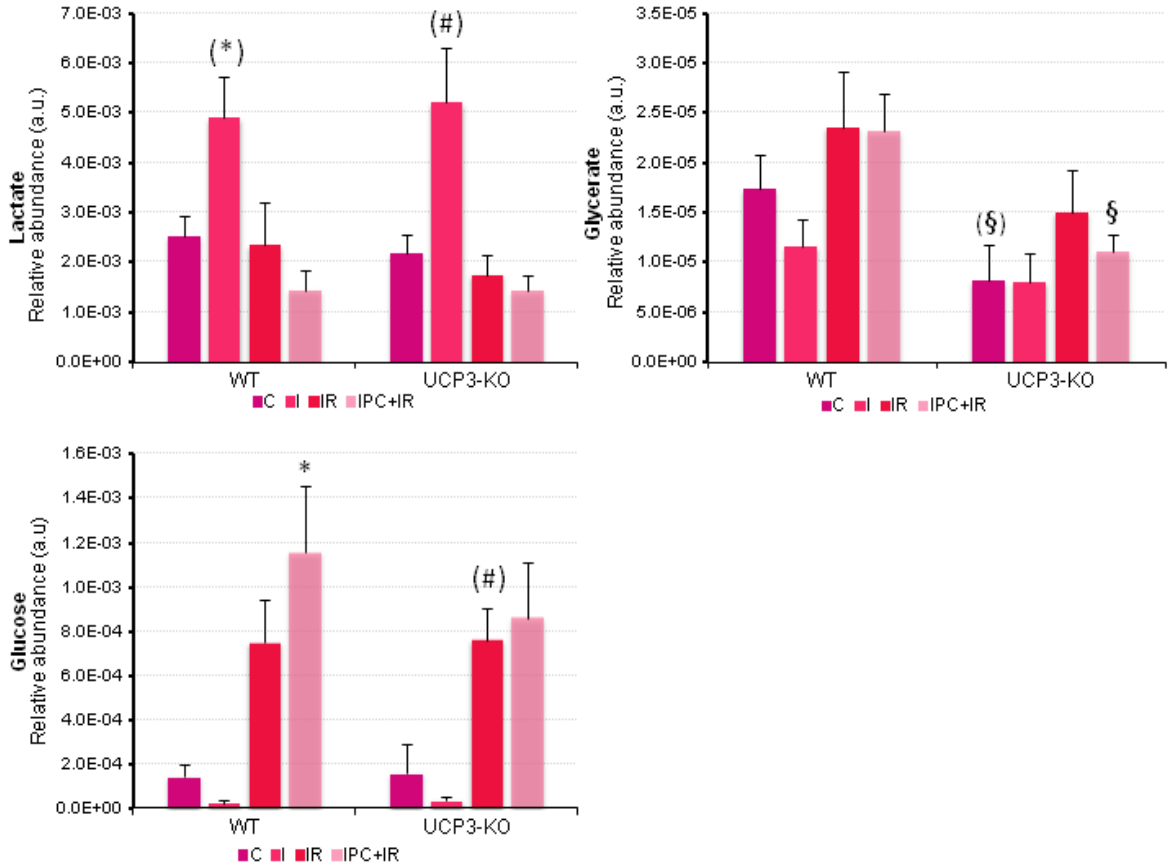

***Fig. 41*. Abundance of metabolites related to glycolysis in hearts from UCP3-KO and wild-type mice subjected to I, IR and IPC**. The histograms show the means ± SEM of 5 hearts per group. $^{(*)}P = 0.058$, $^{*}P < 0.05$ with respect to wild-type control group. $^{(\#)}P = 0.079$ and $^{(\#)}P = 0.077$ with respect to UCP3-KO control group for lactate and glucose graphs, respectively. $^{(\S)}P = 0.066$, $^{\S}P < 0.05$ UCP3-KO with respect to wild-type from the same condition. I, ischemia; IR, ischemia-reperfusion; IPC, ischemic preconditioning.

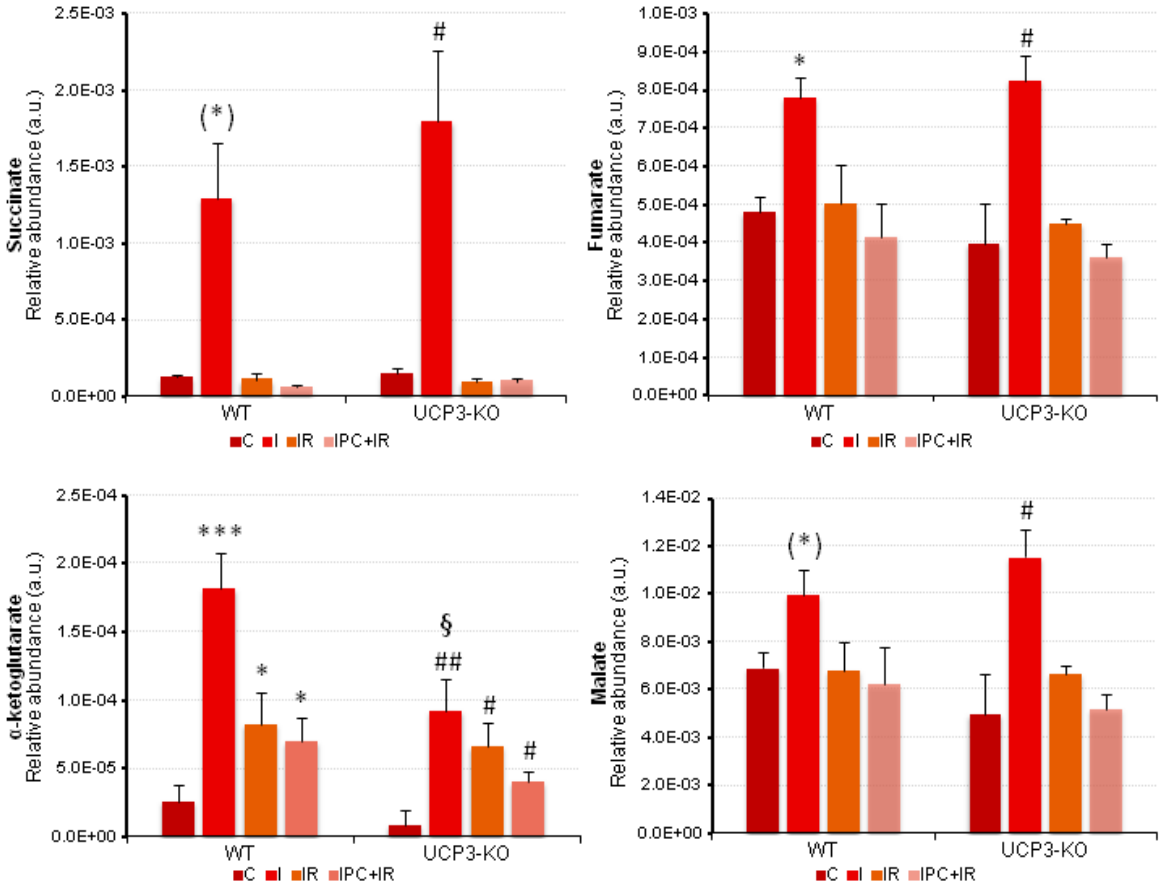

***Fig. 42*. Abundance of intermediary metabolites from the Krebs cycle in hearts from UCP3-KO and wild-type mice subjected to I, IR and IPC.** The histograms show the means ± SEM of 5 hearts per group. $^{(*)}P = 0.056$ for succinate graph, $^{(*)}P = 0.059$ for malate graph, $^{*}P < 0.05$, $^{***}P < 0.001$ with respect to wild-type control group. $^{\#}P < 0.05$, $^{\#\#}P < 0.01$ with respect to UCP3-KO control group. $^{\S}P < 0.05$ UCP3-KO with respect to wild-type from the same condition. I, ischemia; IR, ischemia-reperfusion; IPC, ischemic preconditioning.

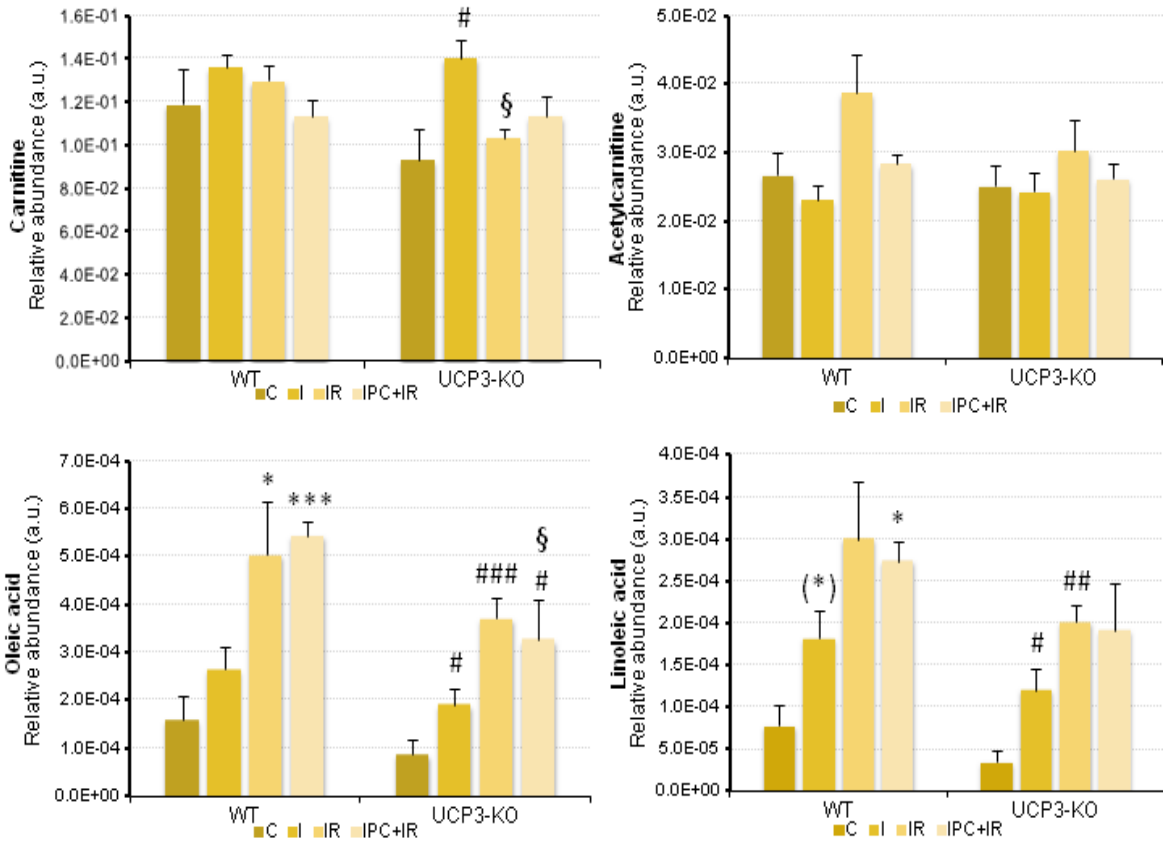

***Fig. 43*. Abundance of metabolites related to lipid metabolism in hearts from UCP3-KO and wild-type mice subjected to I, IR and IPC**. The histograms show the means ± SEM of 5 hearts per group. $^{(*)}P = 0.06$, $^{*}P < 0.05$, $^{***}P < 0.001$ with respect with respect to wild-type control group. $^{\#}P < 0.05$, $^{\#\#}P < 0.01$, $^{\#\#\#}P < 0.001$ with respect to UCP3-KO control group. $^{\S}P < 0.05$ UCP3-KO with respect to wild-type from the same condition. I, ischemia; IR, ischemia-reperfusion; IPC, ischemic preconditioning.

Metabolites related to amino acid metabolism are shown in *Fig. 44*. The amino acids aspartate and asparagine decreased in ischemia and recovered the basal values after reperfusion, although in UCP3-KO mice the aspartate levels were higher after ischemia, IR and IPC, and the asparagine levels were lower after IR. Alanine followed a different trend as it increased in ischemia and returned to basal values after IR in both genotypes. Hypotaurine, an intermediate of taurine biosynthesis, tended to increase in wild-type hearts after I and IR, and the increase was larger but not significant in UCP3-KO mice, which also presented significantly decreased values after IR compared to wild-type mice. The levels of taurine, however, were comparable between protocols and genotypes (data not shown). Creatine levels were similar in all wild-type protocols. However, it decreased in ischemic UCP3-KO hearts and was significantly higher in these hearts after IR than in wild-type hearts. Finally, valine betaine tended to increase in wild-type mice after ischemia and IR but remained low in IPC hearts, whereas in the UCP3-KO the IR values were as low as those of IPC.

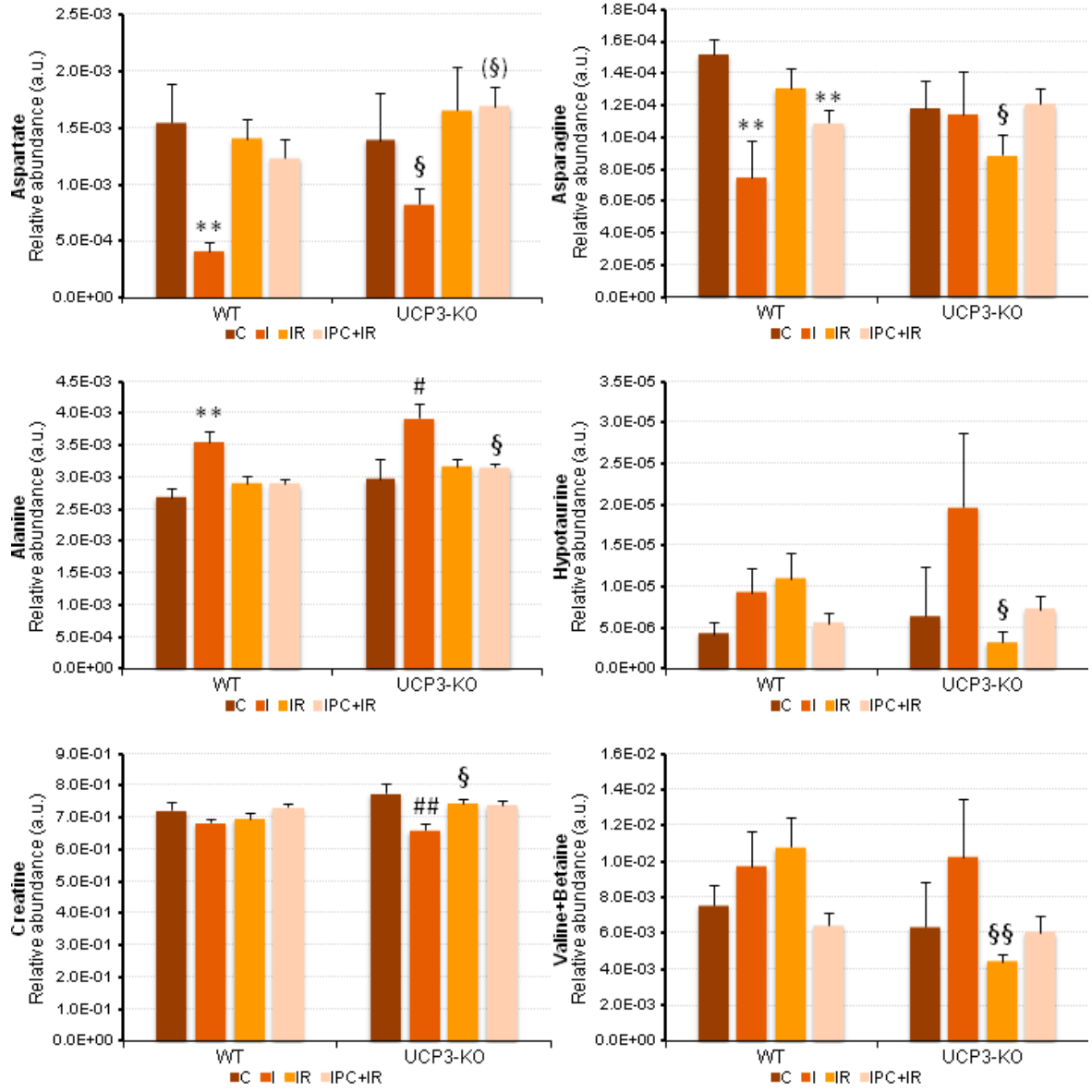

***Fig. 44.* Abundance of amino acids and related metabolites in hearts from UCP3-KO and wild-type mice subjected to I, IR and IPC.** The histograms show the means ± SEM of 5 hearts per group. $^{**}P < 0.01$, with respect to wild-type control group. $^{\#}P < 0.05$, $^{\#\#}P < 0.01$ with respect to UCP3-KO control group. $^{(\S)}P = 0.066$, $^{\S}P < 0.05$, $^{\S\S}P < 0.01$, UCP3-KO with respect to wild-type of the same condition. I, ischemia; IR, ischemia-reperfusion; IPC, ischemic preconditioning.

We also measured the abundance of cofactors and vitamins (*Fig. 45*). NAD is a cofactor that is central to metabolism and is involved in redox reactions. The oxidized form (NAD^+) increased in ischemia in both genotypes, but the increase was higher in the UCP3-KO. After IR, the values decreased below the control value, particularly in preconditioned hearts, although in UCP3-KO hearts the values remained higher than in wild-type hearts. Similar trends were observed for the reduced form (NADH) and the calculated ratio NADH/NAD^+. Ascorbic acid (vitamin C) levels increased in ischemia in both types of mice but only reached statistical significance in UCP3-KO mice. After IR, ascorbic acid behaved differently in wild-type and UCP3-KO hearts: it decreased in the former but increased in the latter. IPC blunted these effects.

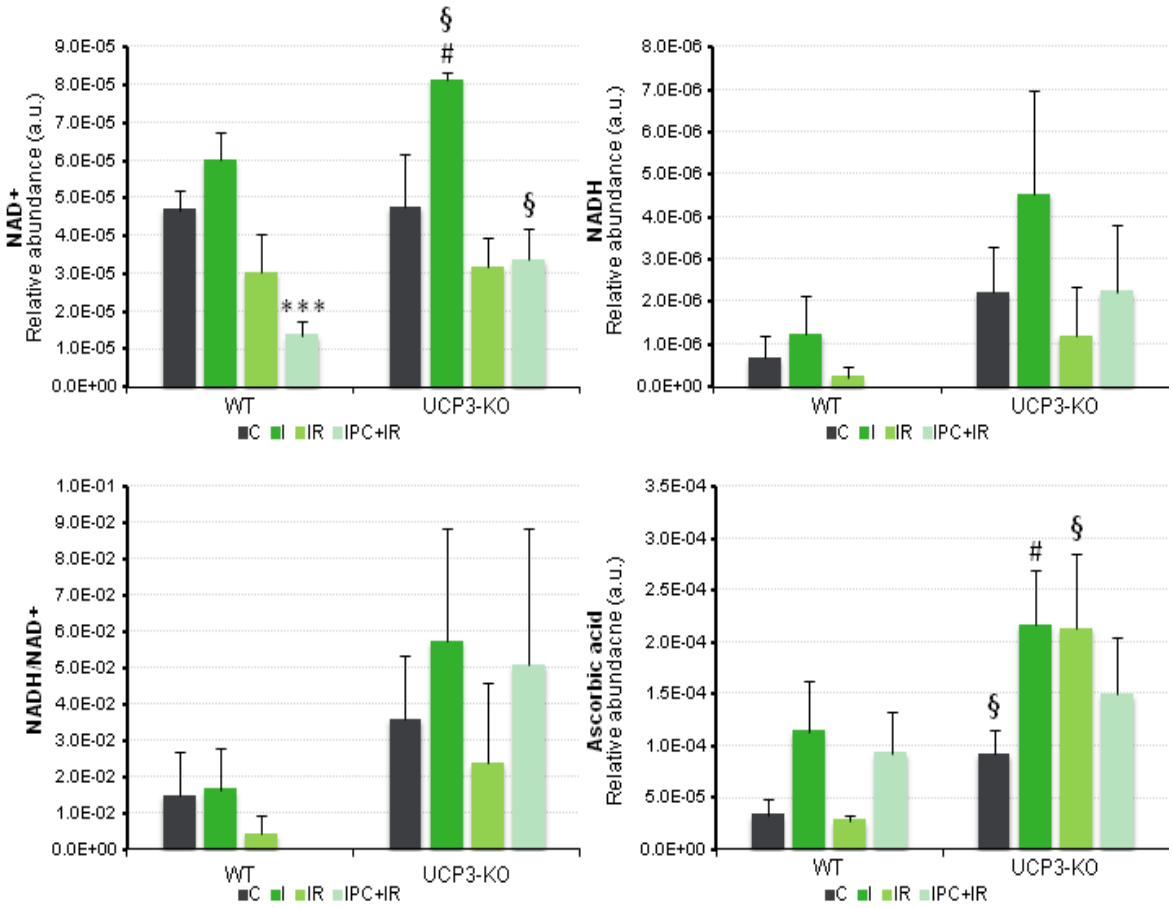

***Fig. 45*. Abundance of metabolites related to cofactors and vitamins in hearts from UCP3-KO and wild-type mice subjected to I, IR and IPC**. The histograms show the means ± SEM of 5 hearts per group. ***$P < 0.001$ with respect to wild-type control group. $^{\#}P < 0.05$ with respect to UCP3-KO control group. $^{\S}P < 0.05$, UCP3-KO with respect to wild-type of the same condition. I, ischemia; IR, ischemia-reperfusion; IPC, ischemic preconditioning.

We finally analyzed the abundance of ATP, ADP and AMP (*Fig. 46*). Surprisingly, we found that the three nucleotides decreased during ischemia in both genotypes. Of note, the levels of ADP after IR were significantly higher in UCP3-KO mice than in wild-type mice. The levels were at least partially recovered upon reperfusion in either conditioned or non-conditioned hearts, except for AMP, whose levels decreased during reperfusion. The ATP/ADP ratio was reduced in control UCP3-KO mice compared to control wild-type mice, contrary to what would be expected for an uncoupling protein. In wild-type hearts, the ratio decreased in ischemia and remained low at reperfusion. By contrast, the ratio slightly decreased in ischemia but recovered to pre-ischemic values after reperfusion in UCP3-KO mice. These differences, however, did not reach statistical significance.

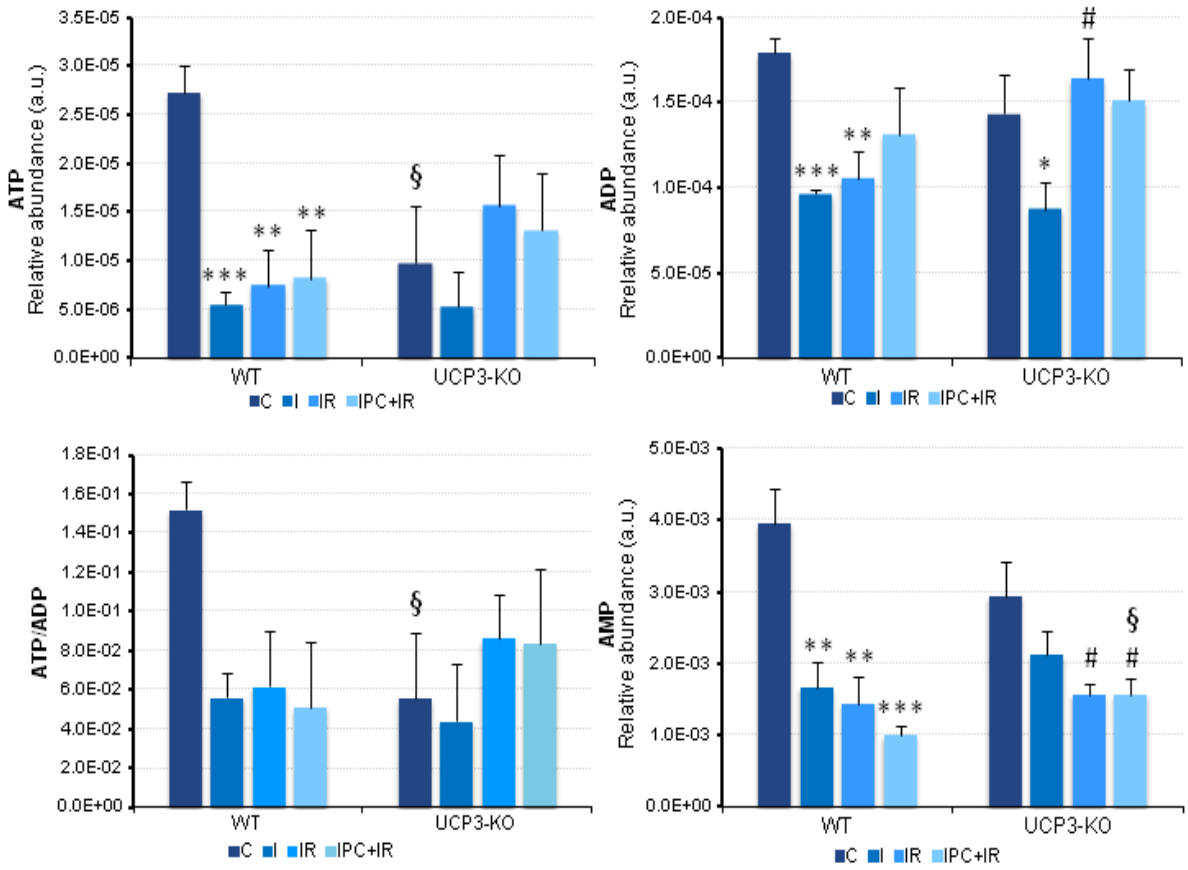

***Fig. 46.* Abundance of adenine nucleotides in hearts from UCP3-KO and wild-type mice subjected to I, IR and IPC**. The histograms show the means ± SEM of 5 hearts per group. **P* < 0.05, ***P* < 0.01, ****P* < 0.001 with respect to wild-type control group. $^{\#}P$ < 0.05 with respect to UCP3-KO control group. $^{\S}P$ < 0.05, UCP3-KO with respect to wild-type of the same condition. I, ischemia; IR, ischemia-reperfusion; IPC, ischemic preconditioning.

In summary, the metabolomics analysis shows that hearts from UCP3-KO and wild-type mice have, in general, a similar response to ischemia: decreased glucose and increased lactate levels, intermediates of the Krebs cycle and products of the catabolism of purine nucleotides. This analysis also suggests that the absence of UCP3 mainly affects pathways related to lipid and energy metabolism.

PART III. *Cardioprotective role of Nrf2 against ischemia-reperfusion injury and its involvement in ischemic preconditioning*

The transcription factor Nrf2 is a primary regulator of the cellular antioxidant response (Itoh *et al.*, 1997). We have shown the nuclear accumulation of Nrf2 in parallel with increased UCP3 expression under oxidative stress (*Fig. 16*), after hypoxia/reoxygenation (*Figs. 17 and 18*) or after SIR (*Figs. 29 and 30*) in HL-1 cells. Nrf2 also accumulates in the nuclear fraction of isolated mouse hearts after IR, regardless of UCP3 expression, although its accumulation is higher in UCP3-KO mice (*Fig. 32*).

We have shown that UCP3 is involved in the protection of the heart against *ex vivo* (*Fig. 39*) and *in vivo* (*Fig. 38*) IR injury. Moreover, previous work from our lab (unpublished) and other labs (Ozcan *et al.*, 2013) indicated that UCP3 is involved in IPC. Since Nrf2 mediates UCP3 upregulation in response to oxidative stress, we wondered whether Nrf2 could also be cardioprotective against IR injury and could be involved in IPC. To address this question, we perfused isolated hearts from adult (20-22 weeks) Nrf2-KO and wild-type mice with the Langendorff system following different protocols as described in Materials and Methods (section 2.2.2): control, IR and IPC+IR. Upon completion of these protocols, we analyzed the infarct size by TTC staining and CK release from the coronary effluent. In addition, the protein levels of HO-1 and caspase-3 were measured in these hearts after the IR protocol (Materials and Methods, section 2.2.3).

1. The absence of Nrf2 reduces HO-1 expression after IR

We first analyzed the expression of the Nrf2 target HO-1 in isolated perfused hearts from Nrf2-KO and wild-type mice subjected to IR. As expected, the absence of Nrf2 resulted in significantly reduced levels of HO-1 after IR (*Fig. 47*), which confirms that HO-1 is a target of Nrf2.

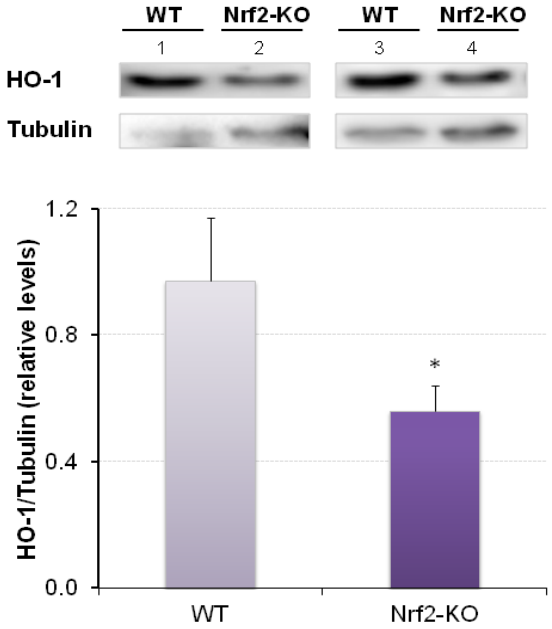

***Fig. 47*. HO-1 expression in Nrf2-KO and wild-type hearts after IR.** Representative immunoblots and histogram of cytosolic levels of HO-1 in the total fraction of isolated perfused hearts from Nrf2-KO and wild-type mice subjected to IR. Numbers 1-4 indicate different mice. Tubulin was used as loading control. The histogram shows the means ± SEM from 4 hearts per group. **P* < 0.05.

2. Nrf2-KO hearts have larger infarct areas, increased creatine kinase release and caspase-3 expression than wild-type hearts after IR

To test whether Nrf2 protects against IR injury, isolated perfused hearts from Nrf2-KO and wild-type mice were subjected to IR followed by TTC staining (*Fig. 48*). The infarct size measured as the percentage of death area (white) divided by the area at risk (total) was significantly larger in Nrf2-KO (78.7%) than in wild-type (67.2%) hearts. We conclude from these experiments that, similar to UCP3, Nrf2 plays an important role in cardioprotection against IR injury.

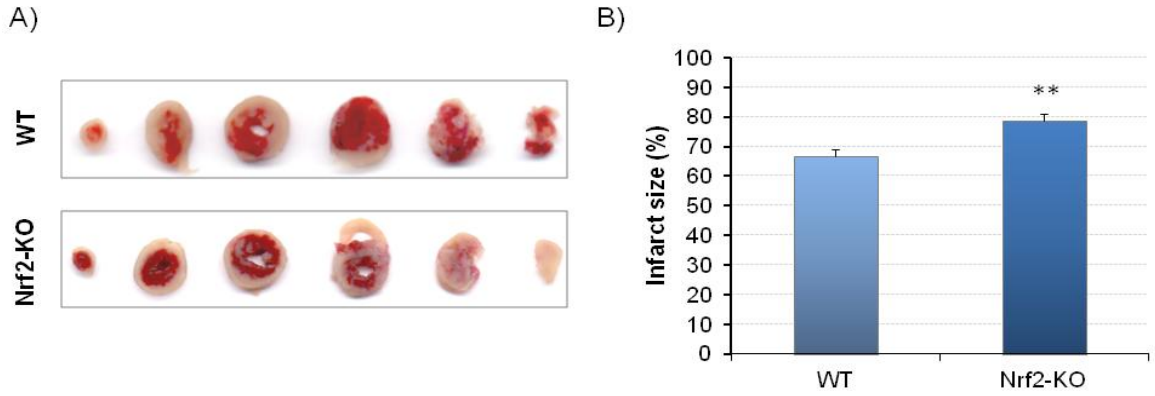

***Fig. 48*. Infarct size in hearts from Nrf2-KO and wild-type mice after IR.** A) Representative images of heart slices stained with tetrazolium chloride (TTC) from adult (20-22 weeks) Nrf2-KO and wild-type (WT) mice after IR. The viable zone was stained in red, while the infarcted area remained white. B) The histogram shows means ± SEM of the percentage of infarct size (infarct area divided by area at risk) from 12-13 hearts per group. ***P* < 0.01.

In addition to the infarct size, we also determined the activity of creatine kinase (CK) in the coronary effluent at different time points up to 60 min during reperfusion (Materials and Methods, section 3). Besides, we measured active caspase-3 levels as an indicator of cell death.

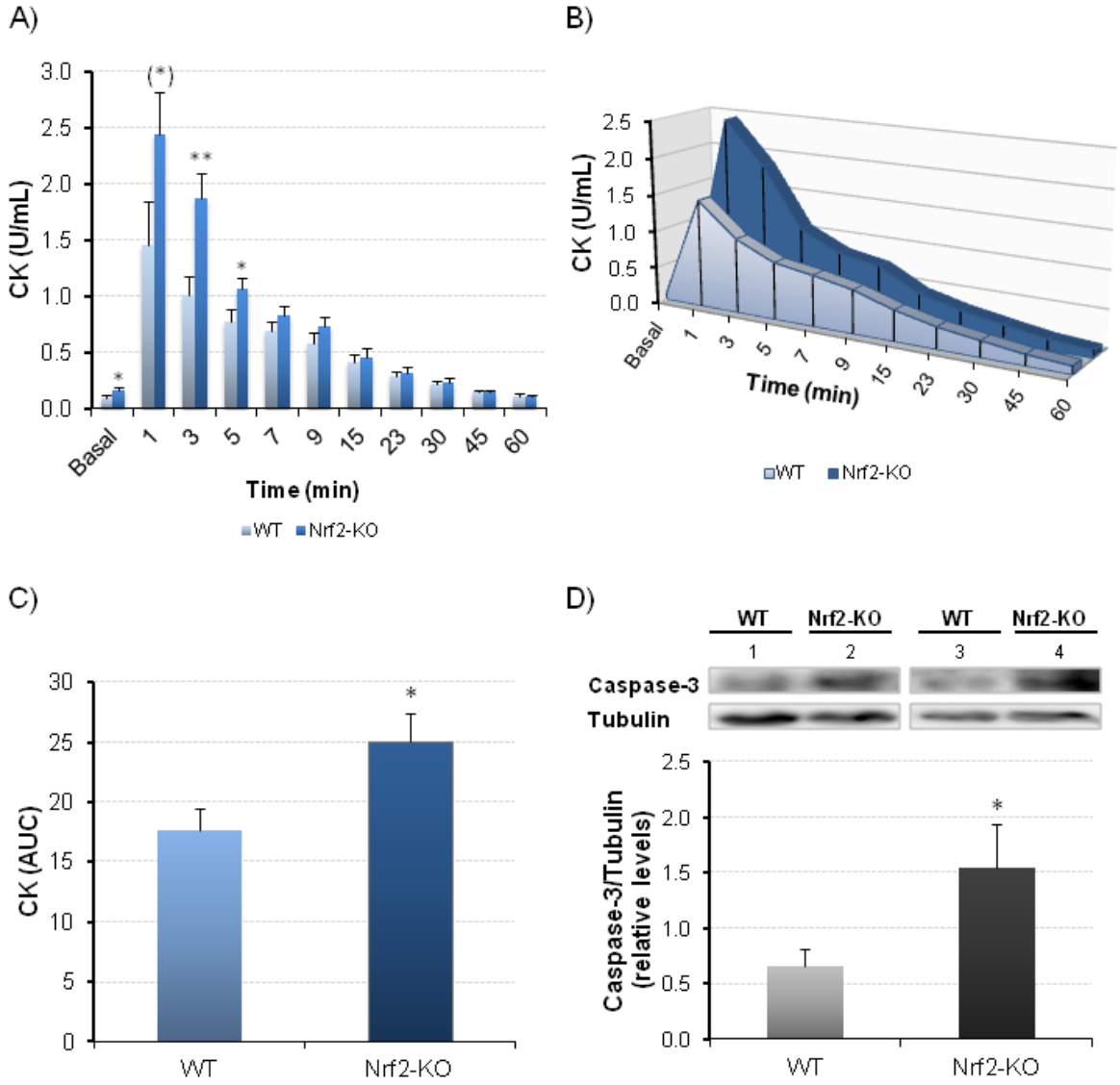

***Fig. 49*. Reperfusion levels of creatine kinase (CK) activity in the coronary effluent of isolated perfused hearts from Nrf2-KO and wild-type mice and active caspase-3 levels in these hearts after IR.** A) Creatine kinase (CK) activity (U/mL) measured in the coronary effluent at different times during reperfusion, in isolated perfused hearts from Nrf2-KO and wild-type (WT) mice. B) Total CK activity (U/mL) measured during reperfusion. C) Area under the curve (AUC) of the total CK activity measured at reperfusion. The histograms show the means ± SEM of CK activity (U/mL) or area under the curve (AUC) from 9-11 hearts per group. D) Representative immunoblot of active caspase-3 in the cytosolic fraction from Nrf2-KO and WT hearts subjected to IR. Numbers 1-4 indicate different mice. Tubulin was used as loading control. The histogram shows the means ± SEM from 4-6 hearts per group. (*)$P = 0.068$; *$P < 0.05$, **$P < 0.01$. Basal, basal levels after 20 min stabilization (time 0).

Both, CK release and active caspase-3 were significantly higher in Nrf2-KO hearts compared to wild-type hearts. These data show that infarct damage is enhanced in Nrf2-KO mice and therefore, suggest a cardioprotective role of Nrf2 against IR injury.

We also determined the infarct size and the activity of CK in Nrf2-KO and wild-type hearts subjected to the control protocol (2 h perfusion) (*Figs. 50 and 51*).

Firstly, we determined the infarct size in Nrf2-KO and wild-type hearts subjected to the control protocol (2 h perfusion) by TTC staining (*Fig. 50*).

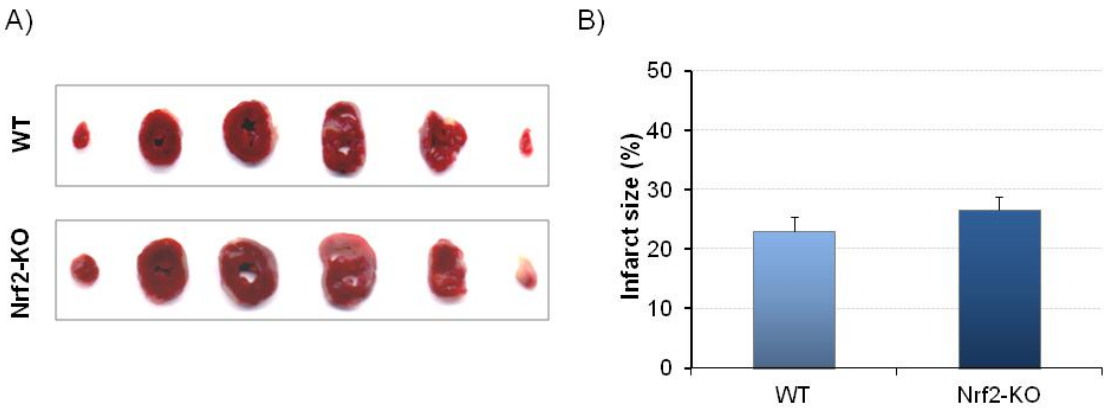

***Fig. 50*. Infarct size in hearts from Nrf2-KO and wild-type mice subjected to 2 h perfusion (control protocol).** A) Representative images of heart slices stained with tetrazolium chloride (TTC) from isolated perfused hearts from Nrf2-KO and wild-type (WT) mice subjected to the control protocol (2 h perfusion). The viable area was stained in red, while the death area remained white. B) The histogram shows the means ± SEM of the percentage of infarct (death area with respect to total area) from 8-9 hearts per group.

The TTC staining showed no statistically significant differences in the infarct size between Nrf2-KO and wild-type hearts subjected to the control protocol (*Fig. 50*). Similarly, CK activity, as determined by the area under the curve (AUC) of total CK activity (U/mL), also did not show significant differences between genotypes (*Fig. 51*), corroborating the TTC result.

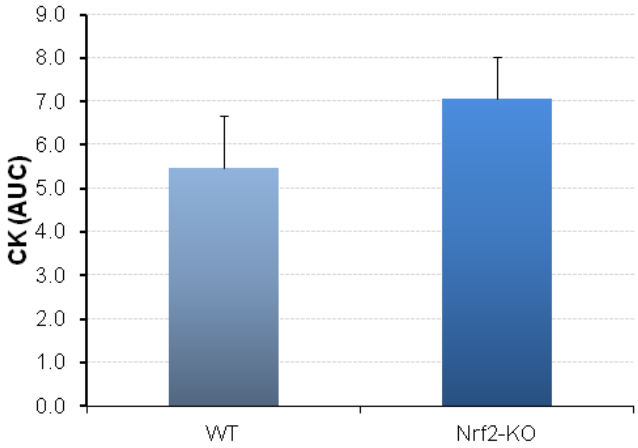

***Fig. 51*. Creatine kinase (CK) activity in the coronary effluent of isolated perfused hearts from Nrf2-KO and wild-type mice after 2 h perfusion (control protocol).** Area under the curve (AUC) of total CK released from Nrf2-KO and wild-type (WT) mice. The histogram shows the means ± SEM of the area under the curve (AUC) of total CK activity (U/mL) of 8-9 hearts per group.

From these results, we conclude that the cardiac damage measured in Nrf2-KO and wild-type mice (*Figs. 50 and 51*) is due to the IR process and not to basal damage due to the cannulation procedure or the perfusion itself.

Taken together, the results obtained in Nrf2-KO mice indicate that Nrf2 plays an important role in the protection of the heart against IR injury.

3. Nrf2 is involved in cardiac ischemic preconditioning

We have shown that mice lacking Nrf2 have larger infarct size after *ex vivo* IR with respect to wild-type mice (*Fig. 48*), as well as elevated CK activity in the coronary effluent (*Fig. 49*), which indicate that Nrf2 has a protective role against IR injury. Moreover, Nrf2 accumulates in the nucleus of isolated perfused hearts from wild-type mice after IR, and Nrf2 nuclear accumulation is even higher after IPC followed by IR (*Fig. 32*). In order to study the involvement of Nrf2 in IPC, isolated hearts from Nrf2-KO and wild-type mice were subjected to IPC followed by IR. Briefly, after stabilization (20 min), the hearts were subjected to two cycles of 5 min ischemia plus 5 min reperfusion followed by IR (40 min ischemia plus 60 min reperfusion). At the end of reperfusion, the hearts were stained with TTC (*Fig. 52*). We also estimated infarct damage by measuring the activity of CK in the coronary effluent during reperfusion (*Figs. 53 and 54*).

In agreement with data shown before (*Fig. 48*), the infarct size in Nrf2-KO mice after IR was larger than in wild-type mice (*Fig. 52*). IPC partially decreased the infarct size in wild-type mice compared to IR alone. By contrast, IPC had no significant effect on the infarct size in Nrf2-KO mice, as they presented a similar percentage of infarct size in conditioned and non-conditioned hearts. These data suggest that, in addition to its role against IR injury, Nrf2 is involved in the cardioprotective phenomenon of IPC.

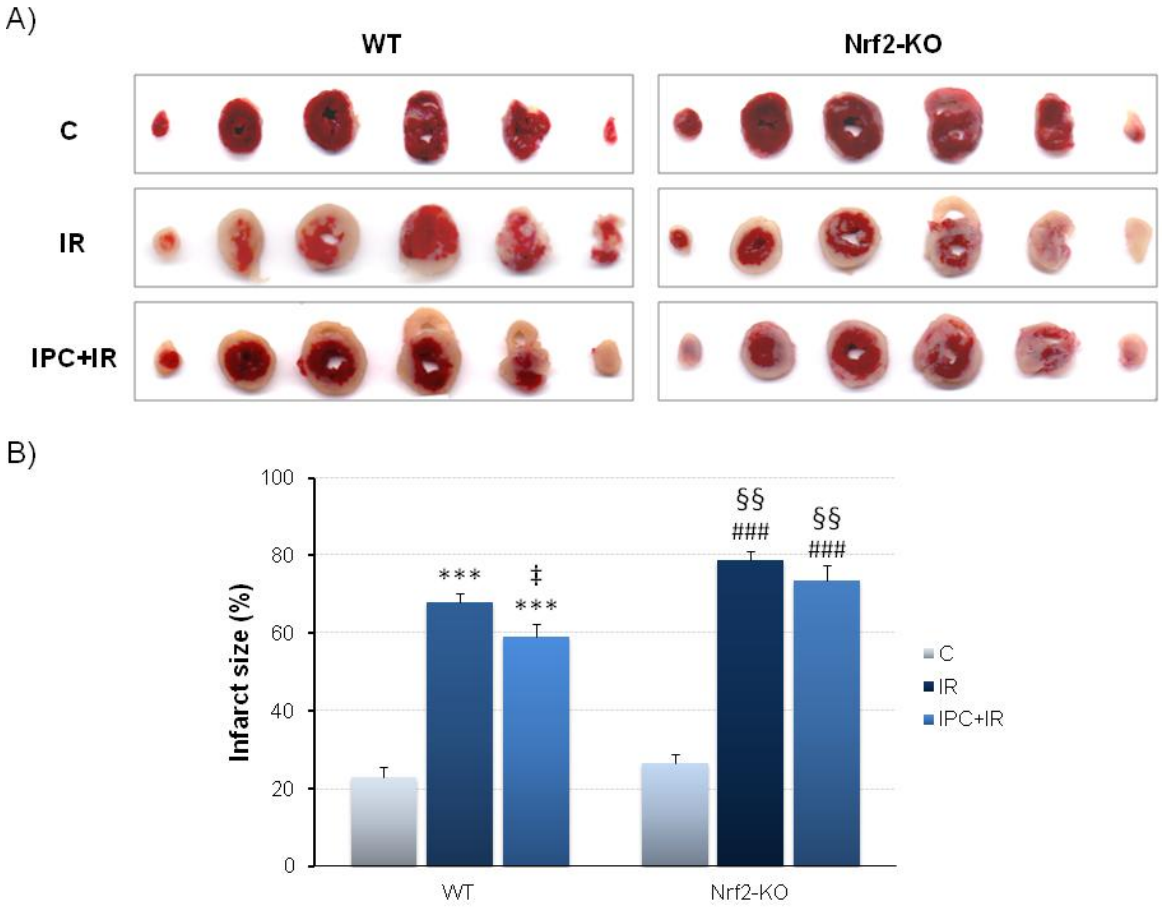

***Fig. 52*. Effect of IPC on the infarct size in Nrf2-KO and wild-type hearts.** A) Representative images of heart slices from isolated perfused hearts from Nrf2-KO and wild-type (WT) mice subjected to IR or IPC+IR and stained with tetrazolium chloride (TTC). The viable area was stained in red, while the infarcted area remained white. B) The histogram shows the means ± SEM of the percentage of infarct size (death area with respect to total area) of Nrf2-KO and wild-type hearts subjected to the different protocols (C, IR and IPC+IR) from 9 (C) or 11-13 (IR and IPC+IR) mice per group. ***$P < 0.001$ with respect to WT control (C). $^{‡}P < 0.05$ IPC with respect to IR. $^{###}P < 0.001$ with respect to Nrf2-KO control (C). $^{§§}P < 0.01$ Nrf2-KO IR and IPC with respect to WT of the same condition. C, control; IR, ischemia-reperfusion; IPC, ischemic preconditioning.

We also determined the CK activity in the coronary effluent during IPC and at different times of reperfusion in isolated perfused hearts from Nrf2-KO and wild-type mice (*Fig. 53*). The results showed that, as expected, IPC *per se* did not generate tissue damage either in Nrf2-KO or wild-type hearts (*Figs. 53A and B*). By contrast, CK increased at reperfusion after 40 min ischemia, especially during the first 5 min. In agreement with the infarct size data, Nrf2-KO mice had a significantly higher CK activity during reperfusion (*Figs. 53A and B*). Correspondingly, the total area under the curve (AUC) of CK release was higher in Nrf2-KO compared to wild-type mice. Taken together, these results support the involvement of Nrf2 in IPC and its protective role against IR injury.

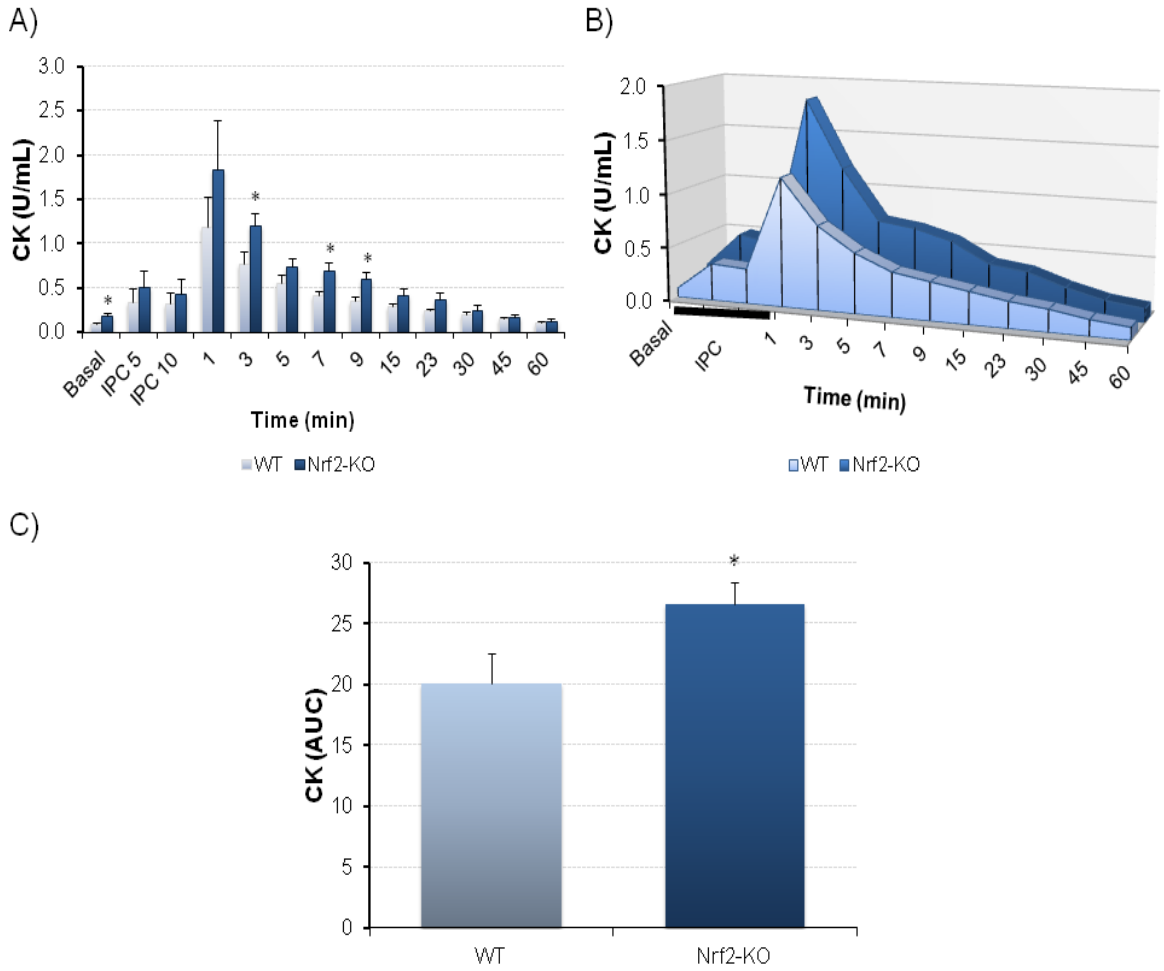

***Fig. 53*. Creatine kinase (CK) release from isolated perfused hearts from Nrf2-KO and wild-type mice subjected to IPC+IR**. A) Creatine kinase (CK) activity (U/mL) released before ischemia (basal), during IPC and at different time points during reperfusion up to 60 min in Nrf2-KO and wild-type (WT) hearts. The histogram shows the means ± SEM of CK (U/mL) from 9-10 hearts per group B) Total enzymatic activity (U/mL) of CK measured in the coronary effluent during IPC+IR in Nrf2-KO and WT mice. C) The histogram shows the means ± SEM of the area under the curve (AUC) from 9-10 hearts per group. **P* < 0.05 with respect to WT mice. Basal, after 20 min stabilization (time 0). IPC, ischemic preconditioning.

We also compared the activity of CK released during reperfusion in Nrf2-KO and wild-type hearts subjected to IR with or without IPC (*Fig. 54*). For this, we determined the activity of CK at different time points up to 60 min during reperfusion.

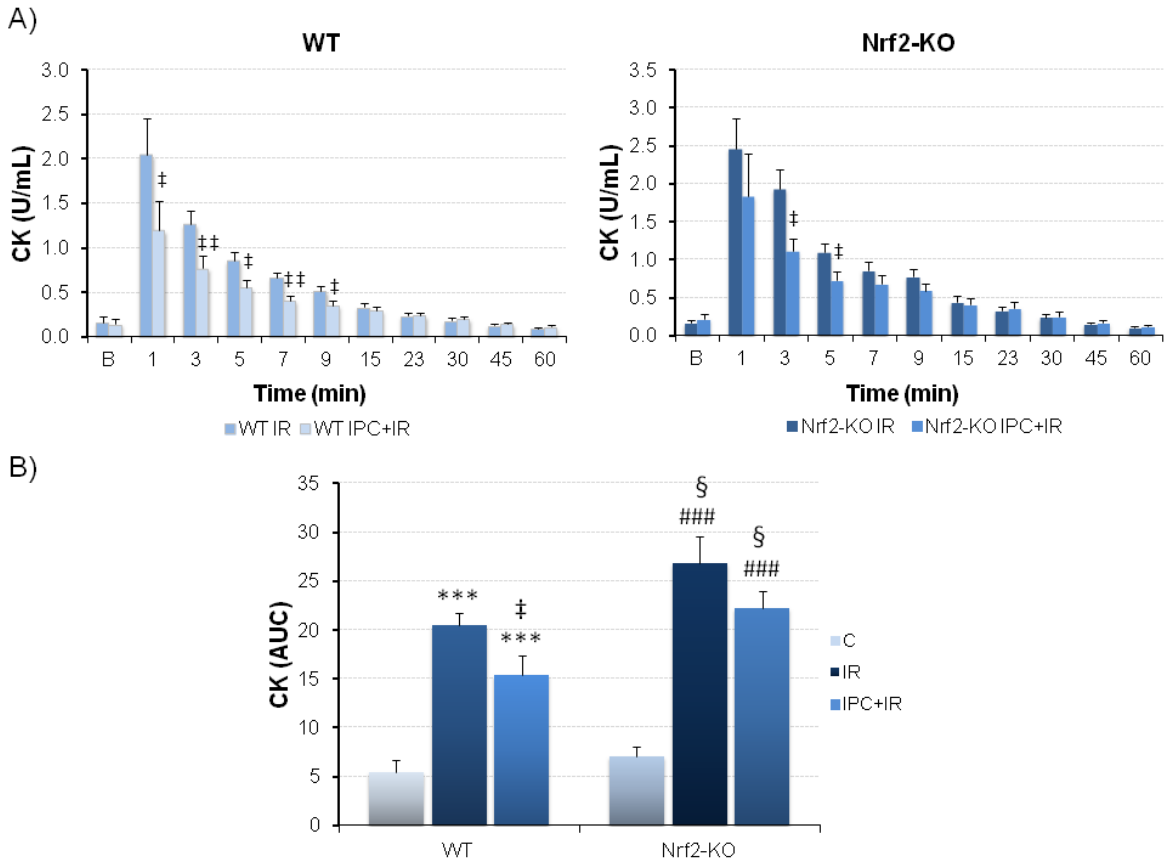

***Fig. 54*. Reperfusion levels of creatine kinase (CK) activity in the coronary effluent of isolated perfused hearts from Nrf2-KO and wild-type mice subjected to IR and IPC+IR.** A) The histograms show the means ± SEM of the enzymatic U/mL of CK measured in the coronary effluent at different times during reperfusion of 11-13 hearts per group, from Nrf2-KO and wild-type (WT) mice subjected to IR or IPC+IR. B) The histogram shows the means ± SEM of the area under the curve (AUC) of the total CK released from 8-9 hearts per C group and 11-13 per IR and IPC+IR groups. ***$P < 0.001$ with respect to WT control (C). $^{###}P < 0.001$ with respect to Nrf2-KO control (C). $^{‡}P < 0.05$, $^{‡‡}P < 0.01$ IPC with respect to IR. $^{§}P < 0.05$ Nrf2-KO IR and IPC with respect to WT of the same condition. C, control; IR, ischemia-reperfusion; IPC, ischemic preconditioning.

Our results show that CK activity in Nrf2-KO mice is higher than in wild-type mice after IR, consistent with the data in *Fig. 49*. Similar to infarct size, IPC partially prevented the increased in CK activity in the wild-type, but did not have a significant effect on Nrf2-KO mice (*Fig. 54*). Therefore, we conclude that Nrf2 is involved in the cardioprotective phenomenon of IPC.

DISCUSSION

Reactive oxygen species (ROS), natural by-products of aerobic respiration, are important cell signaling molecules. However, an excessive and/or sustained increase in ROS production has been implicated in the pathogenesis of cancer, diabetes mellitus, atherosclerosis, neurodegenerative diseases, rheumatoid arthritis, ischemia-reperfusion injury and other diseases (Lenaz, 2012). Mitochondria are a main source of ROS in cells (Murphy, 2009; Wong *et al.*, 2017). The production of superoxide by the mitochondrial ETC is very sensitivity to the electrochemical proton gradient or protonmotive force (Δp) across the inner mitochondrial membrane (Korshunov *et al.*, 1997; Starkov and Fiskum, 2003). Mild uncoupling of mitochondrial oxidative phosphorylation has been suggested as a cytoprotective strategy under conditions of oxidative stress (Hoerter *et al.*, 2004; Nishikawa *et al.*, 2000; Speakman *et al.*, 2004). Mitochondrial uncoupling proteins UCP2 and UCP3 play an important role in the control of ROS production by the ETC (Mailloux and Harper, 2011). These proteins are activated by ROS or ROS-derived products to induce proton leak, thus providing a negative feedback loop for mitochondrial ROS production (Aguirre and Cadenas, 2010; Echtay *et al.*, 2003, 2002). Moreover, they are controlled by covalent modification by glutathione (Mailloux *et al.*, 2011). Previous work from our laboratory, aimed at understanding the regulation of UCP3 expression in response to oxidative stress, showed that UCP3 is upregulated after the treatment with H_2O_2 or HNE, and that this effect is mediated by the antioxidant transcription factor Nrf2 (Anedda *et al.*, 2013; López-Bernardo *et al.*, 2015). Likewise, we showed that isolated perfused hearts from mouse subjected to ischemia-reperfusion (IR) or ischemic preconditioning (IPC) increase UCP3 expression and Nrf2 nuclear accumulation (Anedda *et al.*, 2013). The restoration of blood flow after a prolonged ischemia induces a burst of ROS production from the respiratory chain (Chouchani *et al.*, 2014; Zweier and Talukder, 2006), which causes macromolecular damage and the opening of the permeability transition pore (mPTP) in mitochondria (Halestrap and Richardson, 2015; Hausenloy and Yellon, 2013). Given the importance of the modulation of ROS production in IR injury and the relatively unexplored role of UCP3 and Nrf2 in this pathology, we considered important to study the protective role of UCP3 and Nrf2 against IR injury and their involvement in IPC, as well as their regulation under hypoxic conditions, after hypoxia/reoxygenation or after simulated ischemia-reperfusion (SIR). Indeed, this was the starting point of the work carried out in this thesis.UCP3 has been suggested to play also an important role in regulating fatty acid metabolism, and its overexpression increases fatty acid transport and oxidation (Bezaire *et al.*, 2005; Seifert *et al.*, 2008). Therefore, we aimed at studying the alterations in metabolites related to fatty acid oxidation and other metabolic pathways in isolated perfused hearts from wild-type and UCP3 knockout mice subjected to IR. We thought these studies could contribute to better understand the role of UCP3 and Nrf2 in the heart, and help to clarify both the pathogenic mechanism of IR injury and the endogenous protective phenomenon of IPC.

1. UCP3 expression and Nrf2 activation increase in response to oxidative stress and hypoxia in HL-1 and C2C12 cells

In the first part of this thesis, we studied the effect of two types of cellular stress, oxidative stress and hypoxia, on UCP3 expression and Nrf2 activation. Under normal conditions, the oxidant H_2O_2 and the alkenal HNE, a strong electrophilic compound, are present in cells at low concentrations and act as signalling molecules. However, at high concentrations they become cytotoxic, compromising cell viability (Łuczaj *et al.*, 2017; Sies, 2017). We used sub-lethal concentrations of H_2O_2 (300 µM) and HNE (20 µM) that cause oxidative stress but do not affect cell viability, as shown in previous work from our laboratory (Anedda *et al.*, 2013; López-Bernardo *et al.*, 2015). The results obtained indicate that sub-lethal concentrations of H_2O_2 and HNE upregulate UCP3 and induce the nuclear accumulation of Nrf2 in HL-1 cells, confirming our previous results. HNE and other lipid peroxidation products act as second messengers of free radicals, as they are more stable and diffuse easily, affecting distant targets and enabling their participation in a diverse number of cellular events. HNE is also a known activator of UCPs, inducing mild uncoupling and contributing to ROS reduction by decreasing the mitochondrial membrane potential (Echtay *et al.*, 2003). As stated above, the cellular effects of HNE may induce both damaging and cytoprotective actions, depending on its concentration (Chapple *et al.*, 2013). Thus, high concentrations of HNE can inhibit cellular processes, inducing cellular damage and resulting in apoptosis (Esterbauer *et al.*, 1993, 1991), whereas relatively low concentrations of HNE produced in response to mild oxidative challenge appear to modulate normal physiological processes including the upregulation of endogenous antioxidant defense pathways (Ishii *et al.*, 2004; Zhang *et al.*, 2010). Likewise, physiological concentrations of H_2O_2 have a role in redox signaling, higher concentrations lead to adaptive stress responses, and supraphysiological concentrations lead to damage to biomolecules and oxidative stress (Marinho *et al.*, 2014; Sies, 2017).

Nrf2 activates the cellular antioxidant defenses and modulates oxidative stress, via the upregulation of the expression of various genes such as heme oxygenase-1 (HO-1), aldehyde dehydrogenases (ALDH), glutathione S-transferase (GST), multidrug-resistance proteins (MRP), NAD(P)H quinone oxidoreductase (NQO1) or glutamate-cysteine ligase catalytic subunit (Gclc) (Ma, 2013). In our previous works, we showed that the activation of Nrf2 induced by H_2O_2 and HNE and the subsequent upregulation of UCP3, confirmed in this thesis, promotes survival under conditions of oxidative damage (Anedda *et al.*, 2013; López-Bernardo *et al.*, 2015). Several authors have reported a protective role to sub-toxic concentrations of H_2O_2 and HNE mediated by Nrf2. Thus, a mild dose of H_2O_2 (100 µM) induces Nrf2-dependent antioxidant/detoxyfication genes and elicits resistance against doxorubicin-induced apoptosis in cardiomyocytes (Purdom-Dickinson *et al.*, 2007a). Mild oxidative stress, including sub-toxic H_2O_2, activates Nrf2/ARE-

dependent gene expression in astrocytes, which contributes to neuroprotective IPC (Bell *et al.*, 2011). Similarly, Nrf2 is a key transcriptional regulator for the HNE-mediated induction of antioxidant defenses in cardiomyocytes and in isolated perfused hearts (Dalleau *et al.*, 2013; Zhang *et al.*, 2010).

Lu and Sack (2008) reported that UCP3 expression increases in hypoxia (5% O_2) in mouse C2C12 and rat L6 myotubes, and that this effect is mediated by ATF-1. Our hypoxia time-course experiment showed that UCP3 expression also increases at 1% O_2 in C2C12 myotubes and HL-1 cardiomyocytes. This increase in UCP3 expression was significant at 16 and 24 h and occurred with similar magnitude in both cell lines (around 2.5-fold). Other authors also found an increase in UCP3 expression in skeletal muscle of rats after acute exercise or exposure to hypoxic conditions (10% O_2) (Zhou *et al.*, 2000). The increase in UCP3 expression after acute exercise has been suggested to have an antioxidant function against ROS production (Jiang *et al.*, 2009). Moreover, we found that hypoxia increases Nrf2 nuclear accumulation, in agreement with previous reports in rat cardiomyoblasts (H9C12) subjected to hypoxia (2% O_2), which demonstrated Nrf2 activation and enhanced cell survival under these conditions (Kolamunne *et al.*, 2013).

Here we tested whether the increase in UCP3 and Nrf2 in response to hypoxia was due to new protein synthesis. To address this question, some cells were treated with the protein synthesis inhibitor cycloheximide (CHX) at different times of exposure to hypoxia (1% O_2). The treatment with CHX prevented UCP3 induction in response to hypoxia, an effect that was more evident at 24 h of exposure to low oxygen concentrations. These results suggest that the increase of UCP3 expression in hypoxia is due to new protein synthesis. UCP3 has an exceptionally short half-life (0.5-4 h) compared to that of other mitochondrial proteins such as ANT or UCP1 (Azzu *et al.*, 2010a) and is degraded by the 26S proteasome system (Mookerjee and Brand, 2011). We cannot discard that the increase in UCP3 expression is also due to the inhibition of UCP3 degradation during hypoxia. UCP3 degradation by the 26S proteasome requires matrix ATP and is very sensitive to the membrane potential (Mookerjee and Brand, 2011). Hypoxia reduces ATP so this could negatively affect UCP3 degradation and therefore increase its expression. We also observed that Nrf2 expression in the nucleus in hypoxia was reduced in the presence of CHX, although not significantly, which indicates that there must be some new protein synthesis. Regulation of Nrf2 levels and its activity occurs at several levels, including transcription, translation, degradation, translocation and post-translational modifications such as phosphorylation. One of the most important mechanisms to increase Nrf2 protein levels involves a decreased rate of Nrf2 protein degradation (Kobayashi *et al.*, 2006; Zhang *et al.*, 2004). However, Nrf2 *de novo* synthesis is an important mechanism for the rapid Nrf2 upregulation by oxidative stress (Purdom-Dickinson *et al.*, 2007b, 2007a; Xu *et al.*, 2014). Thus, the treatment with mild doses of H_2O_2 causes a rapid increase in endogenous Nrf2 protein levels in rat cardiomyocytes, through a process that is

independent of Nrf2 protein stabilization. H_2O_2 stress, therefore, could cause selective protein translation, resulting in a rapid increase of Nrf2 protein.

The parallel increase in UCP3 expression and Nrf2 nuclear accumulation suggests that Nrf2 could be involved in UCP3 upregulation under hypoxia, similar to what we found under conditions of oxidative stress (Anedda *et al.*, 2013; López-Bernardo *et al.*, 2015). However, additional experiments are required to confirm this hypothesis.

2. Hypoxia/reoxygenation increases UCP3 expression and Nrf2 activation, enhances mitochondrial superoxide production and induces cell death

In the previous section, we showed that UCP3 expression and Nrf2 activation increase under hypoxia. Likewise, we found that reoxygenation (4 h) after hypoxia (1% O_2, 24 h) induced both UCP3 expression and Nrf2 nuclear accumulation in HL-1 cardiomyocytes, and that these inductions were more evident than those elicited by hypoxia alone. We wondered whether Nrf2 activation could be due to increased ROS production in these conditions. As explained in the Introduction, the generation of ROS in hypoxia is controversial (Clanton, 2005). A positive correlation between oxygen concentration and superoxide generation has been observed in isolated mitochondria (Hoffman *et al.*, 2007) and cells (Sgarbi *et al.*, 2017) due to the low availability of oxygen, which acts as the electron acceptor. However, it has also been shown that hypoxia facilitates the reduction of oxygen to superoxide, as hypoxia might slow the rate of electron transport increasing the reduction of ETC components and the likelihood of superoxide generation (Guzy and Schumacker, 2006; Hamanaka and Chandel, 2009). In contrast to hypoxia, it is well established that reoxygenation induces a burst of ROS production (Granger and Kvietys, 2015).

To study whether hypoxia or hypoxia/reoxygenation could increase ROS production, which may in turn induce Nrf2 activation, we determined mitochondrial superoxide generation after hypoxia or hypoxia/reoxygenation in C2C12 and HL-1 cells. Our experiments using the fluorescent probe MitoSOX Red showed that superoxide increased significantly in cells subjected to hypoxia/reoxygenation compared to control cells. Superoxide levels, however, decreased after the exposure to hypoxia for 24 h with respect to normoxic values. These results are in line with the reports mentioned above that showed a positive correlation between oxygen concentration and superoxide production (Hoffman *et al.*, 2007; Sgarbi *et al.*, 2017) and with the broadly accepted concept of increased ROS production at reperfusion (Granger and Kvietys, 2015). Another report proposes that cells respond to hypoxia with a transient increase in superoxide production for about 10 min (Hernansanz-Agustín *et al.*, 2014). This is also compatible with our data obtained after exposure of the cells to hypoxia for 24 h.

MitoSOX Red (mito-hydroethydine) consists of hydroethidine conjugated to triphenylphosphonium cation (TPP^+) (Robinson *et al.*, 2006). The redistribution of positively

charged MitoSOX Red across the inner mitochondrial membrane depends on the membrane potential. Consequently, evaluation of mitochondrial membrane potential is essential to accurately determine intramitochondrial ROS with this probe (Polster *et al.*, 2014). We therefore analyzed $\Delta\psi_m$ using TMRM (tetramethylrhodamine methyl ester). Our results showed that hypoxia increases $\Delta\psi_m$ significantly compared to normoxia, but reoxygenation returns $\Delta\psi_m$ values to basal levels. Taking these data into account, we confirmed the presence of low mitochondrial superoxide in hypoxia and its increase upon reoxygenation. Besides, increased ROS levels could also explain the activation of Nrf2 and UCP3 upregulation at reoxygenation, but point to a different inducer of this transcription factor and a different mediator of UCP3 upregulation during hypoxia.

In addition to mitochondrial superoxide production, we determined cell viability and caspase-3 levels in HL-1 cells after exposure to hypoxia or hypoxia/reoxygenation. Activated caspase-3 is an important marker of apoptosis. Although hypoxia increased caspase-3 levels, it did not affect cell viability. By contrast, hypoxia/reoxygenation increased both caspase-3 levels and cell viability. Several studies have reported an increase in caspase-3 in cardiomyocytes following hypoxia/reoxygenation (Uchiyama *et al.*, 2004; Zhang *et al.*, 2016). In addition, Freude *et al.* (2000) showed that apoptotic cell death is initiated by ischemia but reperfusion is essential for completion of the apoptotic cascade. Importantly, the execution of apoptosis requires energy, so the depletion of cellular ATP will likely interrupt the apoptotic process (Shiraishi *et al.*, 2001; Tatsumi *et al.*, 2003). These authors proposed that, in the ischemic myocardium, cells are depleted of ATP and forced to die by necrosis; however, upon restoration of sufficient ATP levels, the cells resume the apoptotic process. It would be interesting to test whether ATP is reduced or depleted in HL-1 cells under hypoxic conditions.

We next studied the effects of simulated ischemia and simulated ischemia-reperfusion (SIR) on UCP3 expression and Nrf2 activation in HL-1 cells. For these analyses, the cells were subjected to oxygen and glucose deprivation (OGD) for 2 h followed by the reestablishment of normal oxygen and glucose concentrations for 4 h. Similar to hypoxia and hypoxia/reoxygenation, simulated ischemia and SIR upregulated UCP3 expression and induced the nuclear accumulation of Nrf2. We also analyzed oxidative stress after simulated ischemia or SIR. During lipid peroxidation, 4-hydroxy-2-nonenal (HNE) is produced at high levels and easily reacts with both low molecular weight compounds and macromolecules, such as proteins and DNA (Barrera *et al.*, 2015). Thus, the content of HNE-protein adducts is a reliable marker of oxidative stress. HNE-protein adducts increased after SIR but not during simulated ischemia. These results agree with those obtained in HL-1 cells subjected to hypoxia or hypoxia/reoxygenation, and indicate that although Nrf2 activation and UCP3 upregulation can be mediated by increased ROS under SIR, there must be another mediator during simulated ischemia. Nrf2 activation during hypoxia or hypoxia/reoxygenation enhances survival in H9C2 cardiomyoblasts (Kolamunne *et al.*, 2013).

Similarly, the increase in UCP3 may represent a mechanism to counteract ROS production, as described in cardiomyocytes subjected to anoxia-reoxygenation (McLeod *et al.*, 2005; Sack, 2006).

3. ATF-1 might regulate UCP3 and Nrf2 under hypoxic conditions

We found that hypoxia/reoxygenation or SIR increases the production of ROS, which may in turn activate Nrf2. This transcription factor could mediate the upregulation of UCP3 under these conditions, as we reported to occur in response to oxidative stress (Anedda *et al.*, 2013; López-Bernardo *et al.*, 2015). Hypoxia or simulated ischemia, by contrast, do not increase ROS production, so there must be other pathways involved in Nrf2 activation and UCP3 upregulation in these situations. As mentioned above, UCP3 expression has been reported to increase in hypoxia via ATF-1 (Lu and Sack, 2008). Moreover, CREB-binding protein (CBP)-induced acetylation of Nrf2 regulates its transcriptional activity and nuclear localization (Kawai *et al.*, 2011). Furthermore, ATF-1 and Nrf2 are structurally related, basic zipper transcription factors, so some authors raised the hypothesis of ATF-1/Nrf2 heterodimerization (Boyle *et al.*, 2012). Taking all into consideration, we measured ATF-1 phosphorylation (Ser-133) in HL-1 cardiomyocytes under hypoxia or hypoxia/reoxygenation, as well as under simulated ischemia or SIR. ATF-1 phosphorylation increased in all these conditions. These results support the aforementioned report showing that UCP3 regulation in hypoxia is mediated by ATF-1 (Lu and Sack, 2008). Since ATF-1 phosphorylation also correlates with Nrf2 activation, we speculate about a possible cooperation between these factors. Obviously, additional experiments are necessary to test this hypothesis.

We performed a series of experiments using the p38 MAPK inhibitor SB203580 to study the involvement of this kinase on ATF-1 phosphorylation and UCP3 upregulation in hypoxia in HL-1 and C2C12 cells. ATF-1 phosphorylation was prevented in hypoxia in both cell lines in the presence of SB203580, indicating that ATF-1 phosphorylation is mediated by p38 MAPK in these conditions. Moreover, the inhibitor prevented the increase in UCP3 expression in hypoxia, strongly suggesting that ATF-1 phosphorylation is p38 MAPK-dependent, consistent with data reported previously (Lu and Sack, 2008). Similarly, p38 MAPK inhibition prevented Nrf2 activation and HO-1 upregulation in hypoxia, thus implicating p38 MAPK in ATF-1 phosphorylation that would lead to Nrf2 nuclear translocation. Cerebral ischemia also triggers CREB phosphorylation and CRE-mediated gene expression in neurons (Sugiura *et al.*, 2004), which is believed to be a protective response against ischemic injury (Kitagawa, 2007). Of note, p38 MAPK plays a negative role in the regulation of Nrf2 transactivation domain activity, whereas Raf facilitates Nrf2 activation through the coactivator CBP (Shen *et al.*, 2004; Yu *et al.*, 2000). Moreover, the induction of HO-1 expression by lipid oxidation products has been shown to occur via CREB (Krönke *et al.*, 2003).

We also measured caspase-3 levels in hypoxia in the presence of the p38 MAPK inhibitor S203580. Caspase-3 increased significantly in HL-1 cells in hypoxia regardless of the inhibitor, but only increased significantly in C2C12 skeletal muscle cells in the presence of the inhibitor. It has been reported that p38 MAPK-mediated Bax migration to mitochondria, which can be blocked by SB203580, is an early event in myocardial ischemia that occurs downstream of AMPK activation in isolated rat neonatal cardiomyocytes (Capano and Crompton, 2006). However, we did not find any negative effect of the inhibitor on caspase-3 expression and, although we did not determine cell death, we postulate that other pathways apart from p38 MAPK/Bax could mediate apoptosis in hypoxia.

The results obtained in C2C12 and HL-1 cells subjected to hypoxia, hypoxia/reoxygention, simulated ischemia and SIR, and discussed in sections 1-3, are summarized in *Fig. 55*.

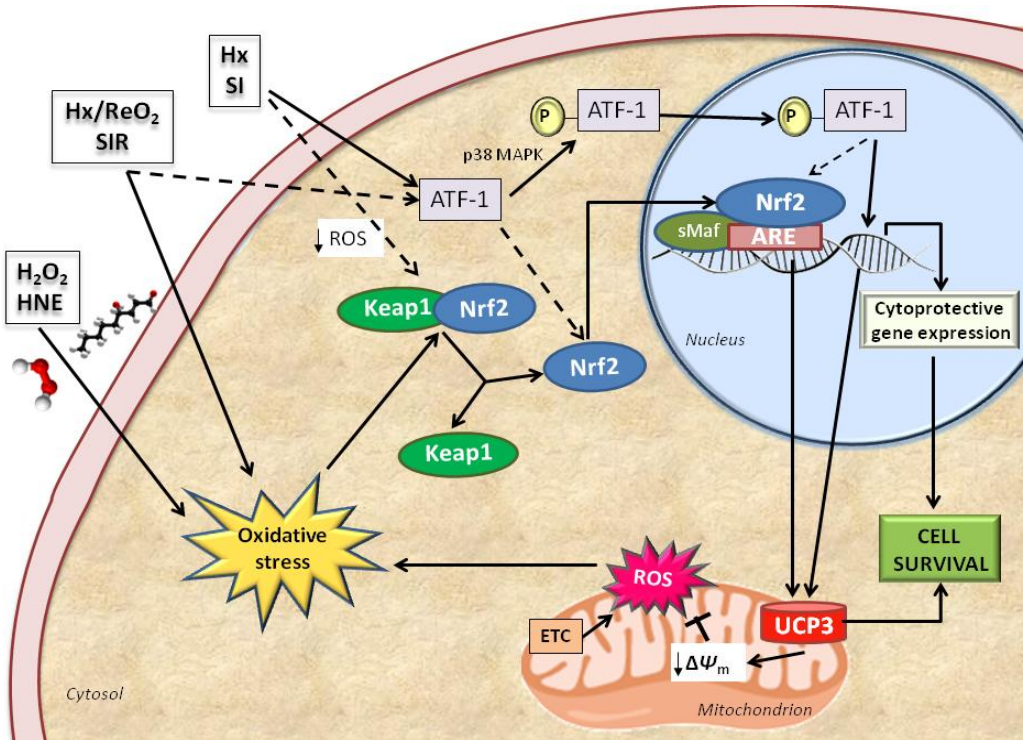

***Fig. 55*. Schematic model of the regulation of UCP3 expression in response to cellular stress and signaling pathways involved.** Hypoxia or simulated ischemia (SI) are proposed to induce the expression of UCP3 via p38 MAPK/ATF-1. Conditions leading to increase oxidative stress such as hypoxia/reoxygenation or simulated ischemia-reperfusion (SIR), as well as the treatment with H_2O_2 or HNE, are proposed to induce the expression of UCP3 via Nrf2. The upregulation of UCP3 by either these two pathways leads to a slight decrease of the mitochondrial membrane potential ($\Delta\psi_m$) (mild uncoupling), reducing superoxide generation by the ETC and promoting cell survival. Activated Nrf2 also induces the expression of cytoprotective genes.

4. Adult and aged UCP3 knockout mice are more susceptible to cardiac IR injury than wild-type mice, present altered content of cardiac metabolites and exhibit a slight cardiac dysfunction

Acute myocardial infarction is a leading cause of morbidity and mortality worldwide (Hausenloy and Yellon, 2013; Murray and Lopez, 1997). Although highly beneficial, prompt myocardial reperfusion is paradoxically associated with cellular injury including cardiomyocyte death (Granger and Kvietys, 2015; Piper *et al.*, 1998). Therefore, novel treatment strategies are required to protect the heart during myocardial reperfusion (Bulluck *et al.*, 2016; Hausenloy *et al.*, 2010). Clearly, understanding the mechanisms underlying ischemia tolerance would help develop cardioprotective strategies.

The experiments performed in HL-1 and C2C12 cells revealed an upregulation of UCP3 during hypoxia/reoxygenation or SIR that could be protective against ROS-induced damage. Moreover, previous work from our laboratory showed that UCP3 expression increases in isolated perfused mouse hearts after IR and IPC (Anedda *et al.*, 2013). Similarly, UCP2 and UCP3 expression increase in rat hearts after IR (Safari *et al.*, 2014). In this thesis, we studied the cardioprotective role of UCP3 against *ex vivo* and *in vivo* IR damage. For this, we analyzed the ischemic damage in isolated perfused hearts (Langendorff system) from UCP3 knockout (UCP3-KO) and wild-type mice subjected to IR, as well as the infarct area of these mice subjected to left anterior descending (LAD) coronary artery ligation followed by reoxygenation.

We initially studied Nrf2 activation and ATF-1 phosphorylation in isolated perfused hearts from UCP3-KO and wild-type mice after IR or IPC+IR. Both treatments increased Nrf2 nuclear accumulation and ATF-1 phosphorylation in these mice. The increase in the activation of these factors was higher in UCP3-KO that in wild-type mice after IR. Moreover, the Nrf2 target HO-1 followed a similar expression pattern. These results support our *in vitro* data in C2C12 and HL-1 cells and our previous report about Nrf2 activation in wild-type hearts after IR or IPC+IR (Anedda *et al.*, 2013). UCP3 regulates ROS levels and cell survival during hypoxia (2% O_2) and modulates infarct size in the ischemic heart (Ozcan *et al.*, 2013; Perrino *et al.*, 2013). UCP3 also mediates proton leak and protects against ROS during IPC (Nadtochiy *et al.*, 2006; Ozcan *et al.*, 2013). The enhanced Nrf2 and ATF-1 activation in the absence of UCP3 might represent a mechanism to compensate the lack of this protective protein.

Cell death is an important component in the pathogenesis of IR injury. Both necrosis and apoptosis occur during ischemia, while the reperfusion event increases apoptosis (Eefting *et al.*, 2004; Konstantinidis *et al.*, 2012). We determined caspase-3 activation as a marker of apoptosis during the different perfusion protocols. Caspase-3 expression increased in both IR and IPC+IR in UCP3-KO and wild-type mice. The expression was higher in UCP3-KO mice compared to wild-

type mice after IR. The apoptotic pathway is therefore activated during IR and IPC+IR, although we cannot exclude the coexistence of other events such as necrosis or autophagy, which also occur in IR (Li *et al.*, 2016). Previous reports also showed significantly higher caspase-3 in UCP3-KO than in wild-type hearts after IR (Perrino *et al.*, 2013). However, conditional expression of UCP3 in 293 cells does not lead by itself to apoptosis but increases the responsiveness of the cells to a mitochondrial apoptotic stimulus, enhances caspase-3 and caspase-9 activation and favors cytochrome *c* release (Dejean *et al.*, 2004). Interestingly, activation of caspase-3 without cell death has been reported as a mechanism for neuroprotection in preconditioning (McLaughlin *et al.*, 2003). Although most studies have shown that early IPC reduces necrotic and apoptotic cell death, it is not clear whether IPC inhibits apoptosis and related mechanisms (Zhao and Vinten-Johansen, 2002). Taking everything into account, these data suggest that UCP3 levels regulate cell survival after cardiac IR or IPC.

We also studied the possible cardioprotective role of UCP3 against cardiac IR in the intact heart. This study was performed in adult (20-22 weeks) and aged (78-80 weeks) UCP3-KO and wild-type mice. Due to the imbalance between antioxidant levels and ROS production, aging is characterized by increased oxidative stress (Beckman and Ames, 1998; Harman, 1956). The antioxidant capacity decreases with age, as does the ability to adjust to diverse environmental or physiological challenges (Jones, 2015). In addition, aged hearts exhibit impaired metabolic flexibility, with a decreased capacity to oxidize fatty acids and enhanced dependence on glucose metabolism (Lesnefsky *et al.*, 2016). Hence, with our experimental approach we tried to answer two questions: first, whether UCP3 is involved in the protection of the heart against IR injury, and second, whether aged mice lacking UCP3 are more susceptible to cardiac IR injury than adult mice. Our data showed that hearts from both adult and aged UCP3-KO mice have larger infarct sizes than those from wild-type mice. Although the infarct size in the wild-type mice was similar in both age groups, it was significantly larger in UCP3-KO hearts from aged than adult mice. The activity of creatine kinase, a marker of infarct damage, also increased in UCP3-KO compared to wild-type hearts. In agreement with the infarct size measurements, the creatine kinase enzymatic activity was higher in aged than in adult UCP3-KO mice. These results indicate that UCP3 is involved in the protection of the heart against IR injury, and that aged UCP3-KO mice are more susceptible to this damage than adult mice. Our results agree with others suggesting a protective effect of UCP3 against cardiac IR injury (Ozcan *et al.*, 2013; Perrino *et al.*, 2013). However, to our knowledge, there are not studies about this protective role of UCP3 in aged mice. There are, nevertheless, reports showing that UCP3 overexpression blunts the age-related increased ROS production and mitochondrial dysfunction (Nabben *et al.*, 2008), and a marked decrease in UCP3 with aging (Kerner *et al.*, 2001; Lee *et al.*, 2002). Of note, UCP3 does not significantly affect longevity in mice (McDonald *et al.*, 2008).

Supporting the results obtained *ex vivo* in Langendorff perfused hearts, we found that UCP3-KO mice subjected to LAD coronary artery ligation had larger infarct areas than wild-type mice. This was evident 21 days after the surgical procedure, when the animals were sacrificed and the hearts were stained with hematoxylin-eosin and Masson's trichrome. These results are consistent with those previously reported (Ozcan *et al.*, 2013; Perrino *et al.*, 2013). Taken together, these data suggest that UCP3 levels regulate cell survival and infarct size after IR, and that this uncoupling protein plays an important role in the protection of the heart against IR injury.

Despite the larger infarct size in UCP3-KO hearts after IR and the increased creatine kinase activity in the coronary effluent, the echocardiographic study did not reveal apparent important functional consequences for the absence of UCP3. Both types of mice have similar alterations in cardiac function. For example, they have a reduced ejection fraction (EF) and increased values for the LV posterior wall (LVPW) thickness and the left atrial diameter (LAd), which indicate heart dysfunction. After 45 min LAD ligation, UCP3-KO hearts tended to have higher LV volumes, reflecting left ventricular dysfunction. Following this protocol, UCP3-KO hearts also had a tendency to present higher infarct damage as determined by the score for the LV wall motion and thickening. Other authors have shown that isolated perfused UCP3-KO hearts have poorer recovery of left ventricular function compared to wild-type hearts after IR (Ozcan *et al.*, 2013). Moreover, the incidence of *in vivo* arrhythmias was higher in UCP3-KO mice. In connection with this, we found an altered QRS duration in these mice. Since calcium ions are essential in normal cardiac function, particularly in excitation-contraction coupling and electrical rhythms (Landstrom *et al.*, 2017), it would be interesting to determine calcium signaling and homeostasis in these mice.

In addition to its role in the modulation of mitochondrial ROS production, UCP3 appears to be involved in promoting fatty acid oxidation, and hence it is likely to influence glucose metabolism indirectly (Bezaire *et al.*, 2005; Giralt and Villarroya, 2016; Schrauwen *et al.*, 2006). In order to study possible alterations in metabolism that could explain the increased sensitivity of UCP3-KO mice to cardiac IR injury, we performed a metabolomics study in isolated perfused hearts from UCP3-KO and wild-type mice subjected to different perfusion protocols: ischemia, IR and IPC+IR. We analyzed 92 metabolites related to carbohydrate, lipid, amino acid and nucleotide metabolism. A number of metabolites have been described to accumulate during ischemia, such as succinate, fumarate, lactate and the metabolites of purine nucleotide catabolism, xanthine and hypoxanthine (Chouchani *et al.*, 2014; Hausenloy and Yellon, 2013). Anaerobic metabolism during ischemia leads to a rise in lactate levels. Xanthine and hypoxanthine are by-products of purine nucleotide breakdown in ischemic hearts (Harmsen *et al.*, 1981). Dihydrothymine is a breakdown product of thymine. These metabolites increased significantly during ischemia in both genotypes and returned to near basal values upon reoxygenation, corroborating the validity of our approach. Interestingly, these values tended to be higher in UCP3-KO than in wild-type hearts.

The intermediate of the Krebs cycle succinate is a mitochondrial feature of ischemia that occurs universally in a range of metabolically diverse tissues (Chouchani *et al.*, 2016, 2014). Succinate accumulates dramatically during ischemia and it is then rapidly metabolized upon reperfusion simultaneously with mitochondrial ROS production increases. Chouchani and col. (2014) showed that succinate accumulates during ischemia from fumarate reduction by the reversal of succinate dehydrogenase. The increase in fumarate was produced by the purine nucleotide cycle and the malate-aspartate shuttle, which consumed glucose and aspartate and led to significant production of lactate and alanine. Indeed, ischemic UCP3-KO and wild-type hearts presented remarkably reduced levels of glucose and high levels of lactate. The fact that UCP3-KO hearts present slightly higher values of succinate, fumarate and malate in ischemia could reflect and increased capacity of these hearts to generate damaging ROS during reperfusion.

Glycerate is obtained from the oxidation of glycerol, and several phosphate derivatives of glycerate are important intermediates in glycolysis. The abundance of this metabolite tended to decrease in ischemia and recover at reperfusion in both types of hearts, although the levels were lower in the UCP3-KO hearts. Moreover, glycerate remained low in preconditioned UCP3-KO hearts in contrast to wild-type hearts. This fact may relate to the loss of protective effect of IPC in mice lacking UCP3.

As mentioned above, UCP3 has been suggested to play an important role in the metabolism of fatty acids, and its overexpression increases fatty acid transport and oxidation (Bezaire *et al.*, 2005; Harmancey *et al.*, 2013; Hilse *et al.*, 2018). A role for UCP3 in the export of fatty acid anions from muscle and brown adipose tissue mitochondria when fatty acids are the predominant substrate was initially proposed (Himms-Hagen and Harper, 2001). Other authors proposed that this protein exported fatty acid peroxides from mitochondria thus preventing lipid-induced oxidative damage (Schrauwen *et al.*, 2006). It was later shown that UCP3 is not itself a fatty acid transporter, but was necessary for fasting-induced enhancement of fatty acid oxidation rate and capacity via mitigated oxidative stress (Seifert *et al.*, 2008). Our data shows that carnitine decreases in UCP3-KO hearts with respect to wild-type hearts after IR. Carnitine is essential for the transfer of long-chain fatty acids across the inner mitochondrial membrane (carnitine shuttle) for subsequent β-oxidation. In order for the acyl-CoA to enter the mitochondria, the acyl group is transferred from the sulfur atom of CoA to the hydroxyl group of carnitine to form acyl-carnitine (Ramsay *et al.*, 2001). This reaction is catalyzed by carnitine acyltransferase I (carnitine palmitoyltransferase 1, CPT1), which is bound to the outer mitochondrial membrane (McGarry and Brown, 1997). Carnitine is necessary for the recovery of lipid metabolism and oxidation of accumulated fatty acids during reperfusion after ischemia (Liedtke *et al.*, 1982). High concentrations of carnitine have been associated with antioxidant capacities as it reduces radical formation (Gülçin, 2006). Carnitine could also protect cardiac metabolism and function in ischemic myocardium by mechanisms such as a reduction of

the toxic effects of long-chain acyl-CoA and acyl-carnitine in myocytes, an increase in coronary blood flow and an anti-arrhythmic effect (Lango *et al.*, 2001). The reduced levels of carnitine in UCP3-KO hearts after IR suggest enhanced oxidative stress and lipid toxicity in these hearts.

Several enzymes of fatty acid oxidation and other pathways of the intermediary metabolism are damaged in isolated perfused mouse hearts after IR (Chen *et al.*, 2018). Moreover, reperfusion of the heart after myocardial ischemia results in high rates of fatty acid oxidation (Kudo *et al.*, 1995; Lopaschuk, 1997). We found that oleic and linoleic acids increased during ischemia and particularly after IR in both types of mice, probably due to impaired fatty acid oxidation. UCP3-KO hearts presented lower levels of both oleic and linoleic acids after IR and IPC. These altered levels of fatty acids in mice lacking UCP3 might reflect a deficient fatty acid metabolism that may lead to increased reperfusion damage.

The heart is capable of utilizing glucose, lactate, fatty acids, ketone bodies and certain amino acids as metabolic substrates. However, the heart's substrate preference under anaerobic conditions is not well understood. Amino acids are of particular interest due to their potential for non-oxidative metabolism and their low contribution to cellular acidification (Drake *et al.*, 2012). Since amino acids are synthesized in a wide variety of pathways and reactions, some amino acids are more readily converted to metabolic intermediates than others. Thus, amino acids like glutamate, glutamine, aspartate, asparagine and the branched chain amino acids, have been shown to be preferentially used as metabolic and anaplerotic substrates in the Krebs cycle during anoxia and ischemia (Mudge *et al.*, 1976). The analysis of amino acids revealed some differences between UCP3-KO and wild-type mice. Aspartate and asparagine abundance was low during ischemia, particularly in wild-type mice and recovered upon reperfusion, probably reflecting their use as metabolic substrates. The amide in asparagine is easily hydrolyzed, converting asparagine to aspartate. Alanine increased in ischemia in both types of hearts, most likely due to the activation of pathways feeding fumarate into the reverse activity of succinate dehydrogenase (Chouchani *et al.*, 2014), and it returned to control values upon reperfusion. Importantly, alanine is interchangeable with pyruvate via transamination. Hypotaurine is an intermediate in the biosynthesis of taurine, which is a very important amino acid for the heart (Huxtable, 1992). Taurine exerts cardioprotective effects by reducing the severity and rate of arrhythmias and improving contractile function. Hypotaurine increased in ischemia in both types of hearts but was drastically reduced after reperfusion only in UCP3-KO hearts. This could contribute to cardiac dysfunction at reperfusion in these hearts. Taurine levels, however, did not show significant differences between groups. Valine betaine follows a similar pattern than hypotaurine, and the levels are not recovered after reperfusion in UCP3-KO mice. Valine was shown to protect the atrioventricular node from hypoxia contributing to the generation of high-energy phosphates in cytoplasm and mitochondria (Nishimura *et al.*, 1989).

The alterations in amino acid abundance in UCP3-KO hearts after reperfusion could affect cardiac metabolism and the contractile activity of the heart.

Nicotinamide adenine dinucleotide (reduced, NADH; oxidized NAD^+) is an essential cofactor for electron transfer in metabolism. Redox reactions catalyzed by various NAD(H)-dependent dehydrogenases are vital for biochemical processes such as glycolysis and mitochondrial metabolism. The mitochondrial NAD pool is relatively distinct from that of the rest of the cell (Yang *et al.*, 2007). In cardiomyocytes, the NAD pool is 70% mitochondrial (Di Lisa *et al.*, 2001). The ratio NADH/NAD^+ is dependent on oxygen levels (Sun *et al.*, 2012). Our results agree with this notion, as they showed that NADH/NAD^+ tends to increase in ischemia, consistent with a reduced oxidative potential, and behaves the opposite way after reperfusion. In preconditioned hearts, the ratio was high in UCP3-KO and low in wild-type hearts, indicating different redox status depending on the genotype.

Ascorbic acid (vitamin C) is an antioxidant that can be oxidized through a two-step oxidation process involving a free radical intermediate, the ascorbyl radical. Ascorbic acid can also behave as a pro-oxidant under certain conditions (Halliwell, 1996). We found that ascorbate levels increase in ischemia and are reduced after IR in wild-type hearts. UCP3-KO hearts present higher levels of ascorbate than wild-type hearts, and this vitamin also increases in ischemia but remains high after IR. The increased levels in ischemia suggest a decreased oxidative potential due to the lack of oxygen. The increased levels of ascorbic acid in UCP3-KO mice may represent a compensatory mechanism for increased ROS damage. Indeed, it was shown that this vitamin inhibits hypoxia-induced damage and apoptosis in cardiomyocytes and ischemic hearts (Guaiquil *et al.*, 2004) and prevents myocardial damage associated with reoxygenation in ischemic rat hearts (Galaris *et al.*, 1989). Other studies, however, do not confirm these findings (Bellows *et al.*, 1995).

The ATP/ADP ratio is a critical parameter of cellular energy status that regulates many metabolic activities. UCP3 is able to increase the proton leak across the inner mitochondrial membrane when activated by fatty acids, superoxide or lipid peroxidation products such as HNE (see Introduction, section 2). However, the lack of UCP3 has no effect on the basal proton conductance of isolated mouse mitochondria (Cadenas *et al.*, 2002, 1999; Echtay *et al.*, 2003, 2002), indicating that this protein does not transport protons in the absence of activators. Our results are consistent with these findings and show that the absence of UCP3 does not increase but even decreases the ratio ATP/ADP in control hearts. As expected, ischemia decreases de ratio in both types of mice and, whereas the values remain low at reperfusion in wild-type mice, they tend to recover in UCP3-KO mice. Creatine levels are not significantly different in any condition in wild-type hearts, but they increase in ischemia and decrease at reperfusion in UCP3-KO compared to the wild-type hearts. The phosphocreatine (PCr) system is fundamental in promoting rapid

recycle of ATP by means of creatine kinase action, and is particularly important in situations of high energy demand.

The proposed model for the cardioprotective role of UCP3 against cardiac IR injury is depicted in *Fig. 56*.

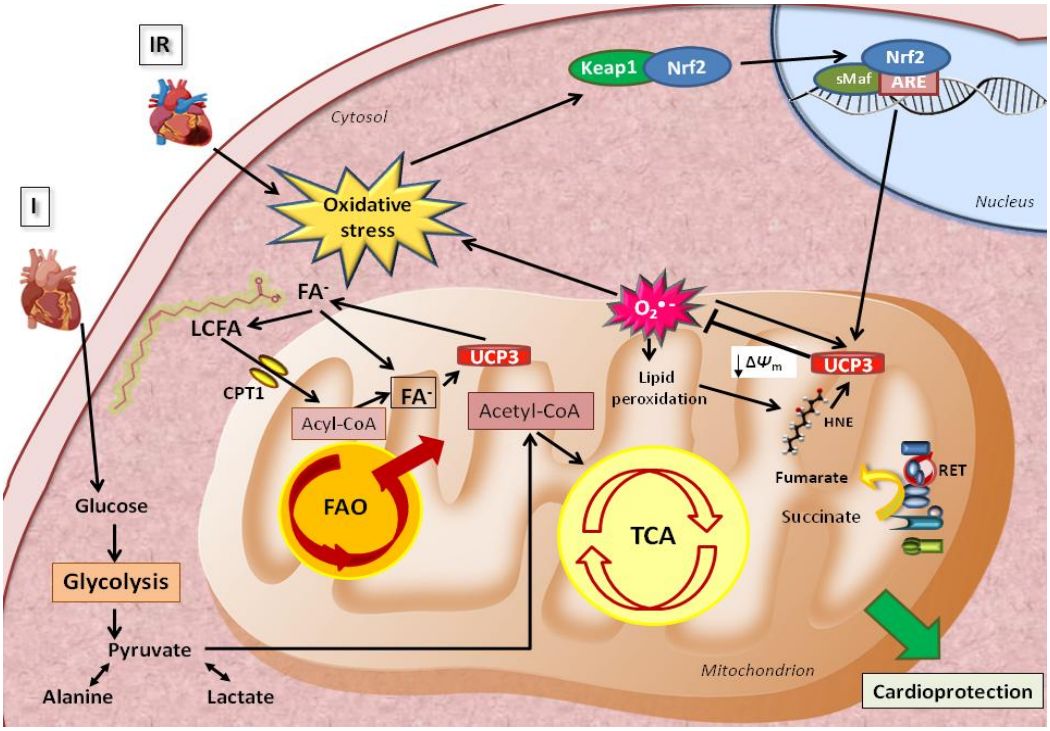

***Fig. 56*. Proposed model for the cardioprotective role of UCP3 against cardiac IR injury.** During myocardial ischemia, the absence of oxygen switches cell metabolism to anaerobic respiration, resulting in the production of lactate. Moreover, succinate dehydrogenase operates in reverse reducing fumarate to succinate. The amino acid alanine is interchangeable with pyruvate via transamination. During reperfusion, the ETC is reactivated producing ROS. Succinate accumulated during ischemia is rapidly oxidized at reperfusion driving ROS generation by RET at complex I. UCP3 expression, probably mediated by Nrf2, increases at reperfusion. Superoxide and HNE activate UCP3 to induce proton conductance across the inner mitochondrial membrane, reducing $\Delta\psi_m$ and in turn superoxide production. Moreover, UCP3 facilitates fatty acid oxidation and participates in the adaptation to perturbed cellular energy balance. These effects promote cardiomyocyte survival and protect against IR injury. ETC, electron transport chain; FAO, fatty acid oxidation; RET, reverse electron transport; ROS, reactive oxygen species; TCA, tricarboxylic acid cycle.

5. Nrf2 knockout mice are more susceptible to cardiac IR injury than wild-type mice and are not protected by ischemic preconditioning

We have confirmed in this thesis that Nrf2 activation increases after exposure of the cells to H_2O_2 or HNE, and have shown that its expression increases after hypoxia/reoxygenation or SIR in HL-1 cardiomyocytes. Likewise, we have confirmed that Nrf2 is upregulated in the hearts of wild-type mice subjected to IR (Anedda *et al.*, 2013). These results reveal the important role of Nrf2 against oxidative stress and cell death. We then reasoned that the Nrf2/ARE pathway might be important in cardioprotection against IR injury.

Several authors have reported the activation of Nrf2 and the induction of cytoprotective gene expression after hypoxia/reoxygenation and in *in vivo* models of IR. These studies indicated that Nrf2 activation is mediated by ROS production during the reoxygenation process (Kolamunne *et al.*, 2013; Leonard *et al.*, 2006). Moreover, Nrf2 is synthesized by *de novo* protein translation in response to the treatment of cardiomyocytes with oxidants (Purdom-Dickinson *et al.*, 2007b) or after myocardial IR (Xu *et al.*, 2014). Importantly, mild oxidative stress mediated by HNE in cardiomyocytes confers protection against oxygen and glucose deprivation followed by reoxygenation, or IR damage in isolated perfused hearts via Nrf2-mediated gene expression and GSH biosynthesis (Zhang *et al.*, 2010). Furthermore, the disruption of the Nrf2/ARE pathway increases cell death due to the impairment of the antioxidant defense pathway (Miller *et al.*, 2012). Along the same line, natural antioxidant compounds such as sulforaphane or the natural flavone acacetin reduce infarct size, inflammation and ROS production after cardiac IR via AMPK-mediated activation of the Nrf2 pathway and downstream antioxidant genes such as SOD and HO-1 (Piao *et al.*, 2010; Wu *et al.*, 2018). Our results in Langendorff perfused hearts showed that Nrf2-KO hearts present larger infarct size than wild-type hearts after IR. This result was supported by the measurement of creatine kinase levels released from the coronary effluent: creatine kinase was higher in Nrf2-KO hearts after the IR protocol compared to wild-type hearts. These results suggest an important role for Nrf2 in cardioprotection against IR damage.

In this thesis, we also analyzed the protein levels of HO-1 in isolated perfused hearts from Nrf2-KO and wild-type mice after IR. As expected, HO-1 levels were significantly lower in mice lacking Nrf2 after IR. In wild-type hearts, Nrf2 nuclear accumulation increased after IR and especially after IPC+IR. This protocol (IPC) partially decreased the infarct size in wild-type mice. The infarct area (TTC staining) and creatine kinase released corroborated this result. In contrast, IPC has no effect on Nrf2-KO hearts, which present a similar percentage of infarct size and creatine kinase activity than non-conditioned hearts. Hence, these results suggest that Nrf2 is involved in IPC. The activation of Nrf2 during IPC will promote the induction of antioxidant enzymes that will protect against IR injury (Huang *et al.*, 2014).

The Nrf2/ARE pathway directly regulates mitochondrial bioenergetics in murine neurons and embryonic fibroblasts (Holmström *et al.*, 2013). Thus, Nrf2 loss leads to mitochondrial depolarization, decreased ATP levels and impaired respiration. In the absence of Nrf2, the activities of the complexes of the respiratory chain in isolated mitochondria and intact cells are substantially impaired. Moreover, Nrf2 is involved in mitochondrial fatty acid oxidation and global metabolism (Ryoo and Kwak, 2018). Nrf2-KO mice have impaired fatty acid oxidation (Ludtmann *et al.*, 2014). In this regard, Nrf2 and UCP3 have a similar function. A recent report showed that UCP1-mediated thermogenesis is a mechanism through which energy expenditure is upregulated in Nrf2 knockout mice (Schneider *et al.*, 2016). These authors also found decreased

UCP3 expression in the skeletal muscle of these mice. It appears, therefore, that Nrf2 has an important role in modulating mitochondrial activity, as recently reported (Dinkova-Kostova and Abramov, 2015; Hayes and Dinkova-Kostova, 2014).

Taken together, these results suggest that Nrf2 protects the heart against IR injury, probably by increasing the antioxidant capacity of cardiomyocytes and preserving fatty acid metabolism and mitochondrial function. The connection of this transcription factor with UCP3 expression and function remains to be explored in the setting of cardiac IR. The involvement of Nrf2 in IPC has been demonstrated in mice lacking this factor, which lose the cardioprotection afforded by IPC. These findings have important implications for the development of strategies aimed at decreasing myocardial damage in patients with high risk of myocardial infarction or undergoing cardiac reperfusion.

CONCLUSIONS/CONCLUSIONES

1. UCP3 expression is upregulated in response to oxidative stress and hypoxia in C2C12 myotubes and HL-1 cardiomyocytes. Similarly, Nrf2 is activated under oxidative stress and hypoxia in these cells. The increase of UCP3 in hypoxia is due to new protein synthesis. As reported to occur under oxidative stress conditions, Nrf2 might mediate UCP3 upregulation in hypoxia.

2. UCP3 expression and Nrf2 activation increase after hypoxia/reoxygenation to a greater extent than after hypoxia alone. Hypoxia/reoxygenation increases mitochondrial superoxide production in both C2C12 myotubes and HL-1 cardiomyocytes, compromising cell viability. The increase in UCP3 expression and Nrf2 activation upon reoxygenation could be due to enhanced oxidative stress.

3. The upregulation of UCP3 and the nuclear accumulation of Nrf2 in response to hypoxia are mediated by the activation of p38 MAPK, since the inhibition of this kinase prevents both effects. Given that p38 MAPK phosphorylates and activates ATF-1, and considering that pATF-1 increases in hypoxia, this transcription factor could mediate UCP3 upregulation and Nrf2 activation in these conditions. The activation of p38 MAPK signalling seems to protect against cell death during hypoxia in skeletal muscle cells.

4. Similar to hypoxia and hypoxia/reoxygenation, both simulated ischemia and simulated ischemia-reperfusion (SIR) increase UCP3 expression and the activation of both Nrf2 and ATF-1 in HL-1 cells. In accordance with enhanced superoxide production after hypoxia/reoxygenation, SIR augments HNE-protein adducts in these cells, indicating increased oxidative stress.

5. Both Nrf2 activation and ATF-1 phosphorylation increase in isolated perfused hearts from UCP3-KO and wild-type mice subjected to IR or IPC+IR, although this increase is higher in hearts lacking UCP3. Likewise, active caspase-3 expression is enhanced in these conditions in both genotypes, but again the increase is higher in UCP3-KO hearts, which reflects augmented damage in hearts lacking UCP3.

6. UCP3 plays a cardioprotective role against IR injury, since isolated perfused hearts from mice lacking UCP3 present larger infarct size than those from wild-type mice. Consistent with this result, creatine kinase activity in the coronary effluent is higher in UCP3-KO than in wild-type mice at reperfusion. This cardioprotective effect of UCP3 against IR injury is even more relevant in aged than in adult mice.

7. The cardioprotective role of UCP3 against IR injury is also evident after LAD coronary artery ligation followed by reperfusion, since the histological analysis showed that UCP3-KO hearts present larger infarct size than wild-type hearts. Moreover, UCP3-KO mice have a tendency to exhibit increased signs of cardiac damage as evaluated by echocardiography.

8. The metabolomics analysis showed that, in ischemic conditions, UCP3 affects, albeit not always significantly, the accumulation of Krebs cycle intermediates. These data suggest that lipid and energy metabolism are the pathways more likely to be modulated by UCP3.

9. The transcription factor Nrf2 plays a cardioprotective role against IR injury, since isolated perfused hearts from mice lacking Nrf2 present larger infarct size than those from wild-type mice. Accordingly, creatine kinase activity in the coronary effluent is higher in Nrf2-KO than in wild-type mice at reperfusion. Our results indicate that Nrf2 is involved in IPC, as the absence of this factor abolishes IPC protective effects.

1. La expresión de UCP3 aumenta en respuesta al estrés oxidativo y la hipoxia en los miotubos C2C12 y en los cardiomiocitos HL-1. Asimismo, Nrf2 se activa en condiciones de estrés oxidativo e hipoxia en estas células. El aumento de UCP3 en hipoxia se debe a la nueva síntesis de proteína. Al igual que lo descrito en condiciones de estrés oxidativo, Nrf2 podría mediar la regulación de UCP3 en hipoxia.

2. El aumento de la expresión de UCP3 y de la activación de Nrf2 es mayor cuando las células se someten a hipoxia/reoxigenación que cuando se someten únicamente a hipoxia. La hipoxia/reoxigenación aumenta la producción de superóxido mitocondrial tanto en los miotubos C2C12 como en los cardiomiocitos HL-1, comprometiendo la viabilidad celular. El aumento en la expresión de UCP3 y en la activación de Nrf2 tras la reoxigenación podría deberse a un mayor estrés oxidativo.

3. El incremento de los niveles de UCP3 y la acumulación nuclear de Nrf2 en respuesta a la hipoxia están mediadas por la activación de la p38 MAPK, ya que la inhibición de esta quinasa previene ambos efectos. Puesto que la p38 MAPK fosforila y activa a ATF-1, y teniendo en cuenta que pATF-1 aumenta en hipoxia, este factor de transcripción podría mediar el incremento de los niveles de UCP3 y la activación de Nrf2 en estas condiciones. La activación de la señalización mediada por la p38 MAPK parece proteger frente a la muerte celular durante la hipoxia en las células del músculo esquelético.

4. Del mismo modo que la hipoxia y la hipoxia/reoxigenación, tanto la isquemia simulada como la isquemia-reperfusión simulada (SIR) aumentan la expresión de UCP3 y la activación de Nrf2 y ATF-1 en las células HL-1. De acuerdo con la producción aumentada de superóxido tras la hipoxia/reoxigenación, la SIR aumenta los aductos de HNE-proteína en estas células, lo que indica un aumento del estrés oxidativo.

5. Tanto la activación de Nrf2 como la fosforilación de ATF-1 aumentan en corazones aislados perfundidos de ratones UCP3-KO y de ratones de tipo silvestre sometidos a IR o IPC+IR, si bien este aumento es mayor en los corazones de ratones que carecen de UCP3. Asimismo, la expresión de caspasa-3 activa aumenta en estas condiciones en ambos genotipos, pero de nuevo el aumento es mayor en los corazones UCP3-KO, lo que refleja un daño aumentado en los corazones que carecen de UCP3.

6. UCP3 juega un papel cardioprotector frente al daño por IR, ya que los corazones aislados perfundidos de ratones que carecen de UCP3 presentan un tamaño de infarto mayor que los ratones de tipo silvestre. De acuerdo con este resultado, la actividad creatina quinasa en el efluente coronario es mayor en ratones UCP3-KO que en ratones de tipo silvestre en la reperfusión. Este efecto cardioprotector de UCP3 frente al daño por IR es aún más relevante en ratones viejos que en adultos.

7. El papel cardioprotector de UCP3 frente al daño por IR también es evidente después de la ligadura de la arteria coronaria anterior descendente izquierda (LAD) seguida de reperfusión, ya que el análisis histológico muestra que los corazones UCP3-KO presentan un mayor tamaño de infarto que los corazones de tipo silvestre. Además, los ratones UCP3-KO tienden a mostrar signos mayores de daño cardiaco según lo evaluado por la ecocardiografía.

8. El análisis metabolómico mostró que, en condiciones de isquemia, UCP3 afecta, aunque no siempre de manera significativa, a la acumulación de intermediarios del ciclo de Krebs. Los datos sugieren que el metabolismo lipídico y el energético son las vías con mayor probabilidad de ser moduladas por UCP3.

9. El factor de transcripción Nrf2 juega un papel cardioprotector frente al daño por IR, ya que los corazones aislados perfundidos de ratones que carecen de Nrf2 presentan un tamaño de infarto mayor que los ratones de tipo silvestre. De acuerdo con este resultado, la actividad creatina quinasa en el efluente coronario es mayor en ratones Nrf2-KO que en ratones de tipo silvestre en la reperfusión. Nuestros resultados indican que Nrf2 está implicado en el IPC, ya que la ausencia de este factor elimina los efectos protectores del IPC.

REFERENCES

Abdul-Ghani, S., Heesom, K.J., Angelini, G.D., Suleiman, M.-S., 2014. Cardiac phosphoproteomics during remote ischemic preconditioning: A role for the sarcomeric Z-Disk proteins. Biomed Res. Int. 2014, 1–11.

Affourtit, C., Brand, M.D., 2008. Uncoupling protein-2 contributes significantly to high mitochondrial proton leak in INS-1E insulinoma cells and attenuates glucose-stimulated insulin secretion. Biochem. J. 409, 199–204.

Affourtit, C., Jastroch, M., Brand, M.D., 2011. Uncoupling protein-2 attenuates glucose-stimulated insulin secretion in INS-1E insulinoma cells by lowering mitochondrial reactive oxygen species. Free Radic. Biol. Med. 50, 609–616.

Aguirre, E., Cadenas, S., 2010. GDP and carboxyatractylate inhibit 4-hydroxynonenal-activated proton conductance to differing degrees in mitochondria from skeletal muscle and heart. Biochim. Biophys. Acta - Bioenerg. 1797, 1716–1726.

Al-Rashed, F., Calay, D., Lang, M., Thornton, C.C., Bauer, A., Kiprianos, A., Haskard, D.O., Seneviratne, A., Boyle, J.J., Schönthal, A.H., Wheeler-Jones, C.P., Mason, J.C., 2018. Celecoxib exerts protective effects in the vascular endothelium via COX-2-independent activation of AMPK-CREB-Nrf2 signalling. Sci. Rep. 8, 6271.

Anedda, A., López-Bernardo, E., Acosta-Iborra, B., Saadeh Suleiman, M., Landázuri, M.O., Cadenas, S., 2013. The transcription factor Nrf2 promotes survival by enhancing the expression of uncoupling protein 3 under conditions of oxidative stress. Free Radic. Biol. Med. 61, 395–407.

Angeloni, C., Motori, E., Fabbri, D., Malaguti, M., Leoncini, E., Lorenzini, A., Hrelia, S., 2011. H 2 O 2 preconditioning modulates phase II enzymes through p38 MAPK and PI3K/Akt activation. Am. J. Physiol. Circ. Physiol. 300, H2196–H2205.

Azzu, V., Affourtit, C., Breen, E.P., Parker, N., Brand, M.D., 2008. Dynamic regulation of uncoupling protein 2 content in INS-1E insulinoma cells. Biochim. Biophys. Acta - Bioenerg. 1777, 1378–1383.

Azzu, V., Brand, M.D., 2010a. The on-off switches of the mitochondrial uncoupling proteins. Trends Biochem. Sci. 35, 298–307.

Azzu, V., Brand, M.D., 2010b. Degradation of an intramitochondrial protein by the cytosolic proteasome. J. Cell Sci. 123, 578–585.

Azzu, V., Jastroch, M., Divakaruni, A.S., Brand, M.D., 2010a. The regulation and turnover of mitochondrial uncoupling proteins. Biochim. Biophys. Acta 1797, 785–791.

Azzu, V., Mookerjee, S.A., Brand, M.D., 2010b. Rapid turnover of mitochondrial uncoupling protein 3. Biochem. J. 426, 13–17.

Babot, M., Birch, A., Labarbuta, P., Galkin, A., 2014. Characterisation of the active/de-active transition of mitochondrial complex I. Biochim. Biophys. Acta - Bioenerg. 1837, 1083–1092.

Balaban, R.S., Nemoto, S., Finkel, T., 2005. Mitochondria, oxidants, and aging. Cell 120, 483–495.

Barreiro, E., Garcia-Martínez, C., Mas, S., Ametller, E., Gea, J., Argilés, J.M., Busquets, S., López-Soriano, F.J., 2009. UCP3 overexpression neutralizes oxidative stress rather than nitrosative stress in mouse myotubes. FEBS Lett. 583, 350–356.

Barrera, G., Pizzimenti, S., Ciamporcero, E.S., Daga, M., Ullio, C., Arcaro, A., Cetrangolo, G.P., Ferretti, C., Dianzani, C., Lepore, A., Gentile, F., 2015. Role of 4-hydroxynonenal-protein adducts in human diseases. Antioxidants Redox Signal. 22, 1681–1702.

Beckman, K.B., Ames, B.N., 1998. The free radical theory of aging matures. Physiol. Rev. 78, 547–581.

Beitner-Johnson, D., Millhorn, D.E., 1998. Hypoxia induces phosphorylation of the cyclic AMP response element- binding protein by a novel signaling mechanism. J. Biol. Chem. 273, 19834–19839.

Bejma, J., Ji, L.L., 1999. Aging and acute exercise enhance free radical generation in rat skeletal muscle. J. Appl. Physiol. 87, 465–470.

Bell, K.F., Al-Mubarak, B., Fowler, J.H., Baxter, P.S., Gupta, K., Tsujita, T., Chowdhry, S., Patani, R., Chandran, S., Horsburgh, K., Hayes, J.D., Hardingham, G.E., 2011. Mild oxidative stress activates Nrf2 in astrocytes, which contributes to neuroprotective ischemic preconditioning. Proc. Natl. Acad. Sci. U. S. A. 108, E1-2.

Bellows, S.D., Hale, S.L., Simkhovich, B.Z., Kay, G.L., Kloner, R.A., 1995. Do antioxidant vitamins reduce infarct size following acute myocardial ischemia/reperfusion? Cardiovasc. Drugs Ther. 9, 117–123.

Bezaire, V., Spriet, L.L., Campbell, S., Sabet, N., Gerrits, M., Bonen, A., Harper, M.-E., 2005. Constitutive UCP3 overexpression at physiological levels increases mouse skeletal muscle capacity for fatty acid transport and oxidation. FASEB J. 19, 977–979.

Bleckmann, S.C., Blendy, J.A., Rudolph, D., Monaghan, A.P., Schmid, W., Schutz, G., 2002. Activating transcription factor 1 and CREB are important for cell survival during early mouse development. Mol. Cell. Biol. 22, 1919–1925.

Boehm, E.A., Jones, B.E., Radda, G.K., Veech, R.L., Clarke, K., 2001. Increased uncoupling proteins and decreased efficiency in palmitate-perfused hyperthyroid rat heart. Am. J. Physiol. - Hear. Circ. Physiol. 280, H977–H983.

Bordone, L., Motta, M.C., Picard, F., Robinson, A., Jhala, U.S., Apfeld, J., McDonagh, T., Lemieux, M., McBurney, M., Szilvasi, A., Easlon, E.J., Lin, S.J., Guarente, L., 2006. Sirt1 regulates insulin secretion by repressing UCP2 in pancreatic β cells. PLoS Biol. 4, e31.

Boss, O., Samec, S., Paoloni-Giacobino, A., Rossier, C., Dulloo, A., Seydoux, J., Muzzin, P., Giacobino, J.P., 1997. Uncoupling protein-3: a new member of the mitochondrial carrier family with tissue-specific expression. FEBS Lett. 408, 39–42.

Bouillaud, F., 2009. UCP2, not a physiologically relevant uncoupler but a glucose sparing switch impacting ROS production and glucose sensing. Biochim. Biophys. Acta - Bioenerg. 1787, 377–383.

Bouillaud, F., Ricquier, D., Thibault, J., Weissenbach, J., 1985. Molecular approach to thermogenesis in brown adipose tissue: cDNA cloning of the mitochondrial uncoupling protein. Proc. Natl. Acad. Sci. U. S. A. 82, 445–448.

Boveris, A., 1977. Mitochondrial production of superoxide radical and hydrogen peroxide. Adv. Exp. Med. Biol. 78, 67–82.

Boyle, J.J., Johns, M., Kampfer, T., Nguyen, A.T., Game, L., Schaer, D.J., Mason, J.C., Haskard, D.O., 2012. Activating transcription factor 1 directs Mhem atheroprotective macrophages through coordinated iron handling and foam cell protection. Circ. Res. 110, 20–33.

Brand, M.D., 2016. Mitochondrial generation of superoxide and hydrogen peroxide as the source of mitochondrial redox signaling. Free Radic. Biol. Med. 100, 14–31.

Brand, M.D., 2000. Uncoupling to survive? The role of mitochondrial inefficiency in ageing. Exp. Gerontol. 35, 811–820.

Brand, M.D., 1990. The proton leak across the mitochondrial inner membrane. Biochim. Biophys. Acta 1018, 128–133.

Brand, M.D., Buckingham, J.A., Esteves, T.C., Green, K., Lambert, A.J., Miwa, S., Murphy, M.P., Pakay, J.L., Talbot, D.A., Echtay, K.S., 2004. Mitochondrial superoxide and aging: uncoupling-protein activity and superoxide production. Biochem Soc Symp 71, 203–213.

Brand, M.D., Esteves, T.C., 2005. Physiological functions of the mitochondrial uncoupling proteins UCP2 and UCP3. Cell Metab. 2, 85–93.

Brand, M.D., Pamplona, R., Portero-Otín, M., Requena, J.R., Roebuck, S.J., Buckingham, J.A., Clapham, J.C., Cadenas, S., 2002. Oxidative damage and phospholipid fatty acyl composition in skeletal muscle mitochondria from mice underexpressing or overexpressing uncoupling protein 3. Biochem. J. 368, 597–603.

Braunersreuther, V., Jaquet, V., 2012. Reactive oxygen species in myocardial reperfusion injury: from physiopathology to therapeutic approaches. Curr. Pharm. Biotechnol. 13, 97–114.

Braunwald, E., Kloner, R.A., 1985. Myocardial reperfusion: A double-edged sword? J. Clin. Invest. 76, 1713–1719.

Breen, E.P., Gouin, S.G., Murphy, A.F., Haines, L.R., Jackson, A.M., Pearson, T.W., Murphy, P. V, Porter, R.K., 2006. On the mechanism of mitochondrial uncoupling protein 1 function. J. Biol. Chem. 281, 2114–9.

Brennan, J., Southworth, R., Medina, R., Davidson, S., Duchen, M.R., Shattock, M.J., 2006. Mitochondrial uncoupling, with low concentration FCCP, induces ROS-dependent cardioprotection independent of KATP channel activation. Cardiovasc. Res. 72, 313–321.

Brindle, P., Linke, S., Montminy, M., 1993. Protein-kinase-A-dependent activator in transcription factor CREB reveals new role for CREM repressers. Nature 364, 821–824.

Brunelle, J.K., Bell, E.L., Quesada, N.M., Vercauteren, K., Tiranti, V., Zeviani, M., Scarpulla, R.C., Chandel, N.S., 2005. Oxygen sensing requires mitochondrial ROS but not oxidative phosphorylation. Cell Metab. 1, 409–414.

Bryan, H.K., Olayanju, A., Goldring, C.E., Park, B.K., 2013. The Nrf2 cell defence pathway: Keap1-dependent and -independent mechanisms of regulation. Biochem. Pharmacol. 85, 705–717.

Bulluck, H., Yellon, D.M., Hausenloy, D.J., 2016. Reducing myocardial infarct size: Challenges and future opportunities. Heart 102, 341–348.

Butler, J., Jayson, G.G., Swallow, A.J., 1975. The reaction between the superoxide anion radical and cytochrome c. Biochem. Biophys. Acta - Bioenerg. 408, 215–222.

Cabaniss, C.D., 1990. Creatine kinase, in: Clinical Methods: The History, Physical, and Laboratory Examinations. Butterworths, p. Chapter 32.

Cadenas, E., Davies, K.J., 2000. Mitochondrial free radical generation, oxidative stress, and aging. Free Radic. Biol. Med. 29, 222–230.

Cadenas, S., 2018a. Mitochondrial uncoupling, ROS generation and cardioprotection. Biochim. Biophys. Acta - Bioenerg. 1859, 940–950.

Cadenas, S., 2018b. ROS and redox signaling in myocardial ischemia-reperfusion injury and cardioprotection. Free Radic. Biol. Med. 117, 76–89.

Cadenas, S., Aragonés, J., Landázuri, M.O., 2010. Mitochondrial reprogramming through cardiac oxygen sensors in ischaemic heart disease. Cardiovasc. Res. 88, 219–228.

Cadenas, S., Buckingham, J.A., Samec, S., Seydoux, J., Din, N., Dulloo, A.G., Brand, M.D., 1999. UCP2 and UCP3 rise in starved rat skeletal muscle but mitochondrial proton conductance is unchanged. FEBS Lett. 462, 257–260.

Cadenas, S., Echtay, K.S., Harper, J.A., Jekabsons, M.B., Buckingham, J.A., Grau, E., Abuin, A., Chapman, H., Clapham, J.C., Brand, M.D., 2002. The basal proton conductance of skeletal muscle mitochondria from transgenic mice overexpressing or lacking uncoupling protein-3. J. Biol. Chem. 277, 2773–2778.

Cai, Z., Zhong, H., Bosch-Marce, M., Fox-Talbot, K., Wang, L., Wei, C., Trush, M.A., Semenza, G.L., 2008. Complete loss of ischaemic preconditioning-induced cardioprotection in mice with partial deficiency of HIF-1α. Cardiovasc. Res. 77, 463–470.

Cannon, B., Nedergaard, J., 2004. Brown Adipose Tissue: Function and Physiological Significance. Physiol. Rev. 84, 277–359.

Capano, M., Crompton, M., 2006. Bax translocates to mitochondria of heart cells during simulated ischaemia: involvement of AMP-activated and p38 mitogen-activated protein kinases. Biochem. J. 395, 57–64.

Carmona, M.C., Hondares, E., Rodríguez de la Concepción, M.L., Rodríguez-Sureda, V., Peinado-Onsurbe, J., Poli, V., Iglesias, R., Villaroya, F., Giralt, M., 2005. Defective thermoregulation, impaired lipid metabolism, but preserved adrenergic induction of gene expression in brown fat of mice lacking C/EBPβ. Biochem. J. 389, 47–56.

Chan, D.C., 2006. Mitochondria: Dynamic Organelles in Disease, Aging, and Development. Cell 125, 1241–1252.

Chan, K., Lu, R., Chang, J.C., Kan, Y.W., 1996. NRF2, a member of the NFE2 family of transcription factors, is not essential for murine erythropoiesis, growth, and development. Proc. Natl. Acad. Sci. U. S. A. 93, 13943–13948.

Chance, B., Sies, H., Boveris, A., 1979. Hydroperoxide metabolism in mammalian organs. Physiol. Rev. 59, 527–605.

Chapple, S.J., Cheng, X., Mann, G.E., 2013. Effects of 4-hydroxynonenal on vascular endothelial and smooth muscle cell redox signaling and function in health and disease. Redox Biol. 1, 319–331.

Chen, Q., Moghaddas, S., Hoppel, C.L., Lesnefsky, E.J., 2008. Ischemic defects in the electron transport chain increase the production of reactive oxygen species from isolated rat heart mitochondria. Am. J. Physiol. Physiol. 294, C460–C466.

Chen, Q., Younus, M., Thompson, J., Hu, Y., Hollander, J.M., Lesnefsky, E.J., 2018. Intermediary metabolism and fatty acid oxidation: Novel targets of electron transport chain-driven injury during ischemia and reperfusion. Am. J. Physiol. - Hear. Circ. Physiol. 314, H787–H795.

Chen, W., Sun, Z., Wang, X.-J., Jiang, T., Huang, Z., Fang, D., Zhang, D.D., 2009. Direct Interaction between Nrf2 and p21Cip1/WAF1 Upregulates the Nrf2-Mediated Antioxidant Response. Mol. Cell 34, 663–673.

Chen, Y., Liu, J., Zheng, Y., Wang, J., Wang, Z., Gu, S., Tan, J., Jing, Q., Yang, H., 2014. Uncoupling protein 3 mediates H2O2 preconditioning-afforded cardioprotection through the inhibition of mPTP opening. Cardiovasc. Res. 105, 192–202.

Cheng, X., Ku, C.H., Siow, R.C.M., 2013. Regulation of the Nrf2 antioxidant pathway by microRNAs: New players in micromanaging redox homeostasis. Free Radic. Biol. Med.

Chouchani, E.T., James, A.M., Frezza, C., Saeb-Parsy, K., Work, L.M., Murphy, M.P., Krieg, T., Pell, V.R., James, A.M., Work, L.M., Saeb-Parsy, K., Frezza, C., Krieg, T., Murphy, M.P., 2016. A Unifying Mechanism for Mitochondrial Superoxide Production during Ischemia-Reperfusion Injury. Cell Metab. 23, 254–263.

Chouchani, E.T., Pell, V.R., Gaude, E., Aksentijevic, D., Sundier, S.Y., Robb, E.L., Logan, A., Nadtochiy, S.M., Ord, E.N.J., Smith, A.C., Eyassu, F., Shirley, R., Hu, C., Dare, A.J., James, A.M., Rogatti, S., Hartley, R.C., Eaton, S., Costa, A.S.H., Brookes, P.S., Davidson, S.M., Duchen, M.R., Saeb-parsy, K., Shattock, M.J., Robinson, A.J., Work, L.M., Frezza, C., Krieg, T., Murphy, M.P., 2014. Ischaemic accumulation of succinate controls reperfusion injury through mitochondrial ROS. Nature 515, 431–435.

Chowdhry, S., Zhang, Y., McMahon, M., Sutherland, C., Cuadrado, A., Hayes, J.D., 2013. Nrf2 is controlled by two distinct β-TrCP recognition motifs in its Neh6 domain, one of which can be modulated by GSK-3 activity. Oncogene 32, 3765–3781.

Ciano, M., Fuszard, M., Heide, H., Botting, C.H., Galkin, A., 2013. Conformation-specific crosslinking of mitochondrial complex I. FEBS Lett. 587, 867–872.

Clanton, T., 2005. Yet another oxygen paradox. J. Appl. Physiol. 99, 1245–1246.

Claycomb, W.C., Lanson, N.A., Stallworth, B.S., Egeland, D.B., Delcarpio, J.B., Bahinski, A., Izzo, N.J., 1998. HL-1 cells: a cardiac muscle cell line that contracts and retains phenotypic characteristics of the adult cardiomyocyte. Proc. Natl. Acad. Sci. U. S. A. 95, 2979–2984.

Cohen, M. V, Downey, J.M., 2007. Cardioprotection: Spotlight on PKG. Br. J. Pharmacol. 152, 833–834.

Conklin, D., Prough, R., Bhatanagar, A., 2007. Aldehyde metabolism in the cardiovascular system. Mol. Biosyst. 3, 136–150.

Cullinan, S.B., Gordan, J.D., Jin, J., Harper, J.W., Diehl, J.A., 2004. The Keap1-BTB protein is an adaptor that bridges Nrf2 to a Cul3-based E3 ligase: Oxidative stress sensing by a Cul3-Keap1 ligase. Mol. Cell. Biol. 24, 8477–8486.

Cullinan, S.B., Zhang, D., Hannink, M., Arvisais, E., Kaufman, R.J., Diehl, J.A., 2003. Nrf2 is a direct PERK substrate and effector of PERK-dependent cell survival. Mol. Cell. Biol. 23, 7198–7209.

Daiber, A., 2010. Redox signaling (cross-talk) from and to mitochondria involves mitochondrial pores and reactive oxygen species. Biochim. Biophys. Acta - Bioenerg. 1797, 897–906.

Dalleau, S., Baradat, M., Guéraud, F., Huc, L., 2013. Cell death and diseases related to oxidative stress: 4-hydroxynonenal (HNE) in the balance. Cell Death Differ. 20, 1615–1630.

Das, D.K., Engelman, R.M., Maulik, N., 1999. Oxygen free radical signaling in ischemic preconditioning, in: Annals of the New York Academy of Sciences. pp. 49–65.

Dawson, T.L., Gores, G.J., Nieminen, A.L., Herman, B., Lemasters, J.J., 1993. Mitochondria as a source of reactive oxygen species during reductive stress in rat hepatocytes. Am. J. Physiol. Physiol. 264, C961–C967.

De Bilbao, F., Arsenijevic, D., Vallet, P., Hjelle, O.P., Ottersen, O.P., Bouras, C., Raffin, Y., Abou, K., Langhans, W., Collins, S., Plamondon, J., Alves-Guerra, M.C., Haguenauer, A., Garcia, I., Richard, D., Ricquier, D., Giannakopoulos, P., 2004. Resistance to cerebral ischemic injury in UCP2 knockout mice: Evidence for a role of UCP2 as a regulator of mitochondrial glutathione levels. J. Neurochem. 89, 1283–1292.

Dehne, N., Brüne, B., 2014. Sensors, transmitters, and targets in mitochondrial oxygen shortage - A hypoxia-inducible factor relay story. Antioxidants Redox Signal. 20, 339–352.

Dejean, L., Ćamara, Y., Sibille, B., Solanes, G., Villarroya, F., 2004. Uncoupling protein-3 sensitizes cells to mitochondrial-dependent stimulus of apoptosis. J. Cell. Physiol. 201, 294–304.

Dhein, S., 2005. The langendorff heart. Pract. Methods Cardiovasc. Res. 155–172.

Di Lisa, F., Menabò, R., Canton, M., Barile, M., Bernardi, P., 2001. Opening of the mitochondrial permeability transition pore causes depletion of mitochondrial and cytosolic NAD+ and is a causative event in the death of myocytes in postischemic reperfusion of the heart. J. Biol. Chem. 276, 2571–2575.

Dinkova-Kostova, A.T., Abramov, A.Y., 2015. The emerging role of Nrf2 in mitochondrial function. Free Radic. Biol. Med. 88, 179–188.

Dinkova-Kostova, A.T., Holtzclaw, W.D., Cole, R.N., Itoh, K., Wakabayashi, N., Katoh, Y., Yamamoto, M., Talalay, P., 2002. Direct evidence that sulfhydryl groups of Keap1 are the sensors regulating induction of phase 2 enzymes that protect against carcinogens and oxidants. Proc. Natl. Acad. Sci. U. S. A. 99, 11908–11913.

Downey, J.M., Davis, A.M., Cohen, M. V., 2007. Signaling pathways in ischemic preconditioning. Heart Fail. Rev. 12, 181–188.

Drake, K.J., Sidorov, V.Y., McGuinness, O.P., Wasserman, D.H., Wikswo, J.P., 2012. Amino acids as metabolic substrates during cardiac ischemia. Exp. Biol. Med. (Maywood, NJ) 237, 1369–1378.

Dröge, W., 2002. Free radicals in the physiological control of cell function. Physiol. Rev. 82, 47–95.

Dröse, S., Stepanova, A., Galkin, A., 2016. Ischemic A/D transition of mitochondrial complex i and its role in ROS generation. Biochim. Biophys. Acta - Bioenerg. 1857, 946–957.

Duranteau, J., Chandel, N.S., Kulisz, A., Shao, Z., Schumacker, P.T., 1998. Intracellular signaling by reactive oxygen species during hypoxia in cardiomyocytes. J. Biol. Chem. 273, 11619–11624.

Ebert, B.L., Bunn, H.F., 1998. Regulation of transcription by hypoxia requires a multiprotein complex that includes Hypoxia-inducible factor 1, an Adjacent transcription factor, and p300/CREB binding protein. Mol. Cell. Biol. 18, 4089–4096.

Echtay, K.S., Esteves, T.C., Pakay, J.L., Jekabsons, M.B., Lambert, A.J., Portero-Otín, M., Pamplona, R., Vidal-Puig, A.J., Wang, S., Roebuck, S.J., Brand, M.D., 2003. A signalling role for 4-hydroxy-2-nonenal in regulation of mitochondrial uncoupling. EMBO J. 22, 4103–4110.

Echtay, K.S., Roussel, D., St-Plerre, J., Jekabsons, M.B., Cadenas, S., Stuart, J.A., Harper, J.A., Roebuck, S.J., Morrison, A., Pickering, S., Clapham, J.C., Brand, M.D., 2002. Superoxide activates mitochondrial uncoupling proteins. Nature 415, 96–99.

Echtay, K.S., Winkler, E., Frischmuth, K., Klingenberg, M., 2001. Uncoupling proteins 2 and 3 are highly active H+ transporters and highly nucleotide sensitive when activated by coenzyme Q (ubiquinone). Proc. Natl. Acad. Sci. 98, 1416–1421.

Eckle, T., Kohler, D., Lehmann, R., Kasmi, K.C. El, Eltzschig, H.K., 2008. Hypoxia-inducible factor-1 is central to cardioprotection a new paradigm for ischemic preconditioning. Circulation 118, 166–175.

Edwards, K.S., Ashraf, S., Lomax, T.M., Wiseman, J.M., Hall, M.E., Gava, F.N., Hall, J.E., Hosler, J.P., Harmancey, R., 2018. Uncoupling protein 3 deficiency impairs myocardial fatty acid oxidation and contractile recovery following ischemia/reperfusion. Basic Res. Cardiol. 113, 47.

Eefting, F., Rensing, B., Wigman, J., Pannekoek, W.J., Liu, W.M., Cramer, M.J., Lips, D.J., Doevendans, P.A., 2004. Role of apoptosis in reperfusion injury. Cardiovasc. Res. 61, 414–426.

Enomoto, A., Itoh, K., Nagayoshi, E., Haruta, J., Kimura, T., O'Connor, T., Harada, T., Yamamoto, M., 2001. High sensitivity of Nrf2 knockout mice to acetaminophen hepatotoxicity associated with decreased expression of ARE-regulated drug metabolizing enzymes and antioxidant genes. Toxicol. Sci. 59, 169–177.

Epstein, A.C.R., Gleadle, J.M., McNeill, L.A., Hewitson, K.S., O'Rourke, J., Mole, D.R., Mukherji, M., Metzen, E., Wilson, M.I., Dhanda, A., Tian, Y.M., Masson, N., Hamilton, D.L., Jaakkola, P., Barstead, R., Hodgkin, J., Maxwell, P.H., Pugh, C.W., Schofield, C.J., Ratcliffe, P.J., 2001. C. elegans EGL-9 and mammalian homologs define a family of dioxygenases that regulate HIF by prolyl hydroxylation. Cell 107, 43–54.

Espinosa-Diez, C., Miguel, V., Mennerich, D., Kietzmann, T., Sánchez-Pérez, P., Cadenas, S., Lamas, S., 2015. Antioxidant responses and cellular adjustments to oxidative stress. Redox Biol. 6, 183–197.

Esterbauer, H., Muskiet, F., Horrobin, D.F., 1993. Cytotoxicity and genotoxicity of lipid-oxidation products. Am. J. Clin. Nutr. 57, 779S-786S.

Esterbauer, H., Schaur, R.J., Zollner, H., 1991. Chemistry and biochemistry of 4-hydroxynonenal, malonaldehyde and related aldehydes. Free Radic. Biol. Med. 11, 81–128.

Fedorenko, A., Lishko, P. V., Kirichok, Y., 2012. Mechanism of fatty-acid-dependent UCP1 uncoupling in brown fat mitochondria. Cell 151, 400–413.

Ferdinandy, P., Schulz, R., Baxter, G.F., 2007. Interaction of cardiovascular risk factors with myocardial ischemia/reperfusion Injury, preconditioning, and postconditioning. Pharmacol. Rev. 59, 418–458.

Firth, J.D., Ebert, B.L., Ratcliffe, P.J., 1995. Hypoxic regulation of lactate dehydrogenase A: Interaction between hypoxia-inducible factor 1 and cAMP response elements. J. Biol. Chem. 270, 21021–21027.

Fischer, F., Hamann, A., Osiewacz, H.D., 2012. Mitochondrial quality control: An integrated network of pathways. Trends Biochem. Sci. 37, 284–292.

Fleury, C., Neverova, M., Collins, S., Raimbault, S., Champigny, O., Levi-Meyrueis, C., Bouillaud, F., Seldin, M., Surwit, R., Ricquier, D., Warden, C., 1997. Uncoupling protein-2: a novel gene linked to obesity and hyperinsulinemia. Nat. Genet. 15, 269–272.

Forbes, R.A., Steenbergen, C., Murphy, E., 2001. Diazoxide-induced cardioprotection requires signaling through a redox-sensitive mechanism. Circ. Res. 88, 802–809.

Forman, H.J., Fukuto, J.M., Miller, T., Zhang, H., Rinna, A., Levy, S., 2008. The chemistry of cell signaling by reactive oxygen and nitrogen species and 4-hydroxynonenal. Arch. Biochem. Biophys. 477, 183–195.

Freude, B., Masters, T.N., Robicsek, F., Fokin, A., Kostin, S., Zimmermann, R., Ullmann, C., Lorenz-Meyer, S., Schaper, J., 2000. Apoptosis is initiated by myocardial ischemia and executed during reperfusion. J. Mol. Cell. Cardiol. 32, 197–208.

Fuhrmann, D.C., Brüne, B., 2017. Mitochondrial composition and function under the control of hypoxia. Redox Biol. 12, 208–215.

Fukuda, R., Zhang, H., Kim, J. whan, Shimoda, L., Dang, C. V., Semenza, G.L.L., 2007. HIF-1 regulates Cytochrome oxidase subunits to optimize efficiency of respiration in hypoxic cells. Cell 129, 111–122.

Galaris, D., Eddy, L., Arduini, A., Cadenas, E., Hochstein, P., 1989. Mechanisms of reoxygenation injury in myocardial infarction: Implications of a myoglobin redox cycle. Biochem. Biophys. Res. Commun. 160, 1162–1168.

Galluzzi, L., Kepp, O., Trojel-Hansen, C., Kroemer, G., 2012. Mitochondrial control of cellular life, stress, and death. Circ. Res. 111, 1198–1207.

Garcia-Dorado, D., Ruiz-Meana, M., Inserte, J., Rodriguez-Sinovas, A., Piper, H.M., 2012. Calcium-mediated cell death during myocardial reperfusion. Cardiovasc. Res. 94, 168–180.

Giaccia, A.J., Simon, M.C., Johnson, R., 2004. The biology of hypoxia: The role of oxygen sensing in development, normal function, and disease. Genes Dev. 18, 2183–2194.

Giralt, M., Villarroya, F., 2016. Mitochondrial uncoupling and the regulation of glucose homeostasis. Curr. Diabetes Rev. 13, 386–394.

Gong, D.W., Monemdjou, S., Gavrilova, O., Leon, L.R., Marcus-Samuels, B., Chou, C.J., Everett, C., Kozak, L.P., Li, C., Deng, C., Harper, M.E., Reitman, M.L., 2000. Lack of obesity and normal response to fasting and thyroid hormone in mice lacking uncoupling protein-3. J. Biol. Chem. 275, 16251–16257.

González-Barroso, M.M., Fleury, C., Bouillaud, F., Nicholls, D.G., Rial, E., 1998. The uncoupling protein UCP1 does not increase the proton conductance of the inner mitochondrial membrane by functioning as a fatty acid anion transporter. J. Biol. Chem. 273, 15528–15532.

Granger, D.N., Kvietys, P.R., 2015. Reperfusion injury and reactive oxygen species: The evolution of a concept. Redox Biol. 6, 524–551.

Griffiths, E.J., Halestrap, A.P., 1995. Mitochondrial non-specific pores remain closed during cardiac ischaemia, but open upon reperfusion. Biochem. J. 307, 93–98.

Guaiquil, V.H., Golde, D.W., Beckles, D.L., Mascareno, E.J., Siddiqui, M.A.Q., 2004. Vitamin C inhibits hypoxia-induced damage and apoptotic signaling pathways in cardiomyocytes and ischemic hearts. Free Radic. Biol. Med. 37, 1419–1429.

Gülçin, I., 2006. Antioxidant and antiradical activities of L-carnitine. Life Sci. 78, 803–811.

Guzy, R.D., Hoyos, B., Robin, E., Chen, H., Liu, L., Mansfield, K.D., Simon, M.C., Hammerling, U., Schumacker, P.T., 2005. Mitochondrial complex III is required for hypoxia-induced ROS production and cellular oxygen sensing. Cell Metab. 1, 401–408.

Guzy, R.D., Schumacker, P.T., 2006. Oxygen sensing by mitochondria at complex III: The paradox of increased reactive oxygen species during hypoxia. Exp. Physiol. 91, 807–819.

Halestrap, A.P., Richardson, A.P., 2015. The mitochondrial permeability transition: A current perspective on its identity and role in ischaemia/reperfusion injury. J. Mol. Cell. Cardiol. 78, 129–141.

Halliwell, B., 1996. Commentary: vitamin C: antioxidant or pro-oxidant in vivo? Free Radic. Res. 25, 439–454.

Hamanaka, R.B., Chandel, N.S., 2009. Mitochondrial reactive oxygen species regulate hypoxic signaling. Curr. Opin. Cell Biol. 21, 894–899.

Handy, D.E., Loscalzo, J., 2012. Redox regulation of mitochondrial function. Antioxidants Redox Signal. 16, 1324–1368.

Harman, D., 1956. Aging: a theory based on free radical and radiation chemistry. J. Gerontol. 11, 298–300.

Harmancey, R., Vasquez, H.G., Guthrie, P.H., Taegtmeyer, H., 2013. Decreased long-chain fatty acid oxidation impairs postischemic recovery of the insulin-resistant rat heart. FASEB J. 27, 3966–3978.

Harmsen, E., Jong, J.W. d., Serruys, P.W., 1981. Hypoxanthine production by ischemic heart demonstrated by high pressure liquid chromatography of blood purine nucleosides and oxypurines. Clin. Chim. Acta 115, 73–84.

Hausenloy, D.J., Baxter, G., Bell, R., Bøtker, H.E., Davidson, S.M., Downey, J., Heusch, G., Kitakaze, M., Lecour, S., Mentzer, R., Mocanu, M.M., Ovize, M., Schulz, R., Shannon, R., Walker, M., Walkinshaw, G., Yellon, D.M., 2010. Translating novel strategies for cardioprotection: The Hatter Workshop Recommendations. Basic Res. Cardiol. 105, 677–686.

Hausenloy, D.J., Lecour, S., Yellon, D.M., 2011. Reperfusion injury salvage kinase and survivor activating factor enhancement prosurvival signaling pathways in ischemic postconditioning: Two sides of the same coin. Antioxidants Redox Signal. 14, 893–907.

Hausenloy, D.J., Tsang, A., Mocanu, M.M., Yellon, D.M., 2005. Ischemic preconditioning protects by activating prosurvival kinases at reperfusion. Am. J. Physiol. - Hear. Circ. Physiol. 288, H971–H976.

Hausenloy, D.J., Yellon, D.M., 2016. Ischaemic conditioning and reperfusion injury. Nat. Rev. Cardiol. 13, 193–209.

Hausenloy, D.J., Yellon, D.M., 2013. Myocardial ischemia-reperfusion injury: a neglected therapeutic target. J. Clin. Invest. 123, 92–100.

Hausenloy, D.J., Yellon, D.M., 2011. The therapeutic potential of ischemic conditioning: an update. Nat. Rev. Cardiol. 8, 619–629.

Hausenloy, D.J., Yellon, D.M., 2010. The Second Window of Preconditioning (SWOP) where are we now? Cardiovasc. Drugs Ther. 24, 235–254.

Hausenloy, D.J., Yellon, D.M., 2004. New directions for protecting the heart against ischaemia-reperfusion injury: Targeting the Reperfusion Injury Salvage Kinase (RISK)-pathway. Cardiovasc. Res. 61, 448–460.

Hayes, J.D., Dinkova-Kostova, A.T., 2014. The Nrf2 regulatory network provides an interface between redox and intermediary metabolism. Trends Biochem. Sci. 39, 199–218.

Henry, T.D., Archer, S.L., Nelson, D., Weir, E.K., From, A.H., 1990. Enhanced chemiluminescence as a measure of oxygen-derived free radical generation during ischemia and reperfusion. Circ. Res. 67, 1453–1461.

Hernansanz-Agustín, P., Izquierdo-Álvarez, A., Sánchez-Gómez, F.J., Ramos, E., Villa-Piña, T., Lamas, S., Bogdanova, A., Martínez-Ruiz, A., 2014. Acute hypoxia produces a superoxide burst in cells. Free Radic. Biol. Med. 71, 146–156.

Heusch, G., 2015. Molecular basis of cardioprotection signal transduction in ischemic pre-, post-, and remote conditioning. Circ. Res. 116, 674–699.

Hilse, K.E., Rupprecht, A., Egerbacher, M., Bardakji, S., Zimmermann, L., Wulczyn, A.E.M.S., Pohl, E.E., 2018. The expression of uncoupling protein 3 coincides with the fatty acid oxidation type of metabolism in adult murine heart. Front. Physiol. 9, 1–11.

Himms-Hagen, J., Harper, M.E., 2001. Physiological role of UCP3 may be export of fatty acids from mitochondria when fatty acid oxidation predominates: an hypothesis. Exp. Biol. Med. (Maywood, NJ) 226, 78–84.

Hoerter, J., Gonzalez-Barroso, M.D.M., Couplan, E., Mateo, P., Gelly, C., Cassard-Doulcier, A.M., Diolez, P., Bouillaud, F., 2004. Mitochondrial uncoupling protein 1 expressed in the heart of transgenic mice protects against ischemic-reperfusion damage. Circulation 110, 528–533.

Hoffman, D.L., Salter, J.D., Brookes, P.S., 2007. Response of mitochondrial reactive oxygen species generation to steady-state oxygen tension: implications for hypoxic cell signaling. Am. J. Physiol. Circ. Physiol. 292, H101–H108.

Holmström, K.M., Baird, L., Zhang, Y., Hargreaves, I., Chalasani, A., Land, J.M., Stanyer, L., Yamamoto, M., Dinkova-Kostova, A.T., Abramov, A.Y., 2013. Nrf2 impacts cellular bioenergetics by controlling substrate availability for mitochondrial respiration. Biol. Open 2, 761–770.

Huang, H.C., Nguyen, T., Pickett, C.B., 2002. Phosphorylation of Nrf2 at Ser-40 by protein kinase C regulates antioxidant response element-mediated transcription. J. Biol. Chem. 277, 42769–42774.

Huang, L.K., Wang, M.J.J., 1995. Image thresholding by minimizing the measures of fuzziness. Pattern Recognit. 28, 41–51.

Huang, X.S., Chen, H.P., Yu, H.H., Yan, Y.F., Liao, Z.P., Huang, Q.R., 2014. Nrf2-dependent upregulation of antioxidative enzymes: A novel pathway for hypoxic preconditioning-mediated delayed cardioprotection. Mol. Cell. Biochem. 385, 33–41.

Hurtaud, C., Gelly, C., Chen, Z., Lévi-Meyrueis, C., Bouillaud, F., 2007. Glutamine stimulates translation of uncoupling protein 2 mRNA. Cell. Mol. Life Sci. 64, 1853–1860.

Huxtable, R., 1992. Physiological actions of taurine. Physiol. Rev. 72, 101–163.

Ishii, T., Itoh, K., Ruiz, E., Leake, D.S., Unoki, H., Yamamoto, M., Mann, G.E., 2004. Role of Nrf2 in the regulation of CD36 and stress protein expression in murine macrophages: Activation by oxidatively modified LDL and 4-Hydroxynonenal. Circ. Res. 94, 609–616.

Itoh, K., Chiba, T., Takahashi, S., Oyake, T., Ishii, T., Chiba, T., Yamamoto, M., Itoh, K., Katoh, Y., Hayashi, N., Satoh, K., Igarashi, K., Hatayama, I., Nabeshima, Y., 1997. An Nrf2/small Maf heterodimer mediates the induction of phase II detoxifying enzyme genes through antioxidant response elements. Biochem. Biophys. Res. Commun. 236, 313–322.

Itoh, K., Wakabayashi, N., Katoh, Y., Ishii, T., Igarashi, K., Engel, J.D., Yamamoto, M., 1999. Keap1 represses nuclear activation of antioxidant responsive elements by Nrf2 through binding to the amino-terminal Neh2 domain. Genes Dev. 13, 76–86.

Itoh, K., Ye, P., Matsumiya, T., Tanji, K., Ozaki, T., 2015. Emerging functional cross-talk between the Keap1-Nrf2 system and mitochondria. J. Clin. Biochem. Nutr. 56, 91–97.

Ivan, M., Kaelin, W.G., 2017. The EGLN-HIF O2-sensing system: multiple inputs and feedbacks. Mol. Cell.

Jabůrek, M., Garlid, K.D., 2003. Reconstitution of recombinant uncoupling proteins. J. Biol. Chem. 278, 25825–25831.

Jabůrek, M., Vařecha, M., Gimeno, R.E., Dembski, M., Ježek, P., Zhang, M., Burn, P., Tartaglia, L.A., Garlid, K.D., 1999. Transport function and regulation of mitochondrial uncoupling proteins 2 and 3. J. Biol. Chem. 274, 26003–26007.

Ji, W., Wang, L., He, S., Yan, L., Li, T., Wang, J., Kong, A.-N.T., Yu, S., Zhang, Y., 2018. Effects of acute hypoxia exposure with different durations on activation of Nrf2-ARE pathway in mouse skeletal muscle. PLoS One 13, e0208474.

Jia, J.-J., Zhang, X., Ge, C.-R., Jois, M., 2009. The polymorphisms of UCP2 and UCP3 genes associated with fat metabolism, obesity and diabetes. Obes. Rev. 10, 519–526.

Jiang, N., Zhang, G., Bo, H., Qu, J., Ma, G., Cao, D., Wen, L., Liu, S., Ji, L.L., Zhang, Y., 2009. Upregulation of uncoupling protein-3 in skeletal muscle during exercise: a potential antioxidant function. Free Radic. Biol. Med. 46, 138–145.

Jones, D.P., 2015. Redox theory of aging. Redox Biol. 5, 71–79.

Jones, D.P., 2006. Redefining oxidative stress. Antioxid. Redox Signal. 8, 1865–1879.

Kaelin, W.G., Ratcliffe, P.J., 2008. Oxygen sensing by metazoans: The central role of the HIF hydroxylase pathway. Mol. Cell 30, 393–402.

Kawai, Y., Garduño, L., Theodore, M., Yang, J., Arinze, I.J., 2011. Acetylation-deacetylation of the transcription factor Nrf2 (nuclear factor erythroid 2-related factor 2) regulates its transcriptional activity and nucleocytoplasmic localization. J. Biol. Chem. 286, 7629–7640.

Kee, B.L., Arias, J., Montminy, M.R., 1996. Adaptor-mediated recruitment of RNA polymerase II to a signal-dependent activator. J. Biol. Chem. 271, 2373–2375.

Kensler, T.W., Wakabayashi, N., Biswal, S., 2007. Cell survival responses to environmental stresses via the Keap1-Nrf2-ARE pathway. Annu. Rev. Pharmacol. Toxicol. 47, 89–116.

Kerner, J., Turkaly, P.J., Minkler, P.E., Hoppel, C.L., 2001. Aging skeletal muscle mitochondria in the rat: Decreased uncoupling protein-3 content. Am. J. Physiol. - Endocrinol. Metab. 281, E1054–E1062.

Kietzmann, T., Fandrey, J., Acker, H., 2000. Oxygen radicals as messengers in oxygen-dependent gene expression. News Physiol. Sci. 15, 202–208.

Kim, J.W., Tchernyshyov, I., Semenza, G.L., Dang, C. V, 2006. HIF-1-mediated expression of pyruvate dehydrogenase kinase: A metabolic switch required for cellular adaptation to hypoxia. Cell Metab. 3, 177–185.

Kitagawa, K., 2007. CREB and cAMP response element-mediated gene expression in the ischemic brain. FEBS J. 274, 3210–3217.

Klingenberg, M., Huang, S.G., 1999. Structure and function of the uncoupling protein from brown adipose tissue. Biochim. Biophys. Acta - Biomembr. 1415, 271–296.

Kobayashi, A., Kang, M.-I., Watai, Y., Tong, K.I., Shibata, T., Uchida, K., Yamamoto, M., 2006. Oxidative and electrophilic stresses sctivate Nrf2 through inhibition of ubiquitination activity of Keap1. Mol. Cell. Biol. 26, 221–229.

Kolamunne, R.T., Dias, I.H.K., Vernallis, A.B., Grant, M.M., Griffiths, H.R., 2013. Nrf2 activation supports cell survival during hypoxia and hypoxia/reoxygenation in cardiomyoblasts; the roles of reactive oxygen and nitrogen species. Redox Biol. 1, 418–426.

Kolwicz, S.C., Purohit, S., Tian, R., 2013. Cardiac metabolism and its interactions with contraction, growth, and survival of cardiomyocytes. Circ. Res. 113, 603–616.

Komatsu, M., Kurokawa, H., Waguri, S., Taguchi, K., Kobayashi, A., Ichimura, Y., Sou, Y.-S., Ueno, I., Sakamoto, A., Tong, K.I., Kim, M., Nishito, Y., Iemura, S., Natsume, T., Ueno, T., Kominami, E., Motohashi, H., Tanaka, K., Yamamoto, M., 2010. The selective autophagy substrate p62 activates the stress responsive transcription factor Nrf2 through inactivation of Keap1. Nat. Cell Biol. 12, 213–223.

Konstantinidis, K., Whelan, R.S., Kitsis, R.N., 2012. Mechanisms of cell death in heart disease. Arterioscler. Thromb. Vasc. Biol. 32, 1552–1562.

Korshunov, S.S., Skulachev, V.P., Starkov, A.A., 1997. High protonic potential actuates a mechanism of production of reactive oxygen species in mitochondria. FEBS Lett. 416, 15–18.

Kovac, S., Angelova, P.R., Holmström, K.M., Zhang, Y., Dinkova-Kostova, A.T., Abramov, A.Y., 2014. Nrf2 regulates ROS production by mitochondria and NADPH oxidase. Biochim. Biophys. Acta - Gen. Subj. 1850, 794–801.

Krauss, S., Zhang, C.-Y., Lowell, B.B., 2002. A significant portion of mitochondrial proton leak in intact thymocytes depends on expression of UCP2. Proc. Natl. Acad. Sci. 99, 118–122.

Krauss, S., Zhang, C.-Y., Scorrano, L., Dalgaard, L.T., St-Pierre, J., Grey, S.T., Lowell, B.B., 2003. Superoxide-mediated activation of uncoupling protein 2 causes pancreatic β cell dysfunction. J. Clin. Invest. 112, 1831–1842.

Krauss, S., Zhang, C.Y., Lowell, B.B., 2005. The mitochondrial uncoupling-protein homologues. Nat. Rev. Mol. Cell Biol. 6, 248–261.

Krönke, G., Bochkov, V.N., Huber, J., Gruber, F., Blüml, S., Fürnkranz, A., Kadl, A., Binder, B.R., Leitinger, N., 2003. Oxidized phospholipids induce expression of human Heme oxygenase-1 involving activation of cAMP-responsive element-binding protein. J. Biol. Chem. 278, 51006–51014.

Kudo, N., Barr, A.J., Barr, R.L., Desai, S., Lopaschuk, G.D., 1995. High rates of fatty acid oxidation during reperfusion of ischemic hearts are associated with a decrease in malonyl-CoA levels due to an increase in 5'-AMP-activated protein kinase inhibition of acetyl-CoA carboxylase. J. Biol. Chem. 270, 17513–17520.

Kulisz, A., Chen, N., Chandel, N.S., Shao, Z., Schumacker, P.T., 2002. Mitochondrial ROS initiate phosphorylation of p38 MAP kinase during hypoxia in cardiomyocytes. Am. J. Physiol. Lung Cell. Mol. Physiol. 282, L1324–L1329.

Kwok, R.P.S., Lundblad, J.R., Chrivia, J.C., Richards, J.P., Bächinger, H.P., Brennan, R.G., Roberts, S.G.E., Green, M.R., Goodman, R.H., 1994. Nuclear protein CBP is a coactivator for the transcription factor CREB. Nature 370, 223–226.

Lando, D., Peet, D.J., Gorman, J.J., Whelan, D.A., Whitelaw, M.L., Bruick, R.K., 2002. FIH-1 is an asparaginyl hydroxylase enzyme that regulates the transcriptional activity of hypoxia-inducible factor. Genes Dev. 16, 1466–1471.

Landstrom, A.P., Dobrev, D., Wehrens, X.H.T., 2017. Calcium Signaling and Cardiac Arrhythmias. Circ. Res. 120, 1969–1993.

Langendorff, O., 1895. Untersuchungen am überlebenden Säugethierherzen. Pflüger, Arch. für die Gesammte Physiol. des Menschen und der Thiere 61, 291–332.

Lango, R., Smolenski, R.T., Narkiewicz, M., Suchorzewska, J., Lysiak-Szydlowska, W., 2001. Influence of L-carnitine and its derivatives on myocardial metabolism and function in ischemic heart disease and during cardiopulmonary bypass. Cardiovasc. Res. 51, 21–29.

Lecour, S., 2009. Multiple protective pathways against reperfusion injury: A SAFE path without Aktion? J. Mol. Cell. Cardiol. 46, 607–609.

Ledesma, A., Lacoba, M.G. De, Rial, E., 2002. Protein family review The mitochondrial uncoupling proteins. Genome Biol 3, 1–9.

Lee, C.K., Allison, D.B., Brand, J., Weindruch, R., Prolla, T.A., 2002. Transcriptional profiles associated with aging and middle age-onset caloric restriction in mouse hearts. Proc. Natl. Acad. Sci. U. S. A. 99, 14988–14993.

Lenaz, G., 2012. Mitochondria and reactive oxygen species. Which role in physiology and pathology?, in: Advances in Mitochondrial Medicine. Advances in Experimental Medicine and Biology. Springer, Dordrecht, pp. 93–136.

Lenaz, G., Genova, M.L., 2010. Structure and organization of mitochondrial respiratory complexes: A new understanding of an old subject. Antioxidants Redox Signal.

Leonard, M.O., Kieran, N.E., Howell, K., Burne, M.J., Varadarajan, R., Dhakshinamoorthy, S., Porter, A.G., O'Farrelly, C., Rabb, H., Taylor, C.T., 2006. Reoxygenation-specific activation of the antioxidant transcription factor Nrf2 mediates cytoprotective gene expression in ischemia-reperfusion injury. FASEB J. 20, 2624–2626.

Lesnefsky, E.J., Chen, Q., Hoppel, C.L., 2016. Mitochondrial metabolism in aging heart. Circ. Res. 118, 1593–1611.

Levonen, A.-L., Landar, A., Ramachandran, A., Ceaser, E.K., Dickinson, D.A., Zanoni, G., Morrow, J.D., Darley-Usmar, V.M., 2004. Cellular mechanisms of redox cell signalling: role of cysteine modification in controlling antioxidant defences in response to electrophilic lipid oxidation products. Biochem. J. 378, 373–382.

Li, M., Gao, P., Zhang, J., 2016. Crosstalk between autophagy and apoptosis: Potential and emerging therapeutic targets for cardiac diseases. Int. J. Mol. Sci. 17, 1–19.

Li, N., Ragheb, K., Lawler, G., Sturgis, J., Rajwa, B., Melendez, J.A., Robinson, J.P., 2003. Mitochondrial complex I inhibitor rotenone induces apoptosis through enhancing mitochondrial reactive oxygen species production. J. Biol. Chem. 278, 8516–8525.

Li, Z., Galli, U., Becker, L.E., Bruns, H., Nickkolgh, A., Hoffmann, K., Karck, M., Schemmer, P., 2013. Sulforaphane protects hearts from early injury after experimental transplantation. Ann. Transplant. 18, 558–566.

Liedtke, A.J., Vary, T.C., Nellis, S.H., Fultz, C.W., 1982. Properties of carnitine incorporation in working swine hearts. Effects of coronary flow, ischemia, and excess fatty acids. Circ. Res. 50, 767–774.

Liesa, M., Shirihai, O.S., 2013. Mitochondrial dynamics in the regulation of nutrient utilization and energy expenditure. Cell Metab. 17, 491–506.

Locke, R.M., Rial, E., Nicholls, D.G., 1982. The acute regulation of mitochondrial proton conductance in cells and mitochondria from the brown fat of cold-adapted and warm-adapted guinea pigs. Eur. J. Biochem. 129, 381–387.

Lopaschuk, G.D., 1997. Alterations in fatty acid oxidation during reperfusion of the heart after myocardial ischemia. Am. J. Cardiol. 80, 11A-16A.

López-Bernardo, E., Anedda, A., Sánchez-Pérez, P., Acosta-Iborra, B., Cadenas, S., 2015. 4-Hydroxynonenal induces Nrf2-mediated UCP3 upregulation in mouse cardiomyocytes. Free Radic. Biol. Med. 88, 427–438.

Lu, Z., Sack, M.N., 2008. ATF-1 is a hypoxia-responsive transcriptional activator of skeletal muscle mitochondrial-uncoupling protein 3. J. Biol. Chem. 283, 23410–23418.

Łuczaj, W., Gęgotek, A., Skrzydlewska, E., 2017. Antioxidants and HNE in redox homeostasis. Free Radic. Biol. Med. 111, 87–101.

Ludtmann, M.H.R., Angelova, P.R., Zhang, Y., Abramov, A.Y., Dinkova-Kostova, A.T., 2014. Nrf2 affects the efficiency of mitochondrial fatty acid oxidation. Biochem. J. 457, 415–424.

Ma, Q., 2013. Role of Nrf2 in Oxidative Stress and Toxicity. Annu. Rev. Pharmacol. Toxicol. 53, 401–426.

Madungwe, N.B., Zilberstein, N.F., Feng, Y., Bopassa, J.C., 2016. Critical role of mitochondrial ROS is dependent on their site of production on the electron transport chain in ischemic heart. Am J Cardiovasc Dis 6, 93–108.

Mahon, P.C., Hirota, K., Semenza, G.L., 2001. FIH-1: A novel protein that interacts with HIF-1α and VHL to mediate repression of HIF-1 transcriptional activity. Genes Dev. 15, 2675–2686.

Mailloux, R.J., Harper, M.E., 2011. Uncoupling proteins and the control of mitochondrial reactive oxygen species production. Free Radic. Biol. Med. 51, 1106–1115.

Mailloux, R.J., Seifert, E.L., Bouillaud, F., Aguer, C., Collins, S., Harper, M.-E., 2011. Glutathionylation acts as a control switch for uncoupling proteins UCP2 and UCP3. J. Biol. Chem. 286, 21865–21875.

Mansfield, K.D., Guzy, R.D., Pan, Y., Young, R.M., Cash, T.P., Schumacker, P.T., Simon, M.C., 2005. Mitochondrial dysfunction resulting from loss of cytochrome c impairs cellular oxygen sensing and hypoxic HIF-α activation. Cell Metab. 1, 393–399.

Marinho, H.S., Real, C., Cyrne, L., Soares, H., Antunes, F., 2014. Hydrogen peroxide sensing, signaling and regulation of transcription factors. Redox Biol. 2, 535–562.

Mattiasson, G., Sullivan, P.G., 2006. The emerging functions of UCP2 in health, disease, and therapeutics. Antioxidants Redox Signal. 8, 1–38.

Mayr, B., Montminy, M., 2001. Transcriptional regulation by the phosphorylation-dependent factor creb. Nat. Rev. Mol. Cell Biol. 2, 599–609.

McDonald, R.B., Walker, K.M., Warman, D.B., Griffey, S.M., Warden, C.H., Ramsey, J.J., Horwitz, B.A., 2008. Characterization of survival and phenotype throughout the life span in UCP2/UCP3 genetically altered mice. Exp. Gerontol. 43, 1061–1068.

McGarry, J.D., Brown, N.F., 1997. The mitochondrial carnitine palmitoyltransferase system. From concept to molecular analysis. Eur. J. Biochem. 244, 1–14.

McLaughlin, B., Hartnett, K.A., Erhardt, J.A., Legos, J.J., White, R.F., Barone, F.C., Aizenman, E., 2003. Caspase 3 activation is essential for neuroprotection in preconditioning. Proc. Natl. Acad. Sci. 100, 715–720.

McLeod, C.J., Aziz, A., Hoyt, R.F., McCoy, J.P., Sack, M.N., 2005. Uncoupling proteins 2 and 3 function in concert to augment tolerance to cardiac ischemia. J. Biol. Chem. 280, 33470–33476.

McMahon, M., Itoh, K., Yamamoto, M., Chanas, S.A., Henderson, C.J., McLellan, L.I., Wolf, C.R., Cavin, C., Hayes, J.D., 2001. The cap "n" collar basic leucine zipper transcription factor Nrf2 (NF-E2 p45-related factor 2) controls both constitutive and inducible expression of intestinal detoxification and glutathione biosynthetic enzymes. Cancer Res. 61, 3299–3307.

McMahon, M., Thomas, N., Itoh, K., Yamamoto, M., Hayes, J.D., 2004. Redox-regulated turnover of Nrf2 is determined by at least two separate protein domains, the redox-sensitive Neh2 degron and the redox-insensitive Neh6 degron. J. Biol. Chem. 279, 31556–31567.

Miao, W., Hu, L., Scrivens, P.J., Batist, G., 2005. Transcriptional regulation of NF-E2 p45-related factor (NRF2) expression by the aryl hydrocarbon receptor-xenobiotic response element signaling pathway. J. Biol. Chem. 280, 20340–20348.

Miller, C.J., Gounder, S.S., Kannan, S., Goutam, K., Muthusamy, V.R., Firpo, M.A., Symons, J.D., Paine, R., Hoidal, J.R., Rajasekaran, N.S., 2012. Disruption of Nrf2/ARE signaling impairs antioxidant mechanisms and promotes cell degradation pathways in aged skeletal muscle. Biochim. Biophys. Acta - Mol. Basis Dis. 1822, 1038–1050.

Mitchell, P., 1966. Chemiosmotic coupling in oxidative and photosynthetic phosphorylation. Biol. Rev. Camb. Philos. Soc. 41, 445–502.

Miwa, S., Brand, M.D., 2003. Mitochondrial matrix reactive oxygen species production is very sensitive to mild uncoupling. Biochem. Soc. Trans. 31, 1300–1301.

Moazed, B., Desautels, M., 2002. Control of proteolysis by norepinephrine and insulin in brown adipocytes: role of ATP, phosphatidylinositol 3-kinase, and p70 S6K. Can. J. Physiol. Pharmacol. 80, 541–552.

Mohanraj, P., Merola, A.J., Wright, V.P., Clanton, T.L., 1998. Antioxidants protect rat diaphragmatic muscle function under hypoxic conditions. J. Appl. Physiol. 84, 1960–1966.

Moi, P., Chan, K., Asunis, I., Cao, A., Kan, Y.W., 1994. Isolation of NF-E2-related factor 2 (Nrf2), a NF-E2-like basic leucine zipper transcriptional activator that binds to the tandem NF-E2/AP1 repeat of the β-globin locus control region. Proc. Natl. Acad. Sci. U. S. A. 91, 9926–9930.

Mookerjee, S.A., Brand, M.D., 2011. Characteristics of the turnover of uncoupling protein 3 by the ubiquitin proteasome system in isolated mitochondria. Biochim. Biophys. Acta - Bioenerg. 1807, 1474–1481.

Motohashi, H., O'Connor, T., Katsuoka, F., Engel, J.D., Yamamoto, M., 2002. Integration and diversity of the regulatory network composed of Maf and CNC families of transcription factors. Gene 294, 1–12.

Motohashi, H., Yamamoto, M., 2004. Nrf2–Keap1 defines a physiologically important stress response mechanism. Trends Mol. Med. 10, 549–557.

Mudge, G.H., Mills, R.M., Taegtmeyer, H., Gorlin, R., Lesch, M., 1976. Alterations of myocardial amino acid metabolism in chronic ischemic heart disease. J. Clin. Invest. 58, 1185–1192.

Murphy, M.P., 2009. How mitochondria produce reactive oxygen species. Biochem. J. 417, 1–13.

Murphy, M.P., Echtay, K.S., Blaikie, F.H., Asin-Cayuelat, J., Cochemé, H.M., Green, K., Buckingham, J.A., Taylort, E.R., Hurrellt, F., Hughes, G., Miwa, S., Cooper, C.E., Svistunenko, D.A., Smith, R.A.J., Brand, M.D., 2003. Superoxide activates uncoupling proteins by generating carbon-centered radicals and initiating lipid peroxidation: Studies using a mitochondria- targeted spin trap derived from α-phenyl-N-tert-butylnitrone. J. Biol. Chem. 278, 48534–48545.

Murray, A.J., Anderson, R.E., Watson, G.C., Radda, G.K., Clarke, K., 2004. Uncoupling proteins in human heart. Lancet 364, 1786–1788.

Murray, A.J., Cole, M.A., Lygate, C.A., Carr, C.A., Stuckey, D.J., Little, S.E., Neubauer, S., Clarke, K., 2008. Increased mitochondrial uncoupling proteins, respiratory uncoupling and decreased efficiency in the chronically infarcted rat heart. J. Mol. Cell. Cardiol. 44, 694–700.

Murray, C.J.L., Lopez, A.D., 1997. Global mortality, disability, and the contribution of risk factors: Global burden of disease study. Lancet 349, 1436–1442.

Murry, C.E., Jennings, R.B., Reimer, K.A., 1986. Preconditioning with ischemia: a delay of lethal cell injury in ischemic myocardium. Circulation 74, 1124–1136.

Murry, C.E., Richard, V.J., Reimer, K.A., Jennings, R.B., 1990. Ischemic preconditioning slows energy metabolism and delays ultrastructural damage during a sustained ischemic episode. Circ. Res. 66, 913–931.

Musa, C. V, Mancini, A., Alfieri, A., Labruna, G., Valerio, G., Franzese, A., Pasanisi, F., Licenziati, M.R., Sacchetti, L., Buono, P., 2012. Four novel UCP3 gene variants associated with childhood obesity: effect on fatty acid oxidation and on prevention of triglyceride storage. Int. J. Obes. (Lond). 36, 207–17.

Nabben, M., Hoeks, J., 2008. Mitochondrial uncoupling protein 3 and its role in cardiac- and skeletal muscle metabolism. Physiol. Behav. 94, 259–269.

Nabben, M., Hoeks, J., Briedé, J.J., Glatz, J.F.C., Moonen-Kornips, E., Hesselink, M.K.C., Schrauwen, P., 2008. The effect of UCP3 overexpression on mitochondrial ROS production in skeletal muscle of young versus aged mice. FEBS Lett. 582, 4147–4152.

Nabben, M., Shabalina, I.G., Moonen-Kornips, E., Van Beurden, D., Cannon, B., Schrauwen, P., Nedergaard, J., Hoeks, J., 2011. Uncoupled respiration, ROS production, acute lipotoxicity and oxidative damage in isolated skeletal muscle mitochondria from UCP3-ablated mice. Biochim. Biophys. Acta - Bioenerg. 1807, 1095–1105.

Nadtochiy, S.M., Tompkins, A.J., Brookes, P.S., 2006. Different mechanisms of mitochondrial proton leak in ischaemia/reperfusion injury and preconditioning: implications for pathology and cardioprotection. Biochem. J. 395, 611–618.

Nègre-Salvayre, A., Hirtz, C., Carrera, G., Cazenave, R., Troly, M., Salvayre, R., Pénicaud, L., Casteilla, L., 1997. A role for uncoupling protein-2 as a regulator of mitochondrial hydrogen peroxide generation. FASEB J. 11, 809–815.

Nguyen, T., Sherratt, P.J., Huang, H.C., Yang, C.S., Pickett, C.B., 2003. Increased protein stability as a mechanism that enhances Nrf2-mediated transcriptional activation of the antioxidant response element: Degradation of Nrf2 by the 26 S proteasome. J. Biol. Chem. 278, 4536–4541.

Nicholls, D.G., 2006. The physiological regulation of uncoupling proteins. Biochim. Biophys. Acta - Bioenerg. 1757, 459–466.

Nicholls, D.G., 2001. A history of UCP1. Biochem. Soc. Trans. 29, 751–755.

Nicholls, D.G., Bernson, V.S., Heaton, G.M., 1978. The identification of the component in the inner membrane of brown adipose tissue mitochondria responsible for regulating energy dissipation. Experientia. Suppl. 32, 89–93.

Nicholls, D.G., Locke, R.M., 1984. Thermogenic mechanisms in brown fat. Physiol. Rev. 64, 1–64.

Nickel, A., Kohlhaas, M., Maack, C., 2014. Mitochondrial reactive oxygen species production and elimination. J. Mol. Cell. Cardiol. 73, 26–33.

Nishikawa, T., Edelstein, D., Du, X.L., Yamagishi, S.I., Matsumura, T., Kaneda, Y., Yorek, M.A., Beebe, D., Oates, P.J., Hammes, H.P., Glardino, I., Brownlee, M., 2000. Normalizing mitochondrial superoxide production blocks three pathways of hyperglycaemic damage. Nature 404, 787–790.

Nishimura, M., Tanaka, H., Homma, N., Matsuzawa, T., Watanabe, Y., 1989. Ionic mechanisms of the depression of automaticity and conduction in the rabbit atrioventricular node caused by hypoxia or metabolic inhibition and protective action of glucose and valine. Am. J. Cardiol. 64, J24–J28.

Niture, S.K., Jain, A.K., Jaiswal, A.K., 2009. Antioxidant-induced modification of INrf2 cysteine 151 and PKC-delta-mediated phosphorylation of Nrf2 serine 40 are both required for stabilization and nuclear translocation of Nrf2 and increased drug resistance. J. Cell Sci. 122, 4452–4464.

Ogryzko, V. V, Schiltz, R.L., Russanova, V., Howard, B.H., Nakatani, Y., 1996. The transcriptional coactivators p300 and CBP are histone acetyltransferases. Cell 87, 953–959.

Opie, L.H., 2014. Cardiac Metabolism in Health and Disease. Cell. Mol. Pathobiol. Cardiovasc. Dis. 3, 23–36.

Orr, A.L., Vargas, L., Turk, C.N., Baaten, J.E., Matzen, J.T., Dardov, V.J., Attle, S.J., Li, J., Quackenbush, D.C., Goncalves, R.L.S., Perevoshchikova, I. V., Petrassi, H.M., Meeusen, S.L., Ainscow, E.K., Brand, M.D., 2015. Suppressors of superoxide production from mitochondrial complex III. Nat. Chem. Biol. 11, 834–836.

Osburn, W.O., Kensler, T.W., 2008. Nrf2 signaling: An adaptive response pathway for protection against environmental toxic insults. Mutat. Res. - Rev. Mutat. Res. 659, 31–39.

Ozcan, C., Palmeri, M., Horvath, T.L., Russell, K.S., Russell, R.R., 2013. Role of uncoupling protein 3 in ischemia-reperfusion injury, arrhythmias, and preconditioning. Am. J. Physiol. Heart Circ. Physiol. 304, H1192–H1200.

Paggio, A., Checchetto, V., Campo, A., Menabò, R., Di Marco, G., Di Lisa, F., Szabo, I., Rizzuto, R., De Stefani, D., 2019. Identification of an ATP-sensitive potassium channel in mitochondria. Nature 572, 609–613.

Papandreou, I., Cairns, R.A., Fontana, L., Lim, A.L., Denko, N.C., 2006. HIF-1 mediates adaptation to hypoxia by actively downregulating mitochondrial oxygen consumption. Cell Metab. 3, 187–197.

Parker, D., Ferreri, K., Nakajima, T., LaMorte, V.J., Evans, R., Koerber, S.C., Hoeger, C., Montminy, M.R., 1996. Phosphorylation of CREB at Ser-133 induces complex formation with CREB-binding protein via a direct mechanism. Mol. Cell. Biol. 16, 694–703.

Pecqueur, C., Alves-Guerra, M.C., Gelly, C., Lévi-Meyrueis, C., Couplan, E., Collins, S., Ricquier, D., Bouillaud, F., Miroux, B., 2001. Uncoupling protein 2, in vivo distribution, induction upon oxidative stress, and evidence for translational regulation. J. Biol. Chem. 276, 8705–8712.

Penna, C., Mancardi, D., Rastaldo, R., Pagliaro, P., 2009. Cardioprotection: A radical view. Biochim. Biophys. Acta - Bioenerg. 1787, 781–793.

Perrino, C., Schiattarella, G.G., Sannino, A., Pironti, G., Petretta, M.P., Cannavo, A., Gargiulo, G., Ilardi, F., Magliulo, F., Franzone, A., Carotenuto, G., Serino, F., Altobelli, G.G., Cimini, V., Cuocolo, A., Lombardi, A., Goglia, F., Indolfi, C., Trimarco, B., Esposito, G., 2013. Genetic deletion of uncoupling protein 3 exaggerates apoptotic cell death in the ischemic heart leading to heart failure. J. Am. Heart Assoc. 2, 1–17.

Piao, C.S., Gao, S., Lee, G.H., Kim, D.S., Park, B.H., Chae, S.W., Chae, H.J., Kim, S.H., 2010. Sulforaphane protects ischemic injury of hearts through antioxidant pathway and mitochondrial KATP channels. Pharmacol. Res. 61, 342–348.

Piper, H.M., García-Dorado, D., Ovize, M., 1998. A fresh look at reperfusion injury. Cardiovasc. Res. 38, 291–300.

Polster, B.M., Nicholls, D.G., Ge, S.X., Roelofs, B.A., 2014. Use of potentiometric fluorophores in the measurement of mitochondrial reactive oxygen species. Methods Enzymol. 547, 225–250.

Puigserver, P., Wu, Z., Park, C.W., Graves, R., Wright, M., Spiegelman, B.M., 1998. A cold-inducible coactivator of nuclear receptors linked to adaptive thermogenesis. Cell 92, 829–839.

Purdom-Dickinson, S.E., Lin, Y., Dedek, M., Morrissy, S., Johnson, J., Chen, Q.M., 2007a. Induction of antioxidant and detoxification response by oxidants in cardiomyocytes: Evidence from gene expression profiling and activation of Nrf2 transcription factor. J. Mol. Cell. Cardiol. 42, 159–176.

Purdom-Dickinson, S.E., Sheveleva, E. V., Sun, H., Chen, Q.M., 2007b. Translational control of Nrf2 protein in activation of antioxidant response by oxidants. Mol. Pharmacol. 72, 1074–1081.

Ramos-Gomez, M., Kwak, M.-K., Dolan, P.M., Itoh, K., Yamamoto, M., Talalay, P., Kensler, T.W., 2001. Sensitivity to carcinogenesis is increased and chemoprotective efficacy of enzyme inducers is lost in nrf2 transcription factor-deficient mice. Proc. Natl. Acad. Sci. 98, 3410–3415.

Ramsay, R.R., Gandour, R.D., Van Der Leij, F.R., 2001. Molecular enzymology of carnitine transfer and transport. Biochim. Biophys. Acta - Protein Struct. Mol. Enzymol. 1546, 21–43.

Rial, E., Aguirregoitia, E., Jiménez-Jiménez, J., Ledesma, A., 2004. Alkylsulfonates activate the uncoupling protein UCP1: implications for the transport mechanism. Biochim. Biophys. Acta 1608, 122–130.

Riss, T., Moravec, R., Niles, A., Duellman, S., Benink, H., Worzella, T., Minor, L., 2013. Cell Viability Assays, In: Sittampalam GS, Grossman A, Brimacombe K, et al., editors. Assay Guidance Manual. Bethesda (MD): Eli Lilly & Company and the National Center for Advancing Translational Sciences; 2004-.

Robidoux, J., Martin, T.L., Collins, S., 2004. β-A drenergic receptors and regulation of energy expenditure: a family affair. Annu. Rev. Pharmacol. Toxicol. 44, 297–323.

Robinson, K.M., Janes, M.S., Pehar, M., Monette, J.S., Ross, M.F., Hagen, T.M., Murphy, M.P., Beckman, J.S., 2006. Selective fluorescent imaging of superoxide in vivo using ethidium-based probes. Proc. Natl. Acad. Sci. U. S. A. 103, 15038–15043.

Rushmore, T.H., Morton, M.R., Pickett, C.B., 1991. The antioxidant responsive element. Activation by oxidative stress and identification of the DNA consensus sequence required for functional activity. J. Biol. Chem. 266, 11632–11639.

Rushworth, S.A., MacEwan, D.J., O'Connell, M.A., 2008. Lipopolysaccharide-induced expression of NAD(P)H:Quinone Oxidoreductase 1 and Heme Oxygenase-1 protects against excessive inflammatory responses in human monocytes. J. Immunol. 181, 6730–6737.

Ryoo, I. geun, Kwak, M.K., 2018. Regulatory crosstalk between the oxidative stress-related transcription factor Nfe2l2/Nrf2 and mitochondria. Toxicol. Appl. Pharmacol. 359, 24–33.

Sack, M.N., 2006. Mitochondrial depolarization and the role of uncoupling proteins in ischemia tolerance. Cardiovasc. Res. 72, 210–219.

Safari, F., Anvari, Z., Moshtaghioun, S., Javan, M., Bayat, G., Forosh, S.S., Hekmatimoghaddam, S., 2014. Differential expression of cardiac uncoupling proteins 2 and 3 in response to myocardial ischemia-reperfusion in rats. Life Sci. 98, 68–74.

Sarri, E., Garcia-Dorado, D., Abellan, A., Soler-Soler, J., 2006. Effects of hypoxia, glucose deprivation and acidosis on phosphatidylcholine synthesis in HL-1 cardiomyocytes. CTP:phosphocholine cytidylyltransferase activity correlates with sarcolemmal disruption. Biochem. J. 394, 325–334.

Schafer, F., Buettner, G., 2001. Redox environment of the cell. Free Radic. Biol. Med. 30, 1191–1212.

Schneider, K., Valdez, J., Nguyen, J., Vawter, M., Galke, B., Kurtz, T.W., Chan, J.Y., 2016. Increased energy expenditure, UCP1 expression, and resistance to diet-induced obesity in mice lacking nuclear factor-erythroid-2-related transcription factor-2 (Nrf2). J. Biol. Chem. 291, 7754–7766.

Schodel, J., Oikonomopoulos, S., Ragoussis, J., Pugh, C.W., Ratcliffe, P.J., Mole, D.R., 2011. High-resolution genome-wide mapping of HIF-binding sites by ChIP-seq. Blood 117, e207–e217.

Schrauwen, P., Hoeks, J., Hesselink, M.K.C., 2006. Putative function and physiological relevance of the mitochondrial uncoupling protein-3: Involvement in fatty acid metabolism? Prog. Lipid Res. 45, 17–41.

Schrauwen, P., Saris, W.H.M., Hesselink, M.K.C., 2001. An alternative function for human uncoupling protein 3: protection of mitochondria against accumulation of nonesterified fatty acids inside the mitochondrial matrix. FASEB J. 15, 2497–2502.

Schulz, E., Wenzel, P., Münzel, T., Daiber, A., 2014. Mitochondrial redox signaling: Interaction of mitochondrial Reactive Oxygen Species with other sources of oxidative stress. Antioxid. Redox Signal. 20, 308–324.

Seifert, E.L., Bézaire, V., Estey, C., Harper, M.E., 2008. Essential role for uncoupling protein-3 in mitochondrial adaptation to fasting but not in fatty acid oxidation or fatty acid anion export. J. Biol. Chem. 283, 25124–25131.

Semenza, G.L., 2013. HIF-1 mediates metabolic responses to intratumoral hypoxia and oncogenic mutations. J. Clin. Invest. 123, 3664–3671.

Semenza, G.L., 2012. Hypoxia-inducible factors in physiology and medicine. Cell 148, 399–408.

Semenza, G.L., Wang, G.L., 1992. A nuclear factor induced by hypoxia via de novo protein synthesis binds to the human erythropoietin gene enhancer at a site required for transcriptional activation. Mol. Cell. Biol. 12, 5447–5454.

Sena, L.A., Chandel, N.S., 2012. Physiological roles of mitochondrial reactive oxygen species. Mol. Cell 48, 158–167.

Sgarbi, G., Gorini, G., Costanzini, A., Barbato, S., Solaini, G., Baracca, A., 2017. Hypoxia decreases ROS level in human fibroblasts. Int. J. Biochem. Cell Biol. 88, 133–144.

Shabalina, I.G., Jacobsson, A., Cannon, B., Nedergaard, J., 2004. Native UCP1 displays simple competitive kinetics between the regulators purine nucleotides and fatty acids. J. Biol. Chem. 279, 38236–38248.

Shabalina, I.G., Nedergaard, J., 2012. Mitochondrial ('mild') uncoupling and ROS production: physiologically relevant or not? Biochem. Soc. Trans. 39, 1305–1309.

Shaywitz, A.J., Greenberg, M.E., 1999. CREB: A stimulus-induced transcription factor activated by a diverse array of extracellular signals. Annu. Rev. Biochem. 68, 821–861.

Shen, G., Hebbar, V., Nair, S., Xu, C., Xu, C., Li, W., Lin, W., Keum, Y.S., Han, J., Gallo, M.A., Kong, A.-N.N.T., 2004. Regulation of Nrf2 transactivation domain activity: The differential effects of mitogen-activated protein kinase cascades and synergistic stimulatory effect of Raf and CREB-binding protein. J. Biol. Chem. 279, 23052–23060.

Shen, Y., Liu, X., Shi, J., Wu, X., 2019. Involvement of Nrf2 in myocardial ischemia and reperfusion injury. Int. J. Biol. Macromol. 125, 496–502.

Shiraishi, J., Tatsumi, T., Keira, N., Akashi, K., Mano, A., Yamanaka, S., Matoba, S., Asayama, J., Yaoi, T., Fushiki, S., Fliss, H., Nakagawa, M., 2001. Important role of energy-dependent mitochondrial pathways in cultured rat cardiac myocyte apoptosis. Am. J. Physiol. - Hear. Circ. Physiol. 281, H1637–H1647.

Sies, H., 2017. Hydrogen peroxide as a central redox signaling molecule in physiological oxidative stress: Oxidative eustress. Redox Biol. 11, 613–619.

Sies, H., 2015. Oxidative stress: A concept in redox biology and medicine. Redox Biol. 4, 180–183.

Sies, H., 1985. Oxidative stress: Introductory remarks. In: Oxidative stress. London, Academic Press.

Skulachev, V.P., 1998. Cytochrome c in the apoptotic and antioxidant cascades. FEBS Lett. 423, 275–280.

Skulachev, V.P., 1997. Membrane-linked systems preventing superoxide formation. Biosci. Rep. 17, 347–366.

Skulachev, V.P., 1991. Fatty acid circuit as a physiological mechanism of uncoupling of oxidative phosphorylation. FEBS Lett. 294, 158–162.

Solanes, G., Pedraza, N., Calvo, V., Vidal-Puig, A.J., Lowell, B.B., Villarroya, F., 2005. Thyroid hormones directly activate the expression of the human and mouse uncoupling protein-3 genes through a thyroid response element in the proximal promoter region. Biochem. J. 386, 505–513.

Solanes, G., Pedraza, N., Iglesias, R., Giralt, M., Villarroya, F., 2003. Functional relationship between MyoD and Peroxisome Proliferator-Activated Receptor-dependent regulatory pathways in the control of the human Uncoupling Protein-3 gene transcription. Mol. Endocrinol. 17, 1944–1958.

Solenkova, N. V., Solodushko, V., Cohen, M. V., Downey, J.M., 2006. Endogenous adenosine protects preconditioned heart during early minutes of reperfusion by activating Akt. Am. J. Physiol. - Hear. Circ. Physiol. 290, H441–H449.

Speakman, J.R., Talbot, D.A., Selman, C., Snart, S., McLaren, J.S., Redman, P., Krol, E., Jackson, D.M., Johnson, M.S., Brand, M.D., 2004. Uncoupled and surviving: Individual mice with high metabolism have greater mitochondrial uncoupling and live longer. Aging Cell 3, 87–95.

Srinivas, V., Zhang, L.P., Zhu, X.H., Caro, J., 1999. Characterization of an oxygen/redox-dependent degradation domain of hypoxia-inducible factor α (HIF-α) proteins. Biochem. Biophys. Res. Commun. 260, 557–561.

St-Pierre, J., Buckingham, J.A., Roebuck, S.J., Brand, M.D., 2002. Topology of superoxide production from different sites in the mitochondrial electron transport chain. J. Biol. Chem. 277, 44784–44790.

Starkov, A.A., Fiskum, G., 2003. Regulation of brain mitochondrial H2O2 production by membrane potential and NAD(P)H redox state. J. Neurochem. 86, 1101–1107.

Sugiura, S., Kitagawa, K., Omura-Matsuoka, E., Sasaki, T., Tanaka, S., Yagita, Y., Matsushita, K., Storm, D.R., Hori, M., 2004. CRE-mediated gene transcription in the peri-infarct area after focal cerebral ischemia in mice. J. Neurosci. Res. 75, 401–407.

Sun, F., Dai, C., Xie, J., Hu, X., 2012. Biochemical issues in estimation of cytosolic free NAD/NADH ratio. PLoS One 7, e34525.

Sun, Z., Chin, Y.E., Zhang, D.D., 2009. Acetylation of Nrf2 by p300/CBP augments promoter-specific DNA binding of Nrf2 during the antioxidant response. Mol. Cell. Biol. 29, 2658–2672.

Tan, Y., Rouse, J., Zhang, a, Cariati, S., Cohen, P., Comb, M.J., 1996. FGF and stress regulate CREB and ATF-1 via a pathway involving p38 MAP kinase and MAPKAP kinase-2. EMBO J. 15, 4629–4642.

Tatsumi, T., Shiraishi, J., Keira, N., Akashi, K., Mano, A., Yamanaka, S., Matoba, S., Fushiki, S., Fliss, H., Nakagawa, M., 2003. Intracellular ATP is required for mitochondrial apoptotic pathways in isolated hypoxic rat cardiac myocytes. Cardiovasc. Res. 59, 428–440.

Tello, D., Balsa, E., Acosta-Iborra, B., Fuertes-Yebra, E., Elorza, A., Ordóñez, Á., Corral-Escariz, M., Soro, I., López-Bernardo, E., Perales-Clemente, E., Martínez-Ruiz, A., Enríquez, J.A., Aragonés, J., Cadenas, S., Landázuri, M.O., 2011. Induction of the mitochondrial NDUFA4L2 protein by HIF-1α decreases oxygen consumption by inhibiting complex I activity. Cell Metab. 14, 768–779.

Thimmulappa, R.K., Lee, H., Rangasamy, T., Reddy, S.P., Yamamoto, M., Kensler, T.W., Biswal, S., 2006. Nrf2 is a critical regulator of the innate immune response and survival during experimental sepsis. J. Clin. Invest. 116, 984–995.

Tompkins, A.J., Burwell, L.S., Digerness, S.B., Zaragoza, C., Holman, W.L., Brookes, P.S., 2006. Mitochondrial dysfunction in cardiac ischemia-reperfusion injury: ROS from complex I, without inhibition. Biochim. Biophys. Acta - Mol. Basis Dis. 1762, 223–231.

Uchiyama, T., Engelman, R.M., Maulik, N., Das, D.K., 2004. Role of Akt signaling in mitochondrial survival pathway triggered by hypoxic preconditioning. Circulation 109, 3042–3049.

Ullery, J.C., Marnett, L.J., 2012. Protein modification by oxidized phospholipids and hydrolytically released lipid electrophiles: Investigating cellular responses. Biochim. Biophys. Acta - Biomembr. 1818, 2424–2435.

Venugopal, R., Jaiswal, A.K., 1996. Nrf1 and Nrf2 positively and c-Fos and Fra1 negatively regulate the human antioxidant response element-mediated expression of NAD(P)H:quinone oxidoreductase1 gene. Proc. Natl. Acad. Sci. U. S. A. 93, 14960–14965.

Venugopal, V., Hausenloy, D.J., Ludman, A., Di Salvo, C., Kolvekar, S., Yap, J., Lawrence, D., Bognolo, J., Yellon, D.M., 2009. Remote ischaemic preconditioning reduces myocardial injury in patients undergoing cardiac surgery with cold-blood cardioplegia: A randomised controlled trial. Heart 95, 1567–1571.

Vidal-Puig, A.J., Grujic, D., Zhang, C.Y., Hagen, T., Boss, O., Ido, Y., Szczepanik, A., Wade, J., Mootha, V., Cortright, R., Muoio, D.M., Lowell, B.B., 2000. Energy metabolism in uncoupling protein 3 gene knockout mice. J. Biol. Chem. 275, 16258–16266.

Villarroya, F., Iglesias, R., Giralt, M., 2007. PPARs in the control of uncoupling proteins gene expression. PPAR Res. 2007, 74364.

Vozza, A., Parisi, G., De Leonardis, F., Lasorsa, F.M., Castegna, A., Amorese, D., Marmo, R., Calcagnile, V.M., Palmieri, L., Ricquier, D., Paradies, E., Scarcia, P., Palmieri, F., Bouillaud, F., Fiermonte, G., 2014. UCP2 transports C4 metabolites out of mitochondria, regulating glucose and glutamine oxidation. Proc. Natl. Acad. Sci. 111, 960–965.

Wang, G.L., Jiang, B.H., Rue, E.A., Semenza, G.L., 1995. Hypoxia-inducible factor 1 is a basic-helix-loop-helix-PAS heterodimer regulated by cellular O2 tension. Proc. Natl. Acad. Sci. U. S. A. 92, 5510–5514.

Wang, G.L., Semenza, G.L., 1995. Purification and characterization of hypoxia-inducible factor. J. Biol. Chem. 270, 1230–1237.

Wasserman, W.W., Fahl, W.E., 1997. Functional antioxidant responsive elements. Proc. Natl. Acad. Sci. U. S. A. 94, 5361–6.

West, A.E., Griffith, E.C., Greenberg, M.E., 2002. Regulation of transcription factors by neuronal activity. Nat. Rev. Neurosci. 3, 921–931.

Winkler, E., Klingenberg, M., 1994. Effect of fatty acids on H+ transport activity of the reconstituted uncoupling protein. J. Biol. Chem. 269, 2508–15.

Wong, H.S., Dighe, P.A., Mezera, V., Monternier, P.A., Brand, M.D., 2017. Production of superoxide and hydrogen peroxide from specific mitochondrial sites under different bioenergetic conditions. J. Biol. Chem. 292, 16804–16809.

Wu, K.C., Cui, J.Y., Klaassen, C.D., 2011. Beneficial role of Nrf2 in regulating NADPH generation and consumption. Toxicol. Sci. 123, 590–600.

Wu, T., Zhao, F., Gao, B., Tan, C., Yagishita, N., Nakajima, T., Wong, P.K., Chapman, E., Fang, D., Zhang, D.D., 2014. Hrd1 suppresses Nrf2-mediated cellular protection during liver cirrhosis. Genes Dev. 28, 708–722.

Wu, W.Y., Li, Y. Da, Cui, Y.K., Wu, C., Hong, Y.X., Li, G., Wu, Y., Jie, L.J., Wang, Y., Li, G.R., 2018. The natural flavone acacetin confers cardiomyocyte protection against hypoxia/reoxygenation injury via AMPK-mediated activation of Nrf2 signaling pathway. Front. Pharmacol. 9, 1–16.

Xu, B., Zhang, J., Strom, J., Lee, S., Chen, Q.M., 2014. Myocardial ischemic reperfusion induces de novo Nrf2 protein translation. Biochim. Biophys. Acta - Mol. Basis Dis. 1842, 1638–1647.

Yaffe, D., Saxel, O., 1977. Serial passaging and differentiation of myogenic cells isolated from dystrophic mouse muscle. Nature 270, 725–727.

Yamamoto, T., Suzuki, T., Kobayashi, A., Wakabayashi, J., Maher, J., Motohashi, H., Yamamoto, M., 2008. Physiological significance of reactive Cysteine residues of Keap1 in determining Nrf2 activity. Mol. Cell. Biol. 28, 2758–2770.

Yanagawa, T., Itoh, K., Uwayama, J., Shibata, Y., Yamaguchi, A., Sano, T., Ishii, T., Yoshida, H., Yamamoto, M., 2004. Nrf2 deficiency causes tooth decolourization due to iron transport disorder in enamel organ. Genes to Cells 9, 641–651.

Yang, H., Yang, T., Baur, J.A., Perez, E., Matsui, T., Carmona, J.J., Lamming, D.W., Souza-Pinto, N.C., Bohr, V.A., Rosenzweig, A., de Cabo, R., Sauve, A.A., Sinclair, D.A., 2007. Nutrient-sensitive mitochondrial NAD+ levels dictate cell survival. Cell 130, 1095–1107.

Yellon, D.M., Hausenloy, D.J., 2007. Myocardial reperfusion injury. N. Engl. J. Med. 357, 1121–1135.

Yoshida, T., Maulik, N., Engelman, R.M., Ho, Y.S., Das, D.K., 2000. Targeted disruption of the mouse Sod I gene makes the hearts vulnerable to ischemic reperfusion injury. Circ. Res. 86, 264–269.

Yu, R., Mandlekar, S., Tan, T.H., Kong, A.N.T., 2000. Activation of p38 and c-Jun N-terminal kinase pathways and induction of apoptosis by chelerythrine do not require inhibition of protein kinase C. J. Biol. Chem. 275, 9612–9619.

Žáčková, M., Škobisová, E., Urbánková, E., Ježek, P., 2003. Activating ω-6 polyunsaturated fatty acids and inhibitory purine nucleotides are high affinity ligands for novel mitochondrial uncoupling proteins UCP2 and UCP3. J. Biol. Chem. 278, 20761–20769.

Zhang, C.-Y., Baffy, G., Perret, P., Krauss, S., Peroni, O., Grujic, D., Hagen, T., Vidal-Puig, A.J., Boss, O., Kim, Y.-B., Zheng, X.X., Wheeler, M.B., Shulman, G.I., Chan, C.B., Lowell, B.B., 2001. Uncoupling protein-2 negatively regulates insulin secretion and is a major link between obesity, β cell dysfunction, and type 2 diabetes. Cell 105, 745–755.

Zhang, C.-Y., Parton, L.E., Ye, C.P., Krauss, S., Shen, R., Lin, C.-T., Porco, J.A., Lowell, B.B., 2006. Genipin inhibits UCP2-mediated proton leak and acutely reverses obesity- and high glucose-induced β cell dysfunction in isolated pancreatic islets. Cell Metab. 3, 417–427.

Zhang, D.D., Hannink, M., 2003. Distinct cysteine residues in Keap1 are required for Keap1-dependent ubiquitination of Nrf2 and for stabilization of Nrf2 by chemopreventive agents and oxidative stress. Mol. Cell. Biol. 23, 8137–8151.

Zhang, D.D., Lo, S.-C., Cross, J. V., Templeton, D.J., Hannink, M., 2004. Keap1 is a redox-regulated substrate adaptor protein for a Cul3-dependent ubiquitin ligase complex. Mol. Cell. Biol. 24, 10941–10953.

Zhang, R., Li, L., Yuan, L., Zhao, M., 2016. Hypoxic preconditioning protects cardiomyocytes against hypoxia/reoxygenation-induced cell apoptosis via sphingosine kinase 2 and FAK/AKT pathway. Exp. Mol. Pathol. 100, 51–58.

Zhang, Y., Sano, M., Shinmura, K., Tamaki, K., Katsumata, Y., Matsuhashi, T., Morizane, S., Ito, H., Hishiki, T., Endo, J., Zhou, H., Yuasa, S., Kaneda, R., Suematsu, M., Fukuda, K., 2010. 4-hydroxy-2-nonenal protects against cardiac ischemia-reperfusion injury via the Nrf2-dependent pathway. J. Mol. Cell. Cardiol. 49, 576–586.

Zhao, Z.Q., Vinten-Johansen, J., 2002. Myocardial apoptosis and ischemic preconditioning. Cardiovasc. Res. 55, 438–455.

Zhou, M., Lin, B.Z., Coughlin, S., Vallega, G., Pilch, P.F., 2000. UCP-3 expression in skeletal muscle: effects of exercise, hypoxia, and AMP-activated protein kinase. Am. J. Physiol. Endocrinol. Metab. 279, E622–E629.

Zorov, D.B., Juhaszova, M., Sollott, S.J., 2014. Mitochondrial Reactive Oxygen Species (ROS) and ROS-Induced ROS Release. Physiol. Rev. 94, 909–950.

Zweier, J.L., Flaherty, J.T., Weisfeldt, M.L., 1987. Direct measurement of free radical generation following reperfusion of ischemic myocardium. Proc. Natl. Acad. Sci. U. S. A. 84, 1404–1407.

Zweier, J.L., Talukder, M.A.H., 2006. The role of oxidants and free radicals in reperfusion injury. Cardiovasc. Res. 70, 181–190.